UNIVERSITÉ DE GENÈVE **FACULTÉ DES SCIENCES**

Section de physique, GAP-Optique **Professeur N. Gisin**

Nonlinear Effects in Optical Fibers

THÈSE

présentée à la Faculté des sciences de l'Université de Genève pour obtenir le grade de Docteur ès sciences mention physique

par

Claudio VINEGONI

d'Italie

Thése N^0 3319

GENÈVE

Atelier de reproduction de la Section de physique

2001

Typeset using LaTeX™
TEX, a trademark of the American Mathematical Society

Thesis Committee

Advisor:

Prof. Nicolas Gisin	*University of Geneva*

Committee:

Dr. J. Faist	*University of Neuchatel*
Dr. H. Chen	*EXFO – Engineering – Quebec, Canada*
Dr. A. Fougere	*GapOptique SA – Geneve*
Dr. Mark Wegmuller	*University of Geneva*

Abstract of the dissertation

In recent years the implementation of Erbium-doped fiber amplifiers allowed to extend high-bit rate transmission to transoceanic distances. But the demand for an increase in transmission capacity is unprecedented and grows continuously. Despite the intrinsically small values of the nonlinear coefficient for silica, the nonlinear effects in optical fibers can be observed even at low powers considering that the light is confined in a relative small area over long (i.e. transoceanic) interaction lengths due to the extremely low attenuation coefficient and the event of optical amplifiers. This is the reason why nonlinear effects can not be ignored when considering light propagation in optical fibers. In the thesis we have studied different ways both to measure the nonlinear coefficient in optical fibers and how to exploit nonlinearities in a useful way in order to build switches or to perform measurements of different optical fibers parameters (e.g. chromatic dispersion, PMD).

Contents

Chapter 1

Introduction.

1.1 Introduction (english)

In recent years the implementation of Erbium-doped fiber amplifiers allowed to extend high-bit rate transmission to transoceanic distances. Despite this achievement, the demand for an increase in transmission capacity is unprecedented and grows continuously. This demand can be accounted for in different ways, like for example increasing the bit-rate per channel (time domain multiplexing, TDM), or by simply increasing the number of channels transmitted along a single fiber (wavelength division multiplexing, WDM). These two methods have different advantages and disadvantages, but nonlinearities start to play an important role for both of them due to the amount of power present in the fibers.

To have an idea of the powers involved in data transmission it could be really interesting to find out as an estimate, what is the minimum amount of power we have to send into a fiber at an entry point A in order to transmit the data at an exit point B distant some kilometers (typically tens of km).

The first step in optical communications corresponds to the conversion from an electrical input signal into an optical bit stream and usually this is done by direct modulation of a semiconductor laser. A non-return-to-zero (NRZ) modulation format is normally used meaning that the pulse remains on throughout the bit slot and its amplitude does not drop to zero between two or more successive bits. Of course the performance of data transmissions has to be characterized through a parameter. This parameter is called bit error rate (BER) and corresponds to the average probability of incorrect bit identification; for example a BER of 10^{-9} corresponds to an average 1 error per billion bits.

So once the light is launched through the fiber, it will be detected at B by an optical

receiver that converts the optical signal into an electrical one. The problem is to find what is the required minimum average received optical power (or receiver sensitivity) such that the signal will result to be error free. To note that the concept of error-free is relative to the kind of transmission we are considering. In the case of voice communications, error-free transmission is defined to corresponds to a BER equal or better than 10^{-9}. For more demanding data communications applications a BER of 10^{-12} could be required. For an ideal detector (no thermal noise, no dark current and 100 % quantum efficiency) 1 bits can be identified without error as long as even one photon is detected. An error is made every time a 1 bit fails to produce even a single electron hole (e-h) pair. For small number of photons (poissonian statistics) we can find that in order to have a BER of 10^{-9} the average number of photons per 1 bits has to be greater than 20. In terms of power that means (at 40 Gbit/s and at a wavelength of 1.55 μm) a minimum power at the detector equal to 100 nW ie. -40 dBm (note that we are working using a NRZ modulation format). Obviously most receivers operate well above the quantum limit (typically 20 dB above). That means the minimum amount of power required in order to detect a 1 is equal to -20 dBm. In a recent experiment performed at Alcatel a 10 Tb/s record transmission capacity over backbone networks was achieved. This was done using 256 channels in the 1.5 μm region (C and L band) spaced by 50 GHz. If we propagate the signal along tens of km of optical fibers considering the natural fiber losses (0.2 dB/km) a BER of 10^{-9} requires an input power at the entry of the fiber line of 0 dBm. For 256 channels this will correspond to a total amount of power at the entry of the fiber of 24 dBm. This if of course an optimistic estimate because in fact we have to take into account even for the losses due to the components along the fiber line (like connectors for example and the WDM and the PBS components that filters the different channels in frequency and polarization respectively out from the fiber). So in practice the power is of the order of Watts!! A further increase in power is required for the case of more demanding data communications (BER of 10^{-12}).

So how do these optical nonlinearities arise [1]? From a simple point of view we can consider a material as made of a collection of charged particles: electrons and ion cores. When an electric field is applied it will move these charges. The positive charges tend to move in the direction of the field while the negative ones move into the opposite way. For dielectric materials (glass in our case) the charges are not free to move and only a slight misplacement will occur. This small movements (ion cores in one direction and electrons in the other) will result in an induced electric dipole moment. Due to the large mass of an ion core and the large frequency of the light (10^{13} - 10^{17} Hz) , it is

only the motion of the electrons that is significant. Usually (Lorenz approximation) we consider the potential in which the electron is immersed as harmonic. But for a high electric field (i.e. high powers) higher order terms have to be included. This implies that the induced polarization will not be linear in the electric field anymore (harmonic approximation) but more generally (for silica) it is given by:

$$\mathbf{P} = \varepsilon_0 \left(\chi^{(1)}\mathbf{E} + \chi^{(3)}\mathbf{EEE} + \cdots \right) \tag{1.1}$$

where ε_0 is the permittivity of vacuum and $\chi^{(j)}$ the j-th order susceptibility. The term $\chi^{(1)}$ is the dominant contribution to the polarization **P** and its effects are included through the refractive index n [2]. The cubic term $\chi^{(3)}$ is responsible for phenomena like third-harmonic generation, four wave mixing and nonlinear refraction [2]. The first two processes (processes that generate new frequencies) are usually not important unless phase matching conditions are satisfied. Nonlinear refraction instead is always present and deeply affects the propagation of intense light in an optical fiber. The electromagnetic wave passing along the optical fiber induces a cubic polarization which is proportional to the third power of the electric field (see Eq. 1.1). This is equivalent to a change in the effective value of $\chi^{(1)}$ to $\chi^{(1)} + \chi^{(3)}\mathrm{E}^2$. In other words the refractive index is changed by an amount proportional to the optical intensity [1].

$$\widetilde{n}(\omega, I) = n(\omega) + n_2 I \tag{1.2}$$

This intensity dependence of the refractive index (optical Kerr effect) is responsible for numerous nonlinear effects.

To note that even if the value of the nonlinear coefficient n_2 is quite small, nonlinear effects in optical fibers assume a relevant importance due to the fact that the magnitudes of these effects depend on the length of the fiber along which the wave travels and on the ratio $\mathrm{n}_2/\mathrm{A}_{eff}$, where n_2 is the nonlinear refractive index of the fiber and A_{eff} the effective area of the lightmode. Despite the intrinsically small values of the nonlinear coefficient for silica, the nonlinear effects in optical fibers can be observed even at low powers considering that the light is confined in a relative small area (ca. 80 $\mu\mathrm{m}^2$) over long interaction lengths (transoceanic as mentioned at the beginning of the introduction) due to the extremely low attenuation coefficient and the event of optical amplifiers. This is the reason why nonlinear effects can not be ignored when considering light propagation in optical fibers. For what concerns the value of the nonlinear

coefficient, due to its importance in the effectiveness of the nonlinear effects, Chapter 2 of the thesis presents an original measurements for this parameter.

Another manifestation of the intensity dependence of the refractive index occurs through self-phase modulation (SPM) a phenomenon that leads to spectral broadening of optical pulses travelling along a fiber [2]. Note that SPM - as for most nonlinear effects - is not necessarily detrimental but can also be exploited as for example by interacting with the group velocity dispersion (GVD) to form optical solitons (i.e. pulses that propagates with undistorted shape).

When two or more optical waves co-propagate they can interact with each other through the fiber nonlinearity. This interaction gives rise to different phenomena like stimulated Raman and Brillouin scattering, harmonic generation, and four wave mixing.

Cross-phase modulation (XPM) is the analogue of SPM but this time the induced phase depends not only on its own intensity, but also on the one of the other co-propagating lightwaves [2]. The strength of XPM is different for the coupling between two waves with different frequencies but the same polarization and the coupling between two waves with the same frequencies but different polarization states. Both these effects are examined in Chapter 3 and exploited for the study of nonlinear polarization rotation (Section 3.1) and for the implementation of an all-optical switch (Section 3.2) respectively.

Another nonlinear effect that can be relevant in optical fibers is four wave mixing (FWM). This phenomenon is not always present but appears only under appropriate conditions (phase matching). This effect is devastating for WDM systems with equally spaced channels as the generated frequencies coincides with a transmission channel, leading to bit dependent interferences which degrade the transmitted signal. Chapter 4 is dedicated to the different aspects of FWM in optical fibers and how we can exploit it in order to produce photon pairs in single mode fibers (SMF) (Section 4.1), to obtain distributed measurements of chromatic dispersion in SMF (Section 4.2) and to obtain longitudinal maps of the nonlinear coefficient in SMF (Section 4.3).

Chapter 5 finally concludes with a description of some other work the author was involved with and not directly related to nonlinear effects in optical fibers. In Section 5.1 we report on a new setup dramatically increasing the sensitivity of near field optical scanning microscopy. In Section 5.2 we report about the possibility to monitor the gain inside an Erbium doped fiber amplifier (EDFA) by using an optical frequency domain reflectometer (OFDR). In Section 5.3 we report on the polarization state evolution in

the different fibers of a ribbon fiber. Finally in Section 5.4 a new type of polarization mode dispersion emulator is presented.

In the following more detailed summaries of the different chapters are given.

1. In Chapter 2 we demonstrate a new method for the measurement of the nonlinear coefficient n_2/A_{eff} in telecom fibers at 1550 nm.

   As mentioned at the beginning of the introduction the implementation of Erbium-doped fiber amplifiers allows for high-bit rate transmission over trans-oceanic distances. At the same time, the technique of wavelength division multiplexing (WDM) is used to increase the transmission rate, leading to an important amount of power inside the fiber. Because of the long distances and high powers, optical nonlinearities due to changes in the refractive index (optical Kerr effect) start to play a significant role. Among them, self-phase modulation (SPM), cross-phase modulation (XPM), and four-wave mixing (FWM) are the most important. The magnitudes of these effects depend on the ratio n_2/A_{eff} , where n_2 is the nonlinear refractive index of the fiber and A_{eff} the effective area of the lightmode. It is therefore important to have a simple and accurate method for the determination of this ratio. Different methods, based on SPM or XPM phase shift detection using interferometric and non-interferometric schemes have been proposed [3]. In this chapter, we present a different method based on the interferometric detection of a phase shift using a self-aligned interferometer with a Faraday mirror. This method has the advantage to be simple and to be all fiber implementable. Moreover, fluctuations from environmental perturbations present in the other schemes mentioned above are avoided. Another important point is the comparison of n_2/A_{eff} (section 2.2) obtained with our method, for Dispersion Shifted Fibers (DSF), Dispersion Compensating Fibers (DCF), and a standard Single Mode Fiber (SMF) with the ones obtained by other institutions on the same fibers. We show that the values found agree quite well with the results from the different measurement methods employed by the other institutions. In particular (Section 2.3) we compare our results with the SPM based cw dual-frequency method [4, 5]. This method with its simple measurement setup, gives the accurate value of n_2/A_{eff} according to the measurement conditions given in Refs. [4]. A brief description of the CW dual method is given and we

present an interlaboratory fiber nonlinear coefficient measurements for Dispersion Shifted Fibers (DSF). The values found are in good agreement among the two methods.

We demonstrate too (Section 2.2) that our results are independent of the length of the test fiber (on a 10 km range) even in the presence of large GVD which cause some problems in other measurement methods [5].

2. In Chapter 3 we analyze the influence of XPM and SPM on the signal propagation.

   - In Section 3.1 we present both a theoretical and experimental analysis of the nonlinear polarization rotation in an optical fiber.

     The potential of the nonlinear polarization rotation (NPR) to build ultrafast devices has been recognized a long time ago and received considerable attention since then. It has been proposed to exploit it for optical switches [6], logic gates [7], multiplexers [8], intensity discriminators [9], nonlinear filters [10], or pulse shapers [11]. However, an inherent problem to all these applications is the stability of the output state of polarization, generally subjected to fluctuations of the linear birefringence caused by temperature changes and drafts in the fiber environment. Of course, the same problem was also encountered in the few experiments dealing with the characterization and measurement of the NPR itself. In Ref. [12], the fluctuations of the output polarization were too strong to allow a meaningful measurement of NPR in a polarization maintaining fiber at 1064 nm, and in Ref. [13] , where 514 nm light was injected into a 60 m long fiber with a beatlength of 1.6 cm, a complicated arrangement had to be employed for the extraction of the changes caused by temperature drifts. As the fluctuations become worse for fibers with a large birefringence, and as the effect of NPR is proportional to the inverse of the wavelength, it is hard to measure NPR directly in a polarization maintaining (PM) fiber at the telecom wavelength of 1.55 μm. In this chapter (Chapter 3.1) we propose a method for removing the overall linear birefringence, and therefore also its fluctuations, in a passive way by employing a Faraday mirror [14] (FM) and a double pass of the fiber under test. To check how this -nowadays standard- method [15, 16, 17, 18] of removing linear birefringence acts on the NPR, we present also in this chapter

a simple model to calculate the action of linear and nonlinear birefringence. Using this model, it is then easy to show that the proposed method removes the overall linear birefringence only, whereas the nonlinear one, leading to NPR, remains unchanged. After describing the experimental set-up, the results of our NPR measurements using a FM are presented also, along with the predictions from our analytical model. The excellent agreement between the two demonstrates that using the FM, the overall linear birefringence is indeed removed completely, allowing to observe the NPR otherwise hidden within the noisy background of polarization changes due to environmental perturbations. This result also validates our method for possible implementation with a variety of other applications like the ones mentioned at the beginning of this section, with the prospect of drastically increasing their polarization stability.

- In Section 3.2 we demonstrate all-optical switching at 1.5 μm based on induced nonlinear polarization rotation, in both a polarization maintaining and a standard telecom fiber.

  All-optical switching techniques based on the optical Kerr effect [8, 19, 20, 21, 22, 23] are very attractive in that respect due to the ultrafast Kerr response [24, 25, 26] of less than a few fs. Indeed, an all optical Kerr switch was demonstrated recently to read out a 10 Gb/s channel from a 40 Gb/s TDM signal [6]. Besides the standard switch parameters like switching ratio, insertion loss or switching time, the stability of the switch is an important issue. Variations in the input control or signal polarizations as well as changes of the intrinsic birefringence of the Kerr medium will affect the switch. The variations of the input signal polarization can be dealt with by adopting a polarization diversity scheme, like e.g. in Ref. [6]. In order to keep the switch stable internally, the control pulse polarization should be kept as stable as possible by using a proper set-up. Moreover, changes in the signal polarization in the Kerr medium (typically a polarization maintaining PM fiber) due to changes in the intrinsic fiber birefringence have to be avoided since they can greatly reduce the extinction ratio of the switch. An active correction scheme (e.g. a polarization controller [12] with a feedback loop) is typically not rapid enough to correct the fast, acoustical perturbations, and may not work at all for large changes due to its limited range of operation.

To avoid these problems, we use on one hand a non-interferometric and on the other hand a passive stabilization scheme. In interferometric switches like Sagnac loops or Mach-Zehnder interferometers (IF), the switching is based on a phase-shift induced between the two different propagation directions or arms, respectively. If the signal is not carefully launched into an axis of a PM fiber, it will split into 4 different polarization modes, two in each propagation direction or interferometer arm, respectively. In addition to the phase-shift between the two different propagation directions or interferometer arms, additional 'local' phase-shifts between the polarization modes with the same propagation direction (or within the same IF arm) will degrade the switch quality. In the switch presented here, this problem is avoided by uniquely using this 'local' phase-shift between the two signal polarization modes in a single fiber, thereby reducing the relevant mode number to two. Having two modes only, we can then use a passive stabilization scheme that works both for fast and slow, arbitrarily large changes in the fiber birefringence. Although in this work an optical fiber is used to induce a nonlinear phase-shift, it should be noted that the stabilization scheme holds as well for any other Kerr elements (e.g. semiconductor saturable absorbers SOA).

- In Section 3.3 we present a way to obtain the polarization coupling length, an important parameter for the PMD probability distribution.

  It is well known that single-mode communication fibers are birefringent and that the orientation and the amount of birefringence are randomly distributed along the fibers. The corresponding polarization mode dispersion (PMD) becomes therefore a statistical quantity, and not only its mean value but also its probability distribution is important to assess the inferred system impairments. This distribution depends on two parameters: the (mean) local birefringence B and the polarization coupling length h, which is the distance over which the E field looses memory of its initial distribution between the local polarization eigenstates [27]. In fibers having a length L long compared to h, the probability distribution is Maxwellian with a mean PMD value of B, whereas for coupling lengths approaching the fiber lengths, the PMD statistic can change considerably [28]. It is therefore important to have knowledge not only of the overall PMD but also of h and the beatlength L_b. Here we present a novel way to directly infer the polarization coupling

length from measurements of the nonlinear polarization rotation (NPR) in a fiber.

3. In Chapter 4 we investigate FWM in optical fibers.

   - In Section 4.1 we present a novel way to generate photon pairs.

     It is well known that pairs of correlated photons entangled in energy and time can be used as a resource for quantum information processing. Up till now, photon pairs are mainly created in nonlinear crystals or waveguides, using parametric down conversion, a nonlinear effect due to the second order susceptibility $\chi^{(2)}$. In this chapter instead, we propose to create photon pairs directly in optical fibres, exploiting four wave mixing processes due to the third order susceptibility $\chi^{(3)}$. As mentioned at the beginning of the introduction this term is responsible for FWM, third harmonic generation, nonlinear refraction. The E dependence of the polarizability reflects on a power dependence of the refractive index of the fiber, inducing a possible intermodulation between different optical signals. If two different signals with frequencies ν_1, ν_2 are then launched into the fiber, the beatnote of these two signals modulates the refractive index with a frequency (ν_2 -ν_1). Through this modulation a third signal at the frequency ν_1 will develop sidebands at the frequencies

     $$\nu_1 + (\nu_1 - \nu_2) \qquad \nu_1 - (\nu_1 - \nu_2)$$

     The situation in fact is much more complex and every possible combination of the single frequencies can combine with each other. In a quantum representation we can say that different photons annihilate to generate new ones at different wavelengths. Different kinds of FWM are possible. The case in which three photons with the same frequency annihilate to give rise to a new one, is called "totally degenerate" FWM; the case of two photons with the same energy that combines to give rise to two photons different in energy, is called "partially degenerate" FWM. "Non-degenerate" FWM is present when all the frequencies are different to each other. It is important to note that as mentioned above not only energy conservation has to be satisfied in the FWM process, but even phase matching conditions. For this reason FWM is referred to as a "parametric process".

     In this chapter we concentrate mainly on "partially degenerate" FWM. In

this process two pump's photons are absorbed by the fiber and two photons are created; one photon at a higher frequency than the pump and one at a lower frequency. Usually low frequency waves are referred as Stokes waves. High frequency wave as Anti-Stokes. As mentioned in the former section, parametric processes are stronger when the process is phase-matched, i.e. when momentum conservation is valid. It follows that due to the dispersion of the refractive index, FWM is not always present but only when phase matching conditions are satisfied. In a SMF fiber this conditions are always satisfied when we work near λ_0, i.e. the wavelength at which the dispersion is equal to zero. If we consider now a pump at a wavelength near λ_0 FWM will create new photons at frequencies distributed symmetrically around the wavelength of the pump. These photons are generated at the same time so they are time correlated.

Now the advantage of creating photon pairs directly in optical fibres is that we can avoid the losses due to the collection of pairs created in an external source into the fibre. It also allows an all fibre operation, which is much more practical for "real life" applications (e.g metrology). Unfortunately in our experiment no photon pairs were detected. This could be due to the low amount of power injected into the FUT and to the poor quality (i.e. signal to background ratio) of the DFB laser. At the same time luminescence due to the glass impurities is covering the signal. Improvements could be obtained with an Erbium doped ring laser (higher signal to noise ratio and higher power) and using short lengths of fibers (like photonic crystal fibers).

- In Section 4.2 we report on distributed measurements of chromatic dispersion along dispersion shifted fibers with different values of polarization mode dispersion and coupling lenght, by way of an OTDR-like method based on four wave mixing.

  As mentioned at the beginning because of the long distances and high powers, optical nonlinearities start to play a significant role in optical fibers. In dispersion shifted fibers (DSF) four wave mixing whose efficiency depends on the chromatic dispersion profile, leads to transmission impairments. From here arise the necessity to have a technique that can allow to map the longitudinal distribution of chromatic dispersion along a fiber. The

method proposed by Mollenauer et al.[29, 30] and based on four wave mixing, is a convenient approach for the measurement of chromatic dispersion maps in DSF fibers. In this chapter we show that when the coupling length h is relatively large (as is typically the case for most older installed DSF cables) the method presents severe limits. In the chapter we present a comparison between DSF fibers with different values of PMD and coupling length and a model is discussed in order to explain the observed phenomena. We show too that mapping of chromatic dispersion in DCF fibers, is strongly affected by the coupling length value present in them.

- In Section 4.3 we report for the first time on distributed measurements of nonlinear coefficient n_2/A_{eff} along dispersion shifted fiber by way of an OTDR-like method based on four wave mixing effect.

  The utility of such a kind of measurements is pretty clear considering what we have said at the beginning of the chapter. It is therefore important to have a simple and accurate method for the determination of this ratio. Different methods, based on SPM or XPM phase shift detection using interferometric [23] and non-interferometric [5] schemes have been proposed (see Chapter 2). But all these measurements techniques give only the integrated value of the nonlinear coefficient over the entire length of the fiber under test (FUT). The only way to obtain a map of the n_2/A_{eff} over the entire fiber length consist in performing a destructive fiber-cutting measurement. In this chapter, we propose a new method based on an OTDR-like technique firstly proposed by Mollenauer et al. [29, 31] to perform distributed measurements of chromatic dispersion along a fiber. The method allows us to obtain longitudinal mapping of the nonlinear coefficient along a 10 km DSF fiber.

4. In Chapter 5 different works the author was involved with during his Ph.D., and not only related to nonlinear effects in optical fibers, are presented.

   - In Section 5.1 we present a a new system combining near-field scanning optical microscopy (NSOM) with single photon detection operating at the wavelength of 1.55 μm. The microscope was used in order to image the splice region between a standard telecom and an Erbium doped fiber. The excellent sensitivity also allowed to detect the Rayleigh scattered light of a standard fiber coming out laterally through the fiber cladding.

- In Section 5.2 we present a new way to obtain distributed gain measurements in Er-doped fibers with high resolution and accuracy using an optical frequency domain reflectometer.
- In Section 5.3 we make an analysis of the polarization evolution in a ribbon cable using high-resolution coherent OFDR.
- Finally in Section 5.4 we present a PMD emulator where the DGD and the ratio between first and second order PMD can be set by the user.

Finally in the appendixes B and C are presented all the articles and proceedings published during the Ph.D. in which the author was actively involved.

1.2 Introduction (française)

Ces dernières années, l'implémentation des amplificateurs à fibre dopée à l'erbium a permis d'étendre les transmissions haut débit aux distances transocéaniques. Malgré cela, la demande d'augmentation de la capacité des transmissions est sans précédent et continue de croître. Il y a différentes façons de combler cette demande, par exemple en augmentant le taux de bits par canaux (time domain multiplexing, TDM) ou simplement en augmentant le nombre de canaux circulant dans une seule fibre (wavelength division multiplexing, WDM). Les deux méthodes ont leurs avantages et leurs inconvénients, mais les effets non linéaires jouent un rôle dans les deux cas.

Quelle est donc l'origine de ces effets non linéaires [1]? Un matériau peut être vu, de façon simpliste, comme étant constitué d'un ensemble de particules chargées: des électrons et des ions. Lorsqu'un champ électrique est appliqué sur celui-ci, les charges se mettent en mouvement. Les charges positives se déplacent dans le sens du champ et les chargent négatives dans le sens inverse. Dans les matériaux diélectriques (dans notre cas le verre) les charges ne sont pas libres de se mouvoir, seul un faible déplacement est permis. Ces petits mouvements de charges (ions dans un sens et électrons dans l'autre) induisent un moment électrique dipolaire. A cause de la masse élevée des ions et des hautes fréquences de la lumière (10^{13} - 10^{17} Hz), seul le déplacement des électrons est significatif. Généralement, on considère que l'électron se trouve dans un potentiel linéaire (approximation de Lorentz). Mais dans le cas de grands champs électriques (c.-à-d. pour des puissances intenses), des harmoniques d'ordre supérieures doivent être considérées. La polarisation induite par le champ électrique ne peut plus être considérée comme linéaire ; pour la silice elle prend la forme générale suivante :

$$\mathbf{P} = \varepsilon_0 \left(\chi^{(1)}\mathbf{E} + \chi^{(3)}\mathbf{EEE} + \cdots \right) \tag{1.3}$$

avec ε_0 permittivité du vide et $\chi^{(j)}$ susceptibilité du j-e ordre. Le terme $\chi^{(1)}$ est la contribution prépondérante de la polarisation $\mathbf{P}$ et ses effets se traduisent par l'indice de réfraction n [2]. Le terme du troisième ordre $\chi^{(3)}$ est à l'origine d'effets comme la génération de troisième harmonique, le mélange à quatre ondes (FWM) et l'indice non linéaire [2]. Les deux premiers processus (processus générant de nouvelles fréquences) sont généralement négligeables si la condition d'accord de phase

n'est pas respectée. L'indice non linéaire est au contraire toujours présent et affecte profondément la propagation de faisceaux lumineux intenses dans les fibres optiques. L'onde électromagnétique passant à travers la fibre induit une polarisation du troisième ordre qui est proportionnelle au cube du champ électrique (voir Eq. 1.3). Cela revient à remplacer le terme $\chi^{(1)}$ par $\chi^{(1)} + \chi^{(3)}\mathrm{E}^2$. En d'autres termes, l'indice de réfraction évolue comme l'intensité optique [1].

$$\widetilde{n}(\omega, I) = n(\omega) + n_2 I \tag{1.4}$$

Cette dépendance de l'indice de réfraction vis à vis de l'intensité (effet Kerr optique) est responsable de nombreux effets non linéaires.

Il faut noter que même si le coefficient non linéaire n_2 est assez faible, les effets non- linéaires dans les fibres optiques sont conséquents, car leur intensité dépend de la longueur de fibre parcourue par l'onde et du rapport $\mathrm{n}_2/\mathrm{A}_{eff}$, où n_2 est l'indice de réfraction non linéaire de la fibre et A_{eff} est l'aire effective du mode optique. Malgré les petites valeurs intrinsèques du coefficient non linéaire de la silice, les effets non-linéaires dans les fibres optiques peuvent être observés même avec de faibles puissances, car la lumière est confinée dans une surface relativement petite (env. 80 $\mu\mathrm{m}^2$) sur de longues distances d'interaction (pour des liaisons transocéaniques comme mentionnées au début de l'introduction). C'est pourquoi les effets non linéaires ne peuvent pas être négligés lorsque l'on considère la propagation de la lumière dans les fibres optiques. Le coefficient non linéaire étant une grandeur physique importante pour tous les effets non linéaires, le chapitre 2 de cette thèse présente une mesure originale de ce paramètre.

Une autre manifestation de la dépendance de l'indice de réfraction vis à vis de l'intensité apparaît à travers l'automodulation de phase (self-phase modulation, SPM), ce phénomène se traduit par un élargissement spectral des pulses optiques se propageant à travers une fibre [2]. La SPM, comme la plupart des effets non linéaires, n'est pas nécessairement néfaste, on peut aussi en tirer partie comme par exemple en la combinant avec la dispersion de vitesse de groupe (group velocity dispersion, GVD) pour réaliser des solitons (c.-à-d. des impulsions se propageant sans se déformer).

Quand il y a co-propagation de deux ondes ou plus, elles peuvent interagir entre elles de façon non linéaire dans la fibre. Cette interaction est à l'origine de nombreux phénomènes comme la stimulation Raman, la diffusion Brillouin, la génération d'harmonique et le mélange à quatre ondes.

L'intermodulation de phase (cross-phase modulation, XPM) est analogue à la SPM; par contre cette fois-ci la phase induite ne dépend pas seulement de l'intensité de l'onde considérée mais aussi de celle des autres ondes présentes [2]. L'ampleur de l'XPM est différente pour le couplage entre deux ondes de fréquences différentes et de même polarisation et pour le couplage entre deux ondes de même fréquence et de polarisations différentes. Dans le chapitre 3, les deux cas sont abordés et exploités dans le cadre de l'étude de la rotation non linéaire de la polarisation (section 3.1) et de l'élaboration d'un interrupteur tout optique (section 3.2).

Un autre effet non linéaire peut être conséquent dans les fibres optiques, le mélange à quatre ondes (four wave mixing, FWM). Ce phénomène n'est pas toujours présent, et il n'apparaît que sous certaines conditions (accord de phase). Cet effet a des conséquences dévastatrices pour les systèmes WDM avec des canaux espacés de façon régulière, car les fréquences générées correspondent à des canaux de transmission. Ceci mène à des dégradations du signal transmis. Le chapitre 4 est dédié à différents aspects du FWM. On peut l'utiliser pour générer des paires de photons dans des fibres monomodes (section 4.1), pour obtenir une mesure distribuée de la dispersion chromatique de fibres monomodes (section 4.2) et pour obtenir un profil longitudinal du coefficient non linéaire dans les fibres (section 4.3).

Le chapitre 5 décrit d'autres travaux que l'auteur a entrepris, mais qui n'ont pas de relation avec les effets non linéaires dans les fibres optiques. La section 5.1 aborde un nouveau montage qui accroît très fortement la sensibilité d'un microscope à champs proche. La possibilité d'observer le gain d'un EDFA à l'aide d'un OFDR est vu dans la section 5.2. Dans la section 5.3 on s'intéresse à l'évolution de la polarisation dans une fibre à ruban. Pour finir, un nouveau type d'émulateur de dispersion des modes de polarisation est présenté dans la section 5.4.

Dans la suite de cette introduction, des résumés plus détaillés des différentes parties sont développés.

1. Dans le chapitre 2, on montre une nouvelle méthode de mesure du coefficient non linéaire n_2/A_{eff} dans les fibres télécoms à 1550 nm.

   Comme nous l'avons déjà mentionné dans le début de cette introduction, l'implémentation des amplificateurs à fibre dopée à l'erbium permet des transmissions haut débit sur des distances transocéaniques. Dans le même temps,

la technique du multiplexage en longueur d'onde (WDM) est utilisée pour accroître les capacités des transmissions, ce qui mène à une forte augmentation de la puissance circulant dans les fibres. A cause de ces longues distances et de ces fortes intensités, les non linéarités optiques causées par les changements de l'indice de réfraction (effet Kerr optique) commence à jouer un rôle conséquent. Ce sont l'automodulation de phase (SPM), l'intermodulation de phase (XPM) et le mélange à quatre ondes (FWM) qui sont prépondérants. L'importance de ces effets dépend du rapport n_2/A_{eff} , où n_2 est l'indice de réfraction non linéaire de la fibre et A_{eff} l'aire effective du mode optique. Il est donc important d'avoir une méthode simple et précise pour la détermination de ce rapport. Différentes méthodes basées sur la détection de la différence de phase induite par la SPM ou la XPM utilisant des schémas interférométriques ou non ont été proposés [3]. Dans ce chapitre, nous proposons une méthode différente basée sur une détection interférométrique de la différence de phase utilisant un interféromètre auto-aligné grâce à des miroirs de Faraday. Cette méthode a l'avantage d'être de réalisation simple et entièrement fibrée. De plus, les fluctuations extérieures présentes dans les autres schémas mentionnés ci-dessus sont éliminées. Un autre point important porte sur la comparaison des résultats de n_2/A_{eff} (section 2.2) obtenus à l'aide de notre méthode avec ceux d'autres instituts pour les même fibres : des fibres à dispersion décalée (dispersion-shifted fiber, DSF), des fibres à dispersion compensée (dispersion-compensating fiber, DCF) et des fibres standards monomodes (single-mode fiber, SMF). On montre que les valeurs trouvées sont en accord avec celles obtenues avec différentes méthodes par les autres instituts. En particulier, dans la section 2.3 nous comparons nos résultats avec la méthode SPM based cw dual-frequency [4, 5]. Cette méthode, avec son principe de mesure très simple, donne des valeurs précises de n_2/A_{eff} , sous réserve que les conditions développées dans la référence [4] soient respectées. Une brève description de cette méthode est donnée et on présente les résultats d'une mesure du coefficient non linéaire effectuée sur une fibre à dispersion décalée (DSF). Les deux méthodes donnent des valeurs qui sont concordantes.

Nous montrons aussi (section 2.2) que nos résultats sont indépendants de la longueur de la fibre sous test, même en présence d'une grande dispersion chromatique qui cause de nombreux problèmes pour les autres méthodes de mesure [5].

2. Dans le chapitre 3 on analyse l'influence de la XPM et de la SPM sur la propagation du signal.

    - Dans la section 3.1, on aborde une analyse théorique et expérimentale de la rotation non linéaire de polarisation (nonlinear polarization rotation, NPR) dans les fibres optiques.

      Les possibilités de réaliser des dispositifs ultra-rapides à l'aide de la rotation non linéaire de polarisation est connue depuis longtemps et reçoit donc une attention toute particulière. Des propositions ont été faites pour réaliser des interrupteurs optiques [6], des portes logiques [7], des multiplexeurs [8], des discriminateurs d'intensité [9], des filtres non linéaires [10] ou des remises en forme d'impulsion [11]. Cependant, la stabilité de l'état de polarisation de sortie est un problème inhérent à toutes ces applications. Généralement, on observe des variations de la biréfringence linéaire causées par les changements de températures et les perturbations de l'environnement de la fibre, ce qui limite la stabilité souhaitée. Bien sûr, ce problème est aussi rencontré dans les expériences traitant de la caractérisation et de la mesure de la NPR elle-même. Dans la référence [12], les fluctuations de la polarisation de sortie étaient trop importantes pour permettre une mesure sensée de la NPR dans une fibre à maintien de polarisation à 1064 nm, et dans la référence [13], où de la lumière à 514 nm a été injectée dans une fibre de 60 m avec une longueur de battement de 1.6 cm, un arrangement compliqué a du être mis en place pour extraire le signal du bruit dû aux dérives de température. Comme les fluctuations empirent dans les fibres avec les biréfringences élevées et que l'effet de la NPR est inversement proportionnel à la longueur d'onde, il est difficile d'effectuer une mesure directe de la NPR dans une fibre à maintien de polarisation et aux longueurs d'onde télécoms (1.55 μm). Dans ce chapitre (section 3.1), on propose une méthode pour éliminer totalement la biréfringence linéaire, et donc ses fluctuations, de façon passive. On utilise un miroir de Faraday [14] (faraday mirror, FM) et un double passage dans la fibre sous test. Pour vérifier comment cette méthode, maintenant courante [15, 16, 17, 18] pour éliminer les effets de la biréfringence linéaire, agit sur la NPR, on présente aussi dans ce chapitre un model simple pour calculer l'effet d'une biréfringence linéaire ou non

linéaire. En utilisant ce model, on montre facilement que la méthode proposée élimine totalement la biréfringence linéaire, alors que la biréfringence non linéaire, menant à la NPR, reste inchangée. Après une description du montage, les résultats obtenus avec notre méthode de mesure de la NPR utilisant un FM sont présentés ainsi que les prédictions de notre modèle analytique. L'excellent accord entre les deux démontre que l'utilisation du FM élimine complètement les effets de la biréfringence linéaire, ce qui permet d'observer la NPR, qui autrement aurait été noyée dans le bruit de fond du changement de la polarisation dû aux fluctuations extérieures. Ce résultat valide aussi notre méthode pour la réalisation d'autres applications comme celles précitées, avec la perspective d'augmenter considérablement leur stabilité en polarisation.

- Dans la section 3.2 on montre un interrupteur entièrement optique à 1.55 μm basé sur la rotation non linéaire de polarisation, dans une fibre à maintien de polarisation et dans une fibre standard télécoms.

  Les techniques d'interrupteur tout-optique basées sur l'effet Kerr optique [8, 19, 20, 21, 22, 23] sont très intéressantes à cause de la réponse ultrarapide de l'effet Kerr [24, 25, 26] , de l'ordre de quelques femtosecondes. En fait, un interrupteur tout optique à effet Kerr a été utilisé récemment pour extraire un canal à 10Gb/s d'un signal TDM à 40Gb/s [6]. En plus des paramètres courants pour caractériser les interrupteurs comme le taux d'extinction, les pertes d'insertion ou le temps de transition, la stabilité de l'interrupteur est un enjeu important. Les variations des polarisations d'entrée du signal et du contrôle vont affecter l'interrupteur tout comme les changements de la biréfringence intrinsèque du milieu. Les variations de la polarisation d'entrée du signal peuvent être gérées grâce à un dispositif insensible à la polarisation, comme dans la référence [6]. Pour garder l'interrupteur stable, la polarisation de l'impulsion de contrôle doit être maintenue aussi stable que possible en utilisant un montage adéquat. De plus, les changements de la polarisation du signal dans le milieu -typiquement une fibre

à maintien de polarisation (PM)- dus aux variations de la biréfringence intrinsèque doivent être éliminés pour ne pas réduire fortement le taux d'extinction de l'interrupteur. Une correction active (un contrôleur de polarisation [12] avec une boucle de contre-réaction) n'est pas assez rapide pour corriger les perturbations rapides et ne fonctionne pas du tout pour de grandes variations à cause de son domaine d'opération limité. Pour résoudre tous ces problèmes, on utilise d'une part un montage non-interférométrique et d'autre part une stabilisation passive. Les interrupteurs interférométriques, comme les boucles de Sagnac ou l'interféromètre de Mach-Zehnder, sont basés sur une différence de phase induite respectivement entre les deux sens de propagation ou les deux bras. Si le signal n'est pas lancé correctement dans un des axes de la fibre PM, il se divise en quatre modes de polarisation différents, respectivement deux dans chaque sens de propagation ou dans chaque bras. En plus de la différence de phase entre les deux sens de propagation ou bras de l'interféromètre, une différence de phase 'locale' supplémentaire entre les modes de polarisation avec le même sens de propagation (ou passant par le même bras) va dégrader la qualité de l'interrupteur. L'interrupteur présenté ici résout ce problème simplement en n'utilisant que cette différence de marche " locale " entre les deux modes de polarisation du signal dans la fibre ; ainsi on réduit le nombre de modes à deux. Ayant simplement deux modes, on peut alors utiliser une stabilisation passive qui fonctionne pour d'importants changements de la biréfringence de la fibre, et ce quelle que soit leur vitesse. Bien que dans ce travail une fibre optique soit utilisée pour induire la différence de phase non linéaire, on peut noter que le principe de la stabilisation marche aussi bien pour tous les autres milieux Kerr (par exemple les semi- conducteurs absorbant saturables SOA).

- Dans la partie 3.3, un moyen d'obtenir la longueur de couplage de la polarisation est présenté ; c'est un paramètre important pour la distribution de probabilité de la PMD.

  Il est bien connu que les fibres monomodes utilisées dans les communications ont de la biréfringence et que l'orientation et l'amplitude de la biréfringence sont distribuées de façon aléatoire le long des fibres. La dispersion des modes de polarisation (PMD) correspondante devient alors une

quantité statistique, et sa valeur moyenne ainsi que sa distribution de probabilité sont importantes pour évaluer les dégradations causées au système. Cette distribution dépend de deux paramètres : la biréfringence locale moyenne B et la longueur de couplage de polarisation h, qui est la distance au bout de laquelle le champ E a perdu la mémoire de sa distribution initiale entre les états propres locaux de la polarisation [27]. Pour les fibres qui ont une distance L grande comparée à h, la distribution de probabilité est maxwellienne avec une PMD moyenne de B, alors que pour une longueur de couplage voisine de la longueur de la fibre la distribution statistique de la PMD peut changer considérablement [28]. Il est donc important d'avoir connaissance non seulement de la PMD mais aussi de h et de la longueur de battement L_b.. Ici, nous décrivons une nouvelle façon de déterminer la longueur de couplage à partir de mesures de la rotation non linéaire de polarisation (NPR) dans une fibre.

3. Dans le chapitre 4, on s'intéresse au FWM dans les fibres optiques.

   - Dans la partie 4.1, on présente une nouvelle façon de générer des paires de photons.

     Il est bien connu que les paires de photons enchevêtrés en énergie et temps peuvent être utilisées comme source dans les processus d'information quantique. Jusqu'à maintenant, les paires de photons ont été principalement créées dans des cristaux non linéaires ou des guides d'onde, en utilisant la conversion paramétrique qui est un effet non linéaire dû à la susceptibilité du deuxième ordre $\chi^{(2)}$. Dans ce chapitre, nous proposons de créer des paires de photon directement dans les fibres optiques en exploitant un processus de mélange à quatre ondes dû à la susceptibilité du troisième ordre $\chi^{(3)}$. Comme nous l'avons mentionné au début de cette introduction, ce terme est responsable du FWM, de la génération de troisième harmonique et de l'indice non linéaire. La dépendance de la polarisabilité avec le champ E se traduit par une dépendance de l'indice de réfraction avec la puissance, ce qui permet d'introduire une intermodulation entre les différents signaux optiques. Alors, si deux différents signaux avec des fréquences ν_1, ν_2 sont lancés dans la fibre, le battement de ces deux signaux module l'indice de réfraction avec la fréquence (ν_2 -ν_1). A cause de cette modulation, un

troisième signal à la fréquence ν_1 va développer des bandes latérales aux fréquences

$$\nu_1 + (\nu_1 - \nu_2) \qquad \nu_1 - (\nu_1 - \nu_2)$$

La situation est en fait plus complexe, car toutes les fréquences peuvent se combiner les unes avec les autres. Une représentation quantique de la chose serait que différents photons s'annihilent pour donner naissance à de nouveaux photons à d'autres longueurs d'onde. Différents types de FWM sont possibles. Le cas où trois photons de même fréquence s'annihilent pour donner naissance à un nouveau photon s'appelle le FWM "totalement dégénéré"; si deux photons de même énergie se combinent pour donner deux photons d'énergie différente on parle de FWM "partiellement dégénéré". Le FWM "non-dégénéré" correspond au cas où toutes les longueurs d'onde seraient différentes. Il est important de remarquer que non seulement la conservation d'énergie doit être respectée mais aussi les conditions d'accord de phase. C'est pour cette raison que le FWM fait partie des "processus paramétriques".

Dans ce chapitre, on se concentre essentiellement sur le FWM "partiellement dégénéré". Dans le processus, deux photons de la pompe sont absorbés par la fibre et deux photons sont créés; le premier à une fréquence supérieure à celle de la pompe et le second à une fréquence inférieure. Couramment l'onde à basse fréquence est appelée raie Stokes et la haute fréquence raie Anti-Stokes. Comme on l'a évoqué précédemment, les processus paramétriques sont plus importants lorsque l'on respecte les conditions d'accord de phase, c'est à dire quand il y a conservation du moment. Il s'ensuit qu'à cause de la dispersion de l'indice de réfraction, le FWM n'est pas toujours présent. Dans une fibre mono-mode, l'accord de phase est toujours respecté lorsque l'on travaille près de λ_0. Si l'on considère maintenant une pompe à la longueur d'onde λ_0,, le FWM crée de nouveaux photons à des fréquences distribuées de façon symétrique de part et d'autre de la longueur de pompe. Ces photons sont générés en même temps et donc sont corrélés en temps.

L'avantage qu'il y a à créer des paires de photons dans les fibres optiques réside dans l'élimination des pertes que l'on peut avoir lorsque l'on crée les paires dans une source externe et qu'on les couple dans une fibre. Cela

permet aussi d'opérer de façon complètement fibrée, ce qui est bien plus pratique dans les applications courantes (par exemple la métrologie). Malheureusement dans notre expérience, aucune paire de photons n'a pu être détectée. Cela peut être dû à la trop faible puissance injectée dans la fibre sous test et à la mauvaise qualité du laser DFB. Dans le même temps, la luminescence provenant des impuretés du verre couvre le signal. Des améliorations peuvent être apportées avec un laser erbium en anneau (un meilleur rapport signal sur bruit et une plus grande puissance) et en utilisant de courts morceaux de fibres (comme des fibres à cristal photonique).

- Dans la section 4.2, on aborde une mesure distribuée de la dispersion chromatique le long de fibres à dispersion décalée avec différentes valeurs de dispersion de mode de polarisation et de longueur de couplage, en utilisant une méthode similaire à un OTDR, basée sur le mélange à quatre ondes.

  Comme mentionné précédemment, les non linéarités optiques commencent à jouer un rôle significatif dans les fibres optiques à cause des distances parcourues et des fortes puissances. Dans les fibres à dispersion décalée (DSF), le mélange à quatre ondes, dont l'efficacité dépend du profil de la dispersion chromatique, mène à des erreurs de transmission. C'est pourquoi il est nécessaire d'avoir une technique qui permet d'obtenir la distribution longitudinale de la dispersion chromatique le long de la fibre. La méthode proposée par Mollenauer et al.[29, 30] et basée sur le mélange à quatre ondes est une bonne approche pour la mesure distribuée de la dispersion chromatique dans les fibres à dispersion décalée. Dans ce chapitre, on montre que lorsque la longueur de couplage h est relativement grande (comme c'est généralement le cas pour la plupart des vieux câbles DSF installés) la méthode présente de sévères limites. Dans le chapitre, on montre une comparaison entre plusieurs fibres DSF avec différentes valeurs de PMD et de longueur de couplage, et un model est élaboré pour tenter d'expliquer les phénomènes observés. On montre aussi que la distribution longitudinale de la dispersion chromatique dans les fibres DCF est fortement affectée par leur longueur de couplage.

- Dans la section 4.3, on montre pour la première fois une mesure distribuée du coefficient non linéaire n_2/A_{eff} le long de fibres à dispersion décalée en utilisant une méthode similaire à un OTDR, basée sur le mélange à quatre

ondes.

L'utilité d'une telle mesure est assez évidente au vu de tout ce que l'on a dit au début de ce chapitre. C'est pourquoi il est important d'avoir une méthode simple et précise de mesure pour la détermination de ce rapport. Différentes méthodes basées sur la détection de la différence de phase induit par la SPM ou la XPM, utilisant des schémas interférométriques [23] ou non [5], ont été proposées (voir chapitre 2). Mais toutes ces techniques ne donnent que la valeur du coefficient non linéaire intégrée sur toute la longueur de la fibre sous test (FUT). Le seul moyen d'obtenir un profil de n_2/A_{eff} le long de la fibre est destructif, il faut couper la fibre en petits bouts. Dans ce chapitre, on propose une nouvelle méthode similaire à une technique élaborée par Mollenauer et al. [29, 31] pour réaliser une mesure distribuée de la dispersion chromatique le long de la fibre. La méthode nous permet d'obtenir un profil longitudinal du coefficient non linéaire le long d'une fibre DSF de 10 km.

4. Dans le chapitre 5, différents travaux réalisés par l'auteur au cours de sa thèse et n'ayant pas de rapport avec les effets non linéaires dans les fibres sont présentés.

   - Dans la section 5.1 on présente une nouvelle méthode combinant microscopie de champ proche à balayage (NSOM) avec détection de photon unique travaillant à la longueur d'onde de 1.55 μm. Le microscope a été utilisé pour réaliser l'image de la soudure entre une fibre standard et une fibre dopée à l'erbium. L'excellente sensibilité permet de détecter la diffusion Rayleigh de la fibre standard sortant latéralement à travers la gaine.
   - Dans la section 5.2 on présente une nouvelle façon d'obtenir une mesure distribuée du gain dans les fibres dopées à l'erbium avec une haute résolution grâce à un OFDR (optical frequency domain reflectometer).
   - Dans la section 5.3 on fait l'analyse de l'évolution de la polarisation dans un ruban de fibre en utilisant un OFDR.
   - Finalement, dans la section 5.4 on présente un émulateur de PMD où le DGD et le rapport entre PMD du premier et du deuxième ordre peut être choisi par l'utilisateur.

A la fin, les appendices B et C présentent tous les articles et proceedings publiés pendant la thèse dans les quel l'auteur s'est activement investi.

Chapter 2

Determination of the Nonlinear Coefficient in Optical Fibers.

2.1 Measurements of n_2/A_{eff} in SMF fibers

In this section we demonstrate a method for the measurement of the nonlinear coefficient n_2/A_{eff} in telecom fibers at 1550 nm. This method is based on the Kerr phase shift detected by a self-aligned interferometer incorporating a Faraday mirror. This makes the set-up very robust, and different test fibers can be measured without any further readjustments.

2.1.1 Introduction

The implementation of Erbium-doped fiber amplifiers allows for high-bit rate transmission over transoceanic distances. At the same time, the technique of wavelength division multiplexing (WDM) is used to increase the transmission rate, leading to an important amount of power inside the fiber. Because of the long distances and high powers, optical nonlinearities due to changes in the refractive index (optical Kerr effect) start to play a significant role. Among them, self-phase modulation (SPM), cross-phase modulation (XPM), and four-wave mixing (FWM) are the most important. The magnitudes of these effects depend on the ratio n_2/A_{eff} , where n_2 is the nonlinear refractive index of the fiber and A_{eff} the effective area of the lightmode. It is therefore important to have a simple and accurate method for the determination of this ratio. Different methods, based on SPM or XPM phase shift detection using interferometric and non-interferometric schemes have been proposed [3]. In this chapter, we present

a different method based on the interferometric detection of a phase shift using a self-aligned interferometer with a Faraday mirror. This method has the advantage to be simple and to be all fiber implementable. Moreover, fluctuations from environmental perturbations present in the other schemes mentioned above are avoided.

2.1.2 Principle of operation

The power dependence of the refractive index leads to a power dependent phase change ϕ of a pulse (peak power P, wave number k) traveling through a fiber of length L:

$$\phi(P) = \phi_l + \phi_{nl} = n_0 kL + n_2 kL_{eff} \frac{P}{A_{eff}} m \tag{2.1}$$

Fiber losses are accounted for by the effective length L_{eff} = 1/α [1-exp(-α L)], with fiber loss coefficient α. The polarization parameter m depends on the polarization characteristics of the test fiber and the signal polarization state. It is equal to 1 for the case of a polarization maintaining fiber if the light is coupled into one of the two axes [32], whereas for a sufficiently long standard telecom fiber with a complete scrambling of the polarization, it was demonstrated that m=8/9 [33]. Using Eq. (2.1), a measure of the acquired phase shift will allow to determine the ratio n_2/A_{eff} or, through an independent measurement of A_{eff}, the value of n_2. The phase shift is measured using the self-aligned interferometer shown in Fig. 2.1. Amplified laser pulses are split at the first coupler (coupling ratio (α/(1-α)). They then move along the two interferometer arms, which are different in length so that the two pulses do not interfere upon recombination at the second coupler (coupling ratio β/(1-β)). One of the exit arms of this last coupler is connected to the fiber under test (FUT) of which n_2/A_{eff} is to be measured. For an adequate choice of α and β, the two pulses in the FUT strongly vary in power, and consequently experience (according to Eq. (2.1)) a different amount of phase-shift. After being reflected at the Faraday mirror (FM) [14, 16], the pulses return back through the FUT towards the first coupler. Four different trajectories through the interferometer are possible during the go- and return path: a double pass of the long-arm (long-long), of the short-arm (short-short), and a forward pass of the short (long) arm with a return pass through the opposite arm (short-long and long-short, respectively). Due to the differences in path length, three different arrival times at the detector can be discerned, as is schematically shown in the inset of Fig. 2.1. Only the middle pulse,

that is due to the interference between short-long and long-short pulses, is interesting and will be further analyzed. Its power at the detector depends on the phase relationship between the two interfering signals, and it can therefore be exploited to calculate the nonlinear phase-shift experienced in the FUT. Note that contrary to regular Mach-Zehnder interferometers, the balancing of the interferometer arms is not critical as the path lengths of the two interfering signals are automatically matched (self-aligned). Obviously, the power of this middle pulse also depends on the polarization states of the two interfering signals, given by

$$|\psi_{LS}>= R_S^{-1}(R_{FUT}^{-1}FR_{FUT})R_L|\psi_0>= R_S^{-1}FR_L|\psi_0>=: A|\psi_0> \tag{2.2}$$

$$|\psi_{SL}>= R_L^{-1}(R_{FUT}^{-1}FR_{FUT})R_S|\psi_0>= R_L^{-1}FR_S|\psi_0>=: B|\psi_0> \tag{2.3}$$

for the long-short and short-long path, respectively. ψ_0 is the input state of polarization, and R_L, R_S, R_{FUT}, and F are the transformation operators for the long- and short arm, the FUT, and the FM, respectively. The use of a FM as a reflector removes polarization transformations of the FUT, thereby fixing its output polarization. Note that using a standard mirror in place of the FM, an additional PC would be required, which not only makes the initial adjustments painful, but also leads to an undesired FUT dependence. For optimum visibility, one needs full interference between the two signals, i.e. A=B in Eq. (2.2) and Eq. (2.3), which can be obtained by properly adjusting the PC such that R_L = R_S. In practice, this is done by setting the PC so that the output intensity is maximized for a low input pulse power and with the FM directly connected to the interferometer (i.e. no FUT and therefore no nonlinear phase-shift is present). This setting can then be used throughout the measurements, without the need for readjustments as long as there is no significant change in R_L or R_S. Using the described adjustment, the detected power becomes proportional to

$$P_{OUT}(P) \propto Pcos^2(\Delta\phi) \tag{2.4}$$

where $\Delta\phi$ is the difference between the nonlinear phase shifts acquired by the short-arm and long-arm pulses, and it is equal to

$$\Delta\phi(P) = \frac{2\pi}{\lambda}PL_{eff}(\alpha-\beta)m\frac{n_2}{A_{eff}} \tag{2.5}$$

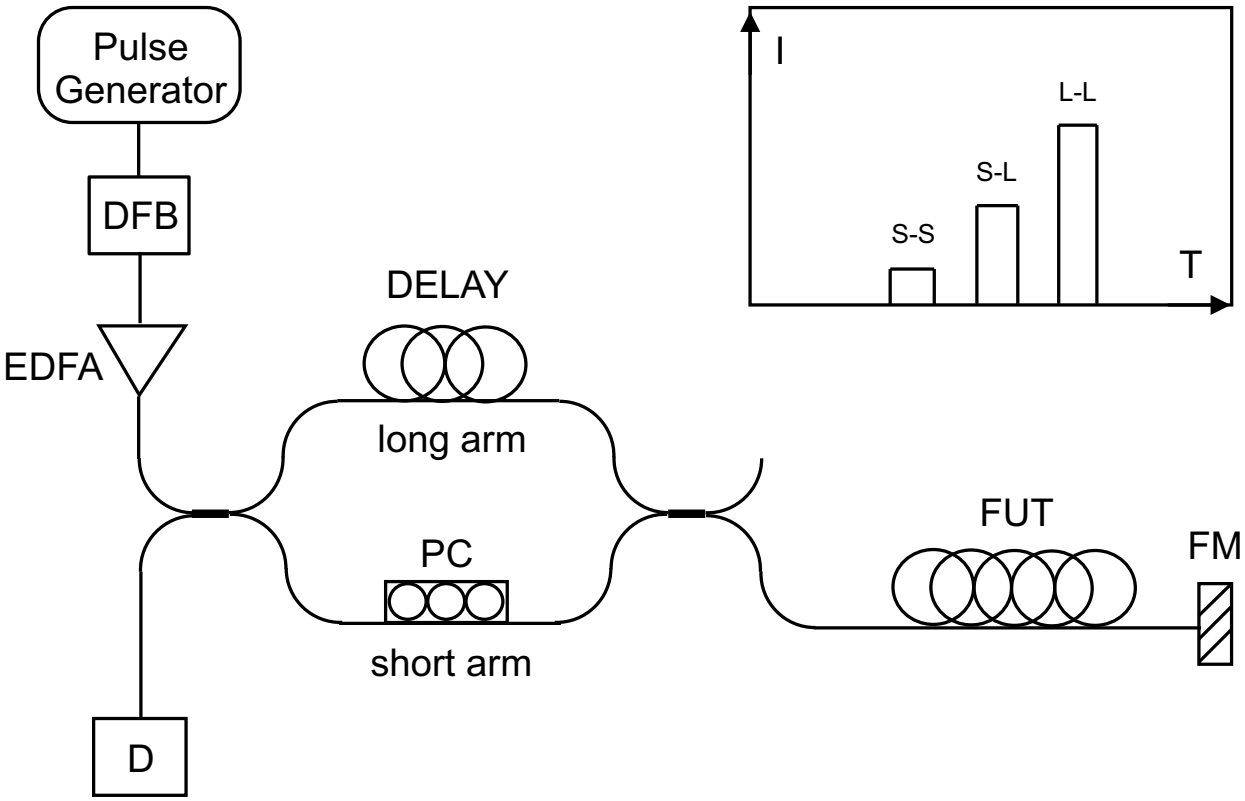

Figure 2.1: Experimental setup of the self-aligned interferometer. DFB distributed feedback laser, EDFA Erbium doped fiber amplifier, PC polarization controller, FUT fiber under test, FM Faraday mirror, D detector.

Straightforward calculation shows that for maximum visibility of the detected signal, one of the two couplers has to be symmetric (50/50). In order to obtain a good accuracy for n_2/A_{eff} , the measurements are done for different launch powers P. Ideally, the length of the FUT is long enough to allow for a good polarization scrambling and to be able to detect the first zero pass at $\Delta\phi = \pi/2$ for the available launch power.

2.1.3 Experimental

The procedure needed to perform the measurements is the following. First of all a calibration of the photodiode and a measurement of the real power sent into the fiber has to be made. In order to do this we have to measure the power from the DFB laser. We do this by using a power meter and measuring the average power for different pulse widths and frequencies in order to check if the power meter is responding linearly with these two parameters. Once linearity is established we calculate the peak power of the laser. If we know now the value of the peak power we can calibrate the photodiode we are using in our setup. To do this we the output of the DFB laser directly onto the photodiode by passing first through a variable attenuator. For different attenuation values we measure the voltage detected at the photodiode and knowing the input power value (determined before) we can find the conversion function from Watts to Volts. When we have the calibration function of the photodiode we can use it to determine the peak power at the entry of our interferometer. Of course higher attenuation during the experiment have to be used due to the high values of the peak power reached after the EDFA. The measurements on the fibers are made in the following way. For different values of amplification (i.e. current set on the EDFA) we measure the peak power value at the exit of the interferometer. But of course we have to take into account that the effective area of the fiber that makes up the interferometer could be different from the one of the FUT. That implies that an amount of power different from the measured one at the entry of the interferometer, is coupled into the FUT. So we have always to check the coupling loss between the different components of the interferometer (i.e. Faraday mirror and exit of the interferometer) and the FUT. Another parameter we have to measure is the attenuation loss of the FUT. This is measured by means of an OTDR. Taking into account all this parameter we obtain an effective length different from the real one. This is the value that has to enter the fitting function of our data. Once we have collected different experimental data changing the power at the entry of the fiber (current) we have to find out to which power these different points

correspond to. To do this we can measure it at the second exit of the last coupler of the interferometer (if we have two photodiodes) or just by removing the FUT and measuring there the input power sent into the FUT. These procedures have to be repeated at least three times in order to accumulate enough statistics. For each measurement the calibration procedure has to be repeated in order to increase the accuracy. In fact the power seems not to be stable with respect to of time for the same current value at the exit of the EDFA.

2.1.4 Results and discussion

For the practical implementation of the above concept, we use a directly modulated DFB laser diode with a wavelength of 1559 nm and consecutive amplification by an EDFA. The pulse duration is 28 ns with a repetition rate of 1 kHz. Note that in some fibers, such pulses can excite acoustic waves through electrostriction, leading to erroneous n_2/A_{eff} values - a laser source with shorter pulses should be used to avoid this risk. For the couplers, a 50/50 ratio is used for the first one and a 90/10 for the second. Fig. 2.2 displays the interference signal as a function of the launch power P for a standard telecom fiber (SMF) with a length of 1100 m used as FUT. The experimentally obtained values (squares) are fitted using Eq. (2.4) (solid line). The data corresponds well with the model (statistical $\chi^2 = 3 \cdot 10^{-3}$). As can be seen, the signal slowly increases reaching a maximum value at 1.4 Watts. For higher powers the nonlinear phase shift becomes more important and the signal decreases reaching a null value at 3.4 Watts corresponding to a full $\pi/2$ phase shift. From the fit we obtain a value of (2.76 ± 0.04) 10^{-10} W^{-1} for the nonlinear coefficient n_2/A_{eff} . Having found with the refracted-near-field method [34] a value of (88 ± 3) μm^2 for A_{eff}, the nonlinear refractive index n_2 becomes (2.4 ± 0.1) 10^{-20} m^2/W.

2.1.5 Conclusion

In this section we have demonstrated a simple method for the measurement of the nonlinear coefficient n_2/A_{eff} based on an all fiber, self-aligned interferometer. The self-alignment characteristic not only allows for an easy and quick initial adjustment of the interferometer, but along with the use of a Faraday mirror also makes it robust against environmental perturbations. Moreover the double-pass configuration allows to characterize shorter span of FUT compared to single-pass implementation. This

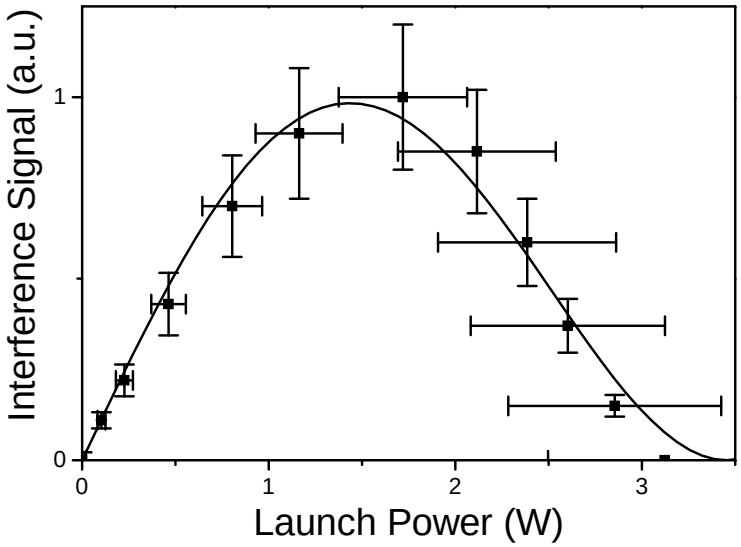

Figure 2.2: Detected interference signal power as a function of launch power. Measured data (squares), theoretical fit (solid line).

leads to a good accuracy for the measured n_2/A_{eff} values. The proposed method is well suited to routinely measure the nonlinear coefficient, as due to the FM the fiber under test can be easily exchanged without necessitating any further readjustments of the interferometer.

2.2 Measurements of n_2/A_{eff} in SMF, DSF, and DCF fibers

In this section we present measurements of the nonlinear coefficient n_2/A_{eff} for standard SMF, DSF, and DCF fibers, using a method based on the detection of the Kerr phase shift by a self-aligned interferometer (see previous section). The presence of a Faraday mirror in the interferometer makes the set-up very robust, and different test fibers can be measured without any further readjustments. Interlaboratory comparisons show that the values found with our method are in good agreement with the other ones. Moreover an analysis of a SMF fiber with large chromatic dispersion shows a good reproducibility of the n_2/A_{eff} measurements as a function of fiber length.

2.2.1 Introduction

As mentioned before in section 2.1.1 there are different methods to measure n_2/A_{eff}, based on SPM or XPM induced phase shift detection [2] using interferometric and non-interferometric schemes. The interferometric detection scheme [32] presents the advantage that it can be implemented more easily. But a disadvantage is its susceptibility to environmental perturbations that leads to a poor stability. In our setup we obtained a considerable improvement of this technique by using a self-aligned interferometer [35] with a Faraday mirror. This method has the advantage to be simple and all fiber implementable. The fluctuations due to the environmental perturbations are completely removed [23]. In this chapter we compare the values of n_2/A_{eff} obtained with our method, for Dispersion Shifted Fibers (DSF), Dispersion Compensating Fibers (DCF), and a standard Single Mode Fiber (SMF) with the ones obtained by other institutions on the same fibers. Our values are found to agree quite well with the results from the different measurement methods employed by the other institutions.

2.2.2 Principle of operation

The experimental setup and the principle of operation is described in Section 2.1.2. A sligthly modified version of the setup is shown in Fig. 2.3

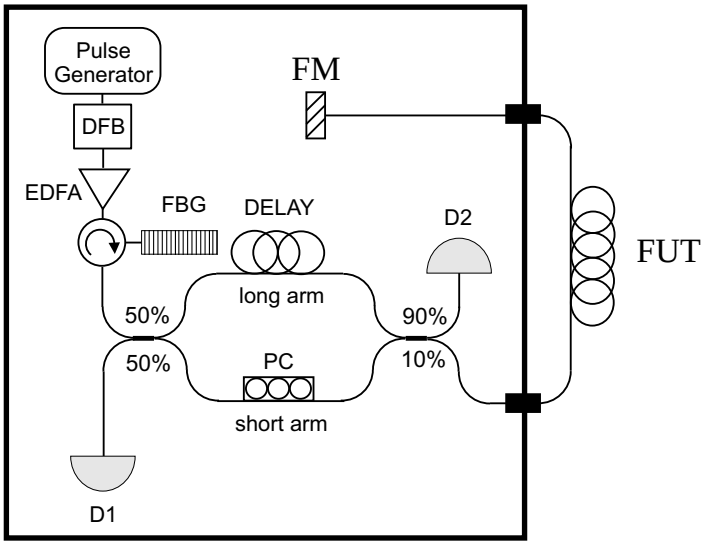

Figure 2.3: Experimental setup of the self-aligned interferometer. DFB distributed feedback laser, EDFA Erbium doped fiber amplifier, PC polarization controller, FUT fiber under test, FM Faraday mirror, D detector.).

2.2.3 Results

n_2/A_{eff} was measured for five different fibers comprising SMF, DSF, and DCF of different lengths. The fibers' parameters are listed in Tab. 2.1 and Tab. 2.2. Fibers DSF-1 and DSF-2 were also measured at NTT [36] utilizing the self-phase modulation based cw dual-frequency method [5, 4]. Fibers NIST-B and NIST-C were measured by six different institutions using the CWDF method and the pulsed method using different fiber lengths and laser wavelengths. Results regarding this North-American round robin were published in [37]. A typical result for a single measurement with our method is shown in Fig. 2.4. The FUT was Fiber G-1 with a fiber length of 2231 m. The interference signal power detected at the exit of the interferometer is plotted as a function of the launch input power P. The experimental values (open circles) are increasing almost linearly in the beginning, demonstrating that nonlinear effects are of little importance up to launched powers of about 0.5 Watt. Then they set in quite heavily, and the measured power eventually starts to decrease with increasing launch power. The maximum of the interference signal power is reached at a launch power of

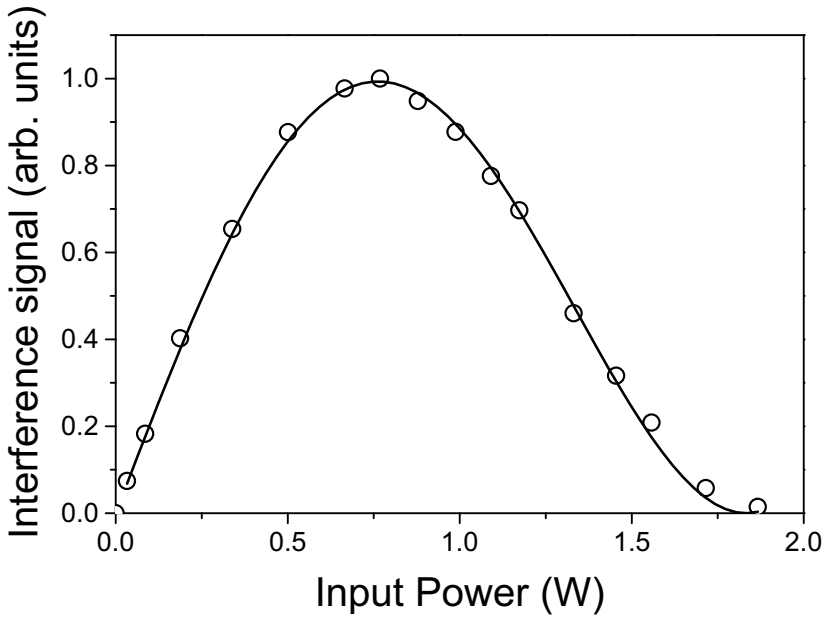

Figure 2.4: Detected interference signal power as a function of launch power: (open circles) measured data, (solid line) theoretical fit (Eq. (2.4)).

0.8 W, whereas a null value, corresponding to a full $\pi/2$ nonlinear phase shift, is obtained for 1.9 W. From this value, n_2/A_{eff} can be calculated using Eq. (2.5). However, we always fitted all the points as the precision is much better. For each fiber three to four different measurements were taken on different days in order to test the reproducibility of our method. The corresponding results are summarized in Table 2.1. Note that the maximum absolute deviation from the average (MD) is used to characterize the reproducibility. Generally the reproducibility is quite good (<10%) although it varies somewhat from fiber to fiber (see Table 2.1 and Table 2.2). Table 2.2 reports the values found by the other laboratories. For the NIST fibers [37], the standard deviation among the n_2/A_{eff} values of the six different round robin participants is given. As one can see the agreement with our values is quite good (with a deviation $< 15\%$ in the worst case). For the NTT fibers [36], the standard deviation of different measurements (using the same measurement method) is given. Once more the agreement with our values is good (<5%). For all measurements of both the NIST and NTT comparison, the deviation of our values are within the error bars. When looking at the maximum deviation of our measurements it is striking that for the NIST-C fiber the value is much larger. A reason for this might be that the GVD in this DCF fiber is much higher. In fact

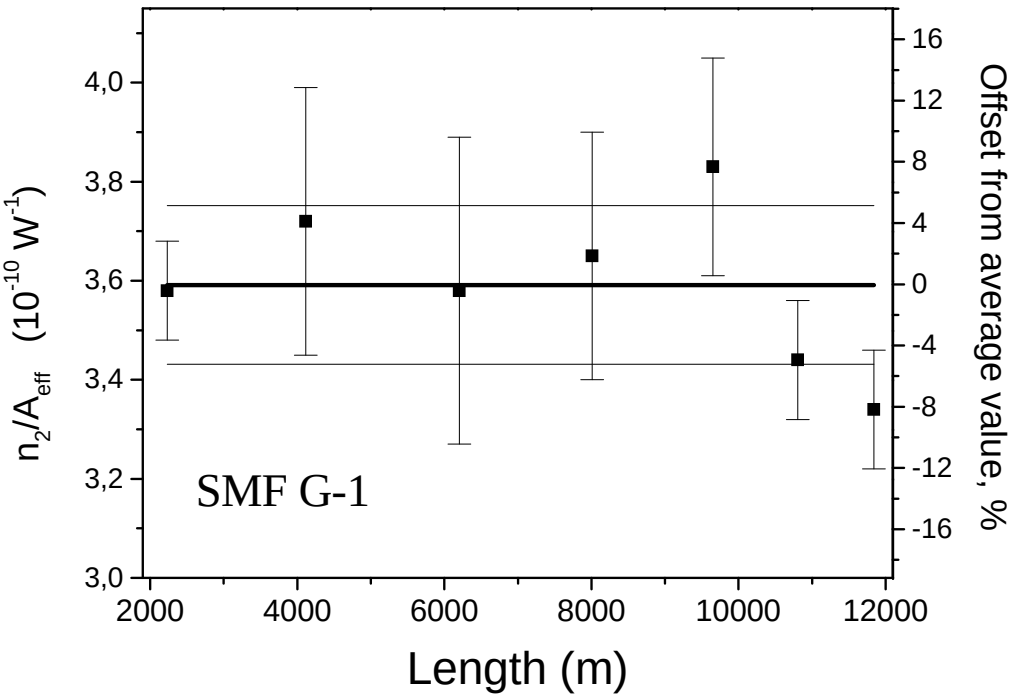

Figure 2.5: Nonlinear coefficient measured for different lengths of the same fiber (G-1).

some methods [5] were found to be very sensitive to the fiber's length for large values of the chromatic dispersion. Therefore, it is interesting to analyze the reproducibility of our method in a large GVD fiber as a function of the fiber length. Consequently we made cut-back measurements of n_2/A_{eff} for a SMF (G-1) changing the length from 12 km to 2 km. For each length at least 3 measurements were taken. The results are reported in Fig. 2.5. The overall standard deviation is only 6%, i.e. a similar amount as the maximum fluctuations for a fixed length (see Table 2.1). Also, no trend of the n_2/A_{eff} values as a function of fiber length can be found, demonstrating that our method is insensitive to the fiber length (in a range of around 10 km) even for large values of chromatic dispersion.

Fiber	Length (m)	λ_0 (nm)	A_{eff} (μm^2	n_2/A_{eff} (VALUE) $10^{-10}W^{-1}$	n_2/A_{eff} (MD) $10^{-10}W^{-1}$
G-1 (SMF)	11840	1302	-	3.6	5%
DSF-1 (DSF)	1990	1556.4	44.5	6.4	2%
DSF-2 (DSF)	1990	1548.6	41.1	6.3	5%
NIST-B (DSF)	1563	-	52.2	4.3	2%
NIST-C (DCF)	1010	-	20.2	15.6	11%

Table 2.1: Values of n_2/A_{eff} for different fibers as measured with the selfaligned interferometric method.

Fiber	Length (m)	λ_0 (nm)	A_{eff} (μm^2	n_2/A_{eff} (VALUE) $10^{-10}W^{-1}$	n_2/A_{eff} (MD) $10^{-10}W^{-1}$
DSF-1 (DSF)	1990	1556.4	44.5	6.3	5%
DSF-2 (DSF)	1990	1548.6	41.1	6.6	5%
NIST-B (DSF)	1563	-	52.2	4.3	14%
NIST-C (DCF)	1010	-	20.2	13.4	15%

Table 2.2: Values of n_2/A_{eff} for different fibers as measured by other institutions.

2.2.4 Conclusion

In this section we have presented a simple and stable method for the measurement of the nonlinear coefficient n_2/A_{eff} based on an all fiber, self-aligned interferometer. Due to its robustness against environmental perturbations, and its ease of adjustment, the proposed method is well suited to routinely measure the nonlinear coefficient. The presence of the FM allows to easily exchange the FUT without necessitating any further readjustments of the interferometer. An inter-laboratory comparison of the n_2/A_{eff} measurements on the same test fibers showed good agreement of our results with the others. Moreover, our method seems to be independent of the fiber's length on a range of 10 km even in the presence of large GVD, known to cause problems with some of the other measurement methods.

2.3 Interlaboratory measurements of n_2/A_{eff} of standard SMF and DSF fibers

In this section we present interlaboratory measurements of the nonlinear coefficient n_2/A_{eff} for standard SMF and DSF fibers. Two different measurement methods were used by two different groups. One of the method is based on the detection of the Kerr phase shift by a self-aligned interferometer (see previous sections). The other method is an SPM based cw dual-frequency method. Interlaboratory comparison shows that the values found with the two methods are in good agreement.

2.3.1 Introduction

There are different methods to measure n_2/A_{eff}, based on SPM or XPM induced phase shift detection using interferometric and non-interferometric schemes [2]. The interferometric detection scheme [32] presents the advantage that it can be implemented more easily. But a disadvantage is constituted by its susceptibility to the environmental perturbations that leads to a poor stability. With one of the setups presented here we reached a considerable improvement of this technique by using a self-aligned interferometer [35] with a Faraday mirror. This method [23] has the advantage to be simple and all fiber implementable and the fluctuations due to the environmental perturbations are completely removed. On the other hand, non-interferometric schemes have the disadvantage that their measurement accuracy strongly depends on the measurement conditions. However, the SPM based cw dual-frequency method [4, 5], with its simple measurement setup, gives accurate value of n_2/A_{eff} according to the measurement conditions given in Refs. [4] and [6]. A description of the interferometric method (method A) is given in the preceding sections. A brief description of the CW dual method (method B) is given in the next section and we present an interlaboratory fiber nonlinear coefficient measurements for Dispersion Shifted Fibers (DSF).

2.3.2 Self aligned interferometer method

The experimental setup and the principle of working is illustrated in Section 2.1.2. This method is hereafter referred to as method A.

2.3.3 SPM based CW dual–frequency method

When two intense signals with wavelength separation of $\Delta\lambda$ are launched into a fiber, SPM acts on the beat envelope to create sidebands in the frequency domain. Then, the optical power ratio of the input signals (I_0) to the first sideband (I_1) is related to the nonlinear phase shift ϕ_{SPM}. When the chromatic dispersion is negligible, this relationship can be expressed as (4) using n-th order Bessel function J_n.

$$\frac{I_0}{I_1} = \frac{J_0^2(\phi_{SPM}/2) + J_1^2(\phi_{SPM}/2)}{J_1^2(\phi_{SPM}/2) + J_2^2(\phi_{SPM}/2)} \tag{2.6}$$

Moreover, the relationship between ϕ_{SPM} and nonlinear coefficient can be expressed as

$$\phi_{SPM} = \frac{4\pi}{\lambda} L_{eff} P \frac{n_2}{A_{eff}} \tag{2.7}$$

where P shows the average launched power. Thus, the nonlinear coefficient can be obtained by measuring the optical power ratio I_0/I_1 with various launched power according to the measurement conditions given in Refs. [4] and [5]. The setup of the SPM based cw dual-frequency method is shown in Fig. 2.6. This method is hereafter referred to as method B.

2.3.4 Experimental results

The measurements were done on three different fibers. A DSF fiber with λ_0 = 1556.4 nm, S=0.067 ps/nm^2/km (DSF-1), a DSF fiber with λ_0 = 1548.6 nm, S=0.060 ps/nm^2/km (DSF-2), and a standard single mode fiber with λ_0 = 1300 nm (G-1). Fibers DSF-1 and DSF-2 were also measured at NTT utilizing the self-phase modulation based cw dual-frequency method. For each fiber different measurements were taken on different days in order to test the reproducibility of our measurements. The corresponding results are summarized in Tab. 2.3 for method A. Note that the maximum absolute deviation from the average (MD) is used to characterize the reproducibility. Generally the reproducibility is quite good (¡5%) although it varies somewhat from fiber to fiber (see Tab. 2.3). Tab. 2.4 reports the values found with method B. Here instead of the MD, the standard deviation (SD) of different measurements is given. As one can see, the values are in good agreement with differences within the experimental errors. Using method A measurements were then performed as a function of the fiber length.

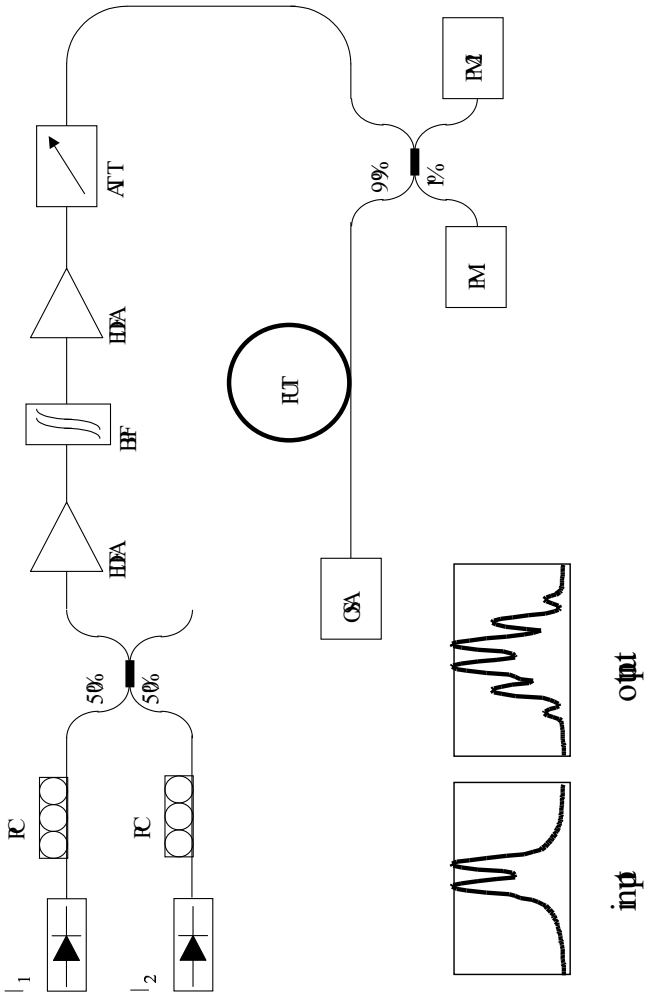

Figure 2.6: Experimental setup of the SPM based cw dual-frequency method. PC polarization controller, EDFA Erbium doped fiber amplifier, BPF Band pass filter, ATT Variable attenuator, PM Power meter, OSA Optical spectrum analyzer, FUT fiber under test. PM1 is used to monitor the power at the entry of the FUT and PM2 to monitor the back-reflected power along the FUT due to Brillouin scattering.

Fiber	Length (m)	λ_0 (nm)	A_{eff} (μm^2)	n_2/A_{eff} (VALUE) $10^{-10}W^{-1}$	n_2/A_{eff} (MD) $10^{-10}W^{-1}$
DSF-1 (DSF)	1990	1556.4	44.5	6.4	2%
DSF-2 (DSF)	1990	1548.6	41.1	6.3	5%

Table 2.3: Values of n_2/A_{eff} for different fibers as measured with the selfaligned interferometric method. For the values measured with method A, the maximum absolute deviation from the average (MD) is used to characterize the reproducibility. For method B the standard deviation is shown.

Fiber	Length (m)	λ_0 (nm)	A_{eff} (μm^2)	n_2/A_{eff} (VALUE) $10^{-10}W^{-1}$	n_2/A_{eff} (MD) $10^{-10}W^{-1}$
DSF-1 (DSF)	1990	1556.4	44.5	6.3	5%
DSF-2 (DSF)	1990	1548.6	41.1	6.6	5%

Table 2.4: Values of n_2/A_{eff} for different fibers as measured by NTT. For the values measured with method A, the maximum absolute deviation from the average (MD) is used to characterize the reproducibility. For method B the standard deviation is shown.

We made a fiber cut-back procedure and for each fiber length we measured the nonlinear coefficient on a standard telecom fiber (G-1) with lengths ranging from 12 km to 2 km. For each length at least 3 measurements were taken in order to acquire some statistics and to find the error bars. All values are within a standard deviation of 6% demonstrating that method A is insensitive to the fiber lengths even for large values of chromatic dispersion.

2.3.5 Conclusion

In this section we have presented an interlaboratory comparison of n_2/A_{eff} measurements on the same test fibers as measured by two different institutions using different methods, an interferometric method and a cw dual-frequency method. Good agreement between the measured values was found.

Chapter 3

Nonlinear Polarization Rotation and Optical Switching in Optical Fibers.

3.1 Nonlinear Polarization Rotation in Optical Fibers

In this section we present both a theoretical and experimental analysis of the non-linear polarization rotation in an optical fiber. Starting from the coupled non-linear Schrödinger equations an analytical solution for the evolution of the state of polarization, valid for fibers with large linear birefringence and quasi cw input light with arbitrary polarization, is given. It allows to model straightforwardly go-and-return paths as in interferometers with standard or Faraday mirrors. In the experiment all the fluctuations in the linear birefringence, including temperature and pressure induced ones, are successfully removed in a passive way by using a double pass of the fiber under test with a Faraday mirror at the end of the fiber. This allows us to use long fibers and relatively low input powers. The match between the experimental data and our model is excellent, except at higher intensities where deviations due to modulation instability start to appear.

3.1.1 Introduction

The potential of nonlinear polarization rotation (NPR) to build ultrafast devices has been recognized a long time ago and received considerable attention since then. It has been proposed to exploit it for optical switches [6], logic gates [7], multiplexers [8], intensity discriminators [9], nonlinear filters [10], or pulse shapers [11]. However, an

inherent problem to all these applications is the stability of the output state of polarization, generally subjected to fluctuations of the linear birefringence caused by temperature changes and perturbations in the fiber environment. Of course, the same problem was also encountered in the few experiments dealing with the characterization and measurement of the NPR itself. In Ref. [12], the fluctuations of the output polarization were too strong to allow a meaningful measurement of NPR in a polarization maintaining fiber at 1064 nm, and in Ref. [13] , where 514 nm light was injected into a 60 m long fiber with a beatlength of 1.6 cm, a complicated arrangement had to be employed for the extraction of the changes caused by temperature drifts.

As the fluctuations become worse for fibers with a large birefringence, and as the effect of NPR is proportional to the inverse of the wavelength, it is hard to measure NPR directly in a polarization maintaining (PM) fiber at the telecom wavelength of 1.55 μm. In this work we propose a method for removing the overall linear birefringence, and therefore also its fluctuations, in a passive way by employing a Faraday mirror [14] (FM) and a double pass of the fiber under test. To check how this -nowadays standard- method [15, 16, 17, 18] of removing linear birefringence acts on the NPR, we develop in Subsection 3.1.2 of this section a simple model to calculate the action of linear and nonlinear birefringence. Using this model, it is then easy to show that the proposed method removes the overall linear birefringence only, whereas the nonlinear one, leading to NPR, remains unchanged. After describing the experimental set-up, the results of our NPR measurements using a FM are presented in Subsection 3.1.3, along with the predictions from our analytical model. The excellent agreement between the two demonstrates that using the FM, the overall linear birefringence is indeed removed completely, allowing to observe the NPR otherwise hidden within the noisy background of polarization changes due to environmental perturbations. This result also validates our method for possible implementation with a variety of other applications like the ones mentioned at the beginning of this subsection, with the prospect of drastically increasing their polarization stability.

3.1.2 Theoretical background

In a dielectric medium, an intense elliptical input pulse induces birefringence - via the optical Kerr effect - due to the different amounts of intensity along the major and minor axis of the polarization ellipse. It is well known that in isotropic media, this self-induced birefringence leads to a rotation of the polarization ellipse while propagating

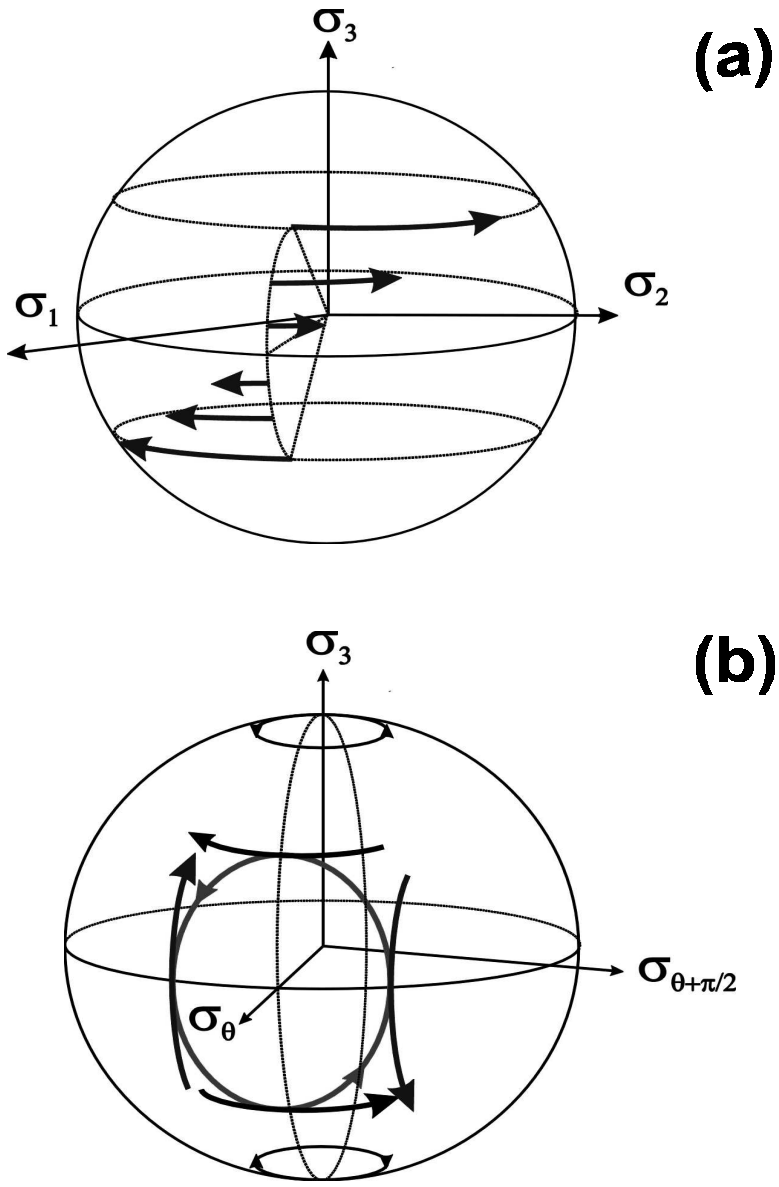

Figure 3.1: Evolution of the state of polarization as represented on the Poincare sphere. (a) Polarization ellipse self rotation in an isotropic medium. The Stokes vector is rotating around the σ_3 axis with an angle proportional to the length of the medium, the input intensity, and the sin of the input ellipticity. (b) High birefringence fiber. The rotation of the Stokes vector mainly consists of a fast rotation around the axis of linear birefringence σ_θ, whereas the slow rotations due to the nonlinear birefringence can be considered as small perturbations.

in the medium [38, 39] (the effect is consequently often called polarization ellipse self-rotation and its representation on the Poincare sphere is shown in Fig. 3.1(a). In fact, measuring this ellipse rotation is one of the standard ways to evaluate the cubic optic nonlinearity of the medium [24]. In an optical fiber however, the situation becomes more complicated as there is also the local intrinsic birefringence to be considered. Generally, the polarization ellipse changes are hard to predict in that case as the linear and nonlinear birefringence interact in a complicated manner.

To formulate this more precisely, we start with the coupled non-linear Schrödinger equations describing the propagation of light in an optical fiber. For cw input light, time derivatives drop out, and we can write the equation in a form similar to that of Menyuk [40] when assuming a lossless, linearly birefringent fiber and by neglecting polarization mode coupling:

$$\partial_z \psi = -i\,(\omega B \sigma_\theta + \omega \alpha < \sigma_3 >_\psi \sigma_3)\,\psi; \qquad B >> \alpha \tag{3.1}$$

$\psi = (E_1, E_2)^t$ is the Jones column vector representing the two components of the complex transverse electric fields $E_1(z)$ and $E_2(z)$ at the position z along the fiber. The first term on the right hand side describes the linear birefringence, where ω is the optical frequency and B the birefringence (in s/m). Note that B is assumed to be independent of ω, an excellent approximation for standard fibers. The phase birefringence ωB is multiplied by $\sigma_\theta = \sigma_1 cos(\theta) + \sigma_2 sin(\theta)$, corresponding to linear birefringence in the θ direction, with $\sigma_{1,2,3}$ being the 2x2 Pauli matrices. The second term on the right hand side of Eq. (3.1) accounts for the nonlinear birefringence, with $\alpha = \frac{n_2 P}{3cA_{eff}}$, and $< \sigma_3 >_{\psi_z} = \frac{|E_1|^2 - |E_2|^2}{|E_1|^2 + |E_2|^2}$. P is the total light power, n_2 the nonlinear refractive index, A_{eff} the effective mode area, and c the speed of light.

For an intuitive understanding of the action of the two terms on the right hand side of Eq. (3.1), it is better to revert to the Stokes formalism. On the Poincare Sphere, the first term describes a rotation of the polarization vector (Stokes vector) around axis σ_θ, lying on the equator and corresponding to linear birefringence. Similarly, the second term is a rotation around the vertical axis corresponding to nonlinear birefringence. However, Eq. (3.1) shows that the speed and the rotation direction in this case depends on the polarization state through $< \sigma_3 >_\psi$, as is illustrated in Fig. 3.1(b). Consequently, the two rotations are linked in a complicated manner, and the resulting evolution of the polarization vector is not obvious.

Fortunately, in standard telecom fibers, the speed of rotation around the vertical

axis is much smaller than the one around the birefringent axis σ_θ even at considerable power levels. This is because in such fibers $B >> \alpha$ (see Eq. (3.1)). For example, a fiber with a beat length of 10 m has B$\approx$ 0.5 ps/km while $\alpha \approx 0.006$ ps/km for a power of 10 Watts (λ=1550 nm, n_2=3.2$\cdot 10^{-20}$, A_{eff}=60 μm^2) (note that in this work, a PM fiber will be used with a beat length in the mm range, making the ratio $\frac{B}{\alpha}$ as large as 10^7). The slow rotation due to the nonlinear birefringence can therefore be treated as a perturbation that merely changes the angular frequency of the fast rotation caused by the linear birefringence. This becomes more obvious by rewriting Eq. (3.1) as

$$\partial_z \psi = -i\omega B \sigma_\theta \psi - i\omega\alpha \frac{1}{2}(< \sigma_3 >_\psi \sigma_3 + (1 - < \sigma_{\theta+\frac{\pi}{2}} >_\psi \sigma_{\theta+\frac{\pi}{2}} - < \sigma_\theta >_\psi \sigma_\theta))\psi \qquad (3.2)$$

where the identity $\psi = < \sigma >_\psi \sigma\psi$, valid for all ψ, has been used. The term proportional to ψ affects only the global phase and can be neglected. Further, the two terms $< \sigma_3 >_\psi \sigma_3$ and $< \sigma_{\theta+\frac{\pi}{2}} >_\psi \sigma_{\theta+\frac{\pi}{2}}$ cancel each other to first order - this can be intuitively understood from Fig. 3.1(b) and was confirmed by numerical simulations - producing only a small (second order) precession of the instantaneous rotation axis. Hence we obtain the following approximation for the evolution of the polarization vector:

$$\partial_z \psi \approx -i\omega B_{eff} \sigma_\theta \psi \qquad (3.3)$$

with the effective birefringence

$$B_{eff} = B - \frac{\alpha}{2} < \sigma_\theta >_\psi \qquad (3.4)$$

depending on the intensity and the polarization state of the input light signal. Note that Eq. (3.3) preserves the square norm $|\psi|^2$ reflecting that we did not take into account losses. Note further that when applying Eq. (3.3) for linearly polarized input light we obtain the same formula as in Ref. [9].

The solution of Eq. (3.3) is straightforward, $\psi_z = exp(-i\omega B_{eff}\sigma_\theta z)\psi_0$, and corresponds to a rotation of the input polarization vector around the linear birefringence axis σ_θ, with a rotation angle β given by

$$\beta = \omega(B - \frac{\alpha}{2} m_\theta(0))z. \qquad (3.5)$$

$m_\theta(0)$ is the projection of the input polarization vector on the birefringence axis σ_θ, and z the distance from the input end.

In principle, the NPR, caused by the nonlinear response of the single mode fiber to the input state, could now be measured by varying the input power and observing the corresponding change in the output polarization vector. However, from a practical standpoint, this will be hardly possible as Eq. (3.5) shows that slightest changes in the linear birefringence B will completely cover the nonlinear, intensity dependent ones (remember that B$>>\alpha$ for reasonable input power levels). Indeed, earlier work [13, 25] greatly suffered from temperature and pressure induced changes of B always present in a lab environment, even though they were using short fibers.

Nowadays, a simple and efficient way to get rid of any kind of fluctuations in the intrinsic birefringence is to make a double pass of the fiber under test by means of a Faraday mirror [14, 15] (FM). The linear birefringence accumulated during the forward path is then automatically compensated on the return path. However, it is not a priori clear what will happen to the nonlinear birefringence.

To investigate this point, we rewrite the solution of Eq. (3.3) in the Stokes formalism,

$$\mathbf{m}(L) = \hat{\mathbf{R}}_\theta(\beta(L))\mathbf{m}(0) \tag{3.6}$$

where $\mathbf{m}(0)$ is the input Stokes vector, $\hat{\mathbf{R}}_\theta$ is a rotation operator around the axis σ_θ, and β is as given by Eq. (3.5). Applying the action of the FM, $\mathbf{m}^F(L) = -\mathbf{m}(L)$ (the suffix F indicates the state of polarization after reflection from the FM), and of the return path, $\hat{R}_\theta^{-1}$, we get

$$\begin{aligned} \mathbf{m}^F(2L) &= \hat{\mathbf{R}}_\theta^{-1}[\omega L(B - \tfrac{\alpha}{2} m_\theta^F(L))]\hat{\mathbf{R}}_\theta[\omega L(B - \tfrac{\alpha}{2} m_\theta(0))]\mathbf{m}(0) = \\ &= -\hat{\mathbf{R}}_\theta[\omega\alpha L m_\theta(0)]\mathbf{m}(0). \end{aligned} \tag{3.7}$$

The result shows that the rotation due to the nonlinear birefringence of the forward and return path do not cancel out but add, giving twice the angle compared to a single (forward) trip through the fiber (Eq. (3.5)). This is because the rotation direction of the nonlinear birefringence is different for the upper and lower hemisphere of the Poincare sphere (see Fig. 3.1(b)) contrary to birefringence in linear optics. Therefore, after reflection at the FM, which transforms the polarization state to its orthogonal counterpart (i.e. flipping it to the other hemisphere), the sense of rotation of the NPR during the return path will be the same as the forward path and the effects add up.

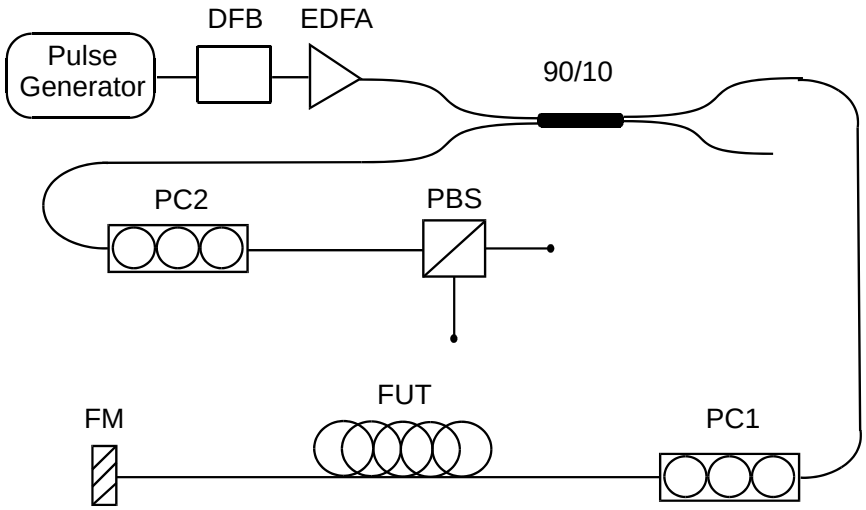

Figure 3.2: Experimental setup of the NPR measurement. DFB distributed feedback laser, EDFA Erbium doped fiber amplifier, PC polarization controller, FUT fiber under test, FM Faraday mirror, PBS polarizing beam splitter

3.1.3 Experimental

Set-up

The experimental setup used to measure the NPR is shown in Fig. 3.2. The light source is a distributed feedback laser diode (DFB) operated in pulsed mode at a wavelength of 1559 nm, consecutively amplified by an EDFA (small signal gain 40dB, saturated output power 23dBm). Typically, pulses with a duration of 30 ns, a repetition rate of 1 kHz, and a peak power of up to 6 W were used. The light is then launched into the test fiber via a 90/10 coupler and a polarization controller. The coupler was inserted for the detection of the backward traveling light after the double pass of the test fiber, with its 90 output port connected to the source in order to maintain the high launch powers into the test fiber. The polarization controller, PC1, allowed to adjust the polarization of the light launched into the test fiber, which is important for the strength of the NPR as demonstrated by Eq. (3.5). In order to satisfy the assumption of neglectable polarization mode coupling used in the previous section, a highly birefringent, polarization maintaining (PM) fiber was used as the test fiber. Its linear birefringence B is of the

order of 5 ps/m, corresponding to a beat length in the mm range. The fiber length was 200 m, giving a total of 400 m round-trip length of the light reflected by the FM.

The polarization state of the light after the double pass of the test fiber was examined by an analyzer consisting of a polarization controller PC2 and a polarizing beam splitter (PBS). To achieve a good sensitivity of the analyzer, it was calibrated to give a 50/50 output of the PBS for low power signals where no nonlinear polarization rotation occurs. Finally, the two PBS output channels were monitored by a fast photodiode (200 ps response time) and a sampling scope.

The measurements were then performed in the following way: for a given launch power, the polarization controller PC1 was adjusted to give the smallest possible output power at the monitored PBS channel. Consequently, the difference between the two PBS output channels is maximized, corresponding to a maximum value of the NPR.

Results

The experimental results are shown in figures 3.3 and 3.4.

In Fig. 3.3, the minimum output power (squares) of the monitored PBS channel is given as a function of the peak power in the test fiber. Note that the reported output power was normalized to account for the analyzer losses and corrected for the PBS extinction ratio. Consequently, without any NPR, the reported output power would equal half of the power in the test fiber (solid line). As can be seen in Fig. 3.3, the effect of NPR is negligibly small up to about 0.5 W. For higher launch powers, NPR manifests itself by a reduction of the power in the monitored PBS channel. In fact, its action becomes so strong that for launch powers above about 2.5 W, the output power starts actually to decrease in spite of the linear increase that would be experienced in the absence of NPR. In principle, this power drop should continue until the nonlinear rotation of the input polarization is such that all the power is in the other PBS channel. However, as Fig. 3.3 shows, this is not happening. The observed increase in the minimum output power could be related to modulation instability a phenomenon in which a CW signal becomes amplitude and phase modulated as a result of the interplay between the nonlinearity and the dispersion of the medium (this effect manifest itself with the appearance of two sidebands one shifted up in frequency and the other

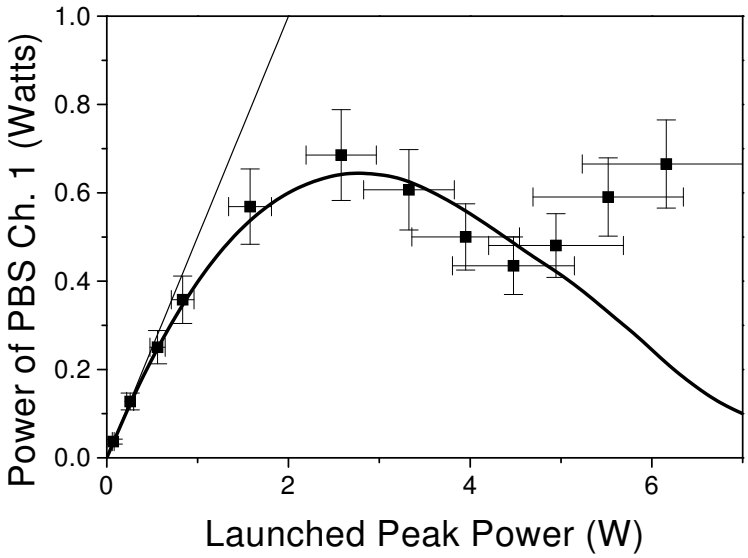

Figure 3.3: Minimum output power of PBS channel 1 as a function of the launched power for a 200 m long PM fiber. Squares: measured data, solid curve: prediction from our model, straight line: prediction in the absence of NPR. The deviations of the experimental data from the predicted values at high powers are due to modulation instability not included in the model.

shifted down by the same amount): above 4.5 W launch power, a Stokes and Anti-Stokes sideband shifted by 2 nm with respect to the laser peak appeared. These sidebands are generated in a distributed fashion along the test fiber, which means that the compensation of the linear fiber birefringence is failing. Therefore, and due to the large birefringence B of the PM fiber used, the sidebands will be almost randomly polarized at the output. As a consequence, about half of the power transferred to the sidebands will appear in the monitored PBS output channel leading to the observed increase in power.

Further, the measured results were compared to the ones predicted by Eq. (3.7) taking into account the analyzer calibration and the adjustment of PC1 as used in the experiment. The parameters used in the computation were the ones from the experiment, i.e. a fiber length of L=200 m, and a nonlinear coefficient of n_2 =3.4·10^{-20} m^2/W. The effective core area of A_{eff} = 41 μm^2 was chosen to give a good match with the experimental results as we had no exact value from the manufacturer. $m_\theta(0)$, the projection of the input state of polarization on the birefringent axis, was varied in order to give a minimum output power from the PBS channel, exactly like in the experiment.

The solid line in Fig. 3.3 shows these computed results. The figure clearly illustrates

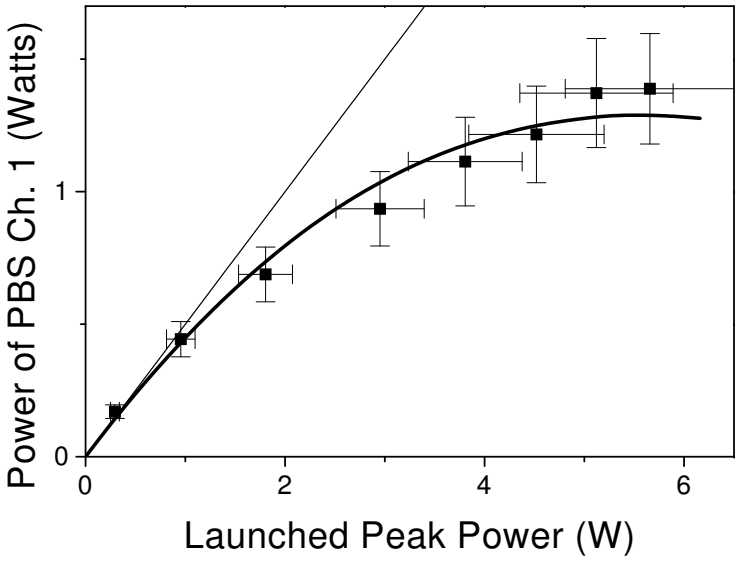

Figure 3.4: Minimum output power of PBS channel 1 as a function of the launched power for a 100 m long PM fiber. Squares: measured data, solid curve: prediction from our model, straight line: prediction in the absence of NPR.

that the measured data corresponds very well to the computed one. This validates our measurement method of NPR in optical fibers and demonstrates that the linear birefringence and its detrimental fluctuations are successfully removed by the FM. Above an input power of 4.5 W, the curves deviate as expected from the onset of MI that was not included in the analytical model.

Fig. 3.4 shows experimental and computed results for a fiber length of 100 m. Note that to avoid cutting our 200 m piece, we emulated the 100 m fiber length by introducing a 20dB attenuation for the reflected light. Consequently, the light power on the return trip is too low to induce NPR, and serves only to compensate for the linear birefringence of the forward trip. As the figure demonstrates, NPR is indeed reduced by a factor of 2 compared to the measurements without attenuator, as expected from Eq. (3.7). Twice the launch power is required to compensate for the shortened length to get the same amount of NPR. Again, experimental and computed data are in excellent agreement.

The experimental results of this section clearly demonstrate that one can indeed use a FM to remove the overall linear birefringence, which allows to observe smallest nonlinear effects otherwise hidden within the noisy linear birefringence. Note that

the change in the output polarization due to environmental perturbations is especially pronounced in PM fibers (when the input is not aligned with one of the two fiber axes) due to its short beat length in the mm range. For example when not using a FM, the output polarization changed drastically from just the body heat when approaching the PM fiber spool, inhibiting any meaningful measurement.

3.1.4 Conclusion

Starting from the non-linear Schrödinger equations, an analytical solution for the evolution of the state of polarization in a high birefringence optical fiber has been developed. It allows for a simple and straightforward modeling of go and return paths as e.g. in interferometers with standard or Faraday mirrors. Using this model, we showed that it is possible to remove the overall linear birefringence in a double-pass arrangement with a FM while leaving at the same time the nonlinear birefringence, resulting in NPR, unchanged. Only this allowed to measure the NPR in a long PM fiber at telecom wavelength in a lab environment where it is otherwise hidden by the changes in the output polarization caused by temperature and pressure fluctuations.

The experimental results for the NPR obtained with a 200 m long PM fiber at a wavelength of 1.55 μm were in excellent agreement with the theoretical predictions from our model for launch power up to 4.5 W. Above that value deviations due to modulation instability, not included in our model, were present.

Due to its generality, the presented method of removing the linear birefringence while leaving the nonlinear one unchanged might prove to be a very valuable tool in numerous other applications as well, like e.g. optical multi-/demultiplexers.

Note that in the case of non-PM fibers, where the coupling between the polarization modes is not negligible, NPR is reduced due to a scrambling related to the ratio between the coupling length and the fiber length. In fact, this effect can be exploited to get information about the important coupling length parameter in standard fibers, as will be shown in Section 3.3.

3.2 All Optical Switching in a PM Fiber and SMF Fiber

In this section we demonstrate all-optical switching at 1.5 μm based on induced nonlinear polarization rotation, in both a polarization maintaining and a standard telecom fiber. We have obtained an excellent switching stability in both cases by removing any detrimental temperature or pressure induced changes of the output polarization state with a Faraday mirror stabilization scheme.

3.2.1 Introduction

Considering the high bit rates of future optical fiber communication systems, optical signal processing could soon become a necessity. In order to demux a single channel from a 100 Gb/s time division multiplexed (TDM) signal e.g., a switching time of less then 5 ps will be required. All-optical switching techniques based on the optical Kerr effect [8, 19, 20, 21, 22, 23] are very attractive in that respect due to the ultrafast Kerr response [24, 25, 26] of less than a few fs. Indeed, an all optical Kerr switch was demonstrated recently that read out a 10 Gb/s channel from a 40 Gb/s TDM signal [6]. Besides the standard switch parameters like switching ratio, insertion loss or switching time, the stability of the switch is an important issue. Variations in the input control or signal polarizations as well as changes of the intrinsic birefringence of the Kerr medium will affect the switch. Variations of the input signal polarization can be dealt with by adopting a polarization diversity scheme, like e.g. in Ref. [6]. In order to keep the switch stable internally, the control pulse polarization should be kept as stable as possible by using a proper set-up. Moreover, changes in the signal polarization in the Kerr medium (typically a polarization maintaining PM fiber) due to changes in the intrinsic fiber birefringence have to be avoided since they can greatly reduce the extinction ratio of the switch. An active correction scheme (e.g. a polarization controller [12] with a feedback loop) is typically not rapid enough to correct the fast, acoustical perturbations, and may not work at all for large changes due to its limited range of operation.

To avoid these problems, we use on one hand a non-interferometric switch[1], and on the other hand a passive stabilization scheme. In interferometric switches like Sagnac loops or Mach-Zehnder interferometers (IF), the switching is based on a phase-shift

[1] "Non-interferometric" in the sense that the signals being interfered are not from two physically separate arms. Of course linear optics is always interferometric in a strict sense of the word (superposition principle).

induced between the two different propagation directions or arms, respectively. If the signal is not carefully launched into an axis of a PM fiber, it will split into 4 different polarization modes, two in each propagation direction or interferometer arm, respectively. In addition to the phase-shift between the two different propagation directions or interferometer arms, additional 'local' phase-shifts between the polarization modes with the same propagation direction (or within the same IF arm) will degrade the switch quality. In the switch presented here, this problem is avoided by uniquely using this 'local' phase-shift between the two signal polarization modes in a single fiber, thereby reducing the relevant mode number to two. Having two modes only, we can then use a passive stabilization scheme that works both for fast and slow, arbitrarily large changes in the fiber birefringence. Although in this work an optical fiber is used to induce a nonlinear phase-shift, it should be noted that the stabilization scheme holds as well for any other Kerr elements (e.g. semiconductor saturable absorbers SOA).

3.2.2 Principle of operation

As mentioned above, the principle of the optical Kerr switch presented here is based on an induced phase-shift between the two signal polarization modes in a single fiber. It is induced by powerful control signal pulses that lead to a different phase-shift (via the optical Kerr effect) for signal components with the same and orthogonal polarization, respectively. The corresponding change in the output signal polarization is maximized if the control signal polarization matches the polarization of one of the two signal polarization modes during the entire propagation in the Kerr fiber. By inserting a polarizing beam splitter (PBS), the signal is switched between the two PBS output ports depending on the amount of the induced phase-shift.

For a control pulse linearly polarized along one of the birefringent axis of a PM fiber, it is easy to show that the phase shift $\Delta\phi$ acquired by a signal linearly polarized at 45 degree is [2]

$$\Delta\phi = \frac{8}{3}\pi(\frac{L_{eff}}{\lambda})n_2\frac{P}{A_{eff}} \tag{3.8}$$

where n_2 is the nonlinear refractive index of the fiber, λ is the signal wavelength, A_{eff} is the effective area of the fiber and P is the peak pump power. Fiber losses are included in the effective length L_{eff}= $1/\alpha$[1-exp(-α L)] where L is the length and α the fiber loss coefficient. For a PBS adjusted so that all the signal is at output port 2 when the control

pulse is absent, the signal at output port 1 becomes

$$T = sin^2 \frac{\Delta\phi}{2}. \tag{3.9}$$

where the induced phase shift $\Delta\phi$ is given by Eq. (3.8). A different wavelength is conveniently used for the control pulses so that they can be combined with the signal using a wavelength division multiplexer (WDM). As a consequence, a walk-off between the control pulses and the signal is introduced, ultimately limiting the switching time. A large walk-off also enlarges the required control peak power because of a reduced interaction length (i.e. smaller L_{eff} in Eq. (3.8)). To keep the switch fast and efficient, either a fiber with low group dispersion has to be used, or the wavelength separation should be kept as small as possible. The latter leads to a trade-off between the switching time (determined by the walk-off) and the extinction ratio (determined by the WDM filtering). For a detailed analysis, the reader is referred to Ref. [20].

It is very important to notice that the transmission given in Eq. (3.9) holds only for a fixed intrinsic birefringence of the fiber. Any fluctuation of this birefringence, caused e.g. by temperature drifts or pressure changes, leads to an additional phase-shift randomly changing the bias of the switch. In order to reduce this effect detrimental for the switch stability, different methods have been proposed [12, 20]. A very promising solution is to make a double pass of the fiber by means of a Faraday mirror (FM) [14, 15, 16, 18]. The FM transforms any input polarization state to the orthogonal one upon reflection. Consequently, the signal components that were polarized parallel to the fast axis during the forward propagation will be polarized parallel to the slow axis during the return path and vice versa. The overall acquired phase is therefore the same for any input polarization, and the intrinsic birefringence is automatically removed as long as it is stable during a single round-trip path. In this way, fluctuations with frequencies up to about 0.5 MHz (200 m long fiber) can be removed.

Although the application of a FM is widely spread in linear optics, we believe to be the first ones having demonstrated its usefulness for nonlinear optics as well. Especially, we showed in Ref. [23] both theoretically and experimentally that only the linear phase fluctuations are removed, whereas the purposefully induced nonlinear effects of the go and return-path add up. This allowed to measure the nonlinear polarization rotation in an optical fiber.

3.2.3 Set-up

The setup of the Kerr switch using the described stabilization scheme is shown in Fig. 3.5. The control signal was generated by a directly modulated DFB laser diode with a wavelength of 1559 nm, amplified by an EDFA with a small signal gain of 40 dB and a saturated output power of 23 dBm. The pulses from the DFB laser had a duration of 28 ns with a repetition rate of 1 kHz. This is good enough to demonstrate the usefulness of the stabilization scheme and the basic functioning of the switch - in an application, shorter control pulses at a higher repetition rate could be used. In order to have a larger side-mode suppression of the DFB output at the signal wavelength, an external small band pass filter ("notch" filter) was inserted after the EDFA. Using a WDM, the control pulses were then coupled into the Kerr fiber along with the signal consisting of cw light generated by a second DFB at 1556 nm. The signal power in the Kerr fiber was -1.8 dBm, whereas several Watts of control pulse peak power were available. For the Kerr medium, we first used a PM fiber with a length L of 200 m. The wavelength difference $\Delta\lambda$ of 3 nm between control and signal light consequently leads to a walk-off of about 10 ps (assuming a GVD value of $D = 17$ ps/km nm):

$$\Delta t \simeq DL\Delta\lambda \simeq 10ps$$

This value represents a lower limit for the (0–100)% rise/fall time of the switch. For even shorter switch times, a dispersion shifted fiber (DSF) would have to be used. For the initial adjustment of the switch, the polarization of both control pulses and signal could be set independently by polarization controller PC1 and PC2, respectively. This allows both for the pump to be launched into a birefringent axis of the PM fiber and for the signal polarization to be set at 45 deg to this axis for a maximum switching ratio at the output. At the end of the PM fiber the pump was removed with a second WDM, whereas the signal was reflected back with a Faraday mirror. Note that the control pulse was removed by the second WDM and not by the first one -after a double pass of the FUT- because one filtering was not enough to remove the control and the signal at the line and switch ports would have been covered by the residual control. After this double pass, the reflected signal is sorted out by a circulator and put on a PBS. The switch is biased by another polarization controller PC3, which allows to set the desired ratio of the signal light at the two PBS output ports. Typically, it was adjusted for maximum power in port 1 (line port), i.e. minimum power in port 2 (switch port)

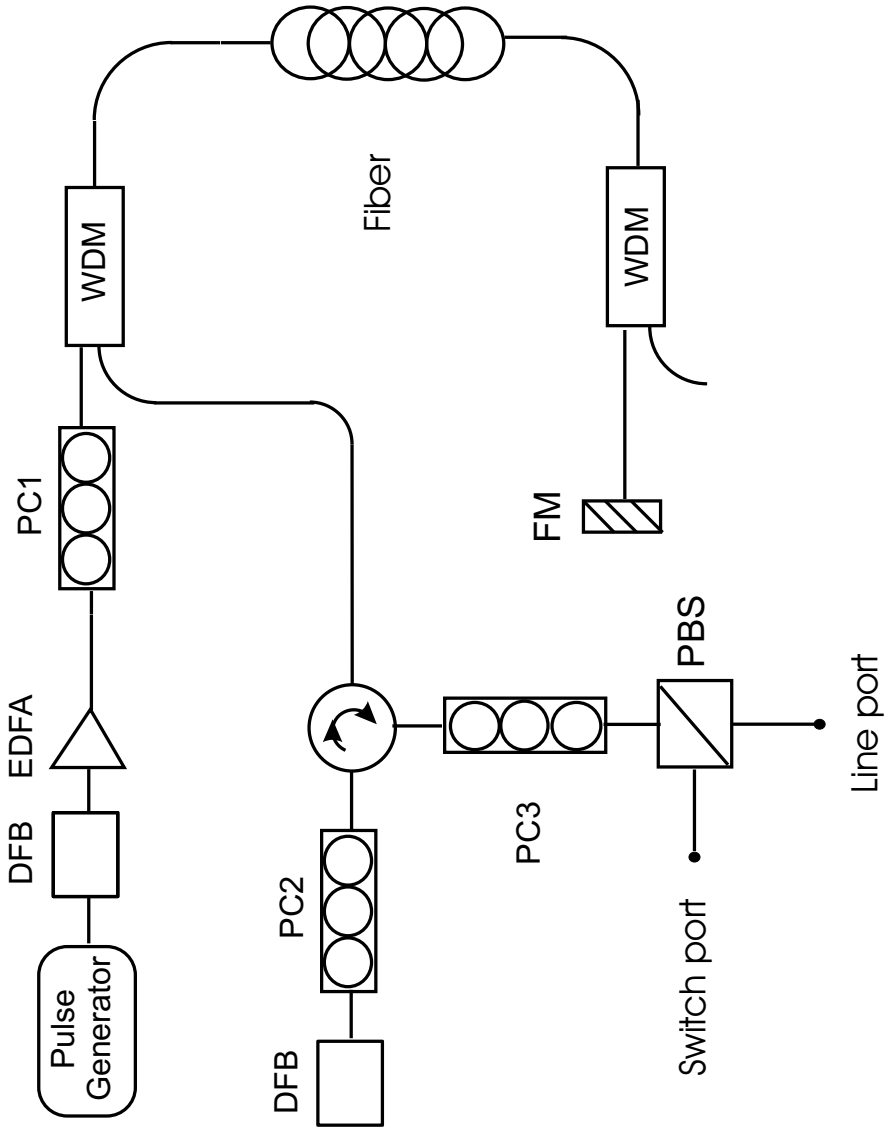

Figure 3.5: Experimental setup. DFB distributed feedback laser, EDFA Erbium doped fiber amplifier, PC polarization controller, FM Faraday mirror, PBS polarizing beam splitter, WDM wavelength division multiplexer

in the absence of control pulses. The switch port, for which Eq. (3.9) holds, was then monitored using a fast photodiode with a response time of 200 ps. The extinction ratio of the switch mainly depends on the extinction ratio of the PBS (20 dB in our case) and on the control signal power suppression at the signal wavelength (60 dB in our set-up). If necessary, higher values could be obtained by using additional polarization selection or filtering. Note that the required control signal peak power (or fiber length) could in principle be reduced to half its value if the pump is not removed at the FM, thereby allowing a double pass of the Kerr fiber. The switch performance is still independent of the control pulse pattern in that case as long as the total power of the control signal within half the round-trip time (1 μs in our case) doesn't change too much, a situation typically realized when switching high bit rate signals.

3.2.4 Experimental results

PM fiber

The experimental results using a 200 m PM fiber as the Kerr medium are shown in Fig. 3.6 and Fig. 3.7.

The proper working of our stabilization scheme was checked by monitoring the output power at the switch port for several hours. After the initial setting of the switch, it was left alone without any re-adjustments for a time period of several hours, while a normal activity in the lab was maintained, with people working around the table. Moreover, a change in the temperature of 5 degrees was observed during that time span. The measured fluctuations of the switch port signal power are shown in Fig. 3.6. Besides the measured data points (squares), the mean value (bold line) and the standard deviation σ (thin lines) are shown. As is demonstrated by the figure, the obtained switch stability was rather good (less than 2% fluctuations) when using the Faraday mirror. When it was replaced by a normal mirror on the other hand, thereby removing the stabilization, the switch port signal output power rapidly changed in the range from zero to full switch power. Indeed, it is well known that the polarization of light coupled into both the birefringent axes of a PM fiber - due to its short beatlength of only a few mm - is very susceptible to any perturbation. The use of a stabilization is therefore an absolute necessity. Fig. 3.7 gives the normalized switching ratio as a function of the applied control signal peak power. The normalized switching ratio is defined as the ratio of the actually measured power from the switch port, divided by

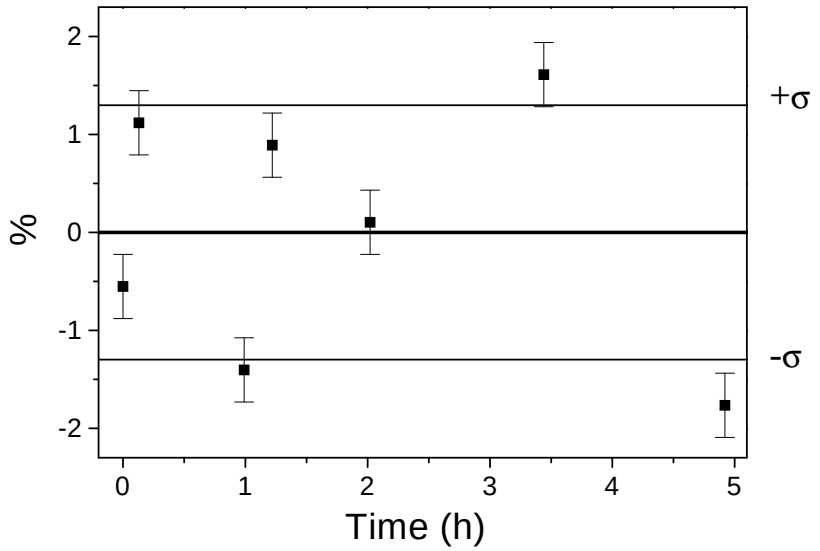

Figure 3.6: Switch performance using a 200 m PM fiber. Relative fluctuations of the switch port signal power as a function of time. Measured data (squares), mean value (bold line), and standard deviation σ (thin lines).

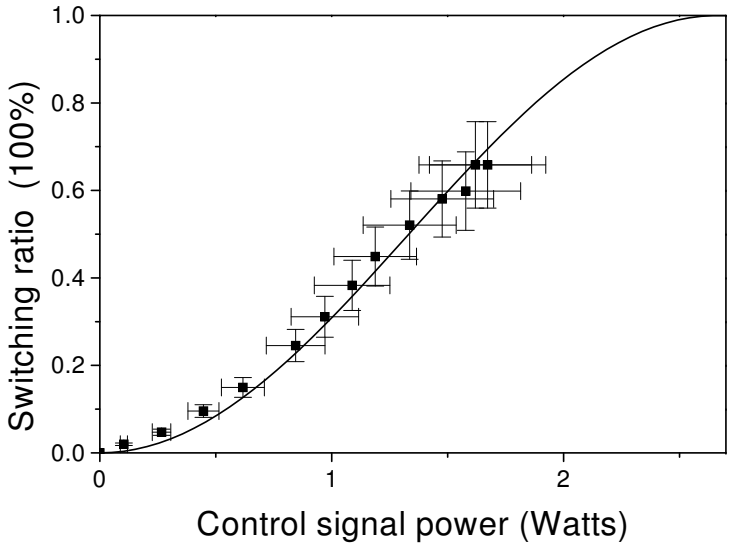

Figure 3.7: Switch performance using a 200 m PM fiber. Normalized switching ratio as a function of the control signal power. Measured data (squares), theoretical fit (solid line).

the maximum signal power obtainable from that same port (measured by adjusting PC3 for maximum transmission to the switch port in the absence of control pulses). The experimentally obtained values (squares) are compared with a fit (solid line) using Eq. (3.9) and requiring a peak normalized switching ratio of 1. As the figure shows, the experimental data corresponds well with the model (statistical $\chi^2 = 0.8$). The maximum switching ratio we could obtain in the measurement was however only 65% for a control peak power of 1.7 W. For higher control powers, the signal started to exhibit strong power fluctuations within the temporal switch window of 28 ns, which inhibited a proper functioning of the switch. As revealed by the optical spectrum, these fluctuations were caused by the onset of concurring nonlinear effects normally absent until much higher peak power times distance values. We believe that our non-optimal control signal source (side-band suppression) was seeding the observed nonlinearities, leading to a much lower threshold power. The observed limit in the switch ratio is therefore not a general problem of the demonstrated switch technique, but was unique to our experimental set-up.

Standard fiber

Further, we analyzed the possibility to use a standard (i.e. non PM) fiber for the Kerr medium. Besides reducing the switch cost, the assembly of the switch is much easier using standard than PM fiber, and the insertion loss can be reduced as the splice losses are lower. In order for the switch to work properly and efficiently, the part of the signal having the same polarization as the control signal at the input should keep the same polarization as the control during propagation, whereas the orthogonal part should stay orthogonally polarized. Only in this way an important phase shift between these two signal components can build-up. It is obvious that the above requirement is perfectly fulfilled in a PM fiber, where a signal component that is coupled into one of the two fiber axes remains there during propagation. In a standard fiber however, the situation is different. The above requirement, which corresponds, on the Poincare sphere, to a conservation of the angle between the control and signal Stokes vectors during propagation, is no longer met exactly. This is because the polarization mode coupling (specified by the coupling length h [28]) present in the standard fiber leads to a coupling of the control and signal light into both the (local) fiber axes, where they will evolve differently due to their different beatlengths. The conservation of the angle

between the control and signal Stokes vectors consequently depends on the fiber characteristics (coupling length h, beatlength L_b) and on the wavelength difference between the control and signal light. We therefore first verified that this angle conservation was sufficiently good in the standard fiber to be used as the Kerr medium. As a simple estimate, we can use

$$\alpha = 2\pi L(1/L_b(\lambda_{signal}) - 1/L_b(\lambda_{control}))$$

where $L_b(\lambda) = \lambda/(cB)$ and the birefringence B [ps/m] is assumed to be independent of the wavelength. The estimate represents a worst case scenario as the coupling length h is assumed to be much larger than the fiber length L and that both signal and control pulses were coupled into both fiber axes at the input. Using the wavelength difference of 3 nm of our experiment, and a typical value of the signal beatlength of 10 m, we get an angle difference of just 7 deg after 100 m of fiber, which should not cause any problems. Analysis of the Jones transfer matrix measured at both the signal and control wavelength further suggests that the angle should be sufficiently conserved. However, these simple estimates neglect nonlinear polarization evolution like e.g. a self-rotation of the intense control signal [23]. The testing of the switch was performed in a similar way as described in the previous subsection. However, as there is no well defined axis into which to couple, the input states of polarization were varied until a maximum in the switching ratio was found, although the differences were not that large due to an apparently small coupling length h of the employed Kerr fiber. This small coupling length quickly leads to a randomization of the fiber axes and makes the results almost independent from the input polarization of the control signal. On the other hand, the effective phase shift acquired by the signal is reduced by this randomization, and we had to use a longer Kerr fiber of 680 m to obtain a sufficiently large rotation of the signal at the fiber output.

As can be seen in Fig. 3.8, the stability was once more excellent when employing the FM. Fig. 3.9 shows the observed switching ratio as a function of the control peak power. The obtained switching ratio corresponds to 90% (for control pulses with a peak power of 2.4 W) before other concurring nonlinear effects once more lead to a pulse break-up. The experimental data are not too different from the ones for the PM fiber (Fig. 3.7), i.e. the longer length of the standard fiber (ΔL= +480 m compared to the PM fiber used before) accounts well for the phase-shift reduction caused by the "polarization scrambling" and the different value of the ratio n_2/A_{eff}. The use of a standard fiber is

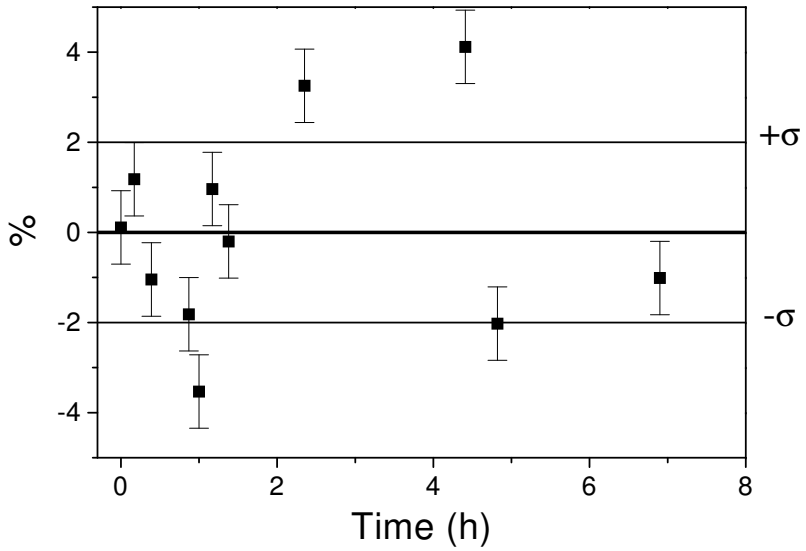

Figure 3.8: Switch performance using a 680 m standard fiber. Relative fluctuations of the switch port signal power as a function of time. Measured data (squares), mean value (bold line), and standard deviation σ (thin lines).

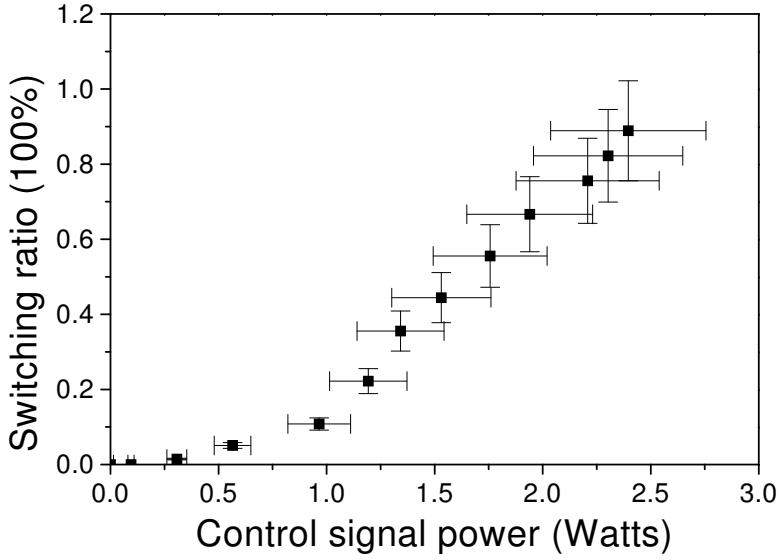

Figure 3.9: Switch performance using a 680 m standard fiber. Normalized switching ratio as a function of the control signal power.

therefore also interesting from a physical point of view, as the functioning of the switch could be exploited to reveal information about the coupling length of the standard fiber as will be seen in the next section.

3.2.5 Conclusion

In this section we have successfully demonstrated all-optical switching at 1.5 μm based on induced nonlinear polarization rotation in both a polarization maintaining and a standard telecom fiber. The insertion of a Faraday mirror after the Kerr fiber led to a very good stability of the switch for both cases.

In the standard fiber, switching was made possible because the small difference between the control and signal wavelength allowed for a similar evolution of both signals along the fiber - the two corresponding Jones transfer matrices were found to be almost equal - thereby well preserving the angle between the two respective Stokes vectors. As a byproduct, the ratio n_2/A_{eff} can be determined, and using an appropriate model, information about the coupling length h might be extracted as well.

3.3 Determination of the coupling length

In this section we present a way to obtain the polarization coupling length, an important parameter for the PMD probability distribution. This parameter is obtained from measurements and modeling of the nonlinear polarization rotation in optical fibers. Results for different types of fibers are presented

3.3.1 Introduction

It is well known that single-mode communication fibers are birefringent and that the orientation and the amount of birefringence are randomly distributed along the fibers. The corresponding polarization mode dispersion (PMD) becomes therefore a statistical quantity, and not only its mean value but also its probability distribution is important to assess the inferred system impairments. This distribution depends on two parameters: the (mean) local birefringence B and the polarization coupling length h, which is the distance over which the E field looses memory of its initial projection over the local polarization eigenstates [27]. In fibers having a length L long compared to h, the probability distribution is Maxwellian with a mean PMD value of B, whereas for coupling lengths approaching the fiber lengths, the PMD statistic can change considerably [28]. It is therefore important to have knowledge not only of the overall PMD but also of h and the beatlength L_b. In this section we present a novel way to directly infer the polarization coupling length from measurements of the nonlinear polarization rotation (NPR) in a fiber.

3.3.2 Principle of operation

In a dielectric medium, an intense elliptical input pulse induces birefringence - via the optical Kerr effect - due to the different amounts of intensity along the major and minor axis of the polarization ellipse. In an isotropic medium this self-induced birefringence leads to polarization ellipse self-rotation. In an optical fiber however, the situation is more complex due to the presence of the local intrinsic birefringence. The polarization changes are hard to predict in that case as the linear and nonlinear birefringences interact in a complicated manner. In general, the linear birefringence will however be much larger than the induced nonlinear one, and the evolution of the polarization vector y

in a polarization maintaining fiber can then be approximated by [23]:

$$\partial_z \psi \approx i\omega B_{eff}\sigma_\theta\psi = \omega(B - \frac{\alpha}{2}m_\theta(0))\sigma_\theta\psi \tag{3.10}$$

where σ_θ accounts for a linear birefringence with axis σ, α =$n_2P/(3cA_{eff})$, n_2 is the nonlinear Kerr coefficient, P the power, and A_{eff} the effective area. $m_\theta(z)$ is defined as the projection of the SOP on the birefringent axis at the position z along the fiber. The term B_{eff} takes into account for the linear birefringence B and the nonlinear birefringence. The solution for Eq. (3.10) is straightforward, and corresponds to a rotation of the input polarization vector around the linear birefringence axis σ_θ, with a rotation angle β given by β=$\omega B_{eff}z$. In principle the NPR can now be measured by varying the input power P and observing the corresponding change in the output SOP. However, an inherent problem for this kind of measurements is the instability of the output SOP at the exit of the fiber. Due to temperature changes and drafts in the fiber environment the dominant linear birefringence B strongly fluctuates and completely covers the nonlinear induced change. We have recently proposed a method for measuring NPR [23] by removing the overall linear birefringence -and therefore also its fluctuations- in a purely passive way by employing a Faraday mirror (FM) and a double pass of the fiber under test. Doing so, the nonlinear birefringence (leading to NPR) was shown to remain unaffected, i.e. the NPR of the forward and backward paths add up (see section 3.1). This allows to measure NPR both in polarization maintaining (PM) fibers and in standard fibers. However, the random variations of the intrinsic local birefringence axis in a standard fiber reduce the NPR. This reduction is due to the increased probability that the NPR action along each fiber's piece where the birefringence is constant, is compensated for by another. The situation becomes more complex, and we therefore resort to numerical simulations. The fiber is modeled as a concatenation of linearly birefringent trunks -for which Eq. (3.10) holds - with a constant physical length L_C. The amount of birefringence of these trunks is fixed (i.e. equal in all trunks), whereas its orientation is driven by a white noise process $g_\theta(z)$ characterized by a dispersion σ_{WN} [27]. For each single trunk, Eq. (3.10) is used to calculate the output SOP from the input one, which is calculated from the output SOP of the previous trunk according to the relative axis orientations. The SOP is therefore calculated piece by piece, with the projection mq being different for each new trunk. The final SOP will depend on the choice of the birefringence axis orientations of the trunks, with variations being larger in the limit of $L_C \to L$. We therefore made 200 runs for each specific trunk length to get

a mean value of the NPR.

3.3.3 Experiment

The experimental setup for the measurement of NPR for different test fibers is shown in Fig. 3.2. The light source consists of a distributed feedback laser (DFB) operated in pulsed mode at a wavelength of 1559 nm. Typically, pulses with a duration of 30 ns, a repetition rate of 1 kHz, and a peak power of up to 6 W (after amplification by an EDFA) are used. The light is then launched into the fiber under test (FUT) via a 90/10 coupler and a polarization controller (PC1). The coupler is inserted for the detection of the backward traveling light after the double pass of the FUT, with its 90% output port connected to the source in order to maintain high launch powers into the FUT. The polarization controller, PC1, allows to adjust the polarization of the light launched into the FUT, i.e. m_θ which is important for the strength of the NPR as demonstrated by Eq. (3.10). Note that for low launch powers (negligible NPR), the action of PC1 is removed by the Faraday mirror, and its setting is therefore of no importance in that case. The output SOP is examined by an analyzer consisting of a polarization controller PC2 and a polarizing beam splitter (PBS). To achieve a good sensitivity of the analyzer, it is calibrated for equal power in the two PBS output arms for low power launch signals where no NPR occurs. The two PBS output channels were monitored by a fast photodiode (200 ps response time) and a sampling scope. The measurements were then performed in the following way: for a given launch power, the polarization launched into the FUT was adjusted (PC1) to give the smallest possible output power at the monitored PBS channel. Consequently, the difference between the two PBS output channels is maximized, corresponding to a maximum value of the NPR.

3.3.4 Results and discussion

We first measured the NPR in a PM fiber with a length of 200 m. The results shown in 3.1 indicate that the NPR manifests itself with a reduction of the power in the monitored PBS channel. The output power starts to decrease in spite of the linear increase that would be experienced in the absence of NPR. The measured data agree well with our model, in which $m_\theta(0)$ was varied in order to give a minimum output power from the PBS channel like in the experiment, and only one fiber trunk was used (L_C = fiber

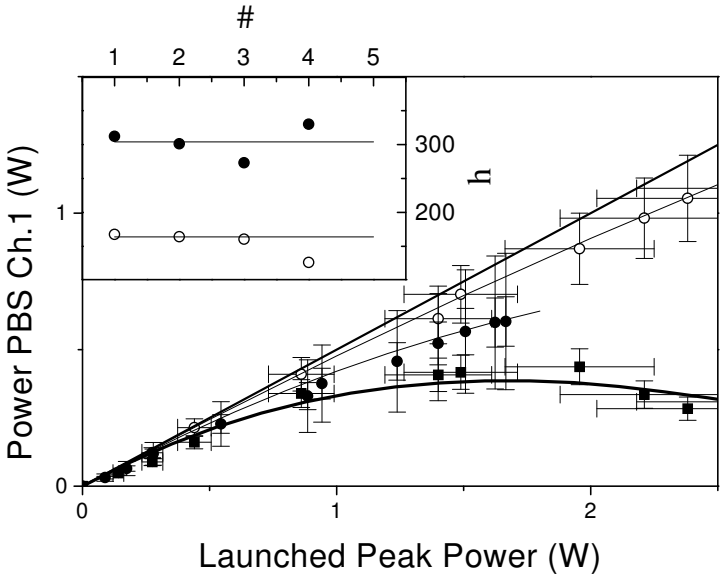

Figure 3.10: Minimum output power of PBS channel 1 as a function of the launched power. Symbols refer to the measured data fiber A (open circles), B (full circles), and C (full squares). Solid curve: prediction from our model. Straight bold line: prediction in the absence of any NPR. Bold curve: PM fiber. In the inset are shown the values of the calculated h for different σ_{WN} and L_C combinations giving curves that fits the experimental data

length L). The model curve for the PM fiber is shown in Fig. 3.10 (bold curve). Measurements were then made on different standard single mode fibers (SMF). The fiber lengths were typically 1 km (simulations were adjusted accordingly to each fiber length and n_2/A_{eff} coefficient). Fig. 3.10 shows the results for 3 different SMF; fiber A and B with a PMD of .05 ps/km (open and full circles) and fiber C with a PMD of 1.9 ps/$\sqrt{km}$ (full squares). The three standard fibers clearly exhibit a different amount of NPR with the fiber C showing a NPR similar to a PM fiber (bold curve). In order to fit the experimental data we have to introduce the polarization coupling length h.

The coupling length is defined as the length at which the fiber autocorrelation function $<\cos[\theta(z) - \theta(0)]>$ is equal to $1/e$. For the discrete case (as in our simulations) in which each piece of fiber has a fixed length L_C, it's easy to show that $h = 2L_C/\sigma_{WN}^2$. The fitting of the experimental data could then be made with two different free parameters; the length L_C and the dispersion σ_{WN} of the white noise process, providing h will remain constant. This is shown to be the case for our data as shown in the inset of Fig. 3.10. Here L_C is varied between 5 and 200 m and σ_{WN}^2 between 10 and 70 degrees. The simulations show that for the three different fibers the coupling length can be estimated to be about 160 m for the fiber A and 300 m for the large PMD fiber

(fiber B). A value of h<100 m is quite reasonable for a state-of-the-art, low PMD fiber. The coupling length of the SMF with high PMD (fiber C), found to e about 1000 m, is surprisingly quite large, indicating that there might be well defined birefringent axes in that fiber.

3.3.5 Conclusion

In this section we presented measurements and a model of NPR in an optical fiber, allowing for direct determination of the polarization mode coupling length. Polarization coupling length values as low as 160 m in state-of-the-art low PMD fibers were found.

Chapter 4

Four Wave Mixing in Optical Fibers.

4.1 Photon Pair Generation in Optical Fibers

Pairs of correlated photons entangled in energy and time can be used as a resource for quantum information processing. Up to now, photon pairs are mainly created in non-linear crystals or waveguides, using parametric down conversion, a non linear effect due to the second order susceptibility (χ^2). Here instead, we propose to create photon pairs directly in optical fibres, exploiting four wave mixing processes due to the third order susceptibility (χ^3). The advantage of creating photon pairs directly in optical fibres is that we can avoid the losses due to the collection of pairs created in an external source into the fibre. It also allows an all fibre operation, which is much more practical for "real life" applications (e.g metrology)

4.1.1 Introduction

The response of a dielectric to the light becomes nonlinear for intense electromagnetic fields. The origin of the phenomena is related to the anharmonic motion of the bound electrons in response to an applied field. As a result the induced polarization is not linear in the electric field E but instead

$$P = \varepsilon_0 \left(\chi^{(0)} E + \chi^{(1)} EE + \chi^{(2)} EEE \right) \tag{4.1}$$

where ε_0 is the vacuum permittivity and $\chi^{(j)}$ the j-th order susceptibility. Silica (SiO_2) is a center-symmetric molecule and symmetry considerations will lead to the result that the second order susceptibility is equal in electric dipole approximation to zero. The consequence is that for example no second harmonic generation is possible in an

optical fiber (in fact this is not true due to the higher order terms neglected in first approximation). The third order term is responsible instead for FWM, third harmonic generation, nonlinear refraction. This E dependence of the polarizability reflects on a power dependence of the refractive index of the fiber, inducing a possible intermodulation between different optical signals. If two different signals with frequencies ν_1,ν_2 are then launched into the fiber, the beatnote of these two signals modulates the refractive index with a frequency (ν_2-ν_1). Through this modulation a third signal at the frequency ν_1 will develop sidebands at the frequencies $\nu_1 + (\nu_1 - \nu_2)$ and $\nu_1 - (\nu_1 - \nu_2)$. The situation in fact is much more complex and every possible combination of the single frequencies can combine with each other. In a quantum representation we can say that different photons annihilate to generate new ones at different wavelengths. Different kinds of FWM are possible. The case in which three photons annihilate to give rise to a new one, is called "totally degenerate" FWM; the case of two photons with the same energy that combines to give rise to two photons different in energy, is called "partially degenerate" FWM. "Non-degenerate" FWM is present when all the frequencies are different to each other. It is important to note that as mentioned above not only energy conservation has to be satisfied in the FWM process, but even phase matching conditions. For this reason FWM is referred to as a "parametric process".

In this chapter we will concentrate mainly on "partially degenerate" FWM. In this process two pump's photons are absorbed by the fiber and two photons are created; one photon at a higher frequency than the pump and one at a lower frequency. Usually low frequency waves are referred as Stokes waves. High frequency wave as Anti-Stokes. As mentioned in the former paragraph, parametric processes are stronger when the process is phase-matched, i.e. when momentum conservation is valid. It follows that due to the dispersion of the refractive index, FWM is not always present but only when the following relation holds:

$$\Delta k = \frac{2n_p\omega_p}{c} - \frac{n_S\omega_S}{c} + \frac{n_{aS}\omega_{aS}}{c} = 0; \tag{4.2}$$

where the ω's refer to the frequencies of the waves (pump, Stokes and Anti-Stokes) and the n's to the different values at each wavelength of the effective refractive index. For the case of an optical fiber, the effective refractive index of the different waves (and consequently Δk) is determined by three factors.

$$\Delta k = \Delta k_M + \Delta k_W + \Delta k_N L \tag{4.3}$$

The first term Δk_M is the dispersion of the bulk medium of which the guide is made. The second is due to the dispersive characteristic of the waveguide itself. The third one represents the mismatch due to nonlinear effects. The single terms can be written as follows

$$\Delta k_M = (n_S\omega_S + n_{aS}\omega_{aS} - 2n_P\omega_P)/c \tag{4.4}$$

$$\Delta k_W = (\Delta n_S\omega_S + \Delta n_{aS}\omega_{aS} - 2\Delta n_P\omega_P)/c \tag{4.5}$$

$$\Delta k_{NL} = 2P\gamma \tag{4.6}$$

where the new n's are equal to the material refractive index n with added the change due to waveguiding. We can immediately note that phase matching in SMF is possible only if at least one of this term is negative. Some considerations are worth to be done. As the pump wavelength changes from below λ_0 to beyond it, the phase mismatch vector (the material one) changes sign from positive to negative. The phase matching (total phase mismatch vector equal to zero) will so occur at longer pump wavelengths because the waveguide contribution causes the shift of the zero crossing point. As the core diameter increases the waveguide contribution changes sign from positive to negative, making phase matching conditions dependent from the core size. Since for a SMF both the material and the waveguide dispersions contribute to phase mismatch the resultant phase matching point depends on

- the dopant
- the doping concentration
- the refractive index difference
- the core diameter of the fiber

Note now that the material contribution Δk_M can be expressed conveniently as a function of the frequency shift between the pump and the Stokes (or anti-Stokes) sideband defined in the following way:

$$\Omega = \omega_P - \omega_S = \omega_{aS} - \omega_P \tag{4.7}$$

To do this we make a Taylor expansion of the propagation constant (momentum) about

the carrier frequency ω_0

$$\beta(\omega) = k(\omega) = n(\omega)\frac{\omega}{c} = \beta_0 + (\omega - \omega_0)\beta_1 + \frac{1}{2}(\omega - \omega_0)^2\beta_2 + \frac{1}{6}(\omega - \omega_0)^3\beta_3 + ... \quad (4.8)$$

where

$$\beta_n = \left(\frac{d^n\beta}{d\omega^n}\right)$$

Now the dispersion parameter D is defined as

$$D = \frac{d\beta_1}{d\lambda} = \frac{d}{d\lambda}\left(\frac{dk}{d\omega}\right) = -\frac{2\pi c}{n\lambda^2}\frac{d^2k}{d\omega^2} \quad (4.9)$$

Let substitute the last expression for the dispersion parameter D into the former equation. Moreover we are interested in the case such that $\lambda_B < \lambda_P$ and two photons from the pump generate one photon at the probe wavelength and another one at the Stokes side ($\lambda_S > \lambda_P$) The phase mismatch Δk will result to be

$$\Delta k = k_B + k_S - 2k_P$$

Substituting the values for k found before (i.e. the Taylor expansion around the pump wavelength) and defining $\Omega = (\omega_S - \omega_P)$ we got

$$\Delta k = -\frac{n\lambda_P^2}{2\pi c}\Omega^2 D(\lambda_P) \quad (4.10)$$

Now making some calculations and considering that $\lambda_S = \lambda_P + \Delta$ and $\lambda_B = \lambda_P - \Sigma$ (it is easy to show that $\Sigma \approx \Delta$) we can easily find that

$$\Delta k = -2\pi c D(\lambda_P)\frac{\Delta^2}{\lambda_P^2}$$

So we can say that the material dispersion

$$\Delta k_M = \beta_2\Omega^2$$

where β_2 is the GVD.

The material dispersion can be rewritten in a more convenient way

$$\Delta k_M = \frac{\lambda^2}{2\pi c} D\Omega^2$$

Now note that this relation is true only when we are not too near the lambda zero dispersion. In fact in this case the formula is no more valid and higher terms in the expansion have to be considered (note that D is zero!). Another important consideration is the following. If we act on the dispersion we can change the value and the sign of the material dispersion, achieving phase matching. We can now consider what is happening for the case of SMF (the one we are considering in this chapter). For this fibers the waveguide dispersion is roughly zero and phase matching can consequently be achieved in different ways. If the pump wavelenght is greater than the zero dispersion wavelength λ_0 the material dispersion becomes negative. So phase matching is achieved when the pump wavelenght is near λ_0. Phase matching can be obtained too, acting on the nonlinear term through the power of the pump.

4.1.2 Phase matching condition near λ_0

We saw in the precedent paragraph when phase matching conditions are allowed. We can now distinguish two different situation depending if we are with the pump wave in a region in which the dispersion D is equal to zero or instead if we are near that one. Depending on that, the phase matching conditions change quite a lot and the FWM gain too. Let consider first the case in which the pump is in a region in which the dispersion D is different from zero (but near that one). Moreover we suppose to work in the normal region of the dispersion (D>0). In the anomalous region things are quite different and the modulation instability plays an important role making impossible to retrieve any information about the chromatic dispersion profile. So under the condition that the fiber has a normal dispersion, the conversion efficiency η which is defined as the ratio of the converted power to the input signal power, is equal to

$$\eta = \gamma P_P L \left[\frac{sin\,(gL)}{gL}\right]^2$$

with

$$g^2 = \frac{1}{2}\left[\Delta k\,(\Delta k + 4\gamma P_P)\right]$$

where P_P is the pump power, L is the length of the fiber under test, γ is the nonlinear factor equal to

$$\gamma = \frac{n_2}{A_{eff}} \frac{2\pi}{\lambda_P}$$

and λ_P is the pump wavelength. Considering the equation we found before for the phase mismatch Δk, t will follow that the conversion efficiency depends on the following parameters

- the pump power
- the phase matching condition
- the nonlinear coefficient γ

Things goes different when the dispersion is equal to zero, i.e. when the wavelength of the pump is equal to λ_0.For this case we have to consider higher order terms in the expansion of the propagation constant, considering that the first derivative of the dispersion parameter D is different from zero. With some calculations (see paragraph before) it's possible to show that the phase mismatch Δk is equal to [41]:

$$\Delta k = -\frac{\pi\lambda^4}{c^2} \frac{dD}{d\lambda} 2 \frac{\Omega^2}{\lambda_S^2} (\lambda_0 - \lambda_P) \Omega^2$$

4.1.3 Photon pair generation and experimental setup

The process we will exploit in order to produce photon pairs in optical fibers is partially degenerated FWM. That means we use two photons at the pump wavelength to create photons at two new frequencies ω_S (called Stokes photon; the reason is that this photon is lower in energy with respect to the pump) and ω_{aS}

$$2\omega_P = \omega_B + \omega_S$$

There is no presence of a probe that will stimulate the process to create one photon at that wavelength and the other at the Stokes or Anti-Stokes. So the FWM will still be present of course, but distributed on the entire spectra. Even if there is some filtering some amplified stimulated emission (ASE) will be present in the FUT stimulating the FWM on the ASE region of the entire available spectrum. So two symmetric sidebands around the pump wavelength should be present arising from the FWM process. The setup for the experiment is shown in Fig. 4.1.

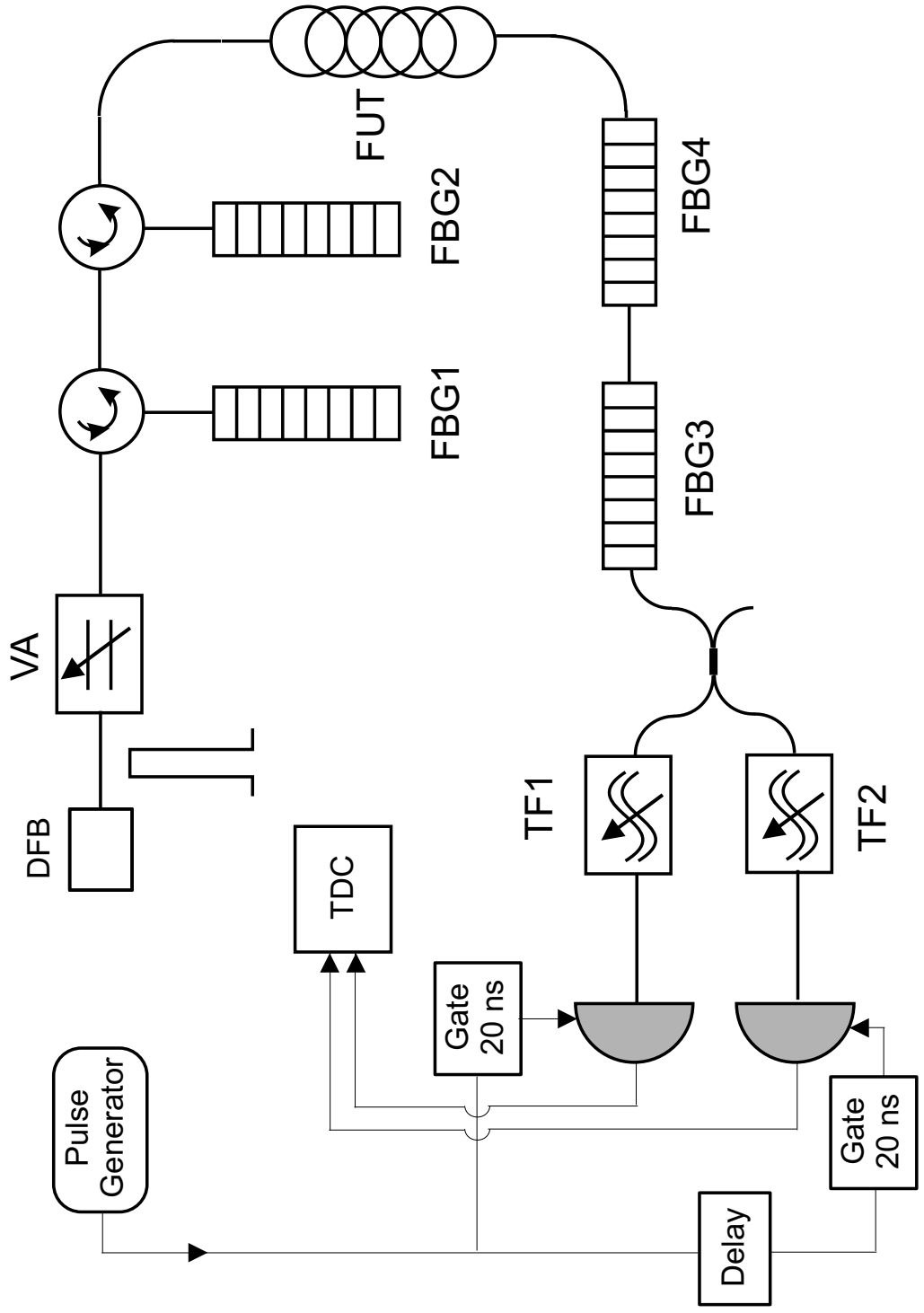

Figure 4.1: DFB Distributed feedback laser; VA variable attenuator; FBG fiber bragg grating; FUT fiber under test; TF tunable filter; TDC time to digital converter.

Light coming from a DFB laser working in CW mode, is filtered twice by way of the fiber bragg gratings FBG1 and FBG2 tuned on the lasing wavelength in order to remove any background signal from the laser itself. Light is then injected into the FUT along which FWM photons are created. At the exit of the FUT the laser line is rejected by the filters FBG3 and FBG4 (80 dB attenuation) because the generated signal is lower than the laser line. After that the photons are splitted in a ration 50/50 at the coupler and two tunable gratings TF (40 dB attenuation) are tuned symmetrically around the laser line. Detection events are collected at the photodiode (InGaAs photodetectors; see Section 5.1) and coincidences between the events are made using a time to digital converter.

The measurements were made in the following way. First of all intensity as a function of wavelength was determined at the exit of the FUT for different fibers. This in order to see that the arising bands were symmetrically located and the signal was higher than the noise. Different spectra are shown in Fig. 4.2 for fibers having different λ_0 and different lengths. The spectra for a high non linear fiber (length 1 km) with λ_0 at the same value of the laser line (λ = 1549.4 nm) is shown in Fig. 4.3. We can clearly distinguish two sidebands located at higher and lower wavelengths compared to the laser line. In the inset of Fig. 4.3 is shown the correlation on the detection of the photons at the two photodiodes. The two tunable gratings are tuned at higher and lower wavelengths symmetrically around the laser line. The correlation spectra shown in the inset was made at the wavelengths evidenced with the arrows in the figure. Correlation measurements were made for different wavelengths and no correlation was ever found suggesting that the bands have their origin in different phenomena than FWM. Measurements as a function of length were made too and even for shorter lengths (meters) no correlation was ever observed.

4.1.4 Conclusion

In conclusion no photon pairs were generated. This could be done to the low amount of power injected into the FUT and to the poor quality of the DFB laser. At the same time luminescence due to the glass impurities is covering the signal. Improvements could be obtained with a Er ring laser (higher signal to noise ration and higher power) and using short lengths of fibers (like photonic crystal fibers).

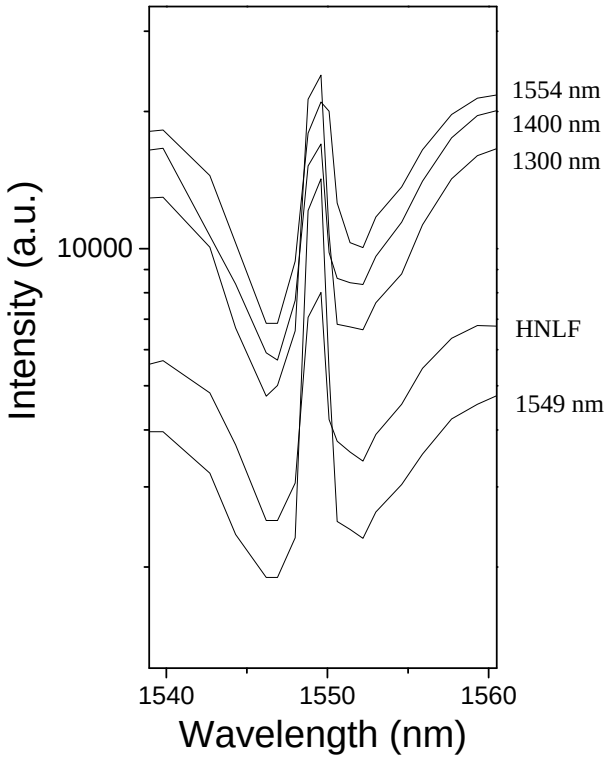

Figure 4.2: Spectra of the created photons. The central peak is due to the pump laser. On the right is indicated the value of λ_0.

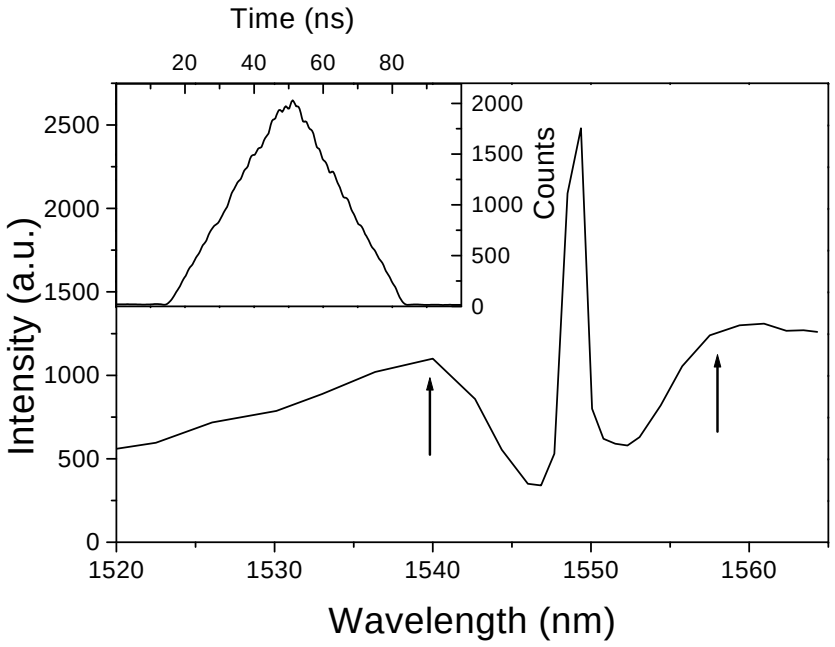

Figure 4.3: Spectra of the created photons. The central peak is due to the pump laser. For these photons,as seen in the inset of the figure, no time correlations have been observed, indicating that they are probably created by another process than FWM (e.g. fluorescence in the fiber).

4.2 Distributed Measurements of CD in DSF fibers

In this section we report on distributed measurements of chromatic dispersion along dispersion shifted fibers with different values of polarization mode dispersion and coupling lenght, by way of an OTDR-like method based on four wave mixing.

4.2.1 Introduction

The implementation of Erbium-doped fiber amplifiers allows for high-bit rate transmission over transoceanic distances. At the same time, the technique of wavelength division multiplexing (WDM) is used to increase the transmission rate, leading to an important amount of power inside the fiber. Because of the long distances and high powers, optical nonlinearities start to play a significant role. In dispersion shifted fibers (DSF) four wave mixing whose efficiency depends on the chromatic dispersion profile, leads to transmission impairments. From here the necessity to have a technique that can allow to map the longitudinal distribution of chromatic dispersion along a fiber. The method proposed by Mollenauer et al.[29, 30] and based on four wave mixing, is a

convenient approach for the measurement of chromatic dispersion maps in DSF fibers. In this work we show that when the coupling length h is relatively large (as is typically the case for most older installed DSF cables) the method presents severe limits. We present a comparison between DSF fiber with different values of PMD and coupling length and a model is discussed in order to explain the observed phenomena.

4.2.2 Theory

The measurement method consists in launching two optical beams at frequencies ω_1 and ω_2 ($\omega_1 < \omega_2$) along a fiber. Due to the nonlinearity of the fiber, the two waves will interact by way of FWM generating two new signals (Stokes and Anti-Stokes) at frequencies $\omega_S = 2\omega_1 - \omega_2$ and $\omega_{AS} = 2\omega_2 - \omega_1$. Being a parametric process, both energy conservation and phase matching conditions must be satisfied. Taking into account the dispersion of the fiber, it is possible to show that the phase mismatch Δk between the two waves (we set the pump power equal to twice the probe power $P_2 = 2P_1$, i.e. the nonlinear contribution to the phase mismatch is equal to zero) is given by

$$\Delta k_1 = D(\lambda_1) c 2\pi \left(\frac{\Delta\lambda}{\lambda_1}\right)^2 \tag{4.11}$$

This phase mismatch is manifest as a spatial intensity oscillation of period λ_{Sp} in both the Stokes and Anti-Stokes waves, that can be observed as a temporal oscillation with frequency ν_t in the intensity of the Rayleigh backscattered light. This oscillations is due to the phase mismatch between the different photons, and the frequency in oscillation is given by

$$F_S = \frac{1}{\Lambda_S} = \frac{\Delta k}{2\pi} = cD(\lambda_1)\left(\frac{\Delta}{\lambda}\right)^2 \tag{4.12}$$

So if we measure the spatial frequency we are measuring in effect $D(\lambda_1)$ with a spatial resolution given by Λ_S. Of course this oscillation can not be observed in forward direction but only in backscattering. In fact here the signal will fluctuate in intensity with a temporal frequency related to the spatial one by

$$F_I(t) = \frac{c}{2n} F_S(z) \tag{4.13}$$

Note that the spatial frequency is a function of the position along the fiber due to possible changes in the D parameter. This spatial frequency will reflect in a temporal

dependence of the temporal frequency $F_I(t)$. So the frequency in the intensity modulation at time t = 2nz/c will give us information about the D at the position z in the fiber.

So finally combining the equation we have that the dispersion parameter D is equal to

$$D(\lambda_1, z) = \frac{2n}{c^2}\left(\frac{\lambda_1}{\Delta}\right)^2 F_I\left(t = z\frac{2n}{c}\right) \tag{4.14}$$

The estimated power can be calculated equal to

$$P_S(z) = 8\left(\frac{\lambda_1}{Dc\Delta^2}\right)^2\left(\frac{n_2}{A_{eff}}P_1\right)^2 P_2 sin^2\left(\frac{\Delta kz}{2}\right) R\Delta z e^{(-4\alpha z)} \tag{4.15}$$

where z is the length occupied by a pulse, and R is the backscattering coefficient. Regarding the nonlinear contribution to the phase mismatch this is usually a fraction of the linear one. In any case keeping the power of the pump twice the one of the probe is easy to show that the nonlinear mismatch is always equal to zero.

So measuring the temporal frequency allows one to obtain the value of the dispersion D(λ_1,z) at the pump wavelength λ_1 and at the position z. Now, it is well known that single-mode communication fibers have residual birefringence and that the orientation and the magnitude of the birefringence is randomly distributed along the fibers. This distribution is characterized by the PMD and depends on two parameters: on the (mean) local birefringence B and on the coupling length h that gives the distance after which a considerable amount of power has coupled into the other polarization mode. If the fiber under test (FUT) does not present a birefringent axis (low values of PMD and coupling length), the pump and probe will travel together remaining parallel to each other for the entire length of the fiber. It follows that the positions along the fiber where the condition of phase matching is satisfied are independent of the entering state of polarization of the pump and of the probe. In the presence of relative large values of PMD the evolution of the SOP for pump and probe is given by [42]

$$< \mathbf{S_1^{out}} \mathbf{S_2^{out}} >= \mathbf{S_1^{in}} \mathbf{S_2^{in}} exp\left(-\Delta\omega^2 \frac{3\pi}{8} \frac{< \Delta\tau >^2}{3}\right) \tag{4.16}$$

For what concerns the efficiency η of the FWM process, this is given by

$$\eta = \frac{1}{2}(1 + \mathbf{S_1}\mathbf{S_2}) \tag{4.17}$$

where $\mathbf{S}_1$ and $\mathbf{S}_2$ represents the Stokes vectors of the state of polarization (SOP) of the pump and probe respectively. For the case of low values of coupling length, even if the PMD results quite high, the net effect consist in a different evolution of pump and probe along the fiber. But due to the short autocorrelation length (i.e. high polarization scrambling) the contribution to the phase mismatch due to the waveguide term is negligible and the phase mismatch will still result to be equal to Eq. (4.11). Only the efficiency η, will change making in some cases difficult to find the position of zero mismatch. But the position will result to be only slightly dependent on the entry state of polarization. However, the situation becomes more complicated, when there are large values of coupling length along the fiber. The asimmetry in the fiber and the concomitant different evolution for pump and probe due to the PMD (Eq. (4.16)) will give rise to polarization dependent effects. In fact depending on the SOP entry angle the two waves will travel along different paths but in this case due to the long coupling length the scrambling is not high enough to make statistically equal the presence of both of them along the birefringence axis with the waveguide phase matching term resulting different from zero. The situation is similar to what is happening in a PM fiber in which two birefringent axis are defined. If one of the two waves will match one of the two axis will travel along it for the entire length of the fiber acquiring a certain phase. The other instead will start to rotate. So the phase matching condition will result to be a function of the entry state of polarization. This will reflect in a SOP dependence of the dispersion maps obtained for this kind of fibers.

4.2.3 Experiment

The experimental setup for the measurements is shown in Fig. 4.4. The light source consists of two tunable distributed feedback lasers (DFB) in cw mode. The SOP of the two waves is controlled via two polarization controllers (PC1, PC2), and made equal in order to maximize FWM (Eq. (4.17)). The two waves are then amplified by a SOA modulated with a frequency of 4 kHz and a pulse width of 30 nsec and then amplified again by an EDFA. Typical values in the range 150-1500 mW are used. The SOP of both the waves is then controlled at the same time by way of a polarization controller (PC3) and the light is then launched into the fiber under test (FUT). The circulator sends the two pulses into the FUT, and collects the Rayleigh backscattered signal to an OTDR after passing through a tunable filter (40 dB attenuation @ 2 nm). The oscillation in the power at the Stokes (or Anti-Stokes) wavelength are monitored in backscattering with

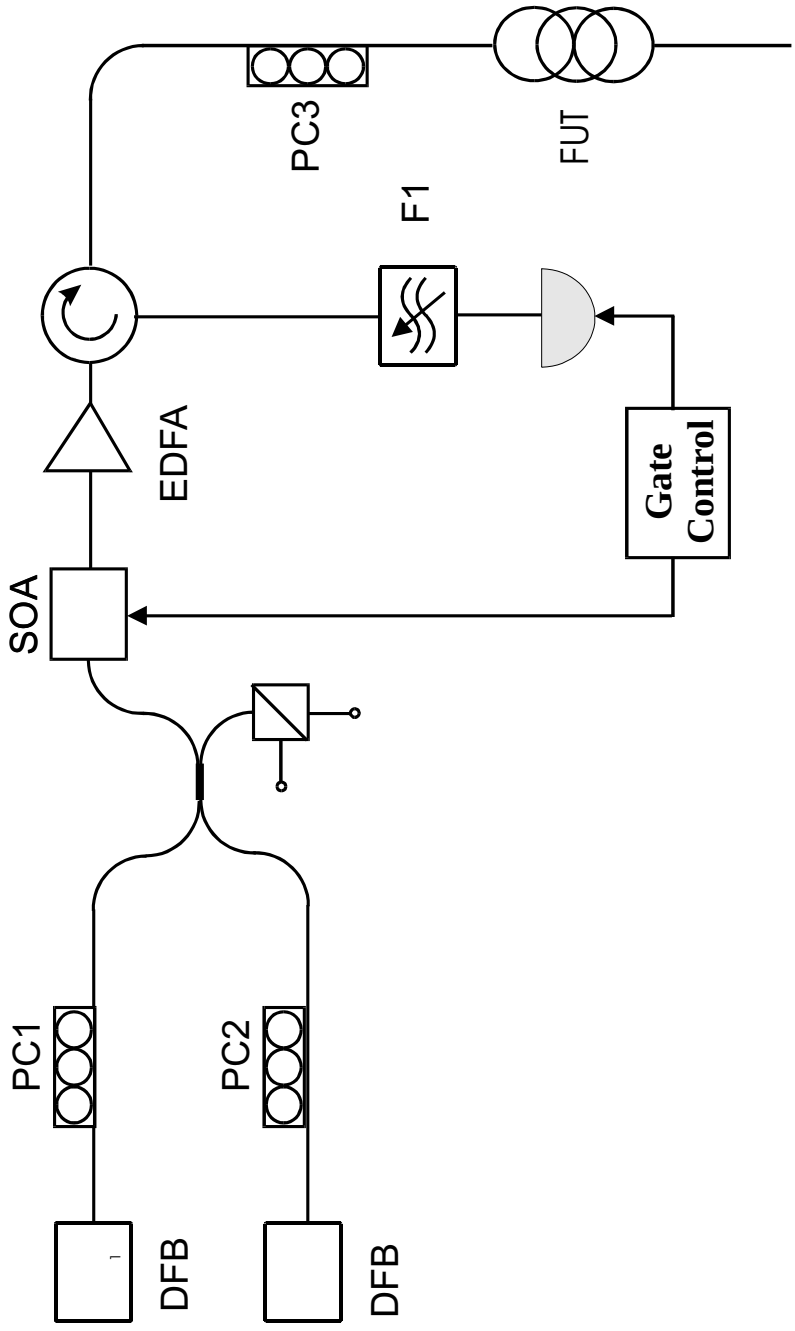

Figure 4.4: Experimental setup.

Fiber	Length (m)	λ_0 (nm)	Coupling Length (m)	PMD (ps/$\sqrt{km}$)
NIST	9700	1547.8	0.53	0.02
AC-2	7400	1545	0.65	0.19

Table 4.1: Parameters for the different fibers.

an OTDR and the dispersion maps are elaborated by a personal computer.

4.2.4 Results

We made measurements on different fibers. The data for two of them are shown in Table 4.1.

First, we map the chromatic dispersion for two different DSF fibers, one with a small and one with a large polarization coupling length h (determined from (polarization sensitive) Optical Frequency Domain Reflectometer traces). In both fibers, the overall PMD is small (¡0.2 ps/km). Fig. 4.5 shows the Stokes signal power for the low coupling length fiber for different input SOPs into the FUT (pump and seed input polarizations are kept identical). No significant dependence of the results on the input polarization is expected for such a fiber, as the pump and seed signals have no time to acquire significantly different phases due to the frequent coupling among the fast and slow axes. Indeed, the figure demonstrates that only small changes in the amplitudes, but not in the locations of the Stokes signal maxima are obtained. For completeness, inset (a) shows the chromatic dispersion map as obtained from entering the fiber from both ends (one of the profiles is inverted), demonstrating the good reproducibility and accuracy of the results. Inset (b) gives the overall dispersion at different wavelengths, where the open circles were obtained from summing up the FWM dispersion map, and the bold line from an alternative method. Good agreement between the two methods can be observed. Fig. 4.6 shows the results for the long coupling length fiber. As can be seen, the maxima locations of the Stokes signal vary strongly due to the additional phase from PMD, which depends on the input polarization states. In fact, the chromatic dispersion map can no longer be estimated from a single trace alone, as the frequency at a given location depends on the (arbitrary) relative polarization states at that location for that input SOP. To remove this arbitrary component, different profiles,

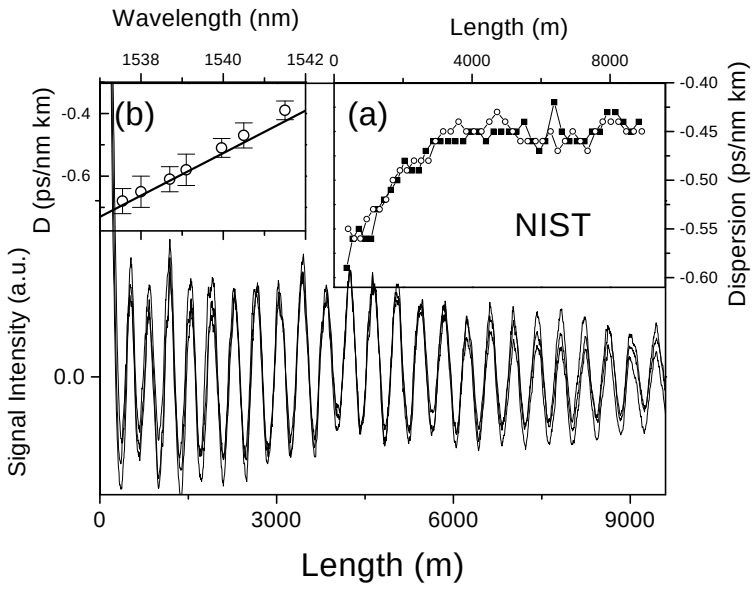

Figure 4.5: Signal intensity profile for the fiber NIST. In the inset is shown the chromatic dispersion profile taken at both FUT entry and the integrated value of the chromatic dispersion.

each corresponding to a different input SOP, have to be taken. For a given location, the mean value of GVD should then be retained. Note that averaging over all the possible SOP during an acquisition (by using a polarization scrambler, bold line in the inset of Fig.3) will not give a meaningful result, as it simply corresponds to a sum of the different individual traces giving -due to arbitrary positions of the different maxima - a curve that is basically flat.

4.2.5 Conclusions

In conclusion in this section we have shown that mapping of chromatic dispersion in DCF fibers, is strongly affected by the coupling length value present in them. The possibility to obtain significative mapping still exist for fibers of this kind and is allowed by way of collecting different signal profiles at different entry SOP.

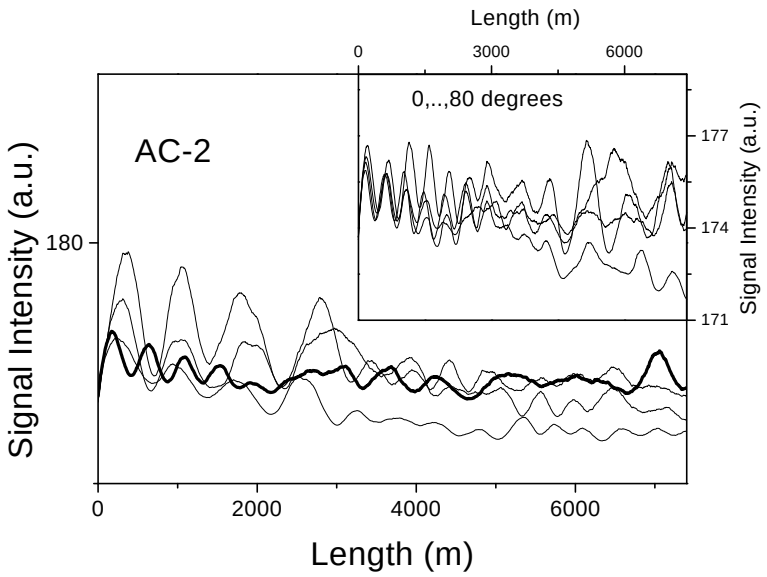

Figure 4.6: Signal intensity profile for the fiber AC-2. In the inset is shown the chromatic dispersion profile taken at both FUT entry.

4.3 Distributed Measurements of n_2/A_{eff} in DSF fibers

In this section we report on distributed measurements of nonlinear coefficient n_2/A_{eff} along dispersion shifted fiber by way of an OTDR-like method based on four wave mixing effect.

4.3.1 Introduction

Because of the long distances and high powers reached nowadays in optical fibers, optical nonlinearities due to changes in the refractive index (optical Kerr effect) start to play a significant role. Among them, self-phase modulation (SPM), cross-phase modulation (XPM), and four-wave mixing (FWM) are the most important. The magnitudes of these effects depend on the ratio n_2/A_{eff} , where n_2 is the nonlinear refractive index of the fiber and A_{eff} the effective area of the lightmode. It is therefore important to have a simple and accurate method for the determination of this ratio. Different methods, based on SPM or XPM phase shift detection using interferometric [23] and non-interferometric [5] schemes have been proposed (see Section 2). But all these measurements techniques give only the integrated value of the nonlinear coefficient over the entire length of the fiber under test (FUT). The only way to obtain a map of the n_2/A_{eff} over the entire fiber length consist in performing a destructive fiber-cutting measurement. In this section, we propose a new method based on an OTDR-like technique firstly proposed by Mollenauer et al. [29, 31] to perform distributed measurements of chromatic dispersion along a fiber. The method allow us to obtain longitudinal mapping of the nonlinear coefficient along a 10 km DSF fiber.

4.3.2 Theory

When two optical beams at frequencies ω_1 and ω_2 (ω_1 ¡ ω_2) propagate along a fiber, due to the nonlinearity of the fiber, they interact by way of FWM generating two new signals (Stokes and Anti-Stokes) at frequencies ω_S and ω_{AS}.

$$\omega_S = 2\omega_1 - \omega_2 \qquad \omega_{AS} = 2\omega_2 - \omega_1$$

The waves at ω_S , ω_1 , and ω_2 are called idler, pump, and signal respectively. Being a parametric process, it is required not only energy conservation but even phase matching conditions have to be satisfied. Taking into account both the dispersion of the fiber

and the nonlinear contribution to the phase matching condition, it is possible to show that the phase mismatch Δk between the two waves is given by

$$\Delta k = \Delta_L + \Delta_{NL} = Dc2\pi \left(\frac{\Delta\lambda}{\lambda}\right)^2 + \gamma(2P_1 - P_2) \tag{4.18}$$

This phase mismatch will reflects itself in a spatial intensity oscillation with period λ_{Sp} in both the Stokes and Anti-Stokes waves, that can be observed as a temporal oscillation with frequency nt in the intensity of the Rayleigh backscattered light [43]

$$\nu_t = \frac{c}{2n}\frac{1}{\lambda_{Sp}} = \frac{c}{2n}\frac{\Delta k}{2\pi} = \nu_L + \nu_{NL} = \frac{c}{2n}Dc\left(\frac{\Delta\lambda}{\lambda}\right)^2 + \frac{c\gamma}{4n\pi}(2P_1 - P_2) \tag{4.19}$$

If $P_2 = 2P_1$ the nonlinear term is vanishing and a measurement of the local frequency will allow to have information on the local value of the dispersion all along the fiber length. Once retrieved a map for the chromatic dispersion D(z,l) and considering a ratio for the pump and probe power different from 2, we can in principle retrieve informations on the local value of the g(z) parameter (i.e. n_2/A_{eff}). Unfortunately local variations due to the coupling length will not allow to obtain good and reproducible map of the nonlinear coefficient. An alternative way, that makes the measurements much more significative, consist in performing two different measurements keeping the ratio P_1/P_2 constant but attenuating it of the same factor a the power of both pump and probe at the entry of the FUT. It follows that the difference between the temporal frequency for the two measurements is indipendent of the chromatic dispersion (the linear term that appears in Eq. (4.19) is equal for both the cases, so it cancels out), but contains instead a dependence in γ.

$$\Delta\nu_t = \nu_t(\alpha = 1) - \nu_t(\alpha = \alpha) = \frac{c\gamma}{4n\pi}(2P_1 - P_2)\frac{1-\alpha}{\alpha} \tag{4.20}$$

That allows us to obtain a map of the nonlinear coefficient along the FUT. To note that typical variations of the n along the fiber, will not contribute significatively to the $\Delta\nu_t$ term.

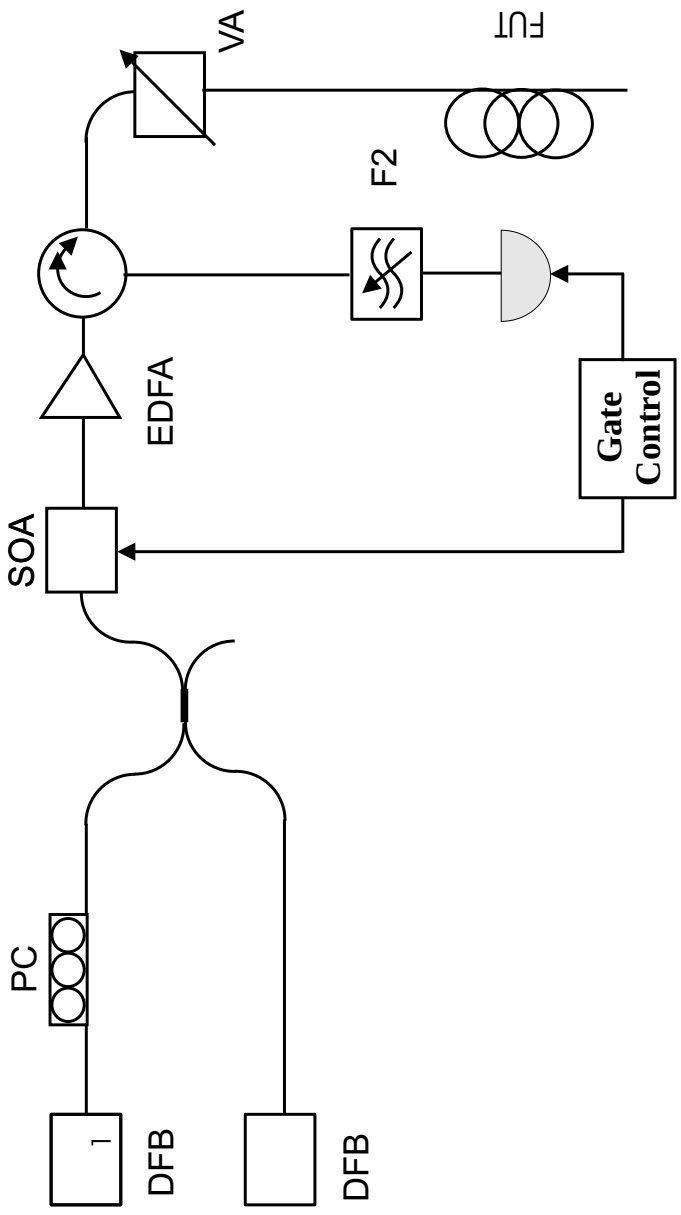

Figure 4.7: Experimental setup.

4.4 Experimental

The experimental setup for the measurements is shown in Fig. 4.7. The light source consists of two tunable distributed feedback lasers (DFB) in cw mode. The state of polarization of the two waves is controlled by way of a polarization controller and monitored by a polarimeter, and made equal in order to maximize FWM process along the FUT. The two waves are then amplified by a SOA modulated with a frequency of 4 kHz and a pulse width of 30 nsec and then amplified again by an EDFA. Typical values in the range 150-1500 mW are used. The circulator sends the two pulses into the FUT, and collects the Rayleigh backscattered signal to an OTDR after passing through a tunable filter (40 dB attenuation @ 2 nm). The oscillation in the power at the Stokes (or Anti-Stokes) wavelength are monitored in backscattering with an OTDR and the dispersion maps are elaborated by a personal computer. The measurements were then performed in the following way: pump and probe were tuned at different wavelengths (λ_2 = 1541.3 nm, $lambda_1$ = 1535.0 nm) and the power was setted at 1150 mW for both of them ($P_1 = P_2$) and at 115 mW for the attenuated measurement (α=10).

4.4.1 Results

A typical signal profile for the fiber under test is shown in Fig. 4.8.

In the inset is shown the CD profile at 1541.3 nm. Measurements at the two different powers are reported in Fig. 4.9. In the inset is shown a simulation using A_{eff} = 39 μm^2, n_2 = 2.6 $10^{-10} W^{-1}$ for the two different powers. The data shown in the figure and in the inset match quite good. From the experimental values using Eq. (4.20) it is possible to determine the longitudinal distribution of the nonlinear coefficient n_2/A_{eff} . This is shown in the inset of Fig. 4.9. The fluctuations are due to the inaccuracy in the determination of the position of the signal peaks. This can be improved averaging the total number of measurements and using a fitting algorithm.

4.4.2 Conclusion

In this section we reported on distributed measurements of nonlinear coefficient n_2/A_{eff} along dispersion shifted fiber by way of an OTDR-like method based on four wave mixing effect.

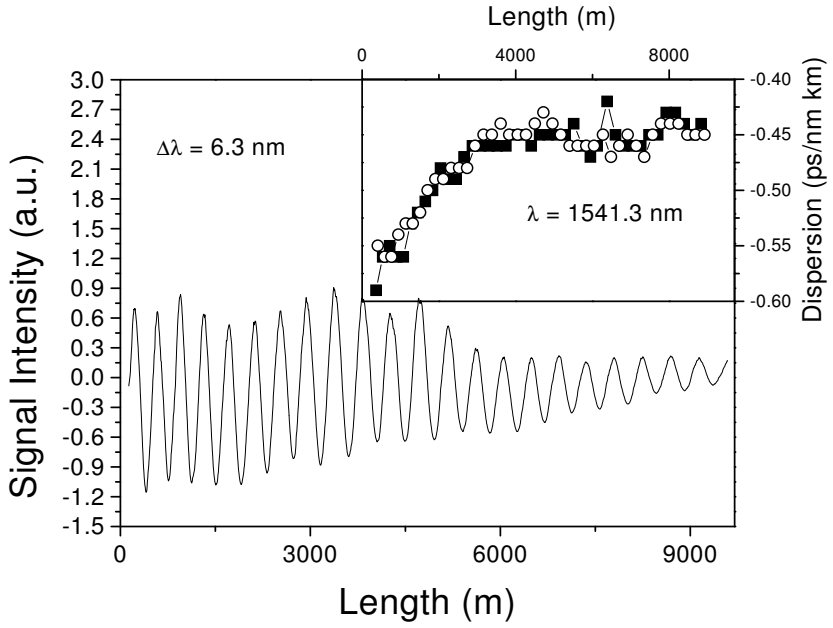

Figure 4.8: A typical signal profile for the fiber under test.

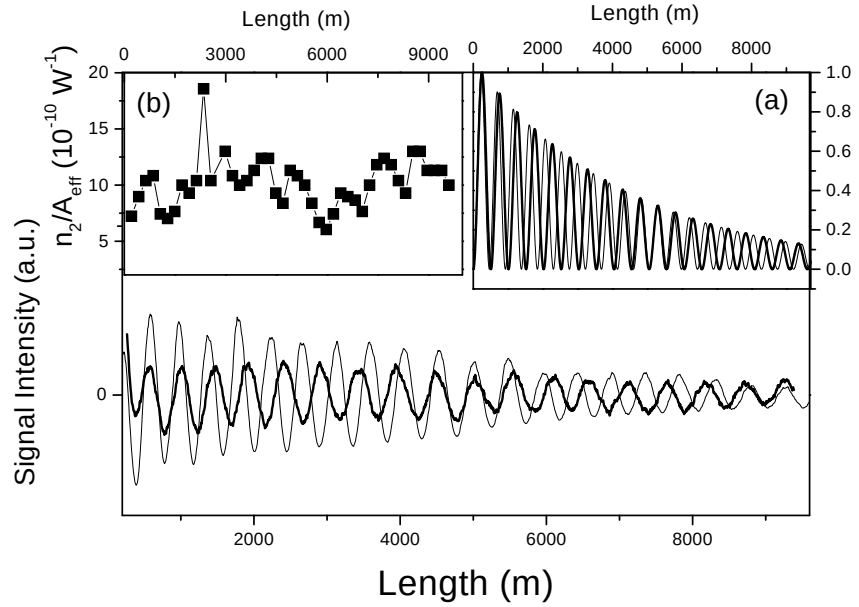

Figure 4.9: Map of the nonlinear coefficient for the short coupling length fiber.

Chapter 5

Different contributions

5.1 Photon Counting Near Field Scanning Optical Microscopy at 1.55 μm

In this section we present a a new system combining near-field scanning optical microscopy (NSOM) with single photon detection operating at the wavelength of 1.55 μm. The microscope was used in order to image the splice region between a standard telecom and an Erbium doped fiber. The excellent sensitivity also allowed to detect the Rayleigh scattered light of a standard fiber coming out laterally through the fiber cladding.

5.1.1 Introduction

Near-field scanning optical microscopy (NSOM) allows to obtain spatial resolutions below the classical diffraction limit [44]. Over the last years, this intriguing possibility has been exploited for numerous applications [44, 45, 46, 47, 48, 49, 50, 51].

In order to increase the sensitivity of the NSOM, photon counting detectors are employed. So far, the use of silicon avalanche photodiodes (APD) operated in the so called Geiger mode has been demonstrated. It is well known that these silicon APDs have very good performances [52]: quantum efficiencies of about 60%, dark count rates below 100 counts per second, and a sub nanosecond timing resolution. But silicon is not sensitive in the near infrared, and other detector materials have to be employed for photon counting in that important wavelength region. Due to their sensitivity from 0.7 to 1.8 μm, Ge APD are potential candidates. However, in order to have a reasonably low dark count rate, these detectors must be cooled to 77 K, reducing their cut-off

wavelength to below 1.45 μm. This problematic is absent in InGaAs/InP photodiodes. Although this 1.55 μm photon counters have been used for several years in quantum optics experiments (e.g. quantum cryptography [53]), they are not yet exploited for NSOM. Using this technique, we demonstrate in this section a photon counting NSOM operating at 1.55 μm. To illustrate its functionality we give some examples relevant for telecommunications. Note however that other interesting applications can be found in the biological field.

The section is structured as follows. In Subsection 5.1.2 we describe the setup of our photon counting NSOM with emphasis on the photon counting detection scheme at 1.55 μm. In Subsection 5.1.3 we first test our NSOM by measuring the optical mode field out of a single mode fiber and by comparing it with a standard measurement method. We then monitor the splice between an Erbium doped and a standard single mode fiber, from which an upper limit for the thermal diffusion length was found. The excellent sensitivity of our NSOM even allowed to detect Rayleigh light scattered out laterally from a piece of standard single mode fiber.

5.1.2 Description of the 1550 nm photon-counting NSOM

The set-up consists of two main parts: the NSOM apparatus and the detection scheme.

The NSOM system is home built and consists of a Physik Instrumente piezo servo-controlled xyz-scanner (100*100*10 μm) mounted on a Nikon TE300 inverted microscope usually used in transmission mode to characterize the fluorescence of biological samples. For the applications discussed in this section, the light coming out from the fiber sample under test is collected by a tapered optical fiber obtained by chemical etching so that the aperture diameter is below 100 nm. To ensure a constant, small tip-sample distance during the scan, we use the shear-force detection technique originally proposed by Karrai et al. [54]. It is based on a mechanically excited tuning fork of well-defined resonant frequency. The optical fiber tip glued to one arm of the tuning fork protrudes less than 1 mm and vibrates parallel to the sample surface with an oscillation amplitude of about 10 nm. Approaching the sample surface, the decrease of the piezoelectric signal amplitude is used to maintain the tip-sample distance at about 5 nm with an electronic feedback loop controlling the z-direction of the scanner.

The heart-piece of the detection scheme is obviously the 1.55 μm photon-counting detector. Due to efficiency and signal-to-noise issues, InGaAs/InP Avalanche Photodiodes (APD) are the only viable candidates for photon counting at 1.55 μm today [55].

In the following, we will therefore concentrate on this type of detectors. Before entering the details, let us briefly recapitulate the working principle of photon-counting. If an APD is biased above the breakdown voltage (Geiger mode), every time a single photon is absorbed by the photodiode, it will trigger an avalanche generating a macroscopic current pulse. The recording of this current pulse with a suitable electronic discriminator circuit indicates the presence of a photon. To link the recorded photon counts to different power levels, many 'real' events have to be recorded so that erroneous (i.e. noise) counts don't falsify the measurement. Further, the probability to detect a single photon in a given time interval has to be much smaller than 1, otherwise the corresponding 'saturation' of the detector corrupts the obtained information After a detection, the APD must be re-initialized to rapidly allow the measurement of other photons arriving. This is done by quenching the avalanche, which can be done actively or passively [56]. If -as in our experiments- the time of arrival of the photons on the APD is known, one typically uses the so called gated mode. Here, the APD bias voltage is raised above its breakdown voltage only during a short gate period, and consequently only during this time interval photons can be measured. At all other times, the APD is operated in standard mode with a reverse bias voltage slightly below the breakdown, inhibiting avalanche formation. The main advantage of gated mode operation is that the number of erroneous counts is very low [55]. To further limit the noise, relatively low repetition rates ($\leq$ MHz) and durations (nsec) for the gate and cooling of the APD (200-300 K) are typically employed.

The choice of the APD to be used as a detector in our setup was a tedious process, as detection efficiency and dark count probability vary from model to model and depend on parameters as gate voltage or APD temperature. Different InGaAs/InP APD from different companies were therefore characterized [57] in order to find the best performances. These results are summarized in Fig. 5.1, where the dark count probability is given as a function of the detection efficiency at different temperatures and for different InGaAs/InP APD's. The figure demonstrates that the quantum efficiency can be as large as 30% with a noise probability of 10^{-2} to 10^{-4} counts per gate of 2.4 ns. The APD we finally used for the NSOM is the one from EG&G (see Fig. 5.1), cooled to -40^o C. The detection efficiency was set to 15%, leading to a noise probability of 10^{-3} counts per 2.4 ns. The gate repetition rate employed in our experiments is 10 kHz, with a gate duration of 40 ns. The number of dark counts was found to be below 250 Hz. From these numbers a sensitivity of 10^{-2} photon per gate can be estimated. Note that the gate can be reduced to as little as 180 ps [55], allowing for time resolved studies.

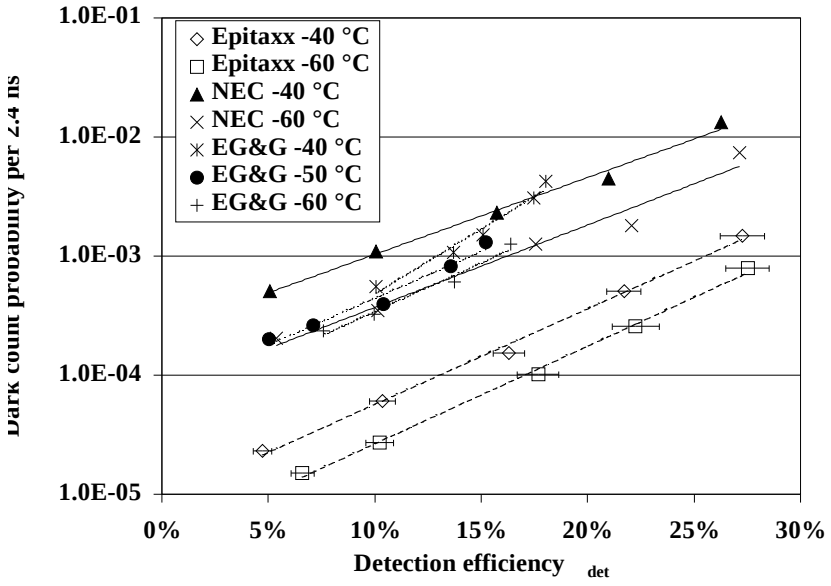

Figure 5.1: Dark count probability as a function of the detection efficiency at 1.55 μm for different InGaAs/InP APD temperatures and models [from Ref.[57]].

The set-up of the driving electronics for the APD is shown schematically in Fig. 5.2. The pulse generator emits at 10 kHz and acts as the timebase of the system. These pulses trigger on one hand the optical source used for the sampling illumination, and on the other hand the voltage generator producing the gate pulse of 4V/40ns. The detection window can be adjusted with respect to the arrival of the photons via a delay generator inserted in front of the voltage generator. In addition to the gate pulse, a continuous voltage offset is put on the APD to optimize both its biasing outside the detection window and the level of the gate voltage. The avalanche signal is detected and registered with the use of discriminator electronics and a counter. A picture of the InGaAs/InP APD module used for the photon-counting NSOM is shown in Fig. 5.3. It includes the Peltier cooling and the detection electronics. The optical source we use in our experiments was a distributed feedback laser (DFB) emitting at 1.559 μm. The pulse duration was set to 100 ns and therefore exceeds the gate duration of 40 ns, creating a quasi-cw illumination. To obtain sufficiently high power levels for the sample illumination, the pulses were consecutively amplified by an Erbium doped fiber amplifier (EDFA) with a small signal gain of 40 dB and a saturated output power of 23 dBm.

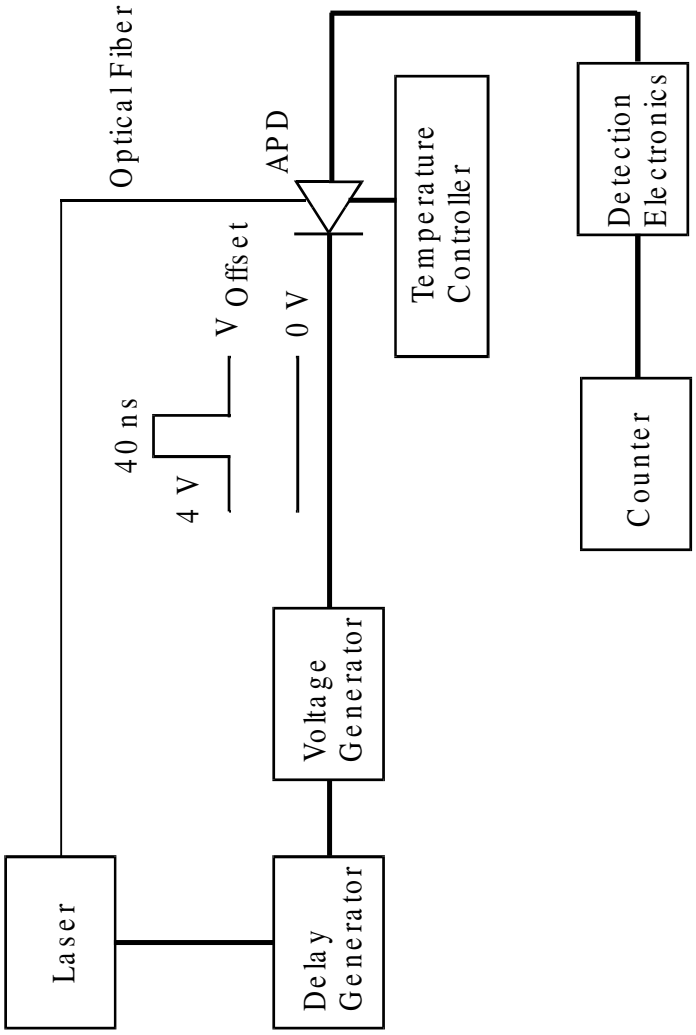

Figure 5.2: Experimental setup. The delay generator is used to trigger the pulsed laser and the voltage generator, such that the gating of the APD coincides with the photons arrival time.

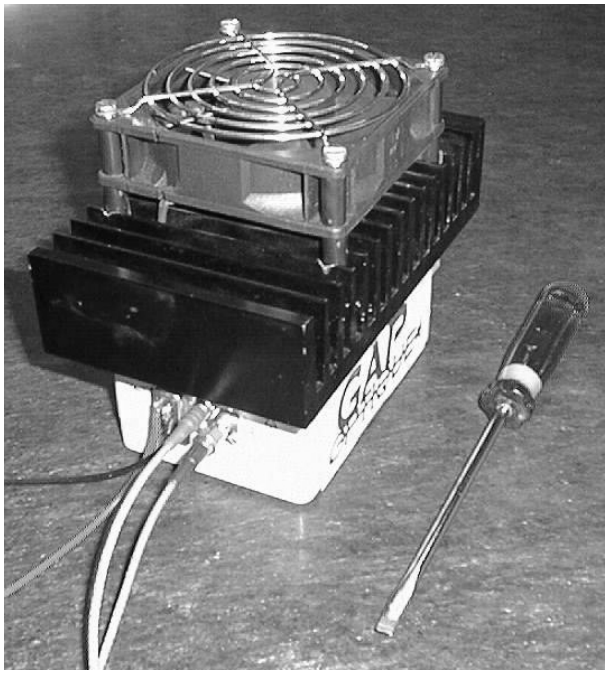

Figure 5.3: Picture of the Peltier cooled InGaAs/InP APD module used for the photon counting NSOM.

5.1.3 Two measurement examples

Optical fiber mode field

As a first test of the 1.55 μm photon-counting NSOM, the mode-field of a single-mode optical fiber (SMF) was measured. Note that this is not a primary application for photon-counting NSOM, as this type of measurement can usually be performed by standard means as well, but rather serves to check the validity of the obtained results.

The measured sample consists of a SMF with a typical diameter of the guiding region (core) of 9 μm. The illumination source is coupled into the SMF with a peak power set to +10dBm. The transverse distribution of the guided light (mode-field) is then measured by performing a near-field scan of the cleaved output surface of the SMF. In order to avoid complete saturation of our high sensitivity photon-counting detection scheme, a loss of 70dB has to be inserted in front of the APD. The result of this scan is shown in Fig. 5.4. As can be seen, the mode is of quite perfect circularity, as expected for a SMF. For better illustration, we choose a slice through the center, along which the measured near-field intensity is plotted (Fig. 5.4). In accordance with the NSOM tip aperture, the spatial resolution is about 100 nm. In order to validate our NSOM measure, a comparative measurement of the mode field using a commercial device (NR 9000 [34]) with specified precision and accuracy was performed. As can be seen in Fig. 5.5, the mode field measured with the NR9000 (bold line) agrees well with our NSOM measurement (open circles), typically to within 10%. From both set of data, a mode-field diameter of 10.0 μm is calculated.

Splice between an Erbium doped fiber and a SMF

In the second measurement example, the splice between an Erbium doped fiber and a SMF is analyzed. It is interesting to look in detail at such a splice as the Erbium ions (and other core dopants like Germanium) are known to thermally diffuse into the cladding material during the splicing process [58]. Control of this diffusion by variation of the splice parameters (electric arc power and duration) allow to better match the mode field in the Erbium doped fiber to the one of the SMF, thereby reducing the transmission loss of the splice.

Our sample consists of a standard SMF spliced to an Erbium doped fiber with a doping concentration of 2000 ppm. The splice region was stripped by mechanically removing the protective plastic coating before the splicing. For the measurements, the

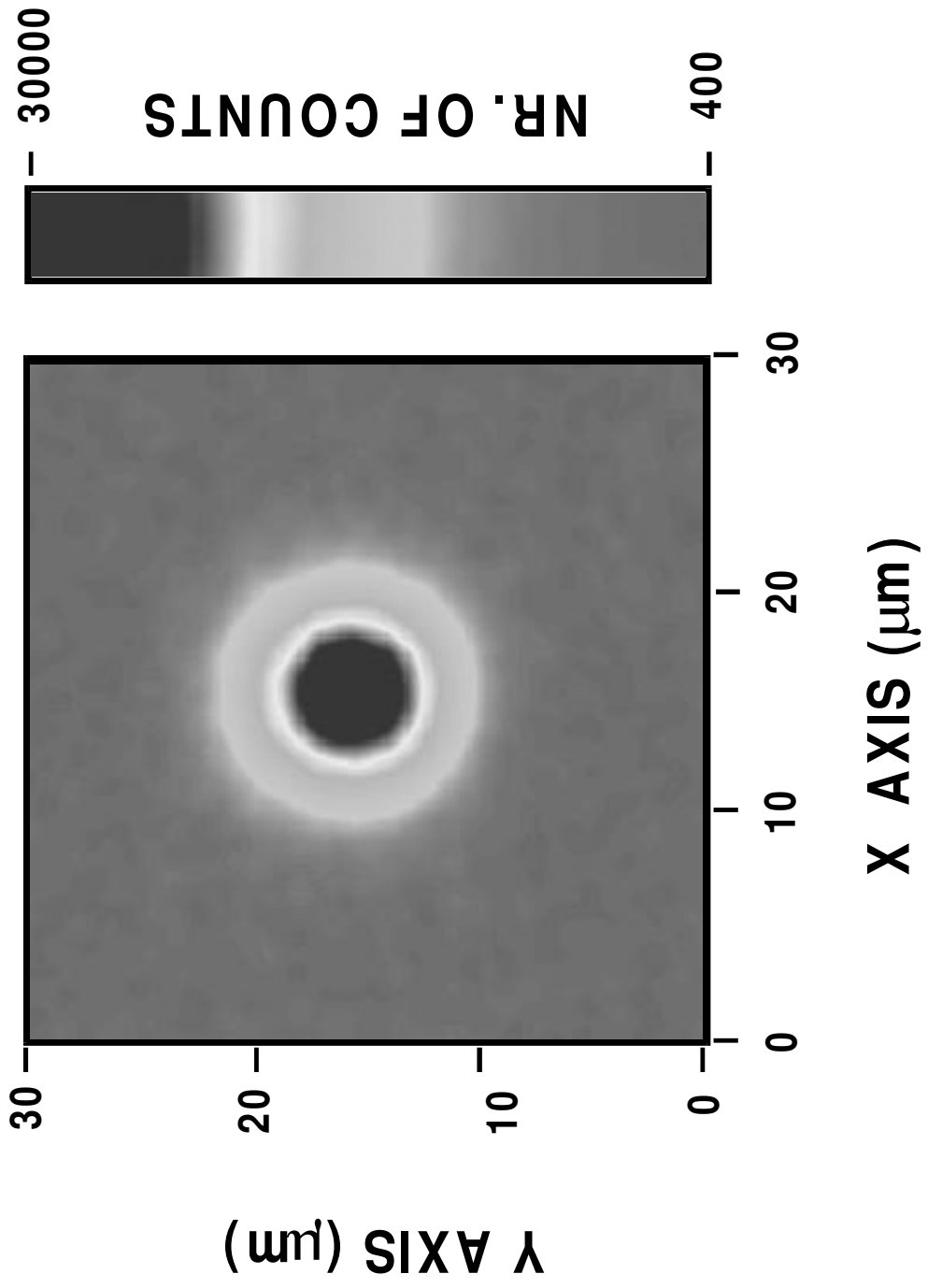

Figure 5.4: Near field image of the mode field at the exit of a cleaved SMF.

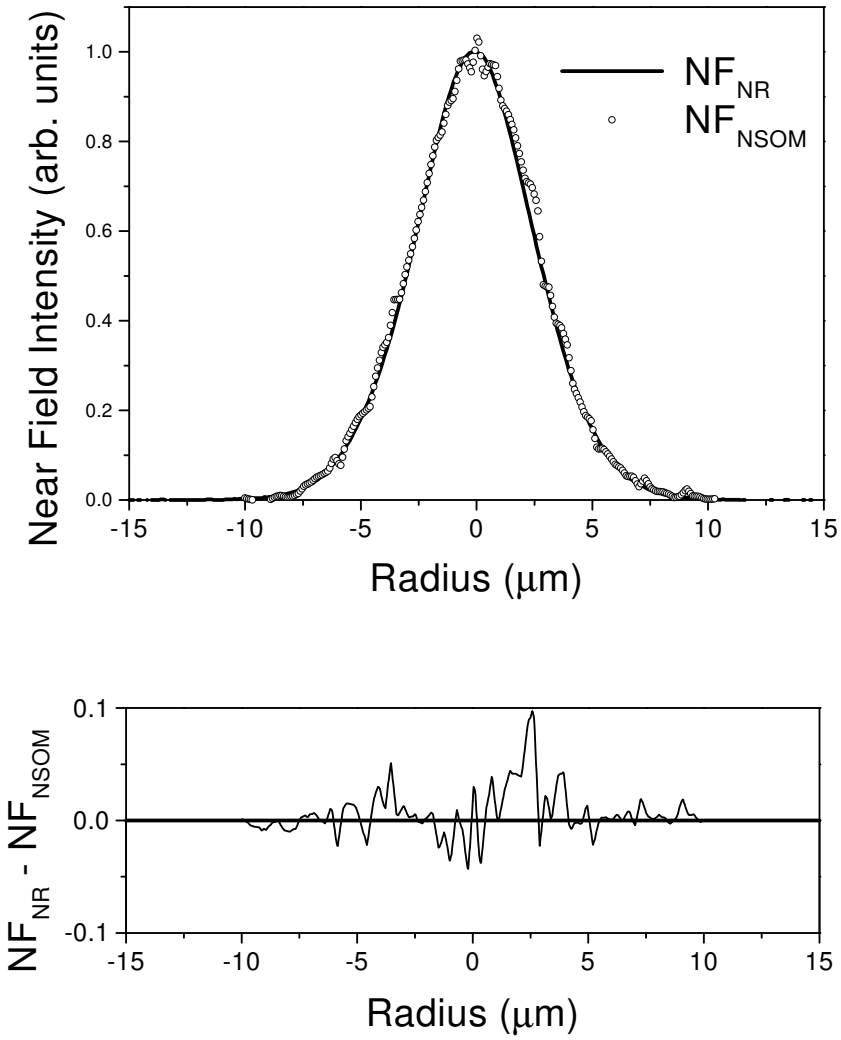

Figure 5.5: Plot of the measured near field intensity along a slice through the center of the fiber. Open circles: NSOM measurements, bold line: measurements with a commercial device [NR9000 Ref.[34]].

NSOM tip was brought close to the cladding surface, and the NSOM was operated in collecting mode to image the light scattered out sidewards of the test fibers (see Fig. 5.6). Along with the optical measurements, a topographical scan of the splice region was performed. This both allows to correctly locate the tip with respect to the fiber sample and to monitor eventual defects in the fiber surface. A typical result of such a topographical scan is shown in Fig. 5.7. The fiber was aligned along the y axis, and the xyz stage of the NSOM allowed for a scan of about 70 μm along x and y axes (top). As the figure demonstrates, the splice topography is completely homogeneous -both the SMF and the Er doped fiber have cladding diameters of 125 μm- and no surface damages or irregularities were detected. Consequently, we can be sure that the optical information is not deteriorated by irregular scattering or diffraction from surface defects.

For the optical scan, the 1.55 μm light source was coupled into the SMF with a peak power of 2.5 W. The result for the splice region is shown in Fig. 5.8. The amount of light collected from the Erbium doped fiber (top) is clearly much larger than the one from the SMF, as the spontaneous emission of the Er ions activated by the 1.55 μm illumination adds to the Rayleigh scattered light. In fact, the collected light stems almost uniquely from this luminescence, as insertion of a filter at the pump wavelength in front of the APD did not lead to significant changes. Also, variation of the delay time of the gate with respect to the pump pulses did not lead to apparent modifications either. The amount of collected light is therefore constant, independently of the presence of a pump pulse at the time of detection - a consequence of the long life time of the Er ions of 1 ms. From Fig. 5.8, it can also be seen that the spatial resolution is not outstanding. The small aperture of the employed tip of 100 nm is not suited for far-field detection. It leads to a large field of view, which -together with the distance of the tip to the region of interest (about 70 μm)- is the cause for the observed resolution exceeding 60 μm. Moreover, the NSOM tip was not coated, allowing photons to penetrate the tip from the side. This might explain the multiple images apparent in Fig. 5.8 along the x axis, and the fact that the maximum power is not detected in the center of the fiber.

We therefore replaced the NSOM tip with a regular, non-tapered fiber with a small mode-field diameter of 5.5 μm. From the numerical aperture of 0.26, a resolution of 40 μm is predicted at the core region of the fiber sample. The corresponding scan is shown in Fig. 5.9. As can be seen, the multiple image structure is now absent, and the collected light power peaks in the center. The observed width of the luminescence is in good agreement with the one predicted from the calculated spatial resolution. The

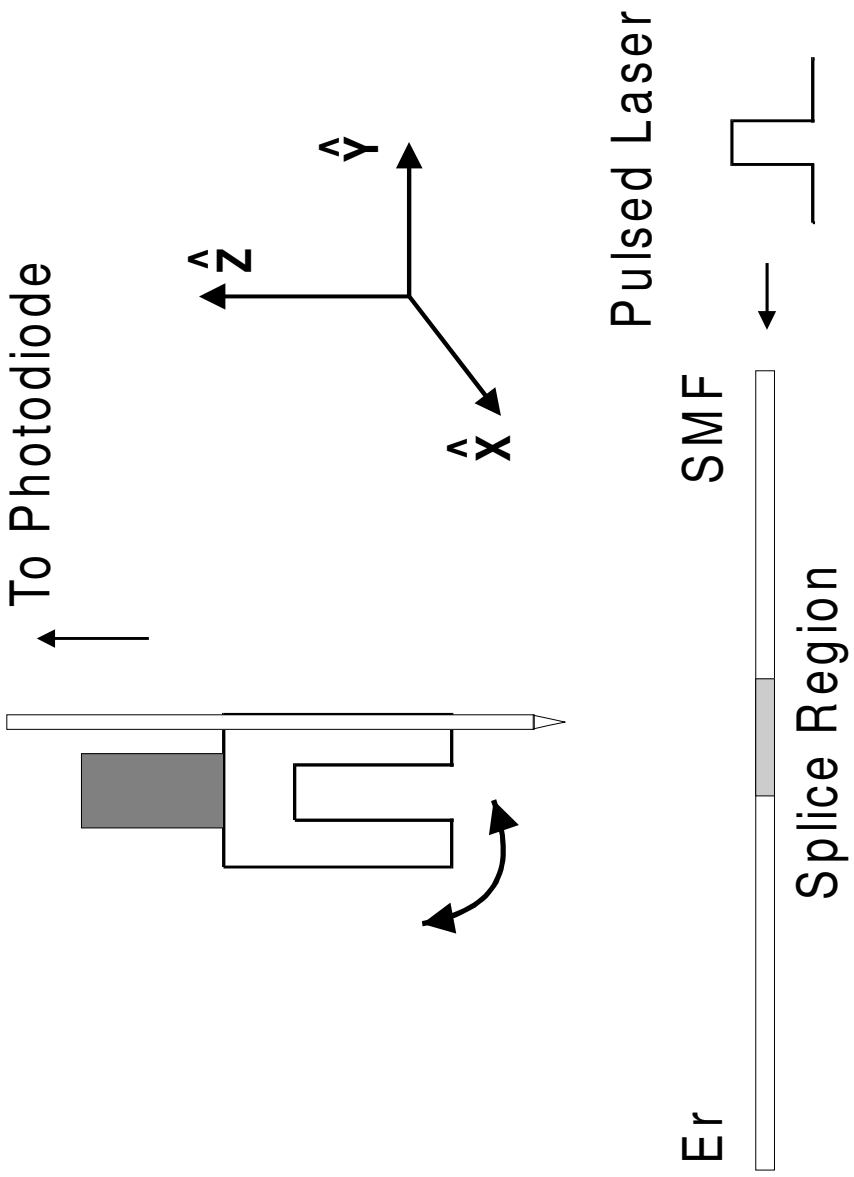

Figure 5.6: The pulse laser source is coupled into the sample under test. The scattered (or luminescent) light is detected by a tapered fiber tip mounted onto the NSOM tuning fork.

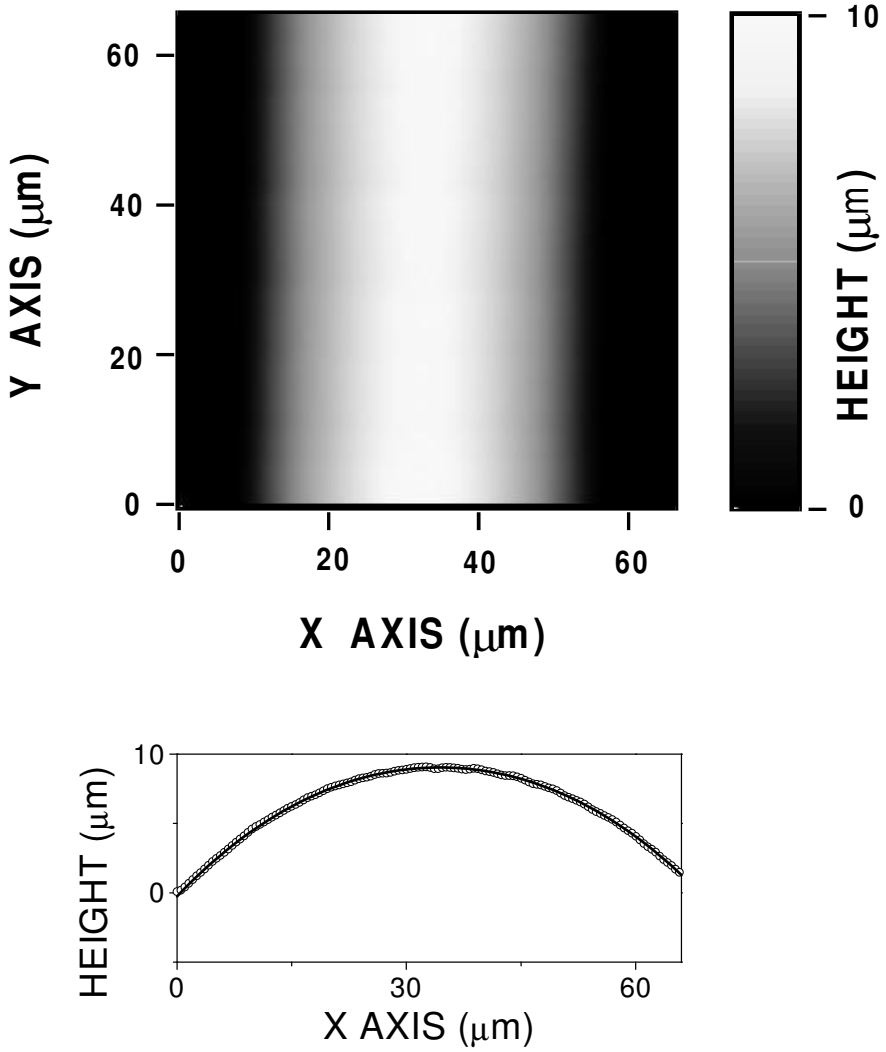

Figure 5.7: Topographical scan of a splice between a standard telecom fiber and an Erbium doped fiber (2000 ppm). The fiber axes are along the y axis, with the Erbium doped fiber on top of the SMF (the splice region is somewhere between 10 and 50 microns). The measured height as a function of the x location is given at the bottom of the figure. Open circles: experimental data, bold line: circular fit.

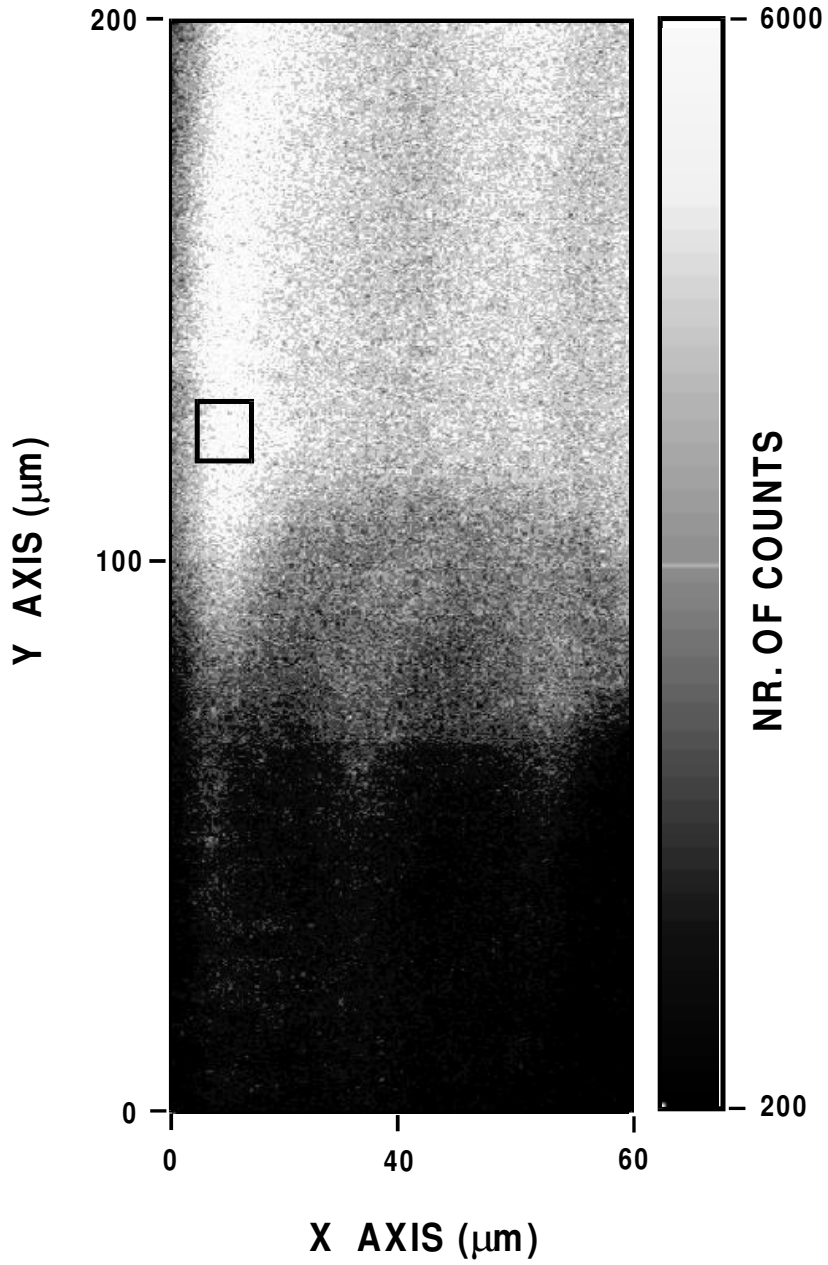

Figure 5.8: Optical image of the splice of Fig. 5.7. The signal of the Erbium fiber is much brighter due to luminescence. Experimental parameters: gate frequency 10 kHz, gate duration 50 ns, dark count rate smaller than 250 Hz.

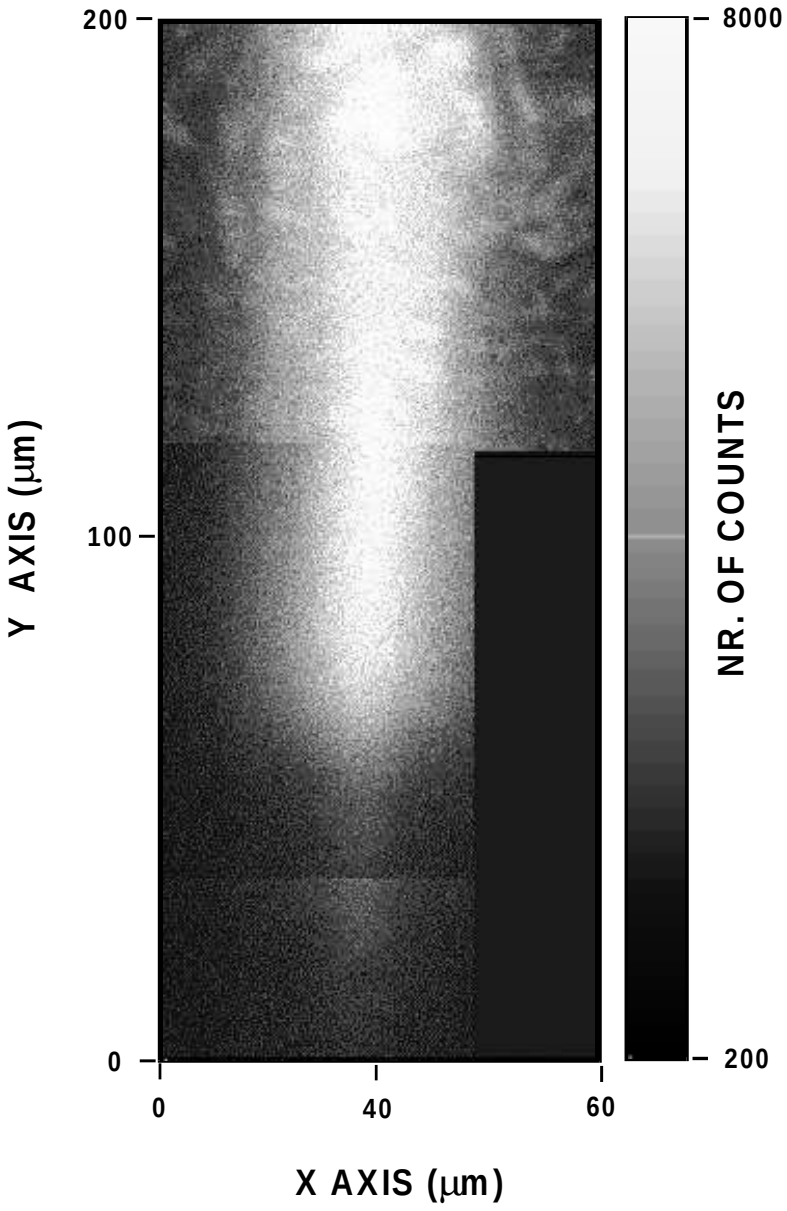

Figure 5.9: Same as Fig. 5.8. Instead of a chemically etched tip, a cleaved fiber with a mode field diameter of 5.5 μm was used for light collection.

transition region between the Er doped and the SMF fiber is smeared out by the same effect. Therefore, one can only conclude from Fig. 5.9 that the Er diffusion length was inferior to 40 μm.

To get more detailed information, a tip with better collimation (e.g. a fiber with a grin lens) could be used to further optimize the spatial resolution. Work in this direction is in progress.

5.1.4 Conclusion

In conclusion in this section we have presented a new system that combines near-field scanning optical microscopy (NSOM) with single photon counting at the wavelength of 1.55 μm. The quantum efficiency of the APD's operating at a temperature of 230 K is 15%. With a gating frequency of 10 kHz and 40 ns gate duration the dark count rate is as low as 250 Hz, leading to a sensitivity of 10^{-2} photon per gate. The timing resolution of the InGaAs/InP APD of better than 180 picoseconds [55] indicates the possibility to employ the microscope for time correlated single photon counting for time resolved measurements [59].

Promising applications of the 1.55 μm photon counting NSOM are in the field of telecom, in high resolution photoluminescence measurements for the study of quantum structures emitting at 1.55 μm, or in the investigation of biological samples. In this chapter we monitored the splice region between an Erbium doped and a SMF fiber, and found the thermal diffusion length to be below 40 μm.

5.2 Distributed gain measurements in Er-doped fibers with high resolution and accuracy using an optical frequency domain reflectometer.

5.2.1 Introduction

We report on distributed gain measurements in Er-doped fibers. It is well known that for critical Erbium doped fiber amplifier design, e.g. gain tilt optimization in WDM booster amplifiers, knowledge of the gain distribution within the active fiber can present a valuable information. Among the different techniques to evaluate the distributed gain in active fibers, the technique of optical frequency domain reflectometry seems most promising as it is a nondestructive measurements method well matched to the task due to its dynamic range, resolution and range. Moreover the background ligth from ASE or residual pump light is strongly rejected due to the coherent detection scheme employed. Using different Erbium-doped fibers with strongly varying doping levels and confinements, we demonstrate the excellent accuracy and reproducibility of the technique. More details can be found in the article reported in Appendix A.5.

5.3 Analysis of the polarization evolution in a ribbon cable using high-resolution coherent OFDR.

5.3.1 Introduction

We exploit the inherent polarization dependence and good spatial resolution of optical frequency domain reflectometry in order to measure the beatlength in a ribbon fiber. The results obtained clearly show the different amount of polarization ordering for inner and outer ribbon fibers due to the stress-induced birefringence from the common outer coating. More details on the work done can be found in the article reported in Appendix A.6.

5.4 First and second order PMD emulator

5.4.1 Introduction

We have built a PMD emulator where the DGD and the ratio between first and second order PMD can be set by the user. Contrary to approaches which try to mimic a standard fiber as closely as possible, our emulator gives one (adjustable) value for the PMD. This allow to directly determine the maximum (instantaneus) values for first and second order PMD for a given permissible system impairment. More details on the work done can be found in the article reported in Appendix B.10.

Appendix A

ITU Round Robin (Step-by-step measurement procedure)

A.1 Introduction

In the following we are going to give a step by step procedure in order to build the setup described in chapter 2. Moreover we give the exact measurement sequence and procedure in order to make the measurements for the n_2/A_{eff} and how to treat the data. This procedure was always followed for all the measurements made in particular for the ITU Round Robin coordinated by Prof. Y. Namihira.

A.2 Components

The following is the list of the components used to make the experiment.

1. Coupler 50/50 Serial Nr. GAP 1061
2. Polarization Controller Serial Nr. GAP 1104
3. Coupler 90/10 Serial Nr. GAP 1035
4. Fiber Bragg Grating filter 3M Part. No. CS-96-6192 Serial No. 6096-3013 Fiber Type CS-96-1914.
5. Fiber optical circulator Serial Nr. GAP 1050
6. Faraday Mirror Serial Nr. GAP 1048
7. Erbium Doped Fiber Amplifier IRE-POLUS 23 dBm Model EAD-200
8. Thermoelectric Control Unit Model 902 A
9. DFB laser Mitsubishi FU-689DF-V5M83A Nr. 982276
10. Power supply

11. Stanford pulse generator Model DG535. Load High impedance. Exit AB positive. 50 Ohm load on exit AB negative. Signal at +1.90 and offset at -1.80.
12. Amplified photodetector Newport Model AD 300/AC 300 ps
13. Oscilloscope Tektronix TDS 580C
14. Fiber splicer Ericsson set on program nr. 2
15. Power meter Wandel/Goltermann Model OLP-18
16. Variable attenuator EXFO FVA 60B
17. One plastic box

In Fig. A.1 is shown the picture of the interferometer. The black points represent the splices reported in Fig. A.3. In Fig. A.2 is shown the picture of the setup used to make the measurements of the n_2/A_{eff} for the ITU Round Robin.

A.3 Characteristics of the laser and of the Bragg grating

The laser is centered at 1558.98 nm with a spectral linewidth of 20 MHz and is made to be operated at 2.5 GHz. CW power can be as high as 10 mW.

The Bragg grating is centered at 1558.81 nm with a bandwidth of 1.63 nm and a reflectivity of 63 dB.

A.4 Building the Setup

In Fig. A.3 is shown the setup used in order to make the measurements of the n_2/A_{eff} for the ITU Round Robin. The black circles indicate the points in which a splice was made and in which it is necessary to make measurements of power in order to estimate the losses of our interferometer. Note that a description of the components is not anymore necessary due to the fact that it is reported in Fig. 2.3.

First of all we have to find out how much is the power we have at the exit of the laser . To do this we use a power meter and we measure the power at the point 1 of the IF. Note that the laser is working in pulsed mode so the measured power is the average power. To convert to the peak power we have to use the formula

$$W_{avg} = W_{peak} \cdot \tau \cdot \nu$$

where W_{avg} is the average power, W_{peak} the peak power, τ the pulse width and ν the repetition rate of the pulse. Now we have to make different measurements of power changing both τ and ν such that their product is constant (i.e. the peak power). In this way we can find out if our power meter gives consistent results. The measurement

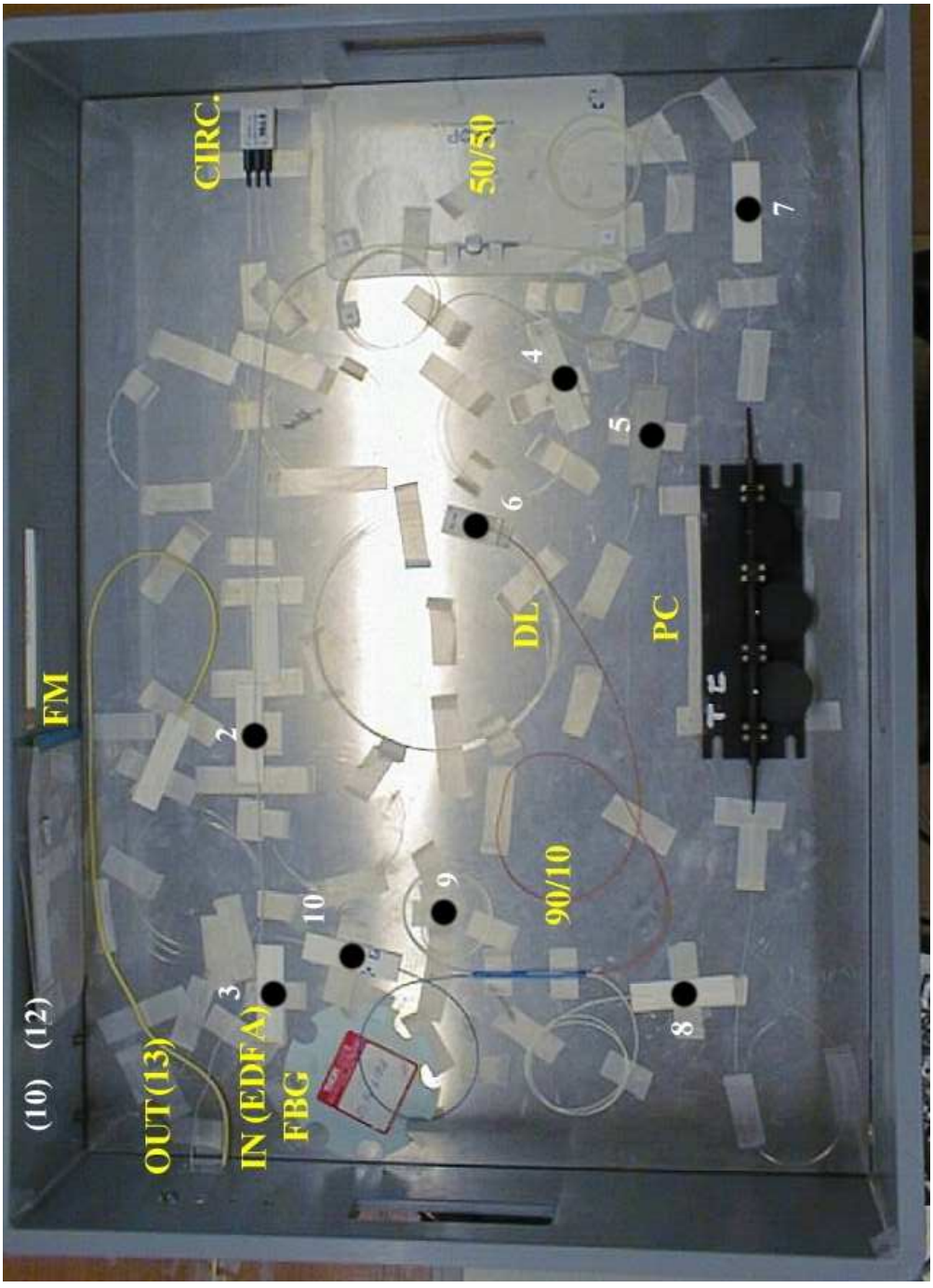

Figure A.1: In the figure is shown the picture of the interferometer used to make the measurements of the n_2/A_{eff} for the ITU Round Robin. Black circles represent the splice points.

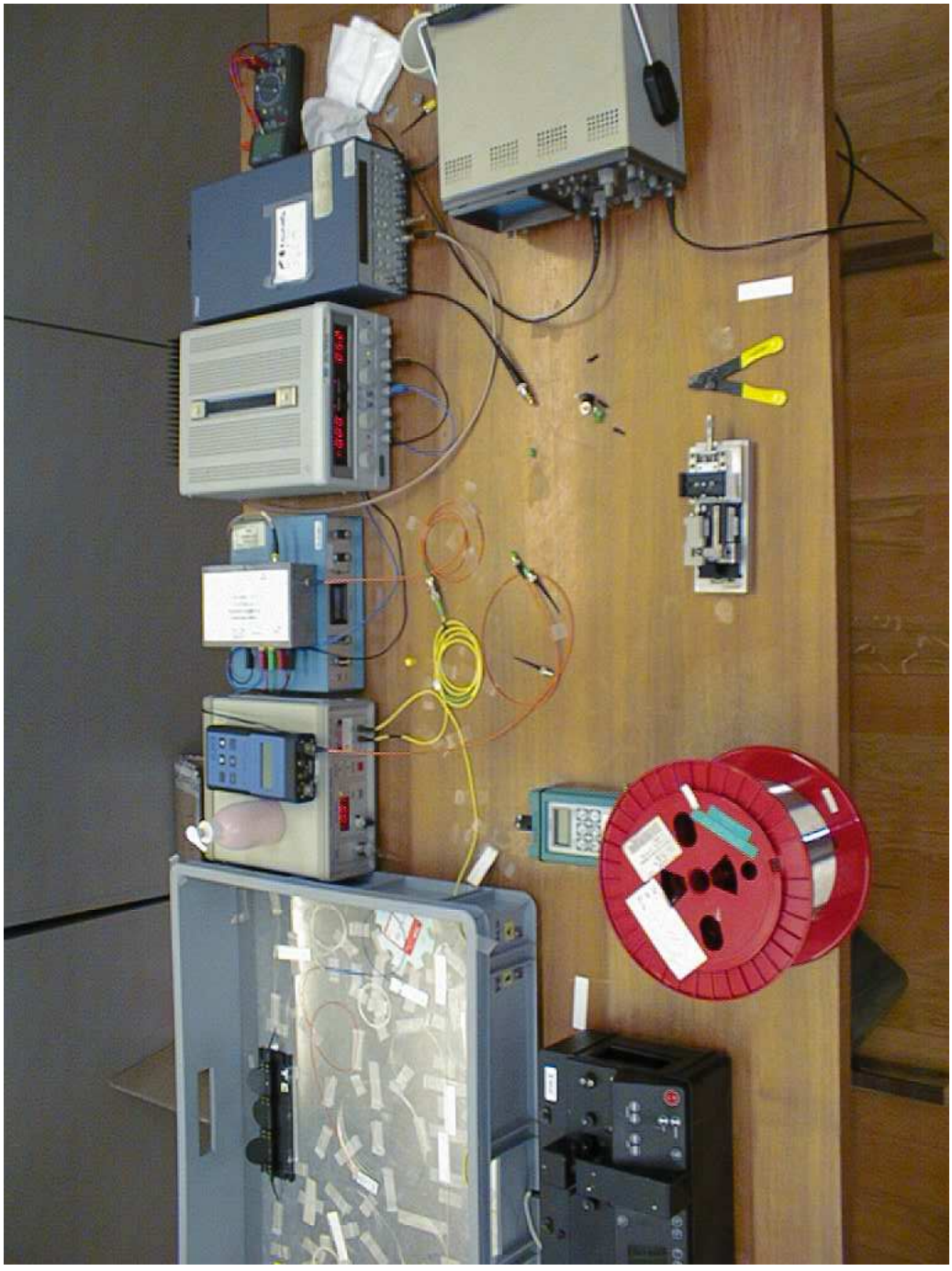

Figure A.2: In the figure is shown the picture of the setup used to make the measurements of the n_2/A_{eff} for the ITU Round Robin.

of power we have made, are done with a frequency of 10kHz and a pulse width of 20 nsec. From this values we can find out what is the peak power and later calibrate our fast photodiode. An error at this point can introduce a systematic error on all the measurements and consequently on the n_2/A_{eff} values.

Now we build the setup as shown in Fig. A.3. We measure the power at 1 (exit of an angled connector) and then we enter into the EDFA. The fiber cable connecting the laser to the EDFA has to be fixed with tape on the table. From the EDFA we have to clean the signal (too much ASE coming from the EDFA) so we enter the optical circulator splicing the fiber coming out from the EDFA to the fiber at the entry of the circulator (point 2). Here we go into the fiber Bragg grating splicing at point 3. The reflection (i.e. the laser signal) is then measured at point 4. Here we have to measure the peak power value. In principle it is not necessary to know how much power we have lost in the splice and connections before, because the power at 4 is the power we consider as the entry power of the interferometer.

Due to the fact that the laser is not exactly matched on the fiber Bragg grating we have to tune its wavelength with the thermoelectric unit. This can be done taking the light at point 4, splicing the fibers at a pigtailed fiber, entering the fast photodiode and monitoring the pulse shape on the scope as a function of the set temperature on the thermoelectric unit. The value used during the measurements is 31.5 Celsius.

After this we have to enter the first coupler (50/50). We measure the power at points 5 and 7 and find out what are the losses and the coupling ratio of the coupler. Then we consider arm 5/6. We have to insert here a delay line in order not to make overlap the pulses (see chapter 2.2). We measure the power at 5 and at 6 and find the loss of the delay line plus splice 5. Then we splice at 6 the 90 entry of the 90/10 coupler and we measure the power at 9 and 10. Then we measure the power at 7 and 8 and we find the loss of the polarization control and splice 7. Then we enter the 10 entry of the 90/10 coupler. We measure the power at 10 and 9. Using the information of before we find the losses and coupling ratio of the 90/10 coupler and losses of splices 6 and 8.

Then we have to characterize the losses of the faraday mirror. To do this we splice the FM directly at 10 without any FUT and measure the power at 13. The loss of the FM (β'') is equal to 1.77 dB.

The results for the interferometer once built up are the following. First of all the losses in the arms are symmetric. Second the power at 10 is equal to 1/2.23 the power measured at 4. From now on we never measure the power at point 4, because we should rebuild the setup every time. But instead we measure the power at point 10 and from this we calculate the power at the entry 4. Point 13 is connectorized.

All the fibers and components have to be attached onto a robust plate in order not to introduce any change in the polarization. Once built the setup is stable over months.

Note that the coupler's fibers are characterized by different colors. Regarding the 50/50 coupler splice 4 at fiber A. Splice 13 at fiber B. Splice 5 at fiber C. Splice D at fiber 7. For what concern the 90/10 coupler, splice 6 at fiber ORANGE. Splice 8 at fiber WHITE-ORANGE. Splice 10 at fiber BLUE. Splice 9 at fiber WHITHE-BLUE.

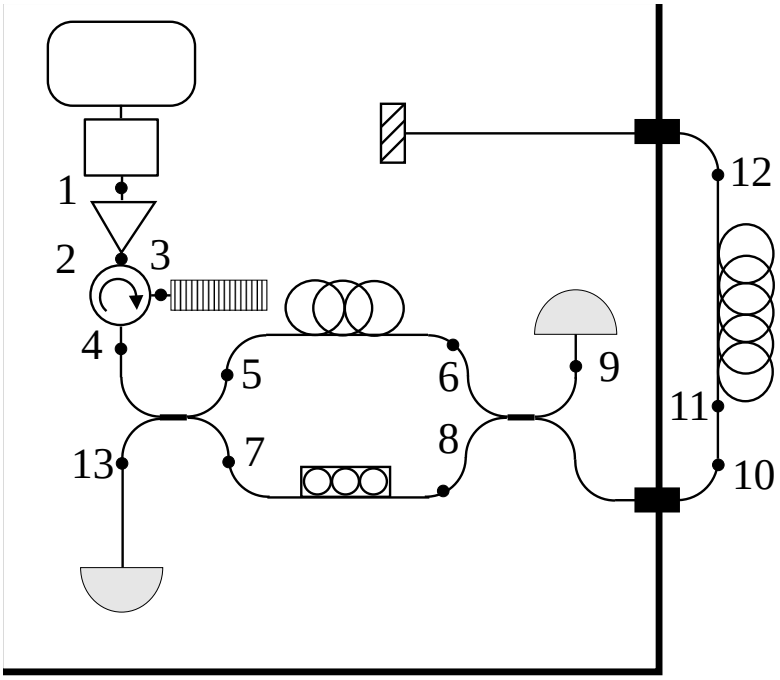

Figure A.3: In the figure is shown the setup used to make the measurements of the n_2/A_{eff} for the ITU Round Robin. The black circles indicate the points in which is crucial to make loss measurements.

A.5 Calibration of the Photodiode

Before we have measured what is the peak power at the exit of the laser. Now we calibrate the fast photodiode. To do this we use a variable attenuator. We measure the power at 1 (it is connectorized). We enter the attenuator. From here we exit with a connectorized fiber. We measure the introduced loss (loss of the connector plus loss of the attenuator) setting the attenuation to zero. Then we check the linearity of the variable attenuator changing the attenuation and measuring the power at the exit of it. The chosen attenuator is very good and the displayed difference in the set power are equal to the real ones (but not the absolute value of course). Then we enter the photodiode and we change the attenuation. We measure on the scope the pulse profile. We acquire the data and elaborate them on a pc. The pulse is not squared as it is possible to see from Fig. A.4. We consider as the height of the pulse the height of it at half width. The value we obtain is in mV. Knowing the value in dBm at the entry of it we can find the factor that transforms the value from mV into dBm. Changing the attenuation we can find until which value the photodiode is linear. The conversion factor η is equal to 264.2. The linearity is valid till 500 mV. As a rule never go above 300 mV.

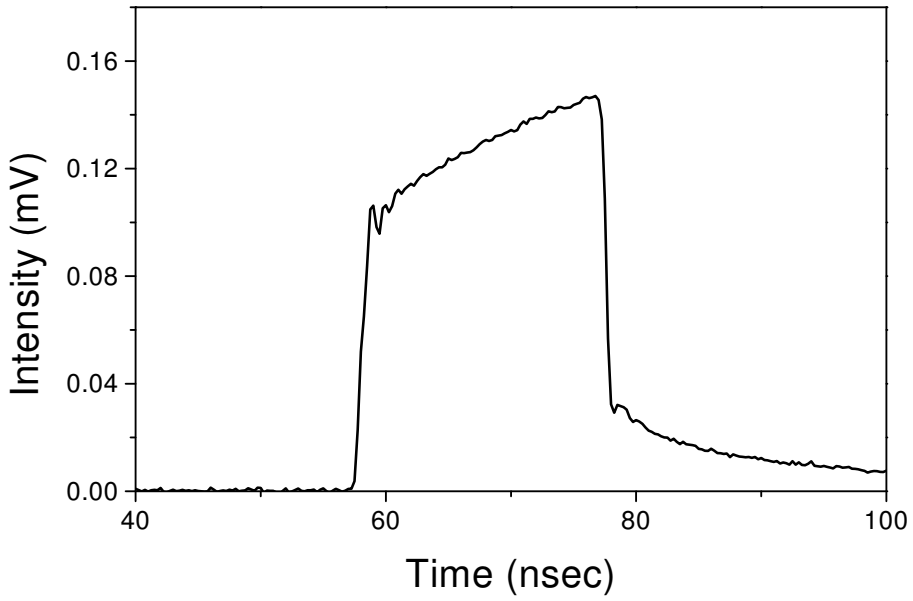

Figure A.4: In the figure is shown the pulse profile as registered from the scope. The pulse is a little irregular. The heigth of the pulse is always considered as the height at half width.

A.6 Measurements

In order to do a measurement it would be good to check with an old fiber that we will obtain the same data as the old ones.

First of all we have to let to heat all the components. We turn on all the equipments and we let it there with a set current on the amplifier at 320 mAmp.

Then we measure the power at point 10 (the average is ok). We splice a piece of the FUT we want to measure. We then measure the power at point 11. We find the coupling loss (the fibers have different diameters). This value is called β. Usually a splice that presents itself good from a visual point of view, it is a good one. So repeat till you reach a good uniformity along the splice length. Then remove the spliced fiber and splice directly the FUT. Measure the power at 12 and find the attenuation of the fiber. This value is called β'. Then the light goes to the FM and pass back into the splice 12. We assume (the fiber we used for our IF is a fiber with a large effective area) that losses are coming only from large to small coupling. This means direction 10 to 11 or 12 to 11.

Now we have to arrange the polarization controller of the IF such that we have maximal interference when no nonlinearity is present (see chapter 2.2). To do this we connect 13 to the fast photodiode. We set a value low in the current on the amplifier (typically 230 mAmp) and we adjust the polarization controller such that the middle pulse on the scope will reach its maximum. Consider 13. Note that we do not have

to know the losses because is the relative power that is interesting to measure here. So we enter an attenuator and we fix an attenuation high enough to remain inside the linearity of the photodiode. Increasing the current of the EDFA the intensity will increase and so the amount of nonlinearity acquired. We write the value of the current and we acquire the pulse profile on the scope. Usually take ten points till you reach an amplification such that the pulse decreases till goes to zero. Note there are three pulses on the scope. Measure the second one.

After this we have to know how much was the power we sent into the interferometer. But as mentioned before we do not measure at point 4 but at point 10. We measure the power at point 10, we splice a pigtailed fiber, we enter a variable attenuator and then we measure the power. We find out what is the attenuation. Then we enter into the calibrated fast photodiode. The total attenuation α_1 has to be such that we have pulses with height below 300 mAmp. Then we set the current on the EDFA such that the values are equal to the one used before for the measurement. And we acquire the pulse profile. There are two pulses. You measure the second one.

To note that every time you make a measurement of losses as a reference you use 31.5 celsius on the thermoelectric unit, and 320 mAmp on the EDFA. Moreover when you make a measurement let the amplifier on the new current value for one minute in order to let it stabilize.

A.7 Elaboration of the Data

Convert the data in ascii format. Use an appropriate software to treat the data (for example Origin). For each current value there is a correspondent pulse profile. Subtract the background from the pulse profile. Measure the height at half width. Take the values and multiply them by the attenuation factor α_1. Multiply the value by 2.23. Divide the value by 262.2. The value you obtain is in Watts.

As an example we consider the calibration done December the 6th, 2001, for the measurement of fiber ITU L-1. In table A.1 we report in the first column the current set on the EDFA in mAmp, in the second column the height at half width of the pulse in V, in the third column the value corrected by the attenuation factor α_1, in the fourth column the values (mW) are corrected by the calibration factor η, in the fifth column there is the correction of the interferometer (2.23) because we want the power at point 4.

The conversion curve is given in Fig. A.5.

Now we treat the data relative to the fiber. Take the pulse profiles, subtract the background and find the height at half width.

Here no conversion into Watts is necessary. It is enough to know the values in arbitrary units. There is a correspondence now between the interference signal and the entry peak power at 4. We have to fit the data using the theoretical equation. Note that in the theoretical equation Eq. (2.4) no losses are taken into account. But we have three different kind of losses. Coupling loss β, attenuation loss β', and FM loss β''. So we find

I (mAmp)	I_0 (V)	I_1 (V)	I_2 (V)	I (W)
300	0.0028	2	0.01	0.02
310	0.0067	6	0.02	0.05
319	0.0126	11	0.04	0.09
330	0.0237	21	0.08	0.17
340	0.032	28	0.11	0.23
360	0.053	46	0.17	0.39
370	0.061	53	0.2	0.45
390	0.074	64	0.24	0.54
410	0.085	74	0.28	0.62
430	0.094	82	0.31	0.69
460	0.106	92	0.35	0.78
490	0.117	102	0.39	0.86
530	0.129	112	0.42	0.95

Table A.1: Experimental values for the calibration of the photodiode. See text for explanation

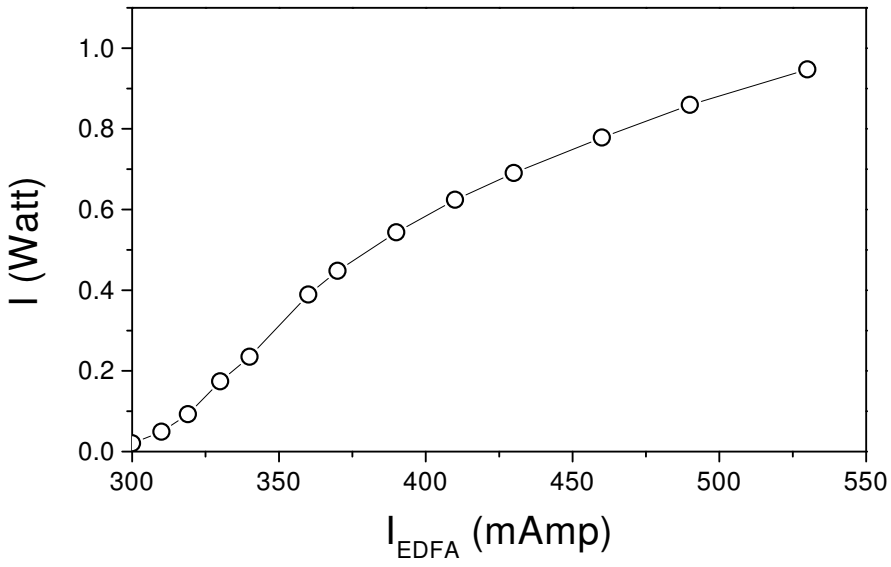

Figure A.5: In the figure is shown the conversion curve from current set on the EDFA and the power in Watts at the entry of the IF.

first the efficient length L_{eff}. Take the attenuation loss of the fiber β' and divide it by the length of the fiber. We obtain the attenuation factor α in dB/km. Then we divide this value by 4.343 and obtain α expressed in km^{-1}. The efficient length L_{eff} is equal to:

$$L_{eff} = \frac{1}{\alpha}(1 - exp(-\alpha \cdot L))$$

where L is the length of the fiber in km, and α is expressed in km^{-1}.

Then we calculate a new L^*_{eff} that takes into account that we have a double pass of the FUT and of the coupling and FM losses.

$$L^*_{eff} = \left(1 + \beta^2 \cdot \beta' \cdot \beta''\right) \beta \cdot L_{eff}$$

At this point we can fit the data with the following function with two free parameters A and n_2/A_{eff} :

$$y = A \cdot x \cdot cos^2\left(\frac{0.1472 \cdot x \cdot L^*_{eff} \cdot \frac{n_2}{A_{eff}}}{2000}\right)$$

where A is a normalization factor.

Usually take at least two measurements on the same fiber in different days and check that you obtain not the same values of itnensity (because they depend on the splice quality of that day) but of the value n_2/A_{eff} . Examples of data acquisition for all the different fibers of the ITU Round Robin are shown in Appendix A.8.

The values of the determined n_2/A_{eff} values are reported in tables A.9.

A.8 Experimental data ITU Round Robin

Here are shown the data relative to the measurements made on the fiber for the ITU Round Robin. For each fiber two measurements were taken in two different days. Every time a new set of measurements was taken a calibration was made. In the figures are reported the data for the L^*_{eff}, for the χ^2, for the n_2/A_{eff} and for the n_2. In figure A.22 is shown a comparison between two measurements taken at a distance of several months on the same fiber but after having rebuilt the setup from scratch. It results that the data are very well reproducible.

Data concerning the measurements:

- December, 6th 2001
  - Fiber NTT #1
  - Fiber 1-L
  - Fiber 2-L
  - Fiber 3-L
  - Fiber 4-L
- December, 7th 2001
  - Fiber NTT #1
  - Fiber 2-L
  - Fiber 5-L
  - Fiber 6-L
  - Fiber 7-L
  - Fiber 8-L
- December, 8th 2001
  - Fiber 2-L
  - Fiber 1-L
  - Fiber 3-L
  - Fiber 4-L
  - Fiber 5-L
  - Fiber 6-L
  - Fiber 7-L
  - Fiber 8-L

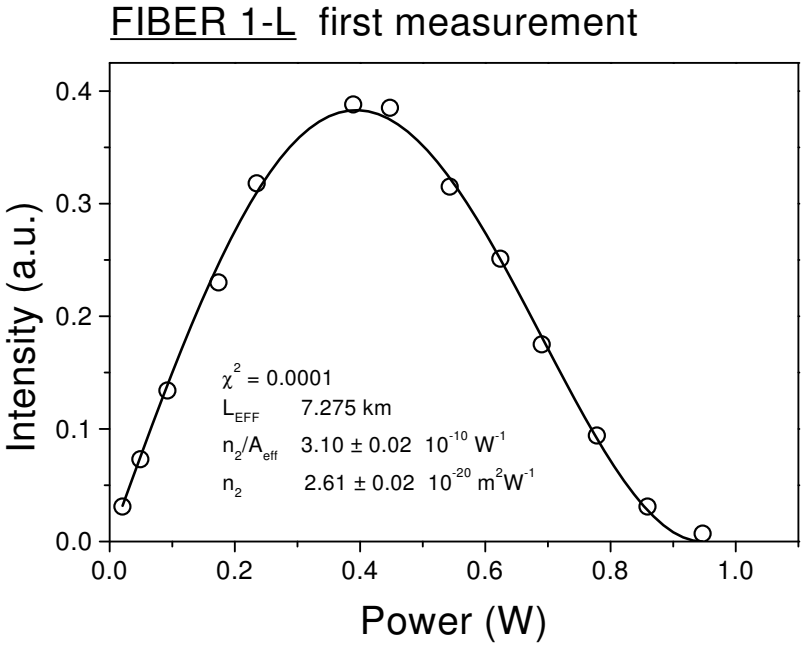

Figure A.6: Detected interference signal power as a function of launch power: (open circles) measured data, (solid line) theoretical fit. Fiber 1-L, measure nr.1.

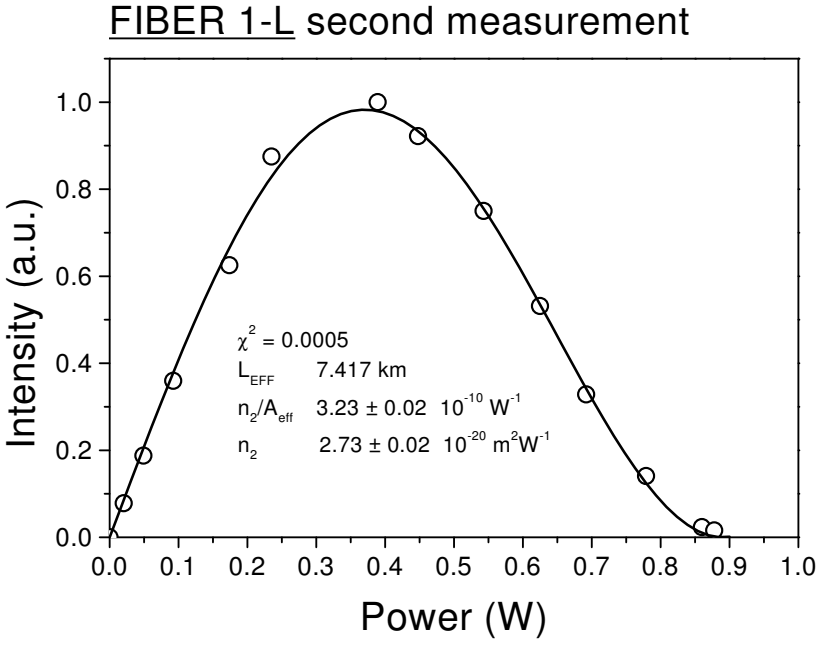

Figure A.7: Detected interference signal power as a function of launch power: (open circles) measured data, (solid line) theoretical fit. Fiber 1-L, measure nr.2.

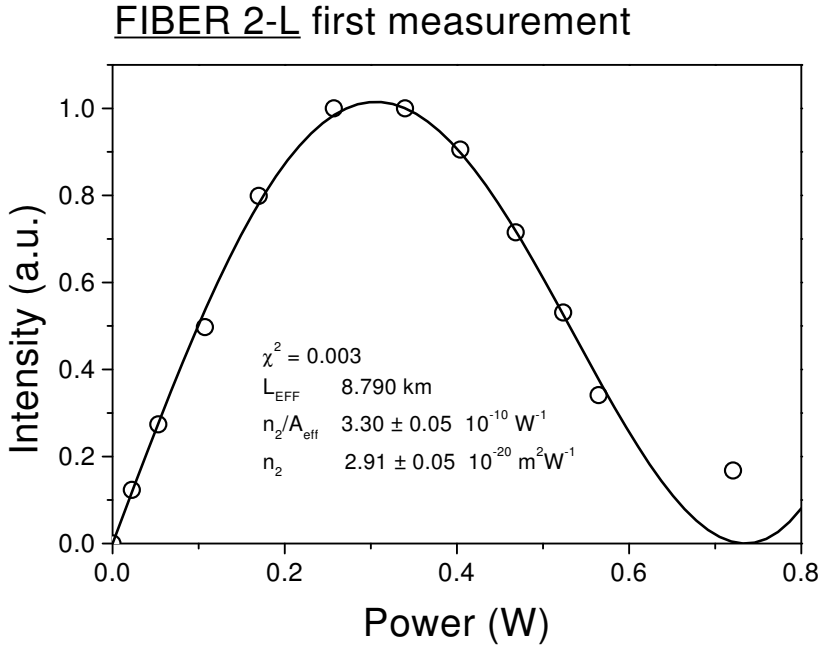

Figure A.8: Detected interference signal power as a function of launch power: (open circles) measured data, (solid line) theoretical fit. Fiber 2-L measure nr.1.

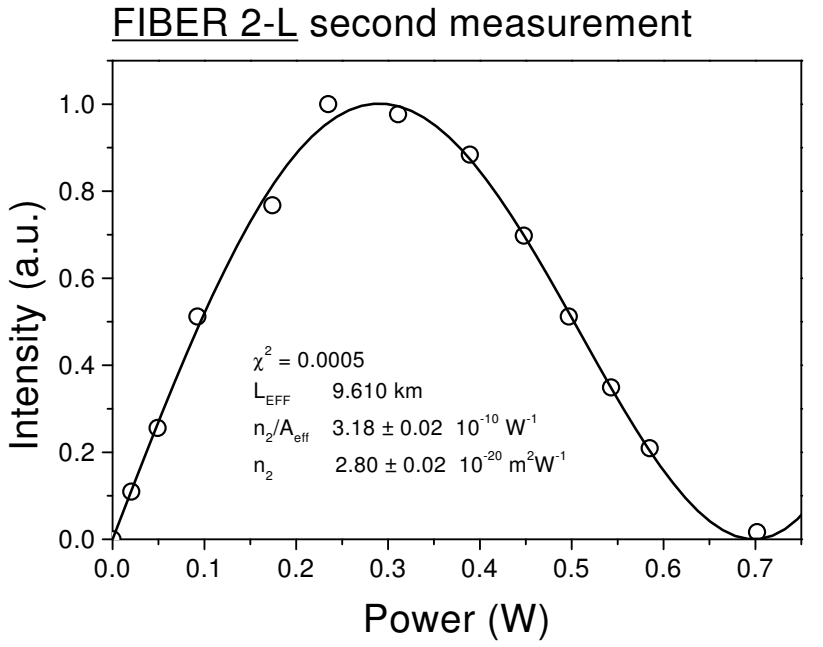

Figure A.9: Detected interference signal power as a function of launch power: (open circles) measured data, (solid line) theoretical fit. Fiber 2-L measure nr.2.

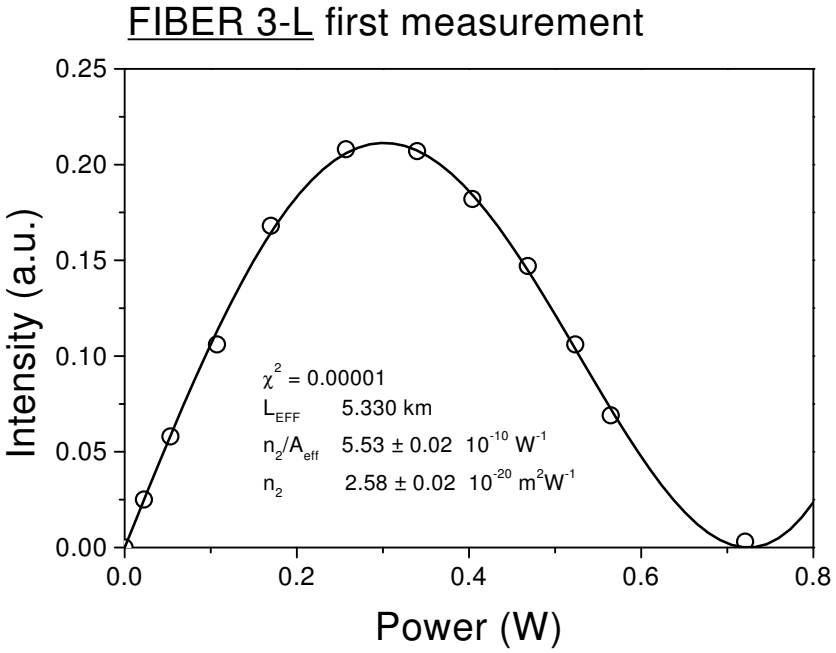

Figure A.10: Detected interference signal power as a function of launch power: (open circles) measured data, (solid line) theoretical fit. Fiber 3-L measure nr.1.

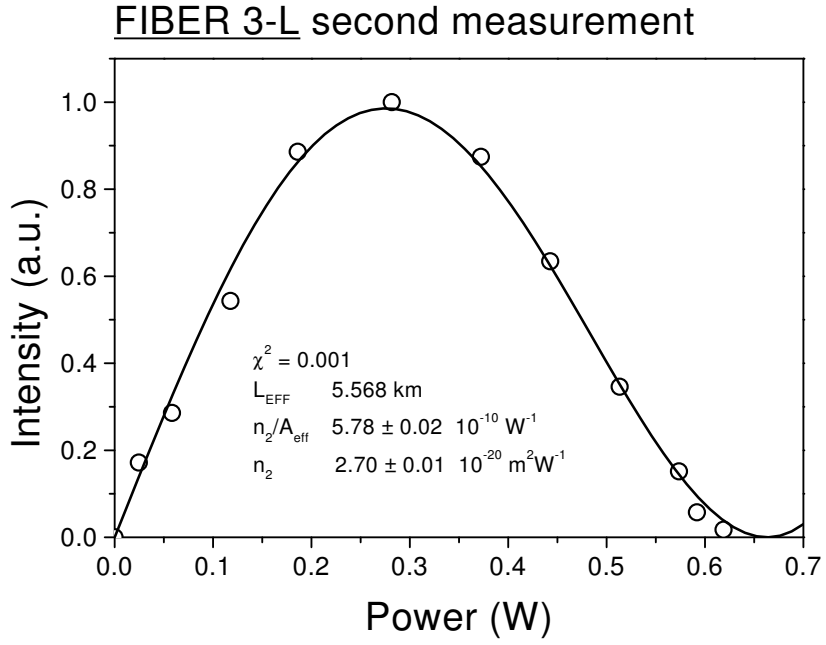

Figure A.11: Detected interference signal power as a function of launch power: (open circles) measured data, (solid line) theoretical fit. Fiber 3-L measure nr.2.

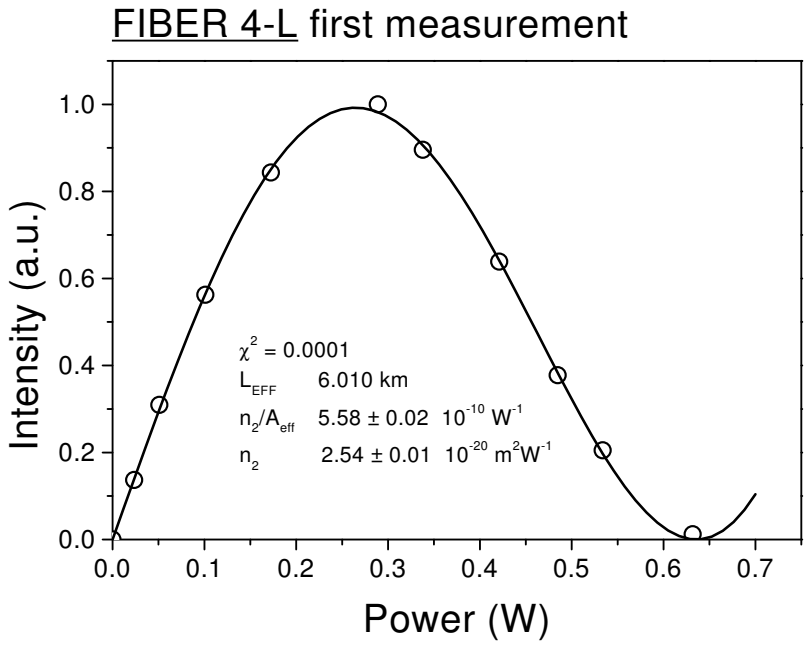

Figure A.12: Detected interference signal power as a function of launch power: (open circles) measured data, (solid line) theoretical fit. Fiber 4-L measure nr.1.

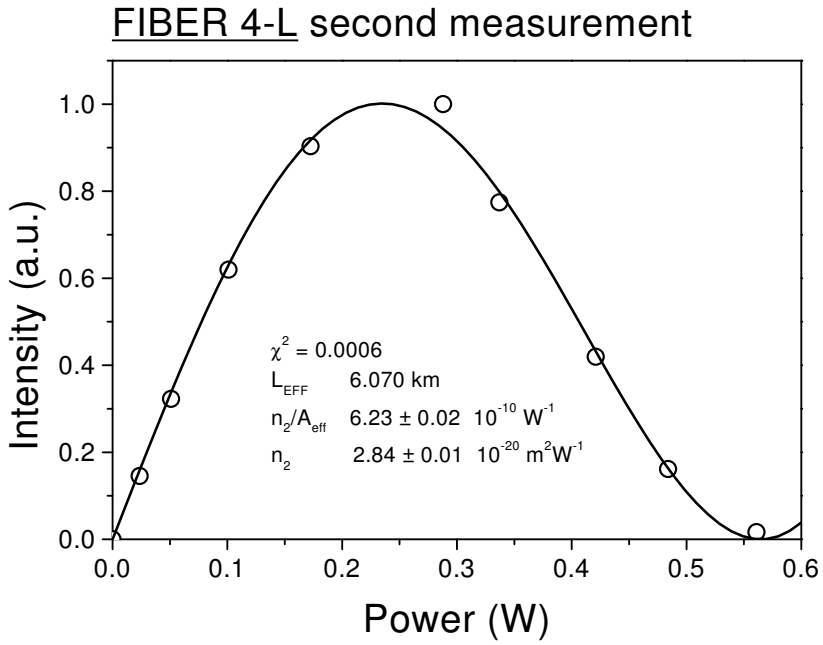

Figure A.13: Detected interference signal power as a function of launch power: (open circles) measured data, (solid line) theoretical fit. Fiber 4-L measure nr.2.

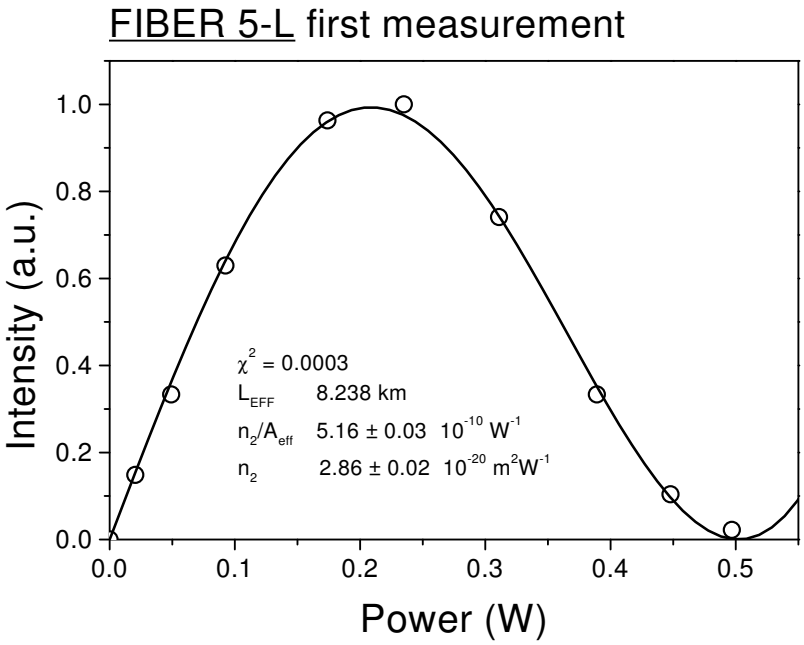

Figure A.14: Detected interference signal power as a function of launch power: (open circles) measured data, (solid line) theoretical fit. Fiber 5-L measure nr.1.

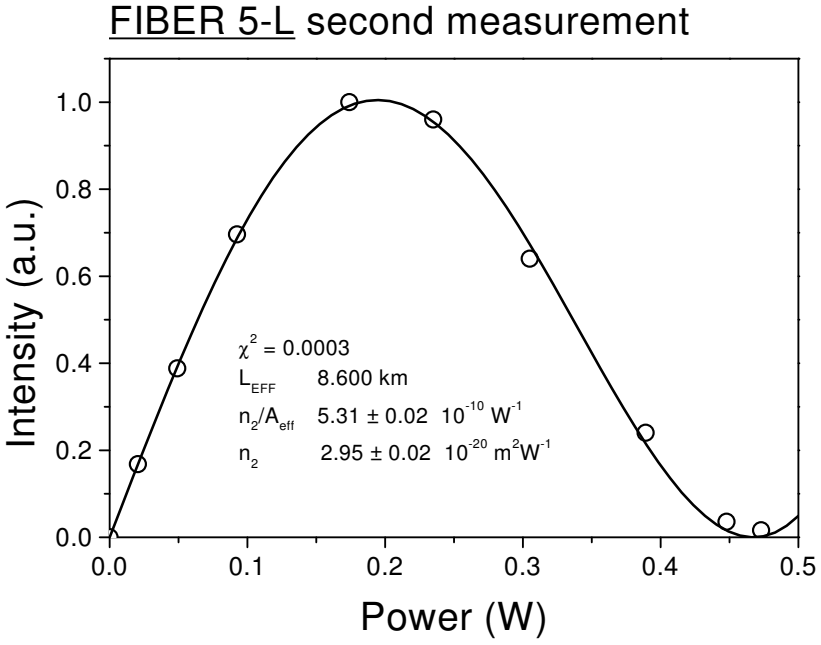

Figure A.15: Detected interference signal power as a function of launch power: (open circles) measured data, (solid line) theoretical fit. Fiber 5-L measure nr.2.

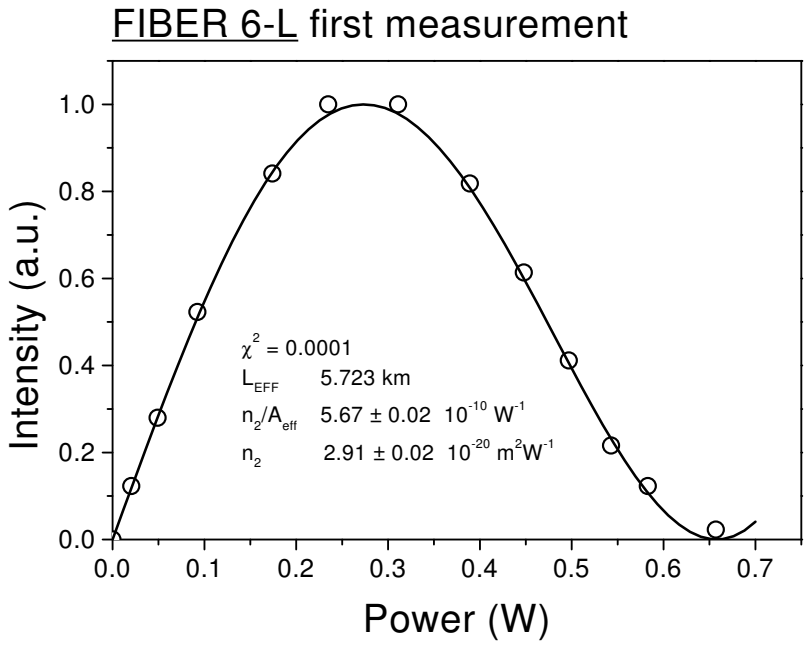

Figure A.16: Detected interference signal power as a function of launch power: (open circles) measured data, (solid line) theoretical fit. Fiber 6-L measure nr.1.

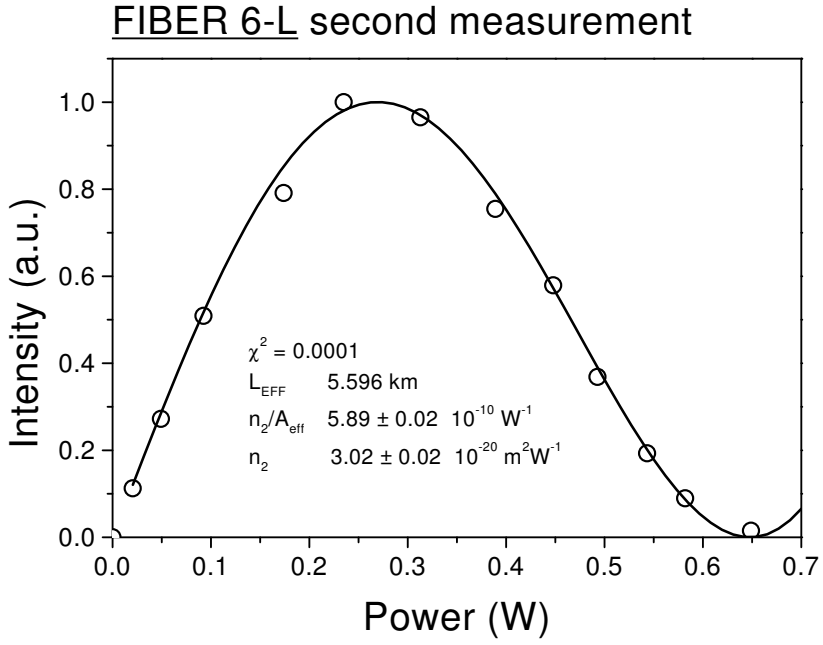

Figure A.17: Detected interference signal power as a function of launch power: (open circles) measured data, (solid line) theoretical fit. Fiber 6-L measure nr.2.

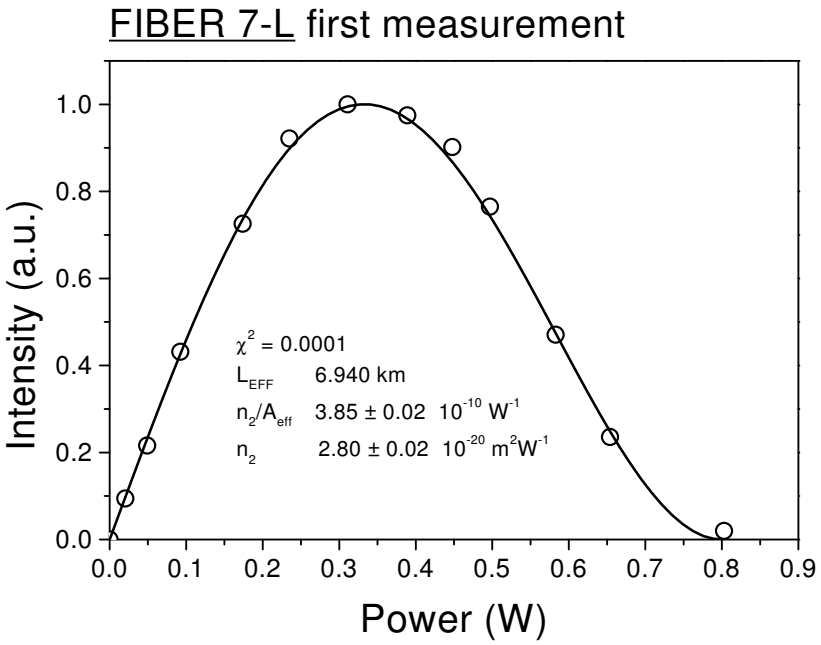

Figure A.18: Detected interference signal power as a function of launch power: (open circles) measured data, (solid line) theoretical fit. Fiber 7-L measure nr.1.

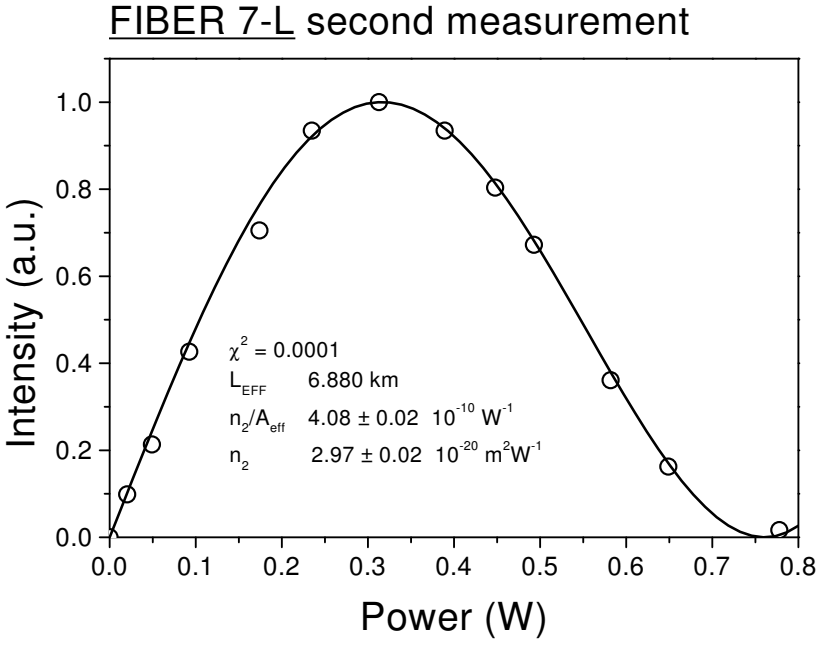

Figure A.19: Detected interference signal power as a function of launch power: (open circles) measured data, (solid line) theoretical fit. Fiber 7-L measure nr.2.

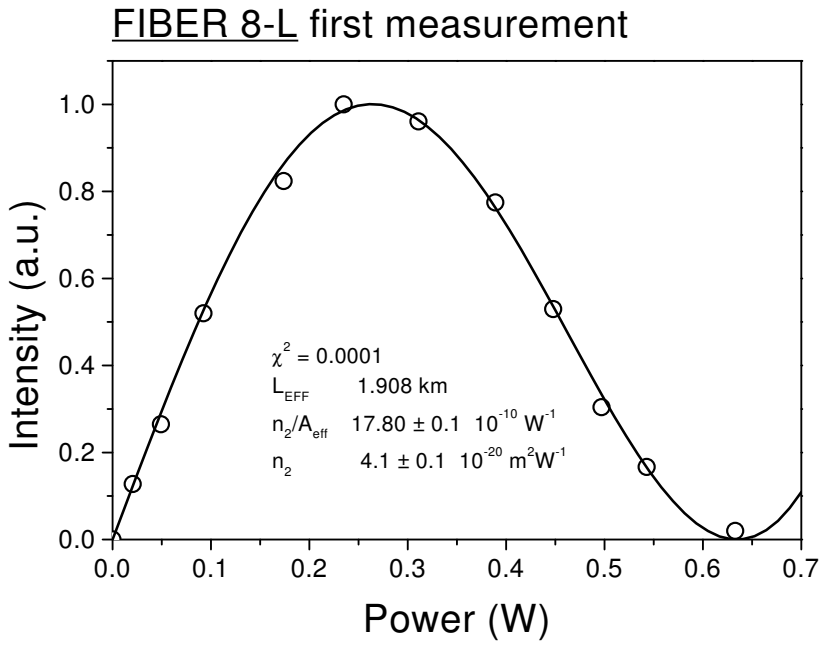

Figure A.20: Detected interference signal power as a function of launch power: (open circles) measured data, (solid line) theoretical fit. Fiber 8-L measure nr.1.

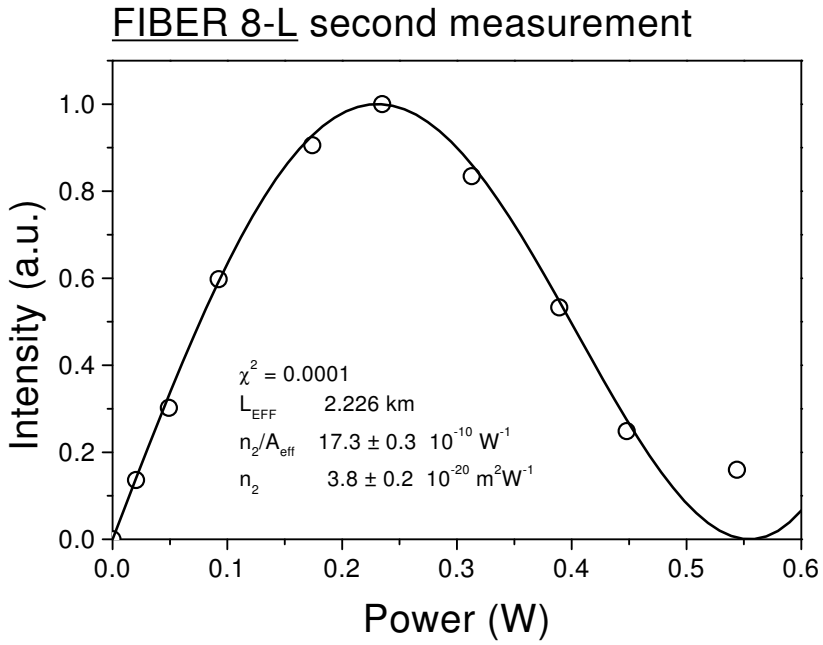

Figure A.21: Detected interference signal power as a function of launch power: (open circles) measured data, (solid line) theoretical fit. Fiber 8-L measure nr.2.

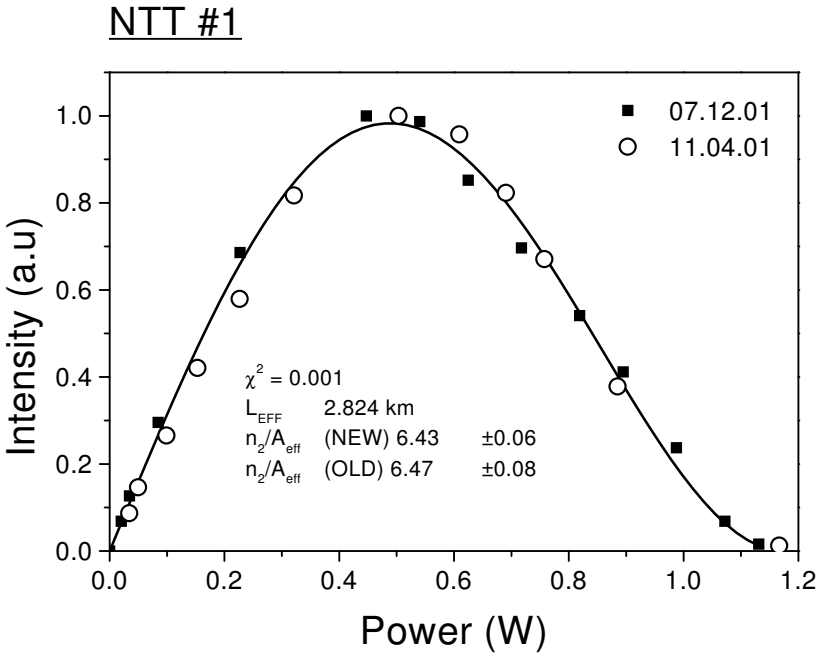

Figure A.22: Detected interference signal power as a function of launch power: (open circles) measured data, (solid line) theoretical fit. Fiber NTT #1 taken at two different dates separated by 8 months.

A.9 Tables ITU Round Robin

Here are reported the results obtained during the measurements for the different fibers of the ITU Round Robin.

In table A.2 and A.3 are shown the characteristics of the fiber as reported by the ITU Round Robin organizer (Prof. Y. Namihira) together with the average values obtained in Geneva for the n_2/A_{eff} and for the n_2 with relative errors. In this case the absolute maximum deviation (MD) from the average is used as an estimate for the error (two measurements were taken).

In the other following tables, in each one are reported in more details the values obtained for all the fibers.

In table A.4 and A.5 are shown the values obtained during each measurement for all the fibers. Are given the splice loss β, the total attenuation along the fiber β', the Faraday Mirror loss β'', the efficient length L^*_{eff}, the n_2/A_{eff} and relative error, the n_2 and relative error, and the χ^2. The errors on n_2/A_{eff} are the one obtained from the fit of the data.

In table A.6 and A.7 are reported the same results but on other measurements taken on a different day.

Final Data for the Fibers L-1 .. L-4

Fiber ID	Fiber 1-L (SMF, G.652)	Fiber 2-L (CSF, G.654)	Fiber 3-L (DSF1, G.653)	Fiber 4-L (DSF2, G.653)
L (km)	5.36	7.65	4.43	4.82
α (dB/km) @1550 nm	0.19	0.17	0.21	0.21
D (ps/nm/km) @1550 nm	+16.0	+19.0	-0.63	-1.30
A_{eff} (μm^2) @1550 nm	84.5	88.2	46.7	45.6
$\mathbf{n_2/A_{eff}}$ (VALUE) ($10^{-10}W^{-1}$)	**3.16**	**3.2**	**5.6**	**5.9**
n_2/A_{eff} (MD) ($10^{-10}W^{-1}$)	0.06	0.1	0.1	0.3
$\mathbf{n_2}$ (VALUE) ($10^{-20}m^2W^{-1}$)	**2.67**	**2.8**	**2.64**	**2.7**
n_2 (MD) ($10^{-20}m^2W^{-1}$)	0.07	0.1	0.09	0.2

Table A.2: Parameters and final values for the n_2/A_{eff} of the first set of fibers. ITU Round Robin. The absolute maximum deviation from the average is used as an estimate for the error.

Final Data for the Fibers L-5 .. L-8

Fiber ID	Fiber 5-L (NZDSF1,G.655)	Fiber 6-L (NZDSF2,G.655)	Fiber 7-L (NZDSF3,G.655)	Fiber 8-L (DSC)
L (km)	6.96	4.4	5.46	2.95
α (dB/km) @1550 nm	0.20	0.20	0.20	0.50
D (ps/nm/km) @1550 nm	-2.27	+4.63	-2.52	-108.4
A_{eff} (μm^2) @1550 nm	55.5	51.3	72.7	22.8
$\mathbf{n_2/A_{eff}}$ (VALUE) ($10^{-10}W^{-1}$)	**5.23**	**5.8**	**4.0**	**17.5**
n_2/A_{eff} (MD) ($10^{-10}W^{-1}$)	0.07	0.1	0.1	0.4
$\mathbf{n_2}$ (VALUE) ($10^{-20}m^2W^{-1}$)	**2.91**	**2.97**	**2.9**	**3.9**
n_2 (MD) ($10^{-20}m^2W^{-1}$)	0.07	0.09	0.1	0.2

Table A.3: Parameters and final values for the n_2/A_{eff} of the second set of fibers. ITU Round Robin. The absolute maximum deviation from the average is used as an estimate for the error.

First Measurement on Fibers L-1 .. L-4

Fiber ID	Fiber 1-L (SMF, G.652)	Fiber 2-L (CSF, G.654)	Fiber 3-L (DSF1, G.653)	Fiber 4-L (DSF2, G.653)
Splice Loss β (dB)	0.1	.15	0.3	0.3
Total Attenuation β′ (dB)	0.9	1.75	1.15	1.6
FM Loss β″ (dB)	1.77	1.77	1.77	1.77
L_{eff} (km)	7.27	8.79	5.33	6.01
$\mathbf{n_2/A_{eff}}$ (VALUE) ($10^{-10}W^{-1}$)	**3.10**	**3.30**	**5.53**	**5.58**
n_2/A_{eff} (FIT ERROR) ($10^{-10}W^{-1}$)	0.02	0.05	0.02	0.02
$\mathbf{n_2}$ (VALUE) ($10^{-20}m^2W^{-1}$)	**2.62**	**2.91**	**2.58**	**2.54**
n_2 (FIT ERROR) ($10^{-20}m^2W^{-1}$)	0.03	0.06	0.04	0.04
χ^2	0.0001	0.003	0.00001	0.0001

Table A.4: Experimental values for the first measurement on the first set of fibers. ITU Round Robin. Errors are from the fit.

First Measurement on Fibers L-5 .. L-8

Fiber ID	Fiber 5-L (NZDSF1,G.655)	Fiber 6-L (NZDSF2,G.655)	Fiber 7-L (NZDSF3,G.655)	Fiber 8-L (DCF)
Splice Loss β (dB)	0.2	0.3	0.1	1.7
Total Attenuation β′ (dB)	1.4	0.7	1.3	1.9
FM Loss β″ (dB)	1.77	1.77	1.77	1.77
L_{eff} (km)	8.24	5.72	6.94	1.91
$\mathbf{n_2/A_{eff}}$ (VALUE) ($10^{-10}W^{-1}$)	**5.16**	**5.67**	**3.85**	**17.8**
n_2/A_{eff} (FIT ERROR) ($10^{-10}W^{-1}$)	0.03	0.02	0.02	0.1
$\mathbf{n_2}$ (VALUE) ($10^{-20}m^2W^{-1}$)	**2.86**	**2.91**	**2.80**	**4.1**
n_2 (FIT ERROR) ($10^{-20}m^2W^{-1}$)	0.04	0.04	0.03	0.1
χ^2	0.0003	0.0001	0.0001	0.0001

Table A.5: Experimental values for the first measurement on the second set of fibers. ITU Round Robin. Errors are from the fit.

Second Measurement on Fibers L-1 .. L-4

Fiber ID	Fiber 1-L (SMF, G.652)	Fiber 2-L (CSF, G.654)	Fiber 3-L (DSF1, G.653)	Fiber 4-L (DSF2, G.653)
Splice Loss β (dB)	0.2	0.1	0.3	0.4
Total Attenuation β′ (dB)	0.8	1.3	1.0	0.9
FM Loss β″ (dB)	1.77	1.77	1.77	1.77
L_{eff} (km)	7.42	9.61	5.57	6.07
$\mathbf{n_2/A_{eff}}$ (VALUE) ($10^{-10}W^{-1}$)	**3.23**	**3.18**	**5.78**	**6.23**
n_2/A_{eff} (FIT ERROR) ($10^{-10}W^{-1}$)	0.02	0.02	0.02	0.02
$\mathbf{n_2}$ (VALUE) ($10^{-20}m^2W^{-1}$)	**2.73**	**2.80**	**2.70**	**2.84**
n_2 (FIT ERROR) ($10^{-20}m^2W^{-1}$)	0.03	0.03	0.04	0.04
χ^2	0.0005	0.003	0.001	0.0006

Table A.6: Experimental values for the second measurement on the first set of fibers. ITU Round Robin. Errors are from the fit.

Second Measurement on Fibers L-5 .. L-8

Fiber ID	Fiber 5-L (NZDSF1,G.655)	Fiber 6-L (NZDSF2,G.655)	Fiber 7-L (NZDSF3,G.655)	Fiber 8-L (DCF)
Splice Loss β (dB)	0.1	0.2	0.2	1.4
Total Attenuation β′ (dB)	1.4	1.0	1.1	1.5
FM Loss β″ (dB)	1.77	1.77	1.77	1.77
L_{eff} (km)	8.60	5.60	6.88	2.23
$\mathbf{n_2/A_{eff}}$ (VALUE) ($10^{-10}W^{-1}$)	**5.31**	**5.89**	**4.08**	**17.3**
n_2/A_{eff} (FIT ERROR) ($10^{-10}W^{-1}$)	0.02	0.02	0.02	0.4
$\mathbf{n_2}$ (VALUE) ($10^{-20}m^2W^{-1}$)	**2.95**	**3.02**	**2.97**	**3.8**
n_2 (FIT ERROR) ($10^{-20}m^2W^{-1}$)	0.04	0.04	0.03	0.2
χ^2	0.0003	0.0001	0.0001	0.0001

Table A.7: Experimental values for the second measurement on the second set of fibers. ITU Round Robin. Errors are from the fit.

Channel N	Bit Rate B (Gbps)	Capacity NB (Gbps)	Distance L (km)	NBL Product (Tbps · km)
10	10	100	50	5

Appendix B

Published Articles

1. Measurement of nonlinear polarization rotation in high birefringence optical fibers at telecom wavelength.
   C. Vinegoni, M. Wegmuller, B. Huttner, and N. Gisin
   J. Opt. A: Pure Appl. Opt., Vol. 2 (2000) pp. 314-18

2. All optical switching in a highly birefringent and a standard telecom fiber using a Faraday mirror stabilization scheme.
   C. Vinegoni, M. Wegmuller, B. Huttner, and N. Gisin
   Opt. Comm., Vol. 182 (2000) pp. 314-18

3. Determination of the nonlinear coefficient n_2/A_{eff} using a self-aligned interferometer and a Faraday mirror.
   C. Vinegoni, M. Wegmuller, N. Gisin
   Electronic Letters, Vol. 36 (2000) pp. 886-87

4. Measurements of the nonlinear coefficient of standard SMF, DSF, and DSC fibers using a self-aligned interferometer and a Faraday mirror.
   C. Vinegoni, M. Wegmuller, and N. Gisin
   Photonics and Technology Lett., December 2001

5. Distributed gain measurements in Er-doped fibers with high resolution and accuracy using an Optical Frequency Domain Reflectometer
   M. Wegmuller, P. Oberson, O. Guinnard, B.Huttner, L. Guinnard, C. Vinegoni, N. Gisin
   J. Lightwave Technol., Vol. 18 (2000) pp. 2127-32

6. Analysis of the polarization evolution in a ribbon cable using high resolution OFDR
   M. Wegmuller, M. Legre, P. Oberson, O. Guinnard, L. Guinnard, C. Vinegoni, N. Gisin
   Photonics and Technology Letters, Vol.. 13 (2000) pp. 145-7

7. A near field scanning optical microscope in single photon detection mode at 1.55 μm.
   C. Vinegoni, H. Deriedmatten, M. Wegmuller, N. Gisin, Y. Mugnier, A. Jalocha, P. Descouts
   Submitted

8. Determination of polarization coupling length in telecom fibers exploiting nonlinear polarization rotation.
   C. Vinegoni, V. Scarani, M. Wegmuller, and N. Gisin
   Submitted

9. Emulator of first and second order polarization mode dispersion.
   M. Wegmuller, S. Demma, C. Vinegoni, and N. Gisin
   Photonics and Technology Lett. , Vol. 14 (2002) pp. 630-2

10. Distributed measurements of chromatic dispersion and nonlinear coefficient in low PMD dispersion shifted fibers.
    C. Vinegoni, H. Chen, M. Leblanc, G. Schinn, M. Wegmuller, and N. Gisin
    Submitted

B.1 Measurement of nonlinear polarization rotation in high birefringence optical fibers at telecom wavelength.

C. Vinegoni, M. Wegmuller, B. Huttner, and N. Gisin

[1] *Group of Applied Physics - Gap Optique*
University of Geneva,
20 Ecole-de-Medecine, CH-1211 Aeneve 4, Switzerland

Claudio.Vinegoni@physics.unige.ch

Abstract : We present both a theoretical and experimental analysis of nonlinear polarization rotation in an optical fiber. Starting from the coupled non-linear Schrödinger equations an analytical solution for the evolution of the state of polarization, valid for fibers with large linear birefringence and quasi cw input light with arbitrary polarization, is given. It allows to model straightforwardly go-and-return paths as in interferometers with standard or Faraday mirrors. In the experiment all the fluctuations in the linear birefringence, including temperature and pressure induced ones, are successfully removed in a passive way by using a double pass of the fiber under test with a Faraday mirror at the end of the fiber. This allows us to use long fibers and relatively low input powers. The match between the experimental data and our model is excellent, except at higher intensities where deviations due to modulation instability start to appear.

PUBLISHED : J. Opt. A: Pure Appl. Opt., Vol. 2 (2000) pp. 314-18

J. Opt. A: Pure Appl. Opt. **2** (2000) 314–318. Printed in the UK PII: S1464-4258(00)10387-3

Measurement of nonlinear polarization rotation in a highly birefringent optical fibre using a Faraday mirror

C Vinegoni, M Wegmuller, B Huttner and N Gisin

Group of Applied Physics, University of Geneva, 20 Ecole-de-Medecine, CH-1211 Geneve 4, Switzerland

E-mail: claudio.vinegoni@physics.unige.ch

Received 14 December 1999, in final form 30 March 2000

Abstract. We present both a theoretical and experimental analysis of nonlinear polarization rotation in an optical fibre. Starting from the coupled nonlinear Schrödinger equations an analytical solution for the evolution of the state of polarization, valid for fibres with large linear birefringence and quasi cw input light with arbitrary polarization, is given. It allows us to model straightforwardly go-and-return paths as in interferometers with standard or Faraday mirrors. In the experiment all the fluctuations in the linear birefringence, including temperature- and pressure-induced ones, are successfully removed in a passive way by using a double pass of the fibre under test with a Faraday mirror at the end of the fibre. This allows us to use long fibres and relatively low input powers. The match between the experimental data and our model is excellent, except at higher intensities where deviations due to modulation instability start to appear.

Keywords: Nonlinear polarization rotation, nonlinear birefringence, Keff effect, Faraday mirror

1. Introduction

The potential of nonlinear polarization rotation (NPR) to build ultrafast devices was recognized a long time ago and has received considerable attention since then. It has been proposed to exploit it for optical switches [1], logic gates [2], multiplexers [3], intensity discriminators [4], nonlinear filters [5], or pulse shapers [6]. However, an inherent problem with all these applications is the stability of the output state of polarization, generally subjected to fluctuations of the linear birefringence caused by temperature changes and drafts in the fibre environment. Of course, the same problem was also encountered in the few experiments dealing with the characterization and measurement of the NPR itself. In [7], the fluctuations of the output polarization were too strong to allow a meaningful measurement of NPR in a polarization maintaining fibre at 1064 nm, and in [8], where 514 nm light was injected into a 60 m long fibre with a beat length of 1.6 cm, a complicated arrangement had to be employed for the extraction of the changes caused by temperature drifts.

As the fluctuations become worse for fibres with a large birefringence, and as the effect of NPR is proportional to the inverse of the wavelength, it is hard to measure NPR directly in a polarization-maintaining (PM) fibre at the telecom wavelength of 1.55 μm. In this work we propose a method for removing the overall linear birefringence, and therefore also its fluctuations, in a passive way by employing a Farady mirror (FM) [9] and a double pass of the fibre under test. To check how this—nowadays standard—method [10–13] of removing linear birefringence acts on the NPR, we develop in section 2 of this paper a simple model to calculate the action of linear and nonlinear birefringence. Using this model, it is then easy to show that the proposed method removes the overall linear birefringence only, whereas the nonlinear one, leading to NPR, remains unchanged. After describing the experimental setup, the results of our NPR measurements using a FM are presented in section 3, along with the predictions from our analytical model. The excellent agreement between the two demonstrates that using the FM, the overall linear birefringence is indeed removed completely, allowing one to observe the NPR otherwise hidden within the noisy background of polarization changes due to environmental perturbations. This result also validates our method for possible implementation with a variety of other applications like the ones mentioned at the beginning of this section, with the prospect of drastically increasing their polarization stability.

2. Theoretical background

In a dielectric medium, an intense elliptical input pulse induces birefringence—via the optical Kerr effect—due to

1464-4258/00/040314+05$30.00

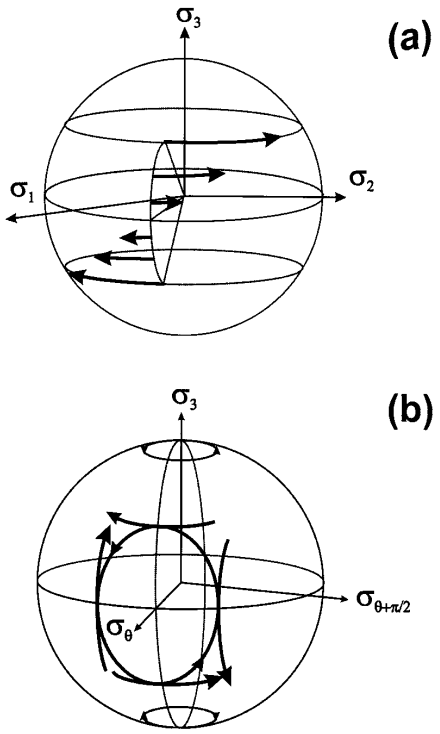

Figure 1. Evolution of the state of polarization as represented on the Poincaré sphere. (*a*) Polarization ellipse self-rotation in an isotropic medium. The Stokes vector is rotating around the σ_3 axis with an angle proportional to the length of the medium, the input intensity, and the sine of the input ellipticity.
(*b*) High-birefringence fibre. The rotation of the Stokes vector mainly consists of a fast rotation around the axis of linear birefringence σ_θ, whereas the slow rotations due to the nonlinear birefringence can be considered as small perturbations.

the different amounts of intensity along the major and minor axis of the polarization ellipse. It is well known that in isotropic media this self-induced birefringence leads to a rotation of the polarization ellipse while propagating in the medium [14, 15] (the effect is consequently often called polarization ellipse self-rotation and its representation on the Poincaré sphere is shown in figure 1(*a*)). In fact, measuring this ellipse rotation is one of the standard ways to evaluate the cubic optic nonlinearity of the medium [16]. In an optical fibre however, the situation becomes more complicated as there is also the local intrinsic birefringence to be considered. Generally, the polarization ellipse changes are hard to predict in that case as the linear and nonlinear birefringence interact in a complicated manner.

To formulate this more precisely, we start with the coupled nonlinear Schrödinger equations describing the propagation of light in an optical fibre. For cw input light, time derivatives drop out, and we can write the equation in a similar form as Menyuk [17] when assuming a lossless, linearly birefringent fibre and by neglecting polarization mode coupling:

$$\partial_z \psi = \mathrm{i}(\omega B \sigma_\theta + \omega\alpha\ \sigma_3\ _\psi \sigma_3)\psi. \qquad (1)$$

ψ $(E_1, E_2)^t$ is the Jones column vector representing the two components of the complex transverse electric fields $E_1(z)$ and $E_2(z)$ at the position z along the fibre. The first term in the right-hand side describes the linear birefringence, where ω is the optical frequency and B the birefringence (in s m ^{1}). Note that B is assumed to be independent of ω, an excellent approximation for standard fibres. The phase birefringence ωB is multiplied by σ_θ $\sigma_1 \cos(\theta) + \sigma_2 \sin(\theta)$, corresponding to linear birefringence in the θ direction, with $\sigma_{1,2,3}$ being the 2 2 Pauli matrices. The second term in the right-hand side of (1) accounts for the nonlinear birefringence, with α $\frac{n_2 P}{3cA_{\mathrm{eff}}}$, and $\sigma_3\ _{\psi_z}$ $\frac{E_1{}^2 - E_2{}^2}{E_1{}^2 + E_2{}^2}$. P is the total light power, n_2 the nonlinear refractive index, A_{eff} the effective mode area, and c the speed of light.

For an intuitive understanding of the action of the two terms in the right-hand side of (1), it is better to revert to the Stokes formalism. On the Poincaré sphere, the first term describes a rotation of the polarization vector (Stokes vector) around axis σ_θ, lying on the equator and corresponding to linear birefringence. Similarly, the second term is a rotation around the vertical axis corresponding to nonlinear birefringence. However, equation (1) shows that the speed and the rotation direction in this case depends on the polarization state through $\sigma_3\ _\psi$, as is illustrated in figure 1(*b*). Consequently, the two rotations are linked in a complicated manner, and the resulting evolution of the polarization vector is not obvious.

Fortunately, in standard telecom fibres, the speed of rotation around the vertical axis is much smaller than the one around the birefringent axis σ_θ even at considerable power levels. This is because in such fibres B α (see (1)). For example, a fibre with a beat length of 10 m has B 0.5 ps km ^{1} while α 0.006 ps km ^{1} for a power of 10 W (λ 1550 nm, n_2 3.2 10 ^{20}, A_{eff} 60 μm^2) (note that in this work, a PM fibre will be used with a beat length in the mm range, making the ratio $\frac{B}{\alpha}$ as large as 10^7). The slow rotation due to the nonlinear birefringence can therefore be treated as a perturbation that merely changes the angular frequency of the fast rotation caused by the linear birefringence. This becomes more obvious by rewriting (1) as

$$\partial_z \psi = \mathrm{i}\omega B \sigma_\theta \psi \quad \mathrm{i}\omega\alpha \tfrac{1}{2}(\ \sigma_3\ _\psi \sigma_3 + (1 \quad \sigma_{\theta+\frac{\pi}{2}}\ _\psi \sigma_{\theta+\frac{\pi}{2}} \quad \sigma_\theta\ _\psi \sigma_\theta))\psi \qquad (2)$$

where the identity ψ $\sigma\ _\psi \sigma \psi$, valid for all ψ, has been used. The term proportional to ψ affects only the global phase and can be neglected. Further, the two terms $\sigma_3\ _\psi \sigma_3$ and $\sigma_{\theta+\frac{\pi}{2}}\ _\psi \sigma_{\theta+\frac{\pi}{2}}$ cancel each other to first order—this can be intuitively understood from figure 1(*b*) and was confirmed by numerical simulations—producing only a small (second-order) precession of the instantaneous rotation axis. Hence we obtain the following approximation for the evolution of the polarization vector:

$$\partial_z \psi = \mathrm{i}\omega B_{\mathrm{eff}} \sigma_\theta \psi \qquad (3)$$

with the effective birefringence

$$B_{\mathrm{eff}} \quad B \quad \frac{\alpha}{2}\ \sigma_\theta\ _\psi \qquad (4)$$

depending on the intensity and the polarization state of the input light signal. Note that equation (3) preserves the square norm ψ^2 reflecting that we did not take into account losses. Note further that when applying (3) for linearly polarized input light we obtain the same formula as in [4].

The solution of (3) is straightforward, ψ_z exp($i\omega B_{\text{eff}}\sigma_\theta z)\psi_0$, and corresponds to a rotation of the input polarization vector around the linear birefringence axis σ_θ, with a rotation angle β given by

$$\beta \quad \omega \quad B \quad \frac{\alpha}{2} m_\theta(0) \quad z. \tag{5}$$

$m_\theta(0)$ is the projection of the input polarization vector on the birefringence axis σ_θ, and z the distance from the input end.

In principle, the NPR, caused by the nonlinear response of the single-mode fibre to the input state, could now be measured by varying the input power and observing the corresponding change in the output polarization vector. However, from a practical standpoint, this will be hardly possible as equation (5) shows that slightest changes in the linear birefringence B will completely cover the nonlinear, intensity-dependent ones (remember that B α for reasonable input power levels). Indeed, earlier work [8, 18] greatly suffered from temperature- and pressure-induced changes of B always present in a laboratory environment, even though they were using short fibres.

Nowadays, a simple and efficient way to get rid of any kind of fluctuation in the intrinsic birefringence is to make a double pass of the fibre under test by means of a FM [9, 10]. The linear birefringence accumulated during the forward path is then automatically compensated on the return path. However, it is not *a priori* clear what will happen to the nonlinear birefringence.

To investigate this point, we rewrite the solution of (3) in the Stokes formalism,

$$\boldsymbol{m}(L) \quad \boldsymbol{R}_\theta(\beta(L))\boldsymbol{m}(0) \tag{6}$$

where $\boldsymbol{m}(0)$ is the input Stokes vector, $\boldsymbol{R}_\theta$ is a rotation operator around the axis σ_θ, and β is as given by (5). Applying the action of the FM, $\boldsymbol{m}^F(L)$ $\boldsymbol{m}(L)$ (the superscript F indicates the state of polarization after reflection from the FM), and of the return path, $\boldsymbol{R}_\theta^{\,1}$, we get

$$\begin{aligned}\boldsymbol{m}^F(2L) \quad \boldsymbol{R}_\theta^{\,1} \quad \omega L \quad B \quad \frac{\alpha}{2} m_\theta^F(L) \quad \boldsymbol{R}_\theta \\ \omega L \quad B \quad \frac{\alpha}{2} m_\theta(0) \quad \boldsymbol{m}(0) \\ \boldsymbol{R}_\theta[\omega\alpha L m_\theta(0)]\boldsymbol{m}(0).\end{aligned} \tag{7}$$

The result shows that the rotation due to the nonlinear birefringence of the forward and return path do not cancel out but add, giving twice the angle compared with a single (forward) trip through the fibre (equation (5)). This is because the rotation direction of the nonlinear birefringence is different for the upper and lower hemisphere of the Poincaré sphere (see figure 1(*b*)) contrary to birefringence in linear optics. Therefore, after reflection at the FM, which transforms the polarization state to its orthogonal counterpart (i.e. flipping it to the other hemisphere), the sense of rotation of the NPR during the return path will be the same as the forward path and the effects add up.

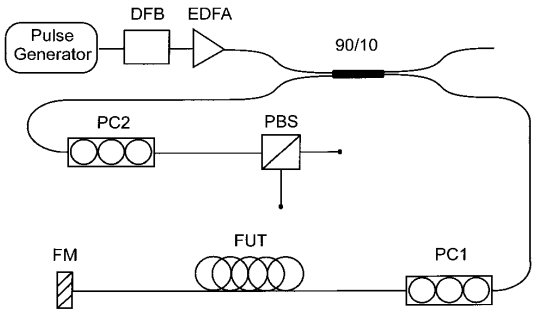

Figure 2. Experimental setup of the NPR measurement. DFB, distributed feedback laser; EDFA, erbium-doped fibre amplifier; PC, polarization controller; FUT, fibre under test; FM, Faraday mirror; PBS, polarizing beam splitter.

3. Experiment

3.1. Setup

The experimental setup used to measure the NPR is shown in figure 2. The light source is a distributed feedback laser diode (DFB) operated in pulsed mode at a wavelength of 1559 nm, consecutively amplified by an EDFA (small signal gain 40 dB, saturated output power 23 dBm, where dBm is a physical unit of power). Typically, pulses with a duration of 30 ns, a repetition rate of 1 kHz and a peak power of up to 6 W were used. The light is then launched into the test fibre via a 90/10 coupler and a polarization controller. The coupler was inserted for the detection of the backward-travelling light after the double pass of the test fibre, with its 90-output port connected to the source in order to maintain the high launch powers into the test fibre. The polarization controller, PC1, allowed us to adjust the polarization of the light launched into the test fibre, which is important for the strength of the NPR as demonstrated by equation (5).

In order to satisfy the assumption of neglectable polarization mode coupling used in the previous section, a highly birefringent, PM fibre was used as the test fibre. Its linear birefringence B is of the order of 5 ps m ^{1}, corresponding to a beat length in the mm range. The fibre length was 200 m, giving a total of 400 m round-trip length of the light reflected by the FM.

The polarization state of the light after the double pass of the test fibre was examined by an analyser consisting of a polarization controller PC2 and a polarizing beam splitter (PBS). To achieve a good sensitivity of the analyser, it was calibrated to give a 50/50 output of the PBS for low-power signals where no nonlinear polarization rotation occurs. Finally, the two PBS output channels were monitored by a fast photodiode (200 ps response time) and a sampling scope.

The measurements were then performed in the following way: for a given launch power, the polarization controller PC1 was adjusted to give the smallest possible output power at the monitored PBS channel. Consequently, the difference between the two PBS output channels is maximized, corresponding to a maximum value of the NPR.

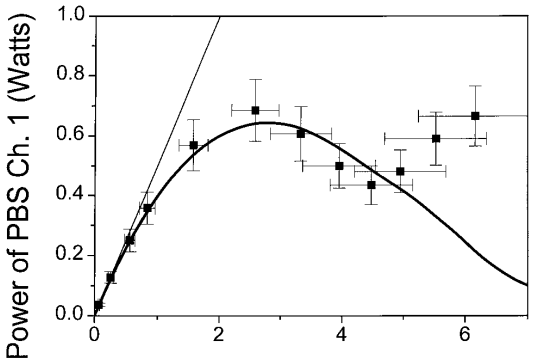

Figure 3. Minimum output power of PBS channel 1 as a function of the launched power for a 200 m long PM fibre. Squares: measured data; solid curve: prediction from our model; straight line: prediction in the absence of NPR. The deviations of the experimental data from the predicted values at high powers are due to modulation instability not included in the model.

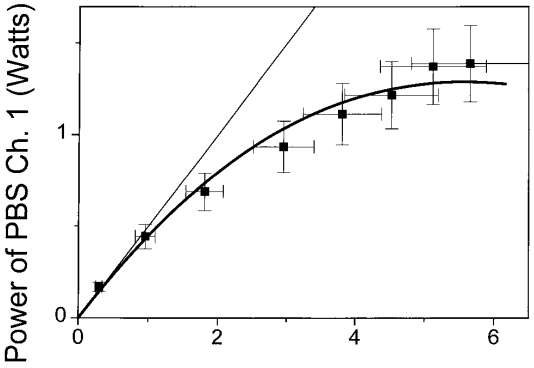

Figure 4. Minimum output power of PBS channel 1 as a function of the launched power for a 100 m long PM fibre. Squares: measured data; solid curve: prediction from our model; straight line: prediction in the absence of NPR.

3.2. Results

The experimental results are shown in figures 3 and 4.

In figure 3, the minimum output power (squares) of the monitored PBS channel is given as a function of the peak power in the test fibre. Note that the reported output power was normalized to account for the analyser losses and corrected for the PBS extinction ratio. Consequently, without any NPR, the reported output power would equal half of the power in the test fibre (straight line). As can be seen in figure 3, the effect of NPR is negligibly small up to about 0.5 W. For higher launch powers, NPR manifests itself by a reduction of the power in the monitored PBS channel. In fact, its action becomes so strong that for launch powers above about 2.5 W, the output power starts actually to decrease in spite of the linear increase that would be experienced in the absence of NPR. In principle, this power drop should continue until the nonlinear rotation of the input polarization is such that all the power is in the other PBS channel. However, as figure 3 shows, this is not happening. The observed increase in the minimum output power could be related to modulation instability: above 4.5 W launch power, a Stokes and anti-Stokes sideband shifted by 2 nm with respect to the laser peak appeared. These sidebands are generated in a distributed fashion along the test fibre, which means that the compensation of the linear fibre birefringence is failing. Therefore, and due to the large birefringence B of the PM fibre used, the sidebands will be almost randomly polarized at the output. As a consequence, about half of the power transferred to the sidebands will appear in the monitored PBS output channel leading to the observed increase in power.

Further, the measured results were compared with the ones predicted by equation (8), taking into account the analyser calibration and the adjustment of PC1 as used in the experiment. The parameters used in the computation were the ones from the experiment, i.e. a fibre length of L 200 m, and a nonlinear coefficient of n_2 3.4 10^{-20} m^2 W^{-1}. The effective core area of A_{eff} 41 μm^2 was chosen to give a good match with the experimental results as we had no exact value from the manufacturer. $m_\theta(0)$, the projection of the input state of polarization on the birefringent axis, was varied in order to give a minimum output power from the PBS channel, exactly like in the experiment.

The solid curve in figure 3 shows these computed results. The figure clearly illustrates that the measured data correspond very well with the computed results. This validates our measurement method of NPR in optical fibres and demonstrates that the linear birefringence and its detrimental fluctuations are successfully removed by the FM. Above an input power of 4.5 W, the curves deviate as expected from the onset of MI that was not included in the analytical model.

Figure 4 shows experimental and computed results for a fibre length of 100 m. Note that to avoid cutting our 200 m piece, we emulated the 100 m fibre length by introducing a 20 dB attenuation for the reflected light. Consequently, the light power on the return trip is too low to induce NPR, and serves only to compensate for the linear birefringence of the forward trip. As the figure demonstrates, NPR is indeed reduced by a factor of two compared with the measurements without attenuator, as expected from equation (8). Twice the launch power is required to compensate for the shortened length to get the same amount of NPR. Again, experimental and computed data are in excellent agreement.

The experimental results of this section clearly demonstrate that one can indeed use a FM to remove the overall linear birefringence, which allows one to observe the smallest nonlinear effects otherwise hidden within the noisy linear birefringence. Note that the change in the output polarization due to environmental perturbations is especially pronounced in PM fibres (when the input is not aligned with one of the two fibre axes) due to its short beat length in the mm range. When not using a FM, the output polarization changed (for example) drastically when just approaching the fibre spool with the hands, inhibiting any meaningful measurement.

4. Conclusion

Starting from the nonlinear Schrödinger equations, an analytical solution for the evolution of the state of polarization in a high-birefringence optical fibre has been developed. It

allows for a simple and straightforward modelling of go and return paths as, for example, in interferometers with standard or Faraday mirrors. Using this model, we showed that it is possible to remove the overall linear birefringence in a double-pass arrangement with a FM while at the same time leaving the nonlinear birefringence, resulting in NPR, unchanged. Only this arrangement allowed us to measure the NPR in a long PM fibre at telecom wavelength in a laboratory environment where it is otherwise hidden by the changes in the output polarization caused by temperature and pressure fluctuations.

The experimental results for the NPR obtained with a 200 m long PM fibre at a wavelength of 1.55 μm were in excellent agreement with the theoretical predictions from our model for launch power up to 4.5 W. Above that value deviations due to modulation instability, not included in our model, were present. Further work to apply our model to standard, non-PM fibres where the coupling between the polarization modes is not negligible, is in progress.

Due to its generality, the presented method of removing the linear birefringence while leaving the nonlinear one unchanged might prove to be a very valuable tool in numerous other applications as well, such as, for example, optical multi-/demultiplexers.

Note that in the case of non-PM fibres, where the coupling between the polarization modes is not negligible, NPR is reduced due to a scrambling related to the ratio between the coupling length and the fibre length. In fact, this effect can be exploited to get information about the important coupling length parameter in standard fibres, as will be shown elsewhere.

Acknowledgments

We acknowledge the financial support from the Swiss Federal Office for Education and Sciences (OFES) in the framework of the European COST P2 action. Further, we would like to thank the Laboratoire de Metrologie des Fibres Optique, EPFL Lausanne, for the loan of the PM fibre, and C R Menyuk for stimulating discussion on the subject.

References

[1] Olssono B E and Andrekson P A 1998 Polarization independent Kerr-switch using a polarization diversity loop *ECOC'98 (Madrid, Spain) Technical Digest* pp 185–6

[2] Kitayama K, Kimura Y and Seikai S 1985 Fibre-optic logic gate *Appl. Phys. Lett.* **46** 317–19

[3] Morioka T, Saruwatari M and Takada A 1987 Ultrafast optical multi/demultiplexer utilizing optical Kerr effect in polarization-maintaining single-mode fibres *Electron. Lett.* **23** 453–4

[4] Stolen R H, Botineau J and Ashkin A 1982 Intensity discrimination of optical pulses with birefringent fibres *Opt. Lett.* **7** 512–14

[5] Horowitz M and Silberberg Y 1997 Nonlinear filtering by use of intensity-dependent polarization rotation in birefringent fibres *Opt. Lett.* **22** 1760–2

[6] Hofer M, Fermann M E, Haberl F, Ober M H and Schmidt A J 1991 Mode locking with cross-phase and self-phase modulation *Opt. Lett.* **16** 502–4

[7] Dianov E M, Zakhidov E A, Karasik A Ya, Kasymdzhanov M A and Mirtadzhiev F M 1987 Optical Kerr effect in glass fibre waveguides with weak and strong birefringence *Sov. J. Quantum Electron.* **17** 517–19

[8] Crosignani B, Piazzola S, Spano P and Di Porto P 1985 Direct measurement of the nonlinear phase shift between the orthogonally polarized states of a single-mode fibre *Opt. Lett.* **10** 89–91

[9] Martinelli M 1989 A universal compensator for polarization changes induced by birefringence on a retracing beam *Opt. Commun.* **72** 341–4

[10] Ribordy G, Gautier J D, Gisin N, Guinnard O and Zbinden H 1998 Automated plug and play quantum key distribution *Electron. Lett.* **34** 2116–17

[11] Breguet J, Pellaux J P and Gisin N 1995 Photoacoustic detection of trace gases with an optical microphone *Sensors Actuators* A **1** 29–35

[12] Yamashita S, Hotate K and Ito M 1996 Polarization properties of a reflective fibre amplifier employing a circulator and a Faraday rotator mirror *J. Lightwave Technol.* **14** 385–90

[13] Alekseev E I, Bazarov E N, Gubin V P, Sazonov A I and Starostin N I 1999 Compensation for spurious polarization modulation in a fibre optic phase modulator with the Faraday mirror *Radiotekh. Elektron.* **44** 122–7

[14] Maker P D, Terhune R W and Savage C M 1964 Intensity-dependent changes in the refractive index of liquids *Phys. Rev. Lett.* **12** 507–9

[15] Unsbo P and Flytzanis C 1997 Degenerate four-wave mixing in isotropic nonlinear-optical gyrotropic media *J. Opt. Soc. Am.* B **14** 560–69

[16] Svirko Yu P and Zheludev N I 1998 *Polarization of Light in Nonlinear Optics* (New York: Wiley)

[17] Menyuk C R 1987 Nonlinear pulse propagation in birefringence optical fibres *IEEE J. Quantum Electron.* **23** 174–6
see also Menyuk C R 1989 Pulse propagation in an elliptically birefringent Kerr medium *IEEE J. Quantum Electron.* **25** 2674–82

[18] Dziedzic J M, Stolen R H and Aschkin A 1981 Optical Kerr effect in long fibres *Appl. Opt.* **20** 1403–6

B.2 All optical switching in a highly birefringent and a standard telecom fiber using a Faraday mirror stabilization scheme.

C. Vinegoni, M. Wegmuller, B. Huttner, and N. Gisin

[1] *Group of Applied Physics - Gap Optique*
University of Geneva,
20 Ecole-de-Medecine, CH-1211 Aeneve 4, Switzerland

Claudio.Vinegoni@physics.unige.ch

Abstract : All-optical switching at 1.5 μm based on induced nonlinear polarization rotation is demonstrated in both a polarization maintaining and a standard telecom fiber. Excellent switching stability is obtained in both cases by removing any detrimental temperature or pressure induced changes of the output polarization state with a Farady mirror stabilization scheme.

PUBLISHED : Opt. Comm., Vol. 182 (2000) pp. 314-18

ELSEVIER

Optics Communications 6822 (2000) xxx

OPTICS COMMUNICATIONS

www.elsevier.com/locate/optcom

All optical switching in a highly birefringent and a standard telecom fiber using a Faraday mirror stabilization scheme

C. Vinegoni *, M. Wegmuller, B. Huttner, N. Gisin

Group of Applied Physics, University of Geneva, 20 Ecole-de-Medecine, CH-1211 Geneve 4, Switzerland

Received 7 March 2000; accepted 9 June 2000

Abstract

All-optical switching at 1.5 μm based on induced nonlinear polarization rotation is demonstrated in both a polarization maintaining and a standard telecom fiber. Excellent switching stability is obtained in both cases by removing any detrimental temperature or pressure induced changes of the output polarization state with a Farady mirror stabilization scheme. © 2000 Published by Elsevier Science B.V.

PACS: 42.65.Pc; 42.81.Gs
Keywords: Kerr effect; All-optical switching; Faraday mirror

1. Introduction

Considering the high bit rates of future optical fiber communication systems, optical signal processing could soon become a necessity. In order to demux a single channel from a 100 Gb/s time division multiplexed (TDM) signal e.g., a switching time of about 5 ps will be required. All-optical switching techniques based on the optical Kerr effect [1–6] are very attractive in that respect due to the ultrafast Kerr response [7–9] of less than a few fs. Indeed, an all optical Kerr switch was demonstrated recently to read out a 10 Gb/s channel from a 40 Gb/s TDM signal [10]. Besides the standard switch parameters like switching ratio, insertion loss or switching time, the stability of the switch is an important issue. Variations in the input control or signal polarizations as well as changes of the intrinsic birefringence of the Kerr medium will affect the switch. Variations of the input signal polarization can be dealt with by adopting a polarization diversity scheme, like e.g. in Ref. [10]. In order to keep the switch stable internally, the control pulse polarization should be kept as stable as possible by using a proper set-up. Moreover, changes in the signal polarization in the Kerr medium (typically a polarization maintaining PM fiber) due to changes in the intrinsic fiber birefringence have to be avoided since they can greatly reduce the extinction ratio of the switch. An active correction scheme (e.g. a polarization controller [11] with a feedback loop) is typically not rapid enough to correct the fast, acoustical perturbations, and may not work at all for large changes due to its limited range of operation.

* Corresponding author. E-mail: claudio.vinegoni@physics.unige.ch

0030-4018/00/$ - see front matter © 2000 Published by Elsevier Science B.V.
PII: S0030-4018(00)00845-2

To avoid these problems, we use on one hand a non-interferometric switch [1], and on the other hand a passive stabilization scheme. In interferometric switches like Sagnac loops or Mach–Zehnder interferometers (IF), the switching is based on a phase-shift induced between the two different propagation directions or arms, respectively. If the signal is not carefully launched into an axis of a PM fiber, it will split into four different polarization modes, two in each propagation direction or interferometer arm, respectively. In addition to the phase-shift between the two different propagation directions or interferometer arms, additional 'local' phase-shifts between the polarization modes with the same propagation direction (or within the same IF arm) will degrade the switch quality. In the switch presented here, this problem is avoided by uniquely using this 'local' phase-shift between the two signal polarization modes in a single fiber, thereby reducing the relevant mode number to two. Having two modes only, we can then use a passive stabilization scheme that works both for fast and slow, arbitrarily large changes in the fiber birefringence. Although in this work an optical fiber is used to induce a nonlinear phase-shift, it should be noted that the stabilization scheme holds as well for any other Kerr elements (e.g. semiconductor saturable absorbers SOA).

2. Principle of operation

As mentioned above, the principle of the optical Kerr switch presented here is based on an induced phase-shift between the two signal polarization modes in a single fiber. It is induced by powerful control signal pulses that lead to a different phase-shift (via the optical Kerr effect) for signal components with the same and orthogonal polarization, respectively. The corresponding change in the output signal polarization is maximized if the control signal polarization matches the polarization of one of the two signal polarization modes during the entire propagation in the Kerr fiber. By inserting a polarizing beam splitter (PBS), the signal is switched between the two PBS output ports depending on the amount of the induced phase-shift.

For a control pulse linearly polarized along one of the birefringent axis of a PM fiber, it is easy to show that the phase shift $\Delta\phi$ acquired by a signal linearly polarized at 45° is [12]

$$\Delta\phi = \tfrac{8}{3}\pi\left(\frac{L_{\text{eff}}}{\lambda}\right) n_2 \frac{P}{A_{\text{eff}}}, \tag{1}$$

where n_2 is the nonlinear refractive index of the fiber, λ is the signal wavelength, A_{eff} is the effective area of the fiber and P is the peak pump power. Fiber losses are included in the effective length $L_{\text{eff}} = (1/\alpha)[1 - \exp(-\alpha L)]$ where L is the length and α the fiber loss coefficient. For a PBS adjusted so that all the signal is at output port 2 when the control pulse is absent, the signal at output port 1 becomes

$$T = \sin^2\frac{\Delta\phi}{2}, \tag{2}$$

where the induced phase shift $\Delta\phi$ is given by Eq. (1). A different wavelength is conveniently used for the control pulses so that they can be combined with the signal using a wavelength division multiplexer (WDM). As a consequence, a walk-off between the control pulses and the signal is introduced, ultimately limiting the switching time. A large walk-off also enlarges the required control peak power because of a reduced interaction length (i.e. smaller L_{eff} in Eq. (1)). To keep the switch fast and efficient, either a fiber with low group dispersion has to be used, or the wavelength separation should be kept as small as possible. The latter leads to a trade-off between the switching time (determined by the walk-off) and the extinction ratio (determined by the WDM filtering). For a detailed analysis, the reader is referred to Ref. [3].

It is very important to notice that the transmission given in Eq. (2) holds only for a fixed intrinsic birefringence of the fiber. Any fluctuation of this birefringence, caused e.g. by temperature drifts or pressure changes, leads to an additional phase-shift randomly changing the bias of the switch. In order to reduce this effect detrimental for the switch stability,

[1] 'Non-interferometric' in the sense that the signals being interfered are not from two physically separate arms. Of course linear optics is always interferometric in a strict sense of the word (superposition principle).

different methods have been proposed [3,11]. A very promising solution is to make a double pass of the fiber by means of a Faraday mirror (FM) [13–16]. The FM transforms any input polarization state to the orthogonal one upon reflection. Consequently, the signal components that were polarized parallel to the fast axis during the forward propagation will be polarized parallel to the slow axis during the return path and vice versa. The overall acquired phase is therefore the same for any input polarization, and the intrinsic birefringence is automatically removed as long as it is stable during a single go-and-return path. In this way, fluctuations with frequencies up to about 0.5 MHz (200 m long fiber) can be removed.

Although the application of a FM is widely spread in linear optics, we believe to be the first ones having demonstrated its usefulness for nonlinear optics as well. Especially, we showed in Ref. [6] both theoretically and experimentally that only the linear phase fluctuations are removed, whereas the purposefully induced nonlinear effects of the go and return-path add up. This allowed to measure the nonlinear polarization rotation in an optical fiber.

3. Set-up

The setup of the Kerr switch using the described stabilization scheme is shown in Fig. 1. The control signal was generated by a directly modulated DFB laser diode with a wavelength of 1559 nm, amplified by an EDFA with a small signal gain of 40 dB and a saturated output power of 23 dBm. The pulses from the DFB laser had a duration of 28 ns with a repetition rate of 1 kHz. This is good enough to demonstrate the usefulness of the stabilization scheme and the basic functioning of the switch – in an application, short control pulses at a high repetition rate could be used. In order to have a larger side-mode suppression of the DFB output at the signal wavelength, an external small pass filter was inserted after the EDFA. Using a WDM, the control pulses were then coupled into the Kerr fiber along with the signal consisting of cw light generated by a second DFB at 1556 nm. The signal power in the Kerr fiber was -1.8 dBm, whereas several Watts of control pulse peak power were available. For the Kerr medium, we first used a PM fiber with a length L of 200 m. The wavelength difference $\Delta\lambda$ of 3 nm between control and signal light consequently leads to a walk-off of about 10 ps (assuming a GVD value of $D = 17$ ps/km nm):

$$\Delta t \simeq DL\Delta\lambda \simeq 10\,\mathrm{ps}\,.$$

This value represents a lower limit for the (0–100)% rise/fall time of the switch. For even shorter switch times, a dispersion shifted fiber (DSF) would have to be used. For the initial adjustment of the switch, the polarization of both control pulses and signal could be set independently by polarization controller PC1 and PC2, respectively. This allows both for the pump to be launched into a birefringent axis of the PM fiber and for the signal polarization to be set at 45° to this axis for a maximum switching ratio at the output. At the end of the PM fiber the pump was removed with a second WDM, whereas the signal was reflected back with a Faraday mirror. After this double pass, the reflected signal is sorted out by a circulator and put on a PBS. The switch is biased by another polarization controller PC3, which allows to set the desired ratio of the signal light at the two PBS output ports. Typically, it was adjusted for maximum power in port 1 (line port), i.e. minimum power in port 2 (switch port) in the absence of control pulses. The switch port, for which Eq. (2) holds, was then monitored using a fast photodiode with a response time of 200 ps. The extinction ratio

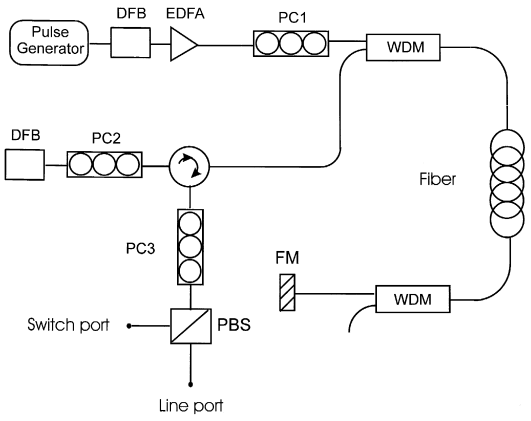

Fig. 1. Experimental setup. DFB distributed feedback laser, EDFA erbium doped fiber amplifier, PC polarization controller, FM Faraday mirror, PBS polarizing beam splitter, WDM wavelength division multiplexer

of the switch mainly depends on the extinction ratio of the PBS (20 dB in our case) and on the pump power suppression at the signal wavelength (60 dB in our set-up). If necessary, higher values could be obtained by using additional polarization selection or filtering. Note that the required control signal peak power (or fiber length) could in principle be reduced to half its value if the pump is not removed at the FM, thereby allowing a double pass of the Kerr fiber. The switch performance is still independent of the control pulse pattern in that case as long as the total power of the control signal within half the round-trip time (1 μs in our case) doesn't change too much, a situation typically realized when switching high bit rate signals.

4. Experimental results

4.1. PM fiber

The experimental results using a 200 m PM fiber as the Kerr medium are shown in Fig. 2.

The proper working of our stabilization scheme was checked by monitoring the output power at the switch port for several hours. After the initial setting of the switch, it was left alone without any re-adjustments for a time period of several hours, while a normal activity in the lab was maintained, with people working around the table. Moreover, a change in the temperature of 5 degrees was observed during that time span. The measured fluctuations of the switch port signal power are shown in Fig. 2a. Besides the measured data points (squares), the mean value (bold line) and the standard deviation σ (thin lines) are shown. As is demonstrated by the figure, the obtained switch stability was rather good (less than 2% fluctuations) when using the Faraday mirror. When it was replaced by a normal mirror on the other hand, thereby removing the stabilization, the switch port signal output power rapidly changed in the range from zero to full switch power. Indeed, it is well known that the polarization of light coupled into both the birefringent axes of a PM fiber – due to its short beatlength of only a few mm – is very susceptible to any perturbation. The use of a stabilization is therefore an absolute necessity.

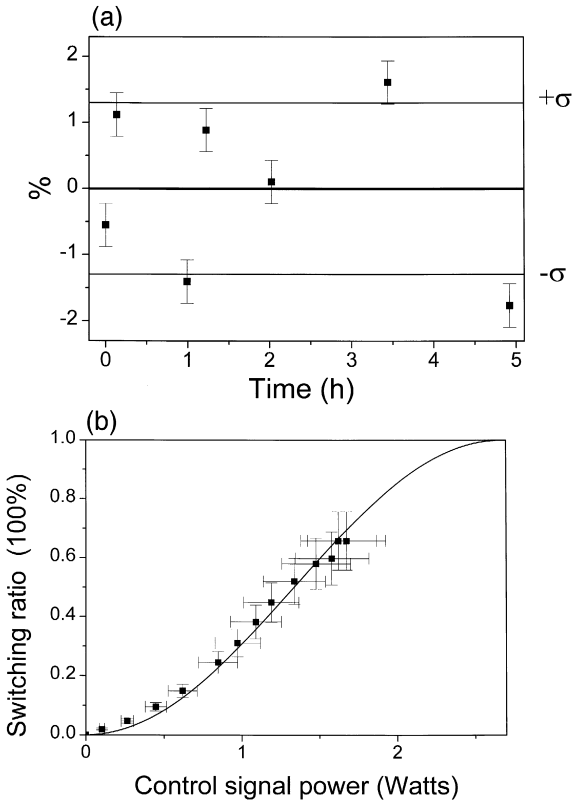

Fig. 2. Switch performance using a 200 m PM fiber. (a) Relative fluctuations of the switch port signal power as a function of time. Measured data (squares), mean value (bold line), and standard deviation σ (thin lines). (b) Normalized switching ratio as a function of the control signal power. Measured data (squares), theoretical fit (solid line).

Fig. 2b gives the normalized switching ratio as a function of the applied control signal peak power. The normalized switching ratio is defined as the ratio of the actually measured power from the switch port, divided by the maximum signal power obtainable from that same port (measured by adjusting PC3 for maximum transmission to the switch port in the absence of control pulses). The experimentally obtained values (squares) are compared with a fit (solid line) using Eq. (2) and requiring a peak normalized switching ratio of 1. As the figure shows, the experimental data corresponds well with the model ($\chi^2 = 0.8$). The maximum switching ratio we could obtain in the measurement was however only 65% for a control peak power of 1.7 W. For higher control

powers, the signal started to exhibit strong power fluctuations within the temporal switch window of 28 ns, which inhibited a proper functioning of the switch. As revealed by the optical spectrum, these fluctuations were caused by the onset of concurring nonlinear effects normally absent until much higher peak power times distance values. We believe that our non-optimal control signal source (side-band suppression) was seeding the observed nonlinearities, leading to a much lower threshold power. The observed limit in the switch ratio is therefore not a general problem of the demonstrated switch technique, but was unique to our experimental set-up.

4.2. Standard fiber

Further, we analyzed the possibility to use a standard (i.e. non PM) fiber for the Kerr medium. Besides reducing the switch cost, the assembly of the switch is much easier using standard than PM fiber, and the insertion loss can be reduced as the splice losses are lower. In order for the switch to work properly and efficiently, the part of the signal having the same polarization as the control signal at the input should keep the same polarization as the control during propagation, whereas the orthogonal part should stay polarized orthogonal. Only in this way an important phase shift between these two signal components can build-up. It is obvious that the above requirement is perfectly fulfilled in a PM fiber, where a signal component that is coupled into one of the two fiber axes remains there during propagation. In a standard fiber however, the situation is different. The above requirement, which corresponds, on the Poincaré sphere, to a conservation of the angle between the control and signal Stokes vectors during propagation, is no longer met exactly. This is because the polarization mode coupling (specified by the coupling length h [17]) present in the standard fiber leads to a coupling of the control and signal light into both the (local) fiber axes, where they will evolve differently due to their different beatlengths. The conservation of the angle between the control and signal Stokes vectors consequently depends on the fiber characteristics (coupling length h, beatlength L_b) and on the wavelength difference between the control and signal light. We therefore first verified that this angle conservation was sufficiently good in the standard fiber to be used as the Kerr medium. As a simple estimate, we can use

$$\alpha = 2\pi L\left(1/L_b(\lambda_{\text{signal}}) - 1/L_b(\lambda_{\text{control}})\right),$$

where $L_b(\lambda) = \lambda/(cB)$ and the birefringence B [ps/m] is assumed to be independent of the wavelength. The estimate represents a worst case scenario as the coupling length h is assumed to be much larger than the fiber length L and that both signal and control pulses were coupled into both fiber axes at the input. Using the wavelength difference of 3 nm of our experiment, and a typical value of the signal beatlength of 10 m, we get an angle difference of just 7° after 100 m of fiber, which should not cause any problems. Analysis of the Jones transfer matrix measured at both the signal and control wavelength further suggests that the angle should be sufficiently conserved. However, these simple estimates neglect nonlinear polarization evolution like e.g. a self-rotation of the intense control signal [6].

The testing of the switch was performed in a similar way as described in the previous section. However, as there is no well defined axis into which to couple, the input states of polarization were varied until a maximum in the switching ratio was found, although the differences were not that large due to an apparently small coupling length h of the employed Kerr fiber. This small coupling length quickly leads to a randomization of the fiber axes and makes the results almost independent from the input polarization of the control signal. On the other hand, the effective phase shift acquired by the signal is reduced by this randomization, and we had to use a longer Kerr fiber of 680 m to obtain a sufficiently large rotation of the signal at the fiber output.

As can be seen in Fig. 3a, the stability was once more excellent when employing the FM. Fig. 3b shows the observed switching ratio as a function of the control peak power. The obtained switching ratio corresponds to 90% (for control pulses with a peak power of 2.4 W) before other concurring nonlinear effects once more lead to a pulse break-up. The experimental data are not too different from the ones for the PM fiber (Fig. 2b), i.e. the longer length of the standard fiber ($\Delta L = +480$ m compared to the PM fiber used before) accounts well for the phase-

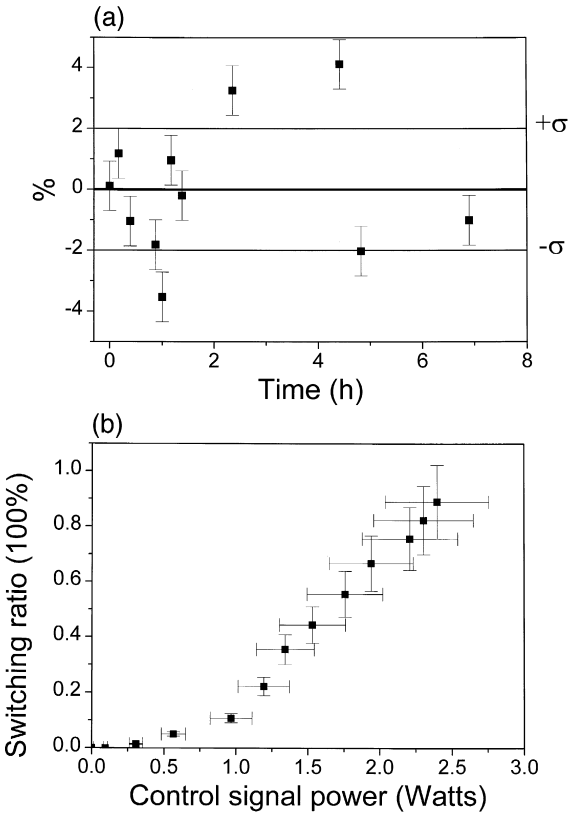

Fig. 3. Switch performance using a 680 m standard fiber. (a) Relative fluctuations of the switch port signal power as a function of time. Measured data (squares), mean value (bold line), and standard deviation σ (thin lines). (b) Normalized switching ratio as a function of the control signal power.

shift reduction caused by the 'polarization scrambling' and the different value of the ratio n_2/A_{eff}. The use of a standard fiber is therefore also interesting from a physical point of view, as the functioning of the switch could be exploited to reveal information about the coupling length of the standard fiber. Such investigations are however beyond the scope of this paper and will be discussed elsewhere.

5. Conclusion

All-optical switching at 1.5 μm based on induced nonlinear polarization rotation was successfully demonstrated in both a polarization maintaining and a standard telecom fiber. The insertion of a Faraday mirror after the Kerr fiber led to a very good stability of the switch for both cases.

In the standard fiber, switching was made possible because the small difference between the control and signal wavelength allowed for a similar evolution of both signals along the fiber – the two corresponding Jones transfer matrices were found to be almost equal – thereby well preserving the angle between the two respective Stokes vectors. As a byproduct, the ratio n_2/A_{eff} can be determined, and using an appropriate model, information about the coupling length h might be extracted as well. Further work in this direction is in progress.

Acknowledgements

We acknowledge the financial support from the Swiss Federal Office for Education and Sciences (OFES) in the framework of the European COST P2 action. Further we would like to thank the Laboratoire de Metrologie des Fibres Optique, EPFL Lausanne, for the lending of the PM fiber.

References

[1] M. Jinno, T. Matsumoto, IEEE J. Quantum Electron. 28 (1992) 875.
[2] T. Morioka, M. Saruwatari, A. Takada, Electron. Lett. 23 (1987) 453.
[3] T. Morioka, M. Saruwatari, IEEE J. on Selected Areas in Comm. 6 (1988) 1186.
[4] K.C. Byron, Electron. Lett. 23 (1987) 1324.
[5] M.J. Lagasse, D. Liu-Wong, J.G. Fujimoto, H.A. Haus, Opt. Lett. 14 (1989) 311.
[6] C. Vinegoni, M. Wegmuller, B. Huttner, N. Gisin, Measurements of nonlinear polarization rotation in a highly birefringent optical fiber using a Faraday mirror, submitted for publication, 1999.
[7] Yu.P. Svirko, N.I. Zheludev, Polarization of Light in Nonlinear Optics, Wiley, New York, 1998.
[8] R.H. Stolen, A. Ashkin, Appl. Phys. Lett. 22 (1978) 294.
[9] J.M. Dziedzic, R.H. Stolen, A. Aschkin, Appl. Opt. 20 (1981) 1403.
[10] B.E. Olssono, P.A. Andrekson, Polarization independent Kerr-switch using a polarization diversity loop, Technical Digest ECOC'98 Madrid, Spain, 1998, p. 185.
[11] E.M. Dianov, E.A. Zakhidov, A.Y. Karasik, M.A.

Kasymdzhanov, F.M. Mirtadzhiev, Sov. J. Quantum Electron. 17 (1987) 517.
[12] G.P. Agrawal, Nonlinear fiber optics, Academic Press, London, 1995.
[13] M. Martinelli, Opt. Commun. 72 (1989) 341.
[14] G. Ribordy, J.D. Gautier, N. Gisin, O. Guinnard, H. Zbinden, Electron. Lett. 34 (1998) 2116.
[15] J. Breguet, J.P. Pellaux, N. Gisin, Sens. Actuators A 1 (1995) 29.
[16] E.I. Alekseev, E.N. Bazarov, V.P. Gubin, A.I. Sazonov, N.I. Starostin, Radiotekh. Elektron. 44 (1999) 122.
[17] N. Gisin, J.P. von der Weid, J.P. Pellaux, J. Lightwave Technol. 9 (1991) 821.

B.3 Determination of the nonlinear coefficient n_2/A_{eff} using a self-aligned interferometer and a Faraday mirror.

C. Vinegoni, M. Wegmuller, N. Gisin

[1] *Group of Applied Physics - Gap Optique*
University of Geneva,
20 Ecole-de-Medecine, CH-1211 Aeneve 4, Switzerland

Claudio.Vinegoni@physics.unige.ch

Abstract : A method for the measurement of the nonlinear coefficient n_2/A_{eff} in telecom fibers at 1550 nm is demonstrated. It is based on the Kerr phase shift detected by a self-aligned interferometer incorporating a Faraday mirror. This makes the set-up very robust, and different test fibers can be measured without any further readjustments.

PUBLISHED : Electronic Letters, Vol. 36 (2000) pp. 886-87

$d_{01} = d_0 + d_1$, it is not the winner and is passed by. We then begin to test the next codevector. As the distance d_{01} is very small, we can determine the winner quickly.

Table 2: Comparison of performance of different codebook search methods

	Full search saving S	Method proposed in [3] saving S	Method proposed in this Letter saving S
	%	%	%
Real image at level 4 (codebook size: 1024, 4 dimensions, 9 bits per vector)	0	76.3	88.9
Real image at level 3 (codebook size: 1024, 4 dimensions, 9 bits per vector)	0	72.9	85.4
Real image at level 2 (codebook size: 512, 4 dimensions, 8 bits per vector)	0	70.5	79.6
Real image at level 1 (codebook size: 256, 4 dimensions)	0	68.3	78.9

Table 2 shows the results in terms of the percentage computational saving obtained over the full search method. It can be observed that use of the codebook searching method proposed in [3] can yield a 60–80% saving. However, if we utilise the special structure of TCVQ, we can reduce the computational complexity further.

Conclusion: We have presented a simple modified set partition method in order to maximise the minimum distance within subsets of a codebook and thus improve the TCVQ performance. The method can maximise the minimum distance within a subset for a small nonuniform distributed codebook. We have also proposed a computation acceleration scheme based on the partial distance search scheme and the codebook structure of TCVQ. This scheme can reduce the computational complexity by ~60–90%.

17 March 2000
Electronics Letters Online No: 20000643
DOI: 10.1049/el:20000643

Hu Mingyou and Tan Boon Tiong (*School of Electrical and Electronic Engineering, Nanyang Technological University, Nanyang Avenue, 639798, Singapore, Republic of Singapore*)

E-Mail: P146587283@ntu.edu.sg

References

1 WANG, H.S., and MOAYERI, N.: 'Trellis coded vector quantization', *IEEE Trans.*, 1992, **COM-40**, (8), pp. 1273–1276
2 FISCHER, T.R., and MARCELLIN, M.W.: 'Trellis coded vector quantization', *IEEE Trans.*, 1991, **IT-37**, (6), pp. 1551–1566
3 DA-BEI, C., and GRAY, R.M.: 'An improvement of the minimum distortion encoding algorithm for vector quantization', *IEEE Trans.*, 1985, **COM-33**, (10), pp. 1132–1133
4 MARCELLIN, M.W., and FISCHER, T.R.: 'Trellis coded quantization of memoryless and Gauss-Markov sources', *IEEE Trans.*, 1990, **COM-38**, (1), pp. 82–93

Determination of nonlinear coefficient n_2/A_{eff} using self-aligned interferometer and Faraday mirror

C. Vinegoni, M. Wegmuller and N. Gisin

A method for measuring the nonlinear coefficient n_2/A_{eff} in telecom fibres at 1550nm is presented. The method is based on determining the Kerr phase shift detected by a self-aligned interferometer incorporating a Faraday mirror. This makes the setup very robust, and different test fibres can be measured without the need for any further readjustments.

Introduction: The implementation of erbium-doped fibre amplifiers allows for high bit rate transmission over transoceanic distances. In addition the technique of wavelength division multiplexing (WDM) is used to increase the transmission rate, leading to a significant amount of power being inside the fibre. Because of the long distances and high powers, optical nonlinearities due to changes in the refractive index (optical Kerr effect) start to play a significant role. Among them, self-phase modulation (SPM), cross-phase modulation (XPM), and four-wave mixing (FWM) are the most important. The magnitudes of these effects depend on the ratio n_2/A_{eff}, where n_2 is the nonlinear refractive index of the fibre and A_{eff} the effective area of the lightmode. It is therefore important to have a simple and accurate method for determining this ratio. Different methods, based on SPM or XPM phase shift detection using interferometric and non-interferometric schemes have been proposed [1]. In this Letter, we present a different method based on the interferometric detection of a phase shift using a self-aligned interferometer with a Faraday mirror. This method has the advantages of being simple and all fibre implementable. Moreover, fluctuations due to environmental perturbations present in the other schemes mentioned above are avoided.

Principle of operation: The power dependence of the refractive index leads to a power dependent phase change ϕ of a pulse (peak power P, wavenumber k) travelling through a fibre of length L:

$$\phi(P) = \phi_1 + \phi_{n1} = n_0 kL + n_2 kL_{eff}\frac{P}{A_{eff}}m \qquad (1)$$

Fibre losses are accounted for by the effective length $L_{eff} = 1/\alpha\,[1 - \exp(-\alpha L)]$, with fibre loss coefficient α. The polarisation parameter m depends on the polarisation characteristics of the test fibre and the signal polarisation state. It is equal to 1 for the case of a polarisation maintaining fibre if the light is coupled into one of the two axes [2], whereas for a sufficiently long standard telecom fibre with a complete scrambling of the polarisation, it was demonstrated that $m = 8/9$ [3]. Using eqn. 1, measurement of the acquired phase shift will enable the ratio n_2/A_{eff} to be determined or, through an independent measurement of A_{eff}, the value of n_2.

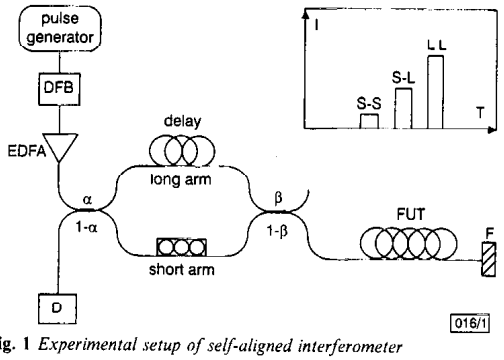

Fig. 1 *Experimental setup of self-aligned interferometer*

DFB: distributed feedback laser; EDFA: erbium doped fibre amplifier; PC: polarisation controller; FUT: fibre under test; FM: Faraday mirror; D: detector

The phase shift is measured using the self-aligned interferometer shown in Fig. 1. Amplified laser pulses are split at the first coupler (coupling ratio $\alpha/(1 - \alpha)$). They then move along the two

interferometer arms, which are different in length so that the two pulses do not interfere on recombination at the second coupler (coupling ratio $\beta/(1-\beta)$). One of the exit arms of this last coupler is connected to the fibre under test (FUT) of which n_2/A_{eff} is to be measured. For an adequate choice of α and β, the two pulses in the FUT strongly vary in power, and consequently experience (according to eqn. 1) a different degree of phase shift. After being reflected at the Faraday mirror (FM) [4, 5], the pulses return back through the FUT towards the first coupler.

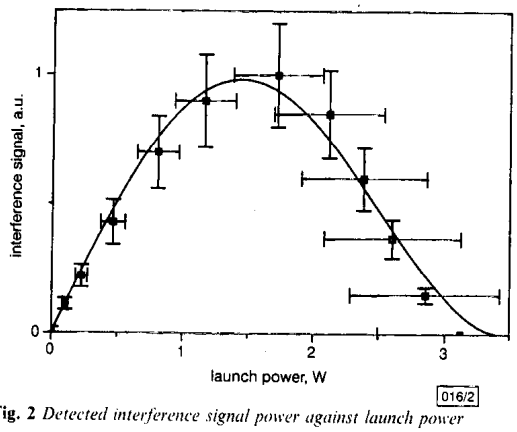

Fig. 2 *Detected interference signal power against launch power*
■ measured
——— theoretical fit

Four different trajectories through the interferometer are possible during the forward and return path: a double pass of the long-arm (long-long), of the short-arm (short-short), and a forward pass of the short (long) arm with a return pass through the opposite arm (short-long and long-short, respectively). Owing to the differences in path length, three different arrival times at the detector can be discerned, as is schematically shown in the inset of Fig. 1. Only the middle pulse, which is due to the interference between the short-long and long-short pulses, is interesting and will be further analysed. Its power at the detector depends on the phase relationship between the two interfering signals, and it can therefore be exploited to calculate the nonlinear phase shift experienced in the FUT. Note that contrary to regular Mach-Zehnder interferometers, the balancing of the interferometer arms is not critical as the path lengths of the two interfering signals are automatically matched (self-aligned).

Obviously, the power of this middle pulse also depends on the polarisation states of the two interfering signals, given by

$$|\psi_{LS}\rangle = R_S^{-1}(R_{FUT}^{-1}FR_{FUT})R_L|\psi_0\rangle = R_S^{-1}FR_L|\psi_0\rangle \equiv A|\psi_0\rangle$$
$$|\psi_{SL}\rangle = R_L^{-1}(R_{FUT}^{-1}FR_{FUT})R_S|\psi_0\rangle = R_L^{-1}FR_S|\psi_0\rangle \equiv B|\psi_0\rangle \quad (2)$$

for the long-short and short-long path, respectively. $|\Psi_0\rangle$ is the input state of polarisation, and R_L, R_S, *RFUT*, and F are the transformation operators for the long arm and short arm, the FUT, and the FM, respectively. The use of an FM as a reflector removes polarisation transformations of the FUT, thereby fixing its output polarisation. Note that using a standard mirror in place of the FM, an additional PC would be required, which not only makes the initial adjustments difficult, but also leads to an undesired FUT dependence. For optimum visibility, full interference is required between the two signals, i.e. $A = B$ in eqn. 2, which can be obtained by properly adjusting the PC such that $R_L = R_S$. In practice, this is achieved by setting the PC so that the output intensity is maximised for low input pulse power and with the FM directly connected to the interferometer (i.e. no FUT and therefore no nonlinear phase shift is present). This setting can then be used throughout the measurements, without the need for readjustments as long as there is no significant change in R_L or R_S. Note that the fact that the bias of our interferometer can be adjusted is due to a geometrical phase (Pancharatnam-effect, [6]): at the PC, the clockwise travelling pulse has experienced a π phase shift (with respect to the anti-clockwise travelling pulse) from the FM reflection. Using the described adjustment, the detected power becomes proportional to

$$P_{out}(P) \propto P\cos^2(\Delta\varphi) \quad (3)$$

where $\Delta\phi$ is the amount of nonlinear phase shift, equal to

$$\Delta\phi(P) = \frac{2\pi}{\lambda}PL_{eff}(\alpha-\beta)m\frac{n_2}{A_{eff}} \quad (4)$$

Straightforward calculation shows that for maximum visibility of the detected signal, one of the two couplers has to be symmetric (50/50). To obtain a good accuracy for n_2/A_{eff}, the measurements are carried out for different launch powers P. Ideally, the length of the FUT is long enough to allow for good polarisation scrambling and to be able to detect the first zero pass at $\Delta\phi = \pi/2$ for the available launch power.

Results and discussion: For the practical implementation of the above concept, we used a directly modulated DFB laser diode with a wavelength of 1559nm and consecutive amplification by an EDFA. The pulse duration was 28ns with a repetition rate of 1kHz. Note that in some fibres, such pulses can excite acoustic waves through electrostriction, leading to erroneous n_2/A_{eff} values: a laser source with shorter pulses should be used to avoid this risk. For the couplers, a 50/50 ratio was used for the first one and a 90/10 for the second.

Fig. 2 displays the magnitude of the interference signal as a function of the launch power P for a standard telecom fibre (SMF) with a length of 1100 m used as the FUT. The experimentally obtained values (squares) are fitted using eqn. 3. The data correspond well with the model ($\chi^2 = 3 \times 10^{-3}$). As can be seen, the signal slowly increases reaching a maximum value at 1.4W. For higher powers the nonlinear phase shift becomes more important and the signal decreases reaching a null value at 3.4W corresponding to a full $\pi/2$ phase shift. From the fit we obtain a value of $(2.76 \pm 0.04)\ 10^{-10}\,W^{-1}$ for the nonlinear coefficient n_2/A_{eff}. Having found with the refracted-near-field method [7] a value of $(88 \pm 3)\ \mu m^2$ for A_{eff}, the nonlinear refractive index n_2 becomes $(2.4 \pm 0.1)\ 10^{-20}\ m^2/W$.

Conclusion: We have described a simple method for the measurement of the nonlinear coefficient n_2/A_{eff} based on an all fibre, self-aligned interferometer. The self-alignment characteristic not only allows for an easy and quick initial adjustment of the interferometer, but along with the use of a Faraday mirror also makes it robust against environmental perturbations. This leads to good accuracy for the measured n_2/A_{eff} values. The proposed method is well suited to the routine measurement of the nonlinear coefficient because, owing to the presence of the FM, the fibre under test can be easily exchanged without necessitating any further readjustments of the interferometer.

Acknowledgments: We acknowledge the financial support from the Swiss Federal Office for Education and Sciences (OFES) in the framework of the European COST 265 programme.

24 March 2000
Electronics Letters Online No: 20000668
DOI: 10.1049/el:20000668

C. Vinegoni, M. Wegmuller and N. Gisin (*Group of Applied Physics, University of Geneva, 20 Ecole-de-Médecine, CH-1211, Geneva 4, Switzerland*)

E-mail: claudio.vinegoni@physics.unige.ch

References

1 FELLEGARA, A., ARTIGLIA, M., ANDREASEN, S.B., MELLONI, A., ESPUNES, F.P., and WABNITZ, S.: 'COST 241 intercomparison of nonlinear refractive index measurements in dispersion shifted optical fibres at λ = 1550nm', *Electron. Lett.*, 1997, 33, pp. 1168–1170

2 WITTL, F., VOBIAN, J., HERCHENROEDER, G., and DULTZ, W.: 'Interferometric determination of the nonlinear refractive index n_2 of optical fibers'. Tech. Dig. Symp. Optical Fiber Measurements, 1996, pp. 71–74 (NIST SP 905)

B.4 Measurements of the nonlinear coefficient of standard SMF, DSF, and DSC fibers using a self-aligned interferometer and a Faraday mirror.

C. Vinegoni, M. Wegmuller, N. Gisin

[1] *Group of Applied Physics - Gap Optique*
University of Geneva,
20 Ecole-de-Medecine, CH-1211 Aeneve 4, Switzerland

Claudio.Vinegoni@physics.unige.ch

Abstract : Using a method based on the detection of the Kerr phase shift by a self-aligned interferometer, we present measurements of the nonlinear coefficient n_2/A_{eff} for standard SMF, DSF, and DCF fibers. The presence of a Faraday mirror in the interferometer makes the set-up very robust, and different test fibers can be measured without any further readjustments. Interlaboratory comparisons show that the values found with our method are in good agreement with the other ones.

Further, analysis of a SMF fiber with large chromatic dispersion shows a good reproducibility of the n_2/A_{eff} measurements as a function of fiber length.

PUBLISHED : Photonics and Technology Lett., December 2001

Measurements of the Nonlinear Coefficient of Standard SMF, DSF, and DCF Fibers Using a Self-Aligned Interferometer and a Faraday Mirror

C. Vinegoni, M. Wegmuller, and N. Gisin

***Abstract*—Using a method based on the detection of the Kerr phase shift by a self-aligned interferometer, we present measurements of the nonlinear coefficient n_2/A_{eff} for standard single-mode fiber (SMF), dispersion-shifted fibers, and dispersion compensating fibers. The presence of a Faraday mirror in the interferometer makes the setup very robust, and different test fibers can be measured without any further readjustments. Interlaboratory comparisons show that the values found with our method are in good agreement with the other ones. Further, analysis of a SMF fiber with large chromatic dispersion shows a good reproducibility of the n_2/A_{eff} measurements as a function of fiber length.**

***Index Terms*—Nonlinear optics, optical fiber measurements, optical kerr effect.**

I. Introduction

THE IMPLEMENTATION of erbium-doped fiber amplifiers and chromatic dispersion compensation allows for long distance data transmission. Along with the technique of wavelength-division multiplexing (WDM), this leads to an important amount of power inside the fiber over long distances, and optical nonlinearities start to play a significant role. Their magnitudes depend on the ratio n_2/A_{eff}, where n_2 is the nonlinear refractive index of the fiber and A_{eff} the effective area of the mode. There are different methods to measure n_2/A_{eff}, based on self-phase modulation (SPM) or cross-phase modulation (XPM) induced phase shift detection [1] using interferometric and noninterferometric schemes. The interferometric detection scheme [2] presents the advantage that it can be implemented more easily, but a disadvantage is its susceptibility to environmental perturbations that leads to a poor stability. In our setup, we obtained a considerable improvement of this technique by using a self-aligned interferometer [3] with a Faraday mirror. This method has the advantage to be simple and all-fiber implementable. The fluctuations due to the environmental perturbations are completely removed [4].

In this letter, after giving a brief description of our measurement method, we compare the values of n_2/A_{eff} obtained with our method for dispersion-shifted fibers (DSF), dispersion compensating fibers (DCF), and a standard single-mode fiber (SMF) with the ones obtained by other institutions on the same fibers. Our values are found to agree quite well with the results from the different measurement methods employed by the other institutions. Moreover, we demonstrate that our results are independent of the length of the test fiber (on a 10-km range) even in the presence of large (17 ps/nm $\cdot$ km)group velocity dispersion (GVD), which cause some problems in other measurement methods [5].

Manuscript received June 13, 2001; revised August 8, 2001. This work was supported by the Swiss Federal Office for Education and Sciences (OFES) in the framework of the European COST 265 action.

The authors are with the Group of Applied Physics, University of Geneva, CH-1211 Geneve 4, Switzerland (e-mail: claudio.vinegoni@physics.unige.ch).

Publisher Item Identifier S 1041-1135(01)09495-2.

II. Principle of Operation

Due to the power dependence of the refractive index, a pulse with peak power P and wave number k, traveling along a fiber of length L, will acquire a power dependent phase change ϕ given by

$$\phi(P) = \phi_l + \phi_{nl} = n_0 kL + kL_{\text{eff}} \frac{n_2}{A_{\text{eff}}} Pm \qquad (1)$$

The fiber losses are accounted for by the effective length $L_{\text{eff}} = 1/\alpha[1 - \exp(-\alpha L)]$, with fiber loss coefficient α [1]. The polarization parameter m depends on the polarization characteristics of the test fiber and the input signal polarization state. It is equal to one for the case of a polarization maintaining fiber if the light is coupled into one of the two axes. For the case of a sufficiently long standard telecom fiber with a complete scrambling of the polarization, it was demonstrated that $m = 8/9$ [6]. Using (1), a measure of the acquired phase shift allows to determine the ratio n_2/A_{eff} (or, through an independent measurement of A_{eff}, the value of n_2).

The setup of the self-aligned interferometer is shown in Fig. 1 and is described in detail in [4]. High peak power pulses (pulse length 20 ns) from an erbium-doped fiber amplifier (EDFA) are split at the entry of the first coupler (coupling ratio 50/50) and move along the two different arms of the interferometer. These arms are different in length such that the two pulses do not interfere when they recombine at the second coupler (coupling ratio 90/10). Due to the asymmetry of the last coupler, the two pulses enter the fiber under test (FUT) with different powers, and according to (1), they will acquire different amounts of phase shift during the propagation along the FUT. The pulses are then reflected at the Faraday mirror (FM) and return back through the

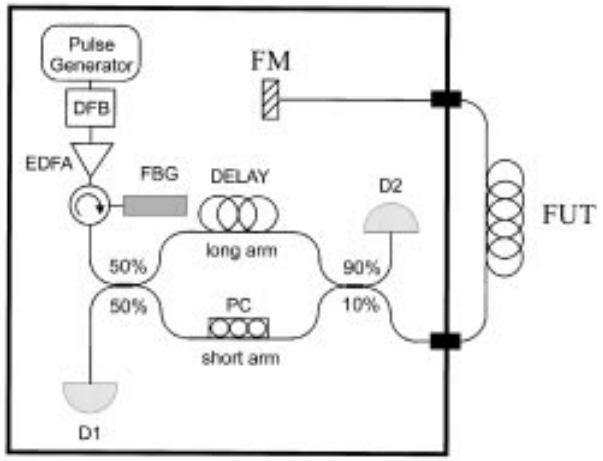

Fig. 1. Experimental setup of the self-aligned interferometer. DFB. EDFA. PC. FUT. FM. D detector. FBG.

FUT and the interferometer, toward the first coupler. During the go and return trip through the interferometer, four different paths are possible. A double pass of the long-arm (LL), of the short-arm (SS), and a forward pass of the short (long) arm with a return pass through the opposite arm (SL and LS, respectively). Due to the difference in arm lengths, three different arrival times at detector D1 can be distinguished. Only the middle pulse arising from the interference between the SL and the LS pulses is further analyzed. The power of this pulse depends on the phase relationship between the two interfering signals and can be exploited to calculate the nonlinear phase shift experienced in the FUT. Note that contrary to regular Mach–Zehnder interferometers, the balancing of the interferometer arms is not critical here as the path lengths of the two interfering signals are automatically matched (self-aligned).

It is possible to show [4] that in order to have the maximum visibility at the exit of the interferometer (i.e., the pulses have the same state of polarization), the polarization controller (PC) inserted in one of the interferometer arms has to be adjusted such that the transfer matrix of the short arm is equal to the transfer matrix of the long one. Note that using a standard mirror in place of the FM , an additional PC would be required [4], making the initial adjustment of the interferometer more difficult. Moreover, both PCs would have to be readjusted for every new FUT. With the FM instead, the interferometer does not require any adjustments after its initial calibration.

In our measurement, the PC was adjusted once for all such that all the light was directed toward detector D1, when no nonlinearity is present (i.e., no FUT is present and at low input power). The detected power $P_{\rm OUT}$ at the exit of the interferometer then becomes

$$P_{\rm OUT}(P) \propto P\cos^2(\Delta\phi) \tag{2}$$

where P corresponds to the pulse power at the entry of the coupler, and $\Delta\phi$ corresponds to the nonlinear phase shift acquired along a double pass of the FUT [4]

$$\Delta\phi(P) = \frac{2\pi}{\lambda} P L_{\rm eff} \frac{16}{45} \frac{n_2}{A_{\rm eff}}. \tag{3}$$

TABLE I
VALUES OF THE NONLINEAR COEFFICIENT $n_2/A_{\rm eff}$ FOR DIFFERENT TEST FIBERS MEASURED WITH THE METHOD PROPOSED IN THIS LETTER (COLUMN A) AND AS MEASURED BY OTHER INSTITUTIONS (COLUMN B). FOR THE VALUES MEASURED WITH OUR METHODS, THE MAXIMUM ABSOLUTE DEVIATION FROM THE AVERAGE (MD) IS USED TO CHARACTERIZE THE REPRODUCIBILITY

Fiber		Length (m)	λ_0 (nm)	$A_{\rm eff}$ (μm^2)	Nonlinear Coefficient $n_2/A_{\rm eff}$ x 10^{-10} W^{-1}			
					A		B	
					Value	MD	Value	SD
G-1	(SMF)	11840	1302	-	3.6	5 %	-	-
DSF-1	(DSF)	1990	1556.4	44.5	6.4	2 %	6.3 [7]	5 % [7]
DSF-2	(DSF)	1990	1548.6	41.1	6.3	5 %	6.6 [7]	5 % [7]
NIST-B	(DSF)	1563	-	52.2 [9]	4.3	2 %	4.3 [9]	14 % [9]
NIST-C	(DCF)	1010	-	20.2 [9]	15.6	11 %	13.4 [9]	15 % [9]

For the values measured at NTT [7]the standard deviation is shown. For the values obtained by the NIST round robin [9] the standard deviation among different participants is reported

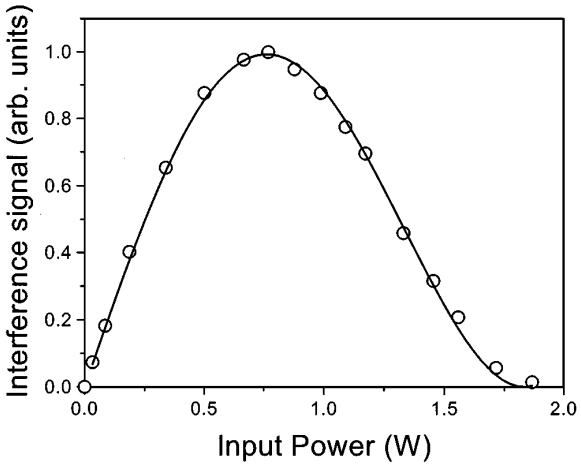

Fig. 2. Detected interference signal power as a function of launch power: (open circles) measured data, (solid line) theoretical fit (2).

Detector D2 is used to measure the power at the entry of the FUT.

III. RESULTS

$n_2/A_{\rm eff}$ was measured for five different fibers comprising SMF, DSF, and DCF of different lengths. The fibers' parameters are listed in Table I.

Fibers DSF-1 and DSF-2 were also measured at NTT [7] utilizing the SPM-based continuous-wave (CW) dual-frequency (DF) method [5], [8]. Fibers NIST-B and NIST-C were measured by six different institutions using the CWDF method and the pulsed method using different fiber lengths and laser wavelengths. Results regarding this North American round robin were published in [9].

A typical result for a single measurement with our method is shown in Fig. 2. The FUT was Fiber G-1 with a fiber length of 2231 m. The interference signal power detected at the exit of the interferometer is plotted as a function of the launch input power P. The experimental values (open circles) are increasing almost linearly in the beginning, demonstrating that nonlinear effects are of little importance up to launched powers of about 0.5 W. Then they set in quite heavily, and the measured power eventually starts to decrease with increasing launch power. The

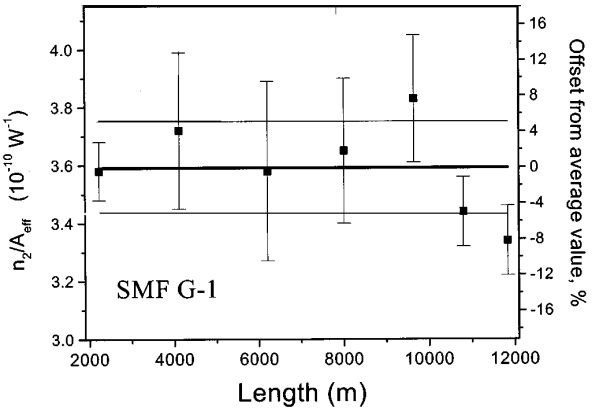

Fig. 3. Nonlinear coefficient measured for different lengths of the same fiber (G-1).

maximum of the interference signal power is reached at a launch power of 0.8 W, whereas a null value, corresponding to a full $\pi/2$ nonlinear phase shift, is obtained for 1.9 W. From this value, n_2/A_{eff} can be calculated using (3). However, we always fitted all the points as the precision is much better.

For each fiber, three to four different measurements were taken on different days in order to test the reproducibility of our method. The corresponding results are summarized in column A of Table I. Note that the maximum absolute deviation from the average (MD) is used to characterize the reproducibility. Generally, the reproducibility is quite good ($<$10%) although it varies somewhat from fiber to fiber (see Table I). Column B of Table I reports the values found by the other laboratories. For the NIST fibers [9], the standard deviation among the n_2/A_{eff} values of the six different round robin participants is given. As one can see the agreement with our values is quite good (with a deviation $<$15% in the worst case). For the NTT fibers [7], the standard deviation of different measurements (using the same measurement method) is given. Once more, the agreement with our values is good ($<$5%). For all measurements of both the NIST and NTT comparison, the deviation of our values are within the error bars.

When looking at the maximum deviation of our measurements, it is striking that for the NIST-C fiber the value is much larger. A reason for this might be that the GVD in this DCF fiber is much higher. In fact, some methods [5] were found to be very sensitive to the fiber's length for large values of the chromatic dispersion. Therefore, it is interesting to analyze the reproducibility of our method in a large GVD fiber as a function of the fiber length.

Consequently, we made cutback measurements of n_2/A_{eff} for a SMF (G-1) changing the length from 12 to 2 km. For each length, at least three measurements were taken. The results are reported in Fig. 3. The overall standard deviation is only 6%, i.e., a similar amount as the maximum fluctuations for a fixed length (see Table I). Also, no trend of the n_2/A_{eff} values as a function of fiber length can be found, demonstrating that our method is insensitive to the fiber length (in a range of around 10 km) even for large values of chromatic dispersion.

IV. Conclusion

In this letter, we have presented a simple and stable method for the measurement of the nonlinear coefficient n_2/A_{eff} based on an all-fiber self-aligned interferometer. Due to its robustness against environmental perturbations, and its ease of adjustment, the proposed method is well suited to routinely measure the nonlinear coefficient. The presence of the FM allows to easily exchange the FUT without necessitating any further readjustments of the interferometer.

An interlaboratory comparison of the n_2/A_{eff} measurements on the same test fibers showed good agreement of our results with the others. Moreover, our method seems to be independent of the fiber's length on a range of 10 km even in the presence of large GVD, known to cause problems with some of the other measurement methods.

Acknowledgment

The authors would like to thank K. Nakajima and N. Ohashi from NTT, A. Pham from EXFO, C. Meneghini from INO and T.J. Drapela from NIST for providing us the test fibers.

References

[1] G. Agrawal, *Nonlinear Fiber Optics*. San Diego, CA: Academic, 1989.
[2] F. Wittl, J. Vobian, G. Herchenroeder, and W. Dultz, "Interferometric determination of the nonlinear refractive index n_2 of optical fibers," in *Tech. Dig.— Symp. Optical Fiber Measure., (NIST SP 905)*, 1996, pp. 71–74.
[3] J. Meier, "Stabile Interferometrie des Nichtlinearen BrechzahlKoeffizienten von Quarzglasfasern der Optischen Nachrichtentechnik," Ph.D., 1995.
[4] C. Vinegoni, M. Wegmuller, and N. Gisin, "Determination of the nonlinear coefficient n_2/A_{eff} using a self-aligned interferometer and a Faraday mirror," *Electron. Lett.*, vol. 36, pp. 886–888, 2000.
[5] T. Omae, K. Nakajima, and M. Ohashi, "Universal conditions for nonlinear refractive index n_2 estimation of dispersion compensating fibers by cw-SPM method," in *OFC 2001*, Anaheim, 2001.
[6] S. V. Chernikov and J. R. Taylor, "Measurement of normalization factor of n_2 for random polarization in optical fibers," *Opt. Lett.*, vol. 21, pp. 1559–1561, 1996.
[7] C. Vinegoni, M. Wegmuller, N. Gisin, K. Nakajima, and M. Ohashi, "Interlaboratory measurements of the nonlinear coefficient of standard SMF and DSF fibers using an interferometric method and an SPM based cw dual-frequency method," in *OFMC 2001*, Cambridge, U.K.
[8] A. Boskovic, S. V. Chernikov, J. R. Taylor, L. Gruner-Nielsen, and O. A. Levring, "Direct continuous-wave measurement of n_2 in various types of telecommunication fiber at 1.55 μm," *Opt. Lett.*, vol. 21, pp. 1965–1967, 1996.
[9] T. Drapela, "Effective area and nonlinear coefficient measurements of single-mode fibers: recent interlaboratory comparison," *Proc. SPIE, ser. Applications of Photonic Technology 4*, vol. 4087, pp. 293–297, 2000.

B.5 Distributed gain measurements in Er-doped fibers with high resolution and accuracy using an optical frequency domain reflectometer.

M. Wegmuller, P. Oberson, O. Guinnard, B. Huttner, L. Guinnard, C. Vinegoni, and N. Gisin

[1] *Group of Applied Physics - Gap Optique*
University of Geneva,
20 Ecole-de-Medecine, CH-1211 Aeneve 4, Switzerland

Claudio.Vinegoni@physics.unige.ch

Abstract : For critical Erbium doped fiber amplifier design, e.g. gain tilt optimization in WDM booster amplifiers, knowledge of the gain distribution within the active fiber can present a valuable information. Among the different techniques to evaluate the distributed gain in active fibers, the technique of optical frequency domain reflectometry seems most promising as it is a nondestructive measurements method well matched to the task due to its dynamic range, resolution and range. Moreover the background ligth from ASE or residual pump light is strongly rejected due to the coherent detection scheme employed. Using different Erbium-doped fibers with strongly varying doping levels and confinements, we demonstrate the excellent accuracy and reproducibility of the technique.

PUBLISHED : J. Lightwave Technol., Vol. 18 (2000) pp. 2127-32

Distributed Gain Measurements in Er-Doped Fibers with High Resolution and Accuracy Using an Optical Frequency Domain Reflectometer

M. Wegmuller, P. Oberson, O. Guinnard, B. Huttner, L. Guinnard, C. Vinegoni, *Member, OSA*, and N. Gisin, *Member, OSA*

***Abstract*—For critical Erbium-doped fiber amplifier (EDFA) design, e.g., gain tilt optimization in WDM booster amplifiers, knowledge of the gain distribution within the active fiber can present a valuable information. Among the different techniques to evaluate the distributed gain in active fibers, the technique of optical frequency domain reflectometry seems most promising as it is a nondestructive measurement method well matched to the task due to its dynamic range, resolution, and range. Moreover, background light from ASE or residual pump light is strongly rejected due to the coherent detection scheme employed. Using different Erbium-doped fibers with strongly varying doping levels and confinements, we demonstrate the excellent accuracy and reproducibility of the technique.**

***Index Terms*—Fiber optics amplifiers and oscillators, metrology, nondestructive testing.**

I. Introduction

THE ERBIUM-DOPED fiber amplifier (EDFA) is one of the key components for the tremendous, fast pace progress in optical telecommunication. Do to its high efficiency, large output power, low noise figure, and compactness, it found its way into diverse applications at different locations in the optical network [1].

In order to exploit the EDFA capabilities to a maximum, theoretical models were soon developed for further optimization of the EDFAs [2], [3]. Although these different models proved as a valuable tool for the proper tuning of parameters like the Erbium ion density and doping confinement, they are typically not capable of predicting important parameters like the distributed gain or optimum fiber length to better than 15% for a specific experimental configuration [2]. This point will be further addressed in the paper. The problem stems on one hand from the fact that models are never perfect as they frequently neglect some aspect of the gain dynamics for the sake of simplicity, e.g., inhomogeneous gain broadening, the number of levels, transverse space integrals, ASE spectrum, etc. [2]. The more important point, however, is that the input parameters for the models can frequently not be measured with a sufficient accuracy. Therefore, several methods to directly measure the gain distribution have been proposed and demonstrated. Cut-back methods are expensive and time consuming, and are not applicable for the measurement of the gain distribution in backward or bi-directionally pumped fibers. Nondestructive methods are consequently advantageous. Using an optical time domain reflectometer (OTDR) with additional ASE filtering, distributed gain curves were obtained [4]. However, the limited dynamic range and spatial resolution (due to the large minimum measurement distance in the order of a kilometer) of OTDRs make it a bad match to measure the gain distribution in typical Erbium-doped fibers (EDF) with lengths of some tens of meters.

Recently, we reported on distributed gain measurements using an optical frequency domain reflectometer (OFDR) [5]. The OFDR is ideally suited for this type of measurement, as its range, resolution, and dynamic range match well with the required values [6], [7]. Further, due to the coherent detection used in the OFDR, disturbing ASE light is largely rejected.

In this paper, an improved OFDR with better resolution, accuracy, and stability is used to give good quantitative results for the gain distributions in different types of EDF at 1550 nm. The reproducibility and accuracy of the distributed gain measurements are investigated carefully and compared to traditionally measured results using the cut-back method.

II. Characteristics of the Improved OFDR

The OFDR technique (Fig. 1) is based on the detection of a beat signal between the distributed reflections from the fiber under test (Rayleigh backscatter, connectors, etc.) and a fixed Fresnel reflection (local oscillator). Using a specific linear frequency sweep of the laser source, one can straightforwardly map the measured beat frequencies on a distance scale, whereas the normed square power for a given beat frequency gives the reflectivity at the corresponding distance.

For a good overview of the OFDR principles and limits, the reader is referred to [6]. In the device used for the measurements presented here, several important improvements have been implemented. First, a different laser source with a much higher coherence length (about 3 km, bandwidth of 10 kHz) is used [8]. The coherence loss leads to a drop in the Rayleigh backscattering level of only about 0.15 dB after 30 m, making a correction of the measured gain curves as in [5] unnecessary. The accuracy of the reflectivity values has been greatly increased by adopting a polarization diversity detection scheme. This assures that the measured reflectivities are independent of the state of polarization of the reflected light—which changes as a function

Manuscript received March 28, 2000; revised August 25, 2000. This work was supported by the Swiss Federal Department for Education and Sciences (OFES) within the European COST 265 Project.

The authors are with the Group of Applied Physics, University of Geneva, CH-1211 Geneve 4, Switzerland (e-mail: mark.wegmuller@physics.unige.ch).

Publisher Item Identifier S 0733-8724(00)10536-5.

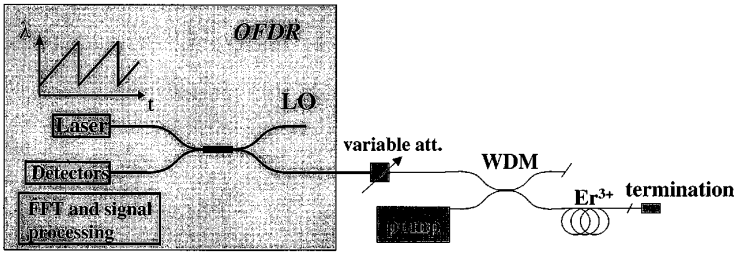

Fig. 1. Sketch of the experimental setup.

of the location of the reflector down the fiber and the fiber beat-length [9]—to within ± 0.5 dB. Note that this value is an upper limit corresponding to the maximum signal deviation, observed when purposefully varying the polarization state in front of a reflector. Assuming a Gaussian probability distribution with a confidence level of 99% for the measured maximum deviation, the typical accuracy becomes $\sigma = 0.25$ dB. Further, the spatial resolution (FWHM of a distinctive reflection peak) was enhanced to 2 cm (30 m range), with a peak location accuracy of a mm.

The OFDR can easily measure the Rayleigh backscattering due to its sensitivity of ~ -120 dB, and the distributed gain in an EDF can be directly measured within 30 s. During the backward path of the reflected light, gain saturation is the same as during the forward path due to the extremely slow gain dynamics of the Erbium ions ($\sim$1 ms, [2]). The measured Rayleigh light therefore undergoes twice the gain (or loss), and the corresponding decibel-values have to be divided by two to get the physical quantity of interest. Note that if the single forward trip gain is to be measured, one has to be careful to avoid strong backreflections after the active fiber (which in an EDFA is ensured by the exit isolator), as the reflected light could saturate the gain. Using an analytic model for the EDF gain [10], we found that for a 25 dB gain, 30 m long fiber backreflections do not add to gain saturation in a significant way (gain reduction of less than 0.5 dB) as long as they are kept below -40 dB.

III. Experimental Results

In all the following measurements, a wavelength division multiplexer (WDM) was inserted between the OFDR test output and the EDF to feed the 1480 nm pump radiation into the active fiber. This corresponds to a forward pumping scheme, but the measurements could be done as easily for backward or bi-directional pumping. For the case of a large part of nonabsorbed pump light exiting the fiber, additional filtering might however be necessary for the latter pump set-ups to remove the backward travelling pump light. This is because noncoherent light reaching the OFDR can saturate its detectors and also leads to a somewhat enhanced noise background.

A standard fiber with a low end reflectance (-65 dB) was spliced to the output end of the active fiber in order to avoid backreflections into the EDF as much as possible.

In order to investigate the accuracy and reproducibility of the measured distributed gain curves from the OFDR we performed several measurements using different fibers and pump powers, and compared them with the gain values obtained from direct transmission measurements using the cut-back technique.

Fig. 2 shows the results for a fiber with a 2000 ppm Er doping level and a length of about 1 m. The lines correspond to the distributed Rayleigh backscattering as measured by the OFDR. The OFDR probe power was held constant at -10 dBm, whereas the pump power was gradually changed from no pump at all to $+15.2$ dBm. Due to the constant input signal, the Rayleigh level is about the same in front of the active fiber that starts at 7.9 m, in spite of the increasing level of backward ASE light. Note that the fluctuations in the backscattered signal is not due to a noisy measurement, but is caused by interference among the different Rayleigh scatterers ("coherent speckle"). The curves shown in Fig. 2 were smoothed by dithering the center frequency of the OFDR by $\sim$0.5 nm and averaging (50 samples). As the fiber was not moved between the consecutive measurements, the remaining interference pattern should not change significantly, which was indeed the case as demonstrated by the figure. At the beginning of the active fiber, a distinctive jump of 8.7 dB in the Rayleigh level can be observed (unfortunately, it is somewhat covered by a Rayleigh peak). This is a known phenomenon due to the often larger numerical aperture (NA) of the EDF, leading to a larger capturing of the Rayleigh scattered light that is emitted in 4π sr (signal power $\propto \mathrm{NA}^2$ [2, ch. 5.8]. As a byproduct, the OFDR curves therefore give a good idea of the amount of possible NA mismatches, which lead to deteriorating internal reflections and losses that can increase the noise figure (input loss) or saturate the gain (reflections) and should consequently be avoided as much as possible.

Looking at the curve within the active fiber (7.9–8.8 m) for a switched off pump, one observes an exponential decay (linear on a decibel scale). It corresponds to the expected 1550 nm absorption of the Er ions in the active fiber, which is calculated from the slope to a value of -62 dB/m. For pump powers larger than about 9.6 dBm, the backscattered signal initially grows, indicating that the fiber is inverted leading to some gain. The figure shows that the location of the maximum gain strongly depends on the pump power. For a full pump of 15.2 dBm e.g., an amplification of 6.3 dB is obtained after 25 cm. After that distance, the fiber is no longer inverted because of pump depletion, and strong signal re-absorption takes place. For a distance of more than 70 cm, the remaining pump power is so small that the signal decays once more with a rate of about -62 dB/m.

A cut-back measurement was performed to obtain directly the transmission through different lengths of the active fiber. The same input signal power of -10 dBm and the same pump

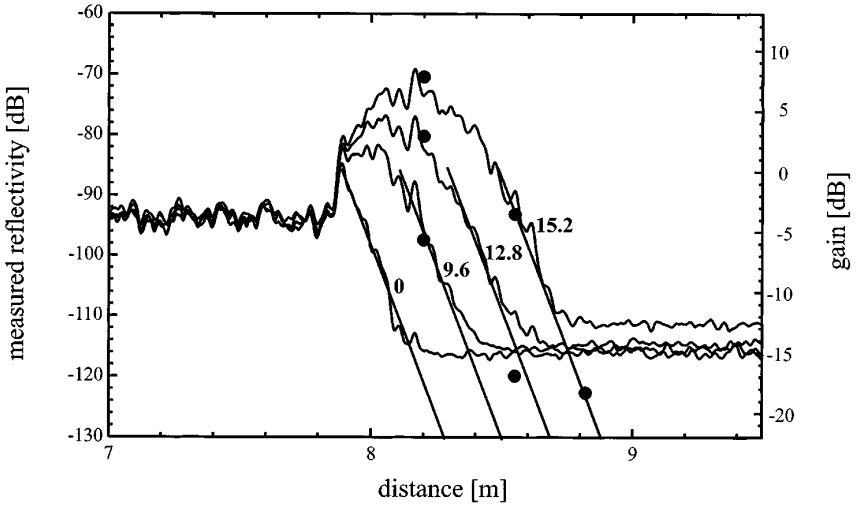

Fig. 2. Analysis of a forward pumped 2000 ppm Er-doped fiber with a length of 1 m. Solid lines: reflectivity traces as measured by the OFDR for pump powers from zero pump (bottom curve) to +15.2 dBm (top curve). Straight lines: guide to the eye of the linear absorption below the OFDR noise level. Dots: measured transmission values from traditional cut-back measures. The signal input power was held constant at −10 dBm.

power levels we used for the OFDR measurements were applied to assure the same saturation behavior. As there is some part of ASE light in the active fiber output, we calculated the transmission values by comparing the input and output optical spectra on an OSA allowing for easy ASE subtraction. The obtained transmission values, doubled (decibel-values) and referred to the fiber input Rayleigh level and location, are shown as dots in Fig. 2. Lines were introduced to indicate the linear decay of the OFDR traces below the instrument noise floor of about −116 dB for better comparison to the measured cut-back transmission values. As can be seen, the correspondence of OFDR and transmission measurements is rather good, clearly demonstrating the proper working of the OFDR for distributed gain measurements. It has to be noted that the presented measurement is a rather rough test with power levels changing at a rate of up to −123 dB/m—nevertheless, the gain value correspondence is typically better than 1 dB.

Fig. 3 shows results for a 3.8-m-long fiber with a 500 ppm Er doping level. Note that the scales have been adjusted in such a way that 0 m/0 dB is located at the input of the fiber, and the measured gain values have been divided by half (in decibels) to give the correct single trip gain values. The solid lines give the OFDR curves obtained for different pump powers and an input power of −11 dBm, whereas the dashed set of curves was obtained for the same pump powers, but for an even larger input signal power of −5 dBm.

Although there is a small reflectivity peak at the beginning of the active fiber, there is practically no difference in the Rayleigh backscattering level at the standard fiber-active fiber transitions. Apparently, the active fiber NA closely matches the one of the standard fibers. The fiber attenuation is −8 dB/m, and for the maximum pump of 15.2 dBm an overall gain of 14.7 dB is obtained for an input signal of −11 dBm. Fig. 3 shows that the gain values obtained from the conventional transmission measurements (dots and triangles for −11 dBm and −5 dBm input signal power, respectively) are all in excellent agreement with the OFDR values. The agreement is better than 0.5 dB in the presented measurement, which is close to the accuracy of the OFDR—the mismatch is probably rather due to uncertainties in the traditional measures anyway.

The gain reduction due to the 6 dB signal input power increase is correctly predicted, demonstrating that the go and return path gain are indeed the same, allowing for exact OFDR measures in a strongly saturated gain regime.

The good reproducibility of the OFDR measurements is shown in Fig. 4. There, the distributed gain was first measured on a 300 ppm-doped Er fiber with a length of 6.3 m. The fiber was then cut down to 2.3 m, and the gain distribution was again measured for the same pump powers. As the figure demonstrates, the curves are overlying well. The attenuation for this fiber is −2.5 dB/m, and for an input power of −5.6 dBm, practically no gain saturation is observed for maximum pump power.

Comparing the attenuation rates of the three fibers [−62 dB/m (2000 ppm), −8 dB/m (500 ppm), −2.5 dB/m (300 ppm)], one observes that they do not scale with the doping level. One reason might be that different co-doping concentrations could have been used for the different fibers. More plausible however is that the confinement factor [2] of the Er doping was different. An indication for this is that the NAs, and with that the signal beam extent, were different in the different fibers as is illustrated by the different amounts of the Rayleigh backscattering: whereas it was enhanced for the 2000 ppm (Fig. 2) and the 300 ppm fiber (Fig. 4), the 500 ppm fiber (Fig. 3) showed about the same backscattering level as a standard fiber. Assuming a very low co-dopant concentration and step doping profiles, the confinement factor can be calculated straightforwardly for the different doping concentrations and attenuation rates [2]. It amounts to 0.65 (2000 ppm), 0.46 (500 ppm), and 0.31 (300 ppm). Apparently, in the fibers with a lower doping concentration, a stronger confinement of the Er-ions was used.

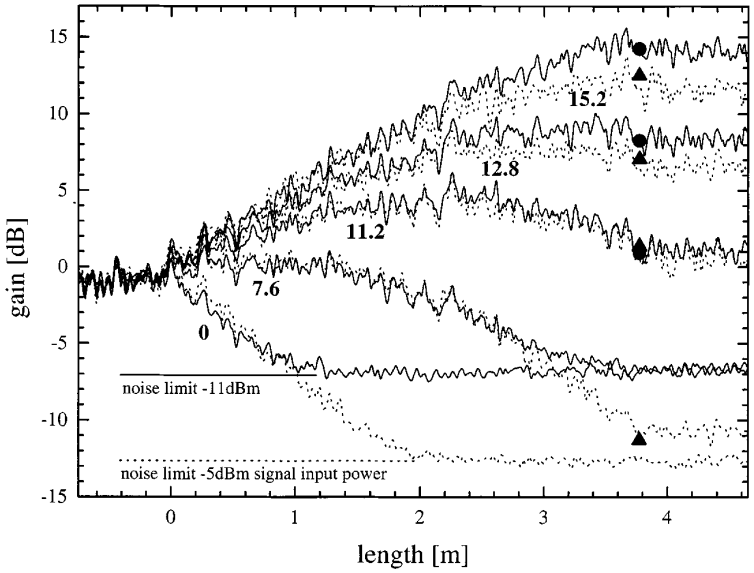

Fig. 3. Distributed gain curves in a 500 ppm Er-doped fiber for pump powers from zero pump (bottom curves) to +15.2 dBm (top curves). Lines: distributed gain calculated from OFDR traces for a signal input power of −11 dBm (solid line) and −5 dBm (dotted line), solid dots and triangles: directly measured transmission values through the Er-fiber. Note that because the gain (and not signal power) is shown, the apparent OFDR noise limit is increased by 6 dB for the set of lower signal input power (lower SNR).

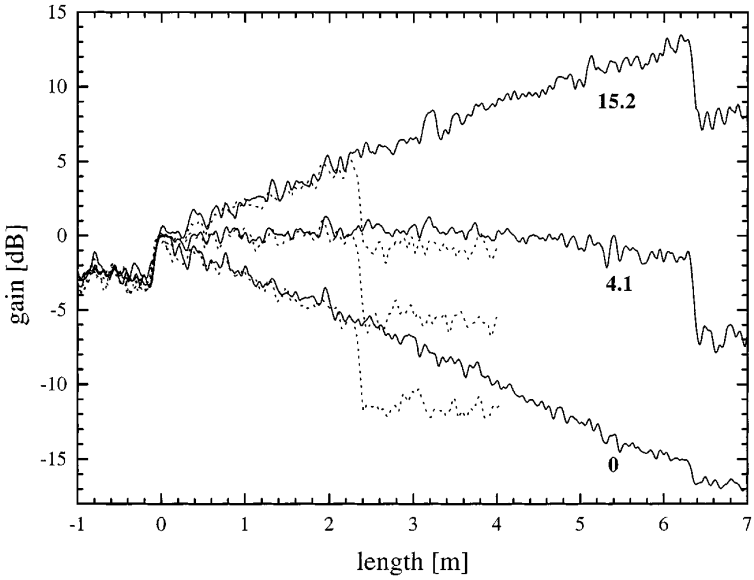

Fig. 4. Demonstration of the reproducibility of the OFDR measurements using a 300 ppm Er-doped fiber, an input signal power of −5.6 dBm, and different pump powers. Lines: distributed gain calculated from OFDR traces for fiber lengths of 6.3 m (solid line) and 2.3 m (dotted line).

IV. A Word on the Modeling of the Gain Distribution

In the introduction, it was mentioned that the accuracy of models for the gain distribution is typically not very good due to a lack of knowing precisely enough the diverse parameters involved. Having seen the excellent precision and repeatability of the OFDR measurements of the distributed gain, we can now illustrate this point more concretely.

A simple analytical model that neglects excited state absorption (which is absent for 1480 nm pumping) and gain saturation caused by ASE is used [10]. It is applicable for moderate gains up to about 20 dB. The model is therefore perfectly applicable for the measurement using a 12 m long 500 ppm Er-doped fiber, which gives a maximum gain of 13 dB for full pump power [Fig. 5(b)]. In order to obtain the necessary model parameters, the small signal absorption and input saturation power were measured both at the pump and signal wavelengths. This can be done on any length of the same active fiber used for the OFDR measurements [10]. Fig. 5(a) shows such a measurement for the signal wavelength of 1550 nm. Using the measured parameters

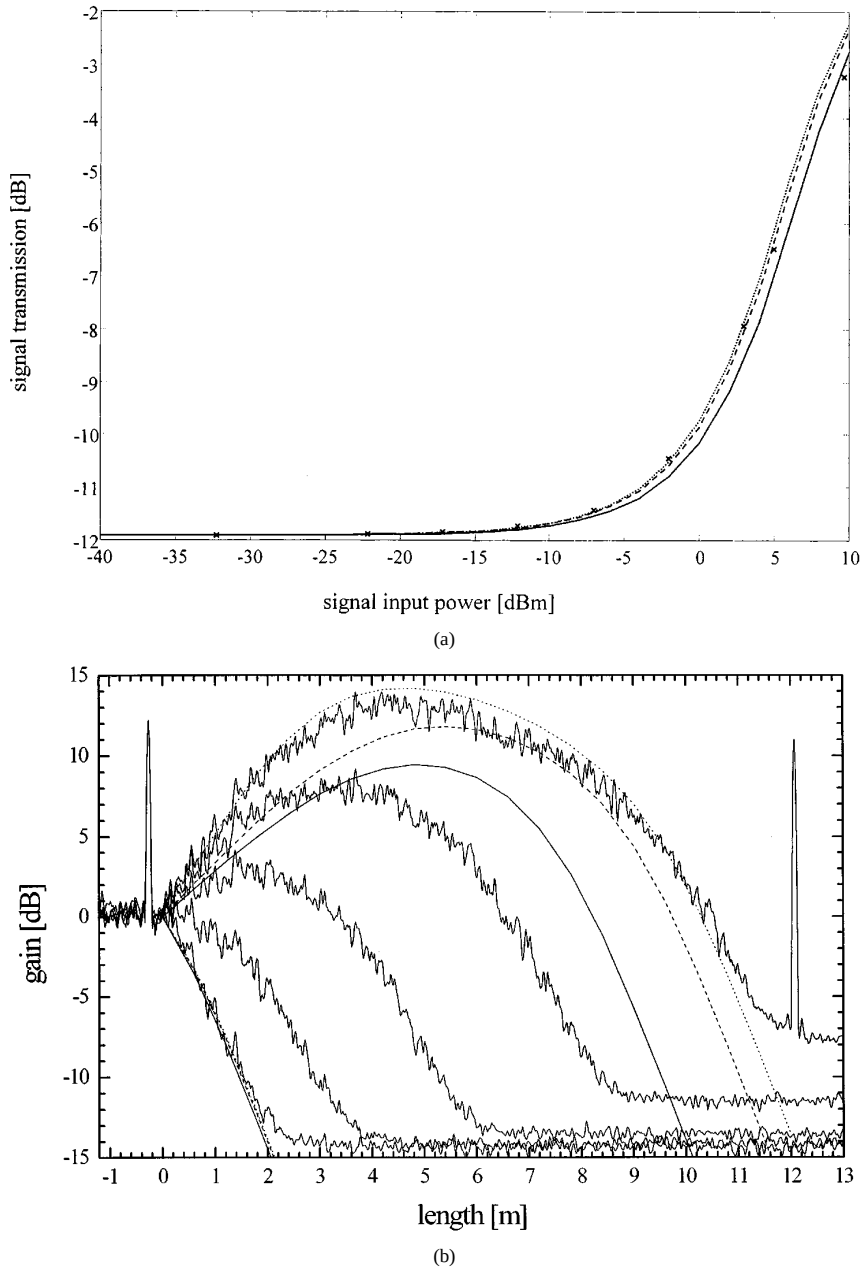

Fig. 5. Modeling of measured gain distributions from a 12-m long 500 ppm Er-doped fiber. (a) signal transmission measurement through an unpumped, 1.5-m long piece of the same fiber for model parameter determination. Crosses: experimental values, lines: calculated transmission using different sets of model parameters (see text for details). (b) Gain distribution. zig-zag lines: measured, smooth lines: modeled using the same sets of parameters as in (a).

and the signal and pump input power used in the OFDR measurements, a gain distribution as shown in Fig. 5(b) for full and zero pump power can be calculated in an easy and rapid way.

The problem however is that the obtained gain distribution strongly depends on the measured parameters. The three different gain distributions for maximum pump power shown in Fig. 5(b) were obtained in the following way. For the solid line, a point measure of the small signal attenuation and saturation power [i.e. measuring the attenuation for a low input power, and measuring the input power for which the absorption is bleached by a factor e (4.34 dB)] has been used. For the dashed line, a fit to the transmission measurements [shown in Fig. 5(a) for the signal wavelength], was used. Finally, the dotted line is a "fit" to the measured OFDR gain curve obtained by manually varying the small signal absorption and saturation values entering the model. As can be seen from Fig. 5(a), where the calculated transmission curves using the three mentioned sets of parameters is shown, all three sets match well with the measured data (crosses), and the differences between the sets are quite small (even smaller for the pump wavelength not shown

in the figure). Nevertheless, these small differences lead to predictions of the gain distribution with strongly varying maximum gain (9.4–14.2 dB) and maximum gain locations (4.7–5.3 m). Moreover, for the curve that matches best, there is still some difference in the shape of the modeled gain distribution to the real one as measured by the OFDR, demonstrating the difficulty to find the correct input parameters for the model.

To predict the maximum gain and especially the maximum gain location in a concrete, critical EDF set-up, it is therefore very useful to have a tool like the OFDR to accurately measure these parameters in a simple and rapid way.

V. Conclusion

Using optical frequency domain reflectometry, distributed gain measurements in Erbium-doped fibers have been performed. The OFDR used is ideally suited for this type of measurement due to its sensitivity (-120 dB), resolution (2 cm at 30 m), and range (150 m). The coherent detection leads to a high background light suppression, and ASE from the active fiber is efficiently rejected. The accuracy and reproducibility of the measured gain distributions has been demonstrated using EDF with strongly varying doping levels and doping confinements. The results were found to be in excellent agreement with traditional cut-back measurements, typically to within the OFDR accuracy of about 0.25 dB. As a byproduct, possible mismatches between the NA of the active fiber and the preceding/following fibers are detected.

Comparison of the measured OFDR curves with an adequate gain model is confirming the difficulty in reproducing the exact gain distribution for a specific situation due to a lack of accuracy in the model input parameters. This clearly points out the importance of being able to accurately measure gain distributions in a rapid and nondestructive way.

References

[1] I. P. Kaminov and T. L. Koch, Eds., *Optical Fiber Telecommunications III*. New York: Academic, 1997.

[2] E. Desurvire, *Erbium Doped Fiber Amplifiers*. New York: Wiley, 1994.

[3] C. R. Giles and E. Desurvire, "Modeling erbium-doped fiber amplifiers," *J. Lightwave Technol.*, vol. 9, pp. 271–283, Feb. 1991.

[4] M. Nakazawa, Y. Kimura, and K. Suzuki, "Gain-distribution measurement along an ultralong erbium doped fiber amplifier using optical time domain reflectometry," *Opt. Lett.*, vol. 15, no. 1, pp. 1200–1202, 1990.

[5] J. P. von der Weid, R. Passy, B. Huttner, O. Guinnard, and N. Gisin, "High-resolution distributed-gain measurements in erbium-doped fibers," *IEEE Photon. Technol. Lett.*, vol. 10, pp. 949–951, July 1998.

[6] J. P. von der Weid, R. Passy, G. Mussy, and N. Gisin, "On the Characterization of optical fiber network components with optical frequency domain reflectometry," *J. Lightwave Technol.*, vol. 15, July 1997.

[7] J. P. von der Weid, R. Passy, and N. Gisin, "Coherent reflectometry of optical fiber amplifiers," *IEEE Photon. Technol. Lett.*, vol. 9, pp. 1253–1255, Sept. 1997.

[8] P. Oberson, B. Huttner, O. Guinnard, L. Guinnard, G. Ribordy, and N. Gisin, "Optical frequency domain reflectometry with a narrow linewidth fiber laser," *IEEE Photon. Technol. Lett.* , submitted for publication.

[9] B. Huttner, J. Reecht, N. Gisin, R. Passy, and J. P. von der Weid, "Local birefringence measurements in single-mode fibers with coherent optical frequency-domain reflectometry," *IEEE Photon. Technol. Lett.*, vol. 10, pp. 1458–1460, Oct. 1998.

[10] A. A. Saleh, R. M. Jopson, J. D. Evankow, and J. Aspell, "Modeling of gain in Erbium-doped fiber amplifiers," *IEEE Photon. Technol. Lett.*, vol. 2, pp. 714–717, Oct..

M. Wegmuller, photograph and biography not available at the time of publication.

P. Oberson, photograph and biography not available at the time of publication.

O. Guinnard, photograph and biography not available at the time of publication.

B. Huttner, photograph and biography not available at the time of publication.

L. Guinnard, photograph and biography not available at the time of publication.

C. Vinegoni, photograph and biography not available at the time of publication.

N. Gisin, photograph and biography not available at the time of publication.

B.6 Analysis of the polarization evolution in a ribbon cable using high-resolution coherent OFDR.

M. Wegmuller, M. Legre, P. Oberson, O. Guinnard, L. Guinnard, C. Vinegoni, and N. Gisin

[1] *Group of Applied Physics - Gap Optique*
University of Geneva,
20 Ecole-de-Medecine, CH-1211 Aeneve 4, Switzerland

Claudio.Vinegoni@physics.unige.ch

Abstract : Exploiting the inherent polarization dependence and good spatial resolution of optical frequency domain reflectometry the beatlength in a ribbon fiber can be straightforwardly measured. The results clearly show the different amount of polarization ordering for inner and outer ribbon fibers due to the stress-induced birefringence from the common outer coating.

PUBLISHED : Photonics and Technology Letters, Vol. 13 (2000) pp. 145-7.

Analysis of the Polarization Evolution in a Ribbon Cable Using High-Resolution Coherent OFDR

M. Wegmuller, *Member, IEEE*, M. Legré, P. Oberson, O. Guinnard, L. Guinnard, C. Vinegoni, and N. Gisin, *Member, IEEE*

***Abstract*—Exploiting the inherent polarization dependence and good spatial resolution of optical frequency domain reflectometry (OFDR), the beatlength in a ribbon fiber can be straightforwardly measured. The results clearly show the different amount of polarization ordering for inner and outer ribbon fibers due to the stress-induced birefringence from the common outer coating.**

***Index Terms*—Birefringence, fiber metrology, optical fiber ribbons, optical reflectometry, polarization-mode coupling.**

I. Introduction

FIBER ribbons, where the individual fibers are densely arranged in a common outer coating, can present a popular low-cost solution—mainly for access networks—because of the possibility of mass splicing. With the bit rates ever increasing down to the end user, polarization-mode dispersion (PMD) of these fibers is becoming an issue. Several studies [1]–[4] address this topic, and often a different polarization evolution was found in the inner and outer fibers of the ribbon. For the four-fiber ribbon used in [4], e.g., the PMD was three times larger for the inner fibers than for the outer ones. A possible explanation is the birefringence induced by the stress of the ribbon itself. A finite element method was used in [4] to model the stress distribution within the ribbon, and the corresponding induced birefringence was found to be larger for the inner fibers by a factor of three as well.

The influence of a uniform external perturbation (usually of fiber twist) on the polarization evolution in an ideal fiber having a uniform, constant intrinsic birefringence and no polarization coupling has been investigated long ago [5]. In a real fiber, however, the intrinsic birefringence has random relative orientations of its (local) birefringent axes leading to polarization-mode coupling. In fiber ribbons, it is on such fibers that the external stress from the common coating is acting, and it is therefore not *a priori* clear to what extent the induced stress birefringence will change the polarization evolution (namely the polarization-coupling length). These points are clarified in this paper using high-resolution coherent optical frequency domain reflectometry (OFDR) measurements [6].

II. Experimental Setup

The OFDR technique (Fig. 1) is based on the detection of a beat signal between the distributed reflections from the fiber under test (Rayleigh backscatter, connectors, etc.) and a fixed Fresnel reflection (local oscillator). Using a linear frequency sweep of the laser, one can straightforwardly map the measured beat frequencies on a distance scale, whereas the normed square power for a given beat frequency gives the reflectivity at the corresponding distance. The polarization dependence of the coherent detection used in the OFDR can be exploited to get information about the evolution of the polarization state along the fiber [6], [7]. For a good general overview of the OFDR principles and limits, the reader is referred to [8], [9].

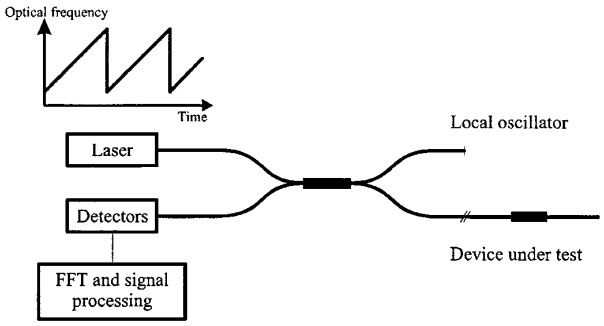

Fig. 1. Sketch of the OFDR setup.

In the device used for the measurements presented here, several important improvements have been implemented. A polarization-diversity detection allows to subtract the (polarization-independent) Rayleigh structure from the polarization-dependent channel, thereby removing the frequencies that are not related with the fiber birefringence. Along with the greatly enhanced range (2 km) and two-point resolution (0.08% of the range, i.e., 5 mm for a range of 6 m, 1.5 m for 2 km), this allows for precise measurements of the polarization evolution.

III. Results and Discussion

The fiber ribbon analyzed here consists of four fibers. Its length is 1.5 km, loosely spooled on a drum with a diameter of 35 cm.

First, PMD was measured both with the Jones matrix eigenanalysis (JME) and the interferometric method. The results are summarized in Table I. The inner fibers have a consistently larger PMD than the outer ones, the difference being as large as a factor of 3.6. As predicted by the model in [4], we found the DGD to vary more for the inner fibers between the measurement series done at different times during the day (different temperatures).

Manuscript received August 7, 2000; revised October 25, 2000.

The authors are with the Group of Applied Physics, University of Geneva, CH-1211, Geneve 4, Switzerland.

Publisher Item Identifier S 1041-1135(01)01048-5.

TABLE I
PMD, BEATLENGTH, AND COUPLING LENGTH FOR INNER AND OUTER FIBERS

	inner fibers	outer fibers
JME	0.4 ± 0.2 ps/√km	0.13 ± 0.05 ps/√km
interferometric	0.4 ± 0.2 ps/√km	0.11 ± 0.05 ps/√km
beatlength L_b	2.4 m	4.2 m
coupling length h	36 m	9.5 m

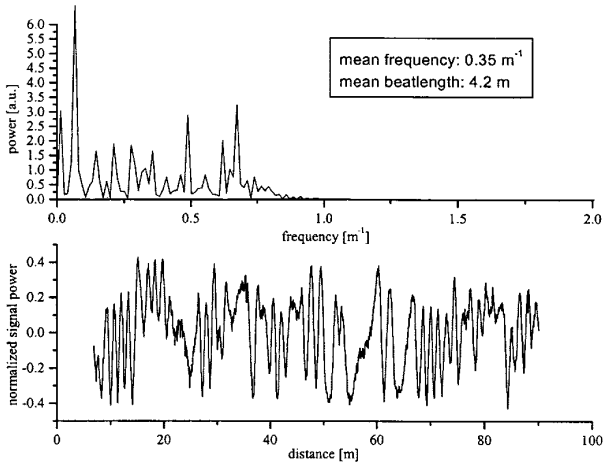

Fig. 2. Reflected signal and spectrum for an outer fiber.

We then used the OFDR to analyze the polarization evolution in the four different fibers. Fig. 2 shows the polarization-dependent reflections from an outer fiber, after removal of the Rayleigh noise and normalization-to-zero mean power. This curve is then Fourier transformed to get information about the rotation period of the polarization vector, i.e., the beatlength. The figure shows that there is not one specific, well-defined beatlength period, but a distribution of such values. While the structure of the peaks changes somewhat for different launch polarizations, the mean value of the distribution is fairly constant, giving a mean beatlength of about 4 m. The uneven structure of the signal is typical for a low PMD, standard fiber with a relatively short coupling length. The influence of the ribbon stress is small, but still induces some ordering (e.g., at distances around 10 m and 70 m in Fig. 2).

On the other hand, the situation is drastically changed for the inner ribbon fibers. As is shown in Fig. 3, the backreflected signal is now very regular, indicating a long coupling length and well-defined birefringent axes induced by the larger external ribbon stress. Accordingly, the Fourier transform now shows a distinctive peak corresponding to $L_b/2$ [7], giving a beatlength value of $L_b = 2.4$ m. Consequently, the external stress both enhanced the coupling length *and* the local birefringence. It is interesting to note that when the fibers are torn out of the ribbon, inner and outer fibers show the same characteristics. A typical example is shown in Fig. 4. Comparing the spectrum of the "free fiber" (Fig. 4) and the outer ribbon fiber (Fig. 2), one observes that the two strong low-frequency components, corresponding to an intrinsic beatlength of about 55 m, are present

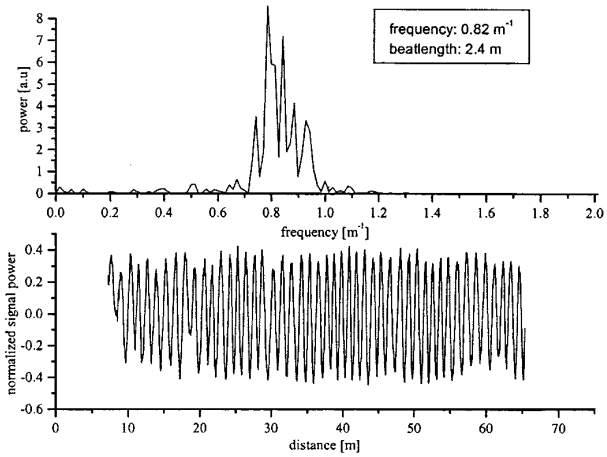

Fig. 3. Reflected signal and spectrum for an inner fiber.

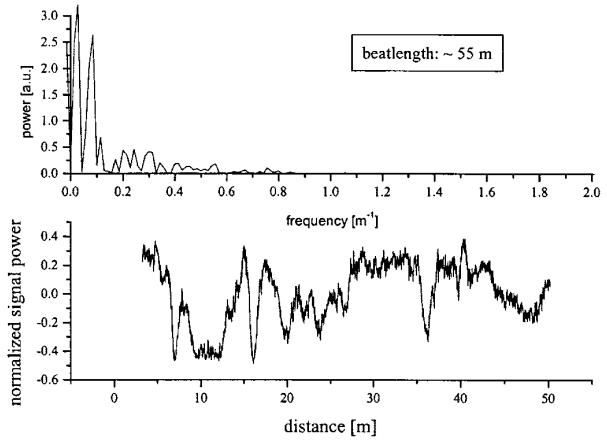

Fig. 4. Reflected signal and spectrum from a "deribbonized" fiber.

in both cases. For the outer ribbon fiber, there are, however, additional peaks due to the stress-induced birefringence, demonstrating that in that fiber intrinsic and induced birefringence are of similar magnitudes.

The coupling lengths h for inner and outer fibers can be determined more precisely by using the measured PMD (Table I) and beatlength values and applying the well-known relation $\mathrm{PMD} = (\lambda/cL_b)\sqrt{hL}$, valid for fibers where the fiber length $L \gg (h, L_b)$. The obtained coupling lengths are 36 m for the inner, and 9.5 m for the outer fiber (see, also, Table I), confirming the qualitative observations given above. These findings are also in good qualitative agreement with those reported in [1].

IV. CONCLUSION

Using high-resolution coherent optical frequency domain reflectometry, the polarization evolution in fibers of a ribbon cable have been straightforwardly measured. The reflected signal for inner ribbon fibers shows a well-defined, regularly varying structure. This demonstrates that the ordering from the external stress, induced by the common ribbon coating,

is important. Consequently, a small beatlength and a large coupling length were obtained. For the outer ribbon fibers, the signal variations were more random, indicating that the externally induced stress birefringence is of the same order than the intrinsic one.

The measurements further point out that for long-range applications of fiber ribbons, a careful design of the common coating is important, as PMD values as large as 0.4 ps/$\sqrt{}$km are otherwise experienced.

REFERENCES

[1] A. Galtarossa, L. Palmieri, M. Schiano, and T. Tambosso, "Measurement of beat length and perturbation length in long single-mode fibers by backscattered signal analysis," in *Proc. OFC*, Baltimore, MD, 2000, Paper ThR4.

[2] H. Ishikawa, Y. Suetsugu, Y. Kitayama, M. Nishimura, and S. Tanaka, "Polarization mode dispersion in optical fiber ribbon-slot cable," in *Proc. ECOC*, Firenze, Italy, 1994, pp. 443–446.

[3] A. Galtarossa, G. Gianello, C. G. Someda, and M. Schiano, "Stress investigation in optical fiber ribbon cable by means of polarization sensitive techniques," *IEEE Photon. Technol. Lett.*, vol. 6, pp. 1232–1234, Oct. 1994.

[4] A. Galtarossa, C. G. Someda, A. Tommasini, B. A. Schrefler, G. Zavarise, and M. Schiano, "Stress distribution in optical fiber ribbons," *IEEE Photon. Technol. Lett.*, vol. 9, pp. 354–356, Mar. 1997.

[5] R. Ulrich and A. Simon, "Polarization optics of twisted single-mode fibers," *Appl. Opt.*, vol. 18, no. 13, pp. 2241–2251, 1979.

[6] M. Wegmuller, J. P. von der Weid, P. Oberson, and N. Gisin, "High resolution fiber distributed measurements with coherent OFDR," in *Proc. ECOC*, vol. 4, Munich, Germany, 2000, pp. 109–110.

[7] B. Huttner, J. Reecht, N. Gisin, R. Passy, and J. P. von der Weid, "Local birefringence measurements in single-mode fibers with coherent optical frequency-domain reflectometry," *IEEE Photon. Technol. Lett.*, vol. 10, pp. 1458–1460, Oct. 1998.

[8] J. P. von der Weid, R. Passy, G. Mussi, and N. Gisin, "On the characterization of optical fiber network components with optical frequency domain reflectometry," *J. Lightwave Technol.*, vol. 15, pp. 1131–1141, July 1997.

[9] M. Wegmuller, P. Oberson, J. P. von der Weid, O. Guinnard, L. Guinnard, C. Vinegoni, M. Legré, and N. Gisin, "Overview of coherent reflectometry techniques: Characterization of components and small systems," in *Proc. Symp. Optical Fiber Measurements SOFM*, Boulder, CO, 2000, pp. 155–160.

B.7 A near field scanning optical microscope in single photon detection mode at 1.55 μm.

C. Vinegoni[1], H. Deriedmatten[1], M. Wegmuller[1], N. Gisin[1], Y. Mugnier[2], A. Jalocha[2], P. Descouts[2]

[1] *Group of Applied Physics - Gap Optique*
University of Geneva,
20 Ecole-de-Medecine, CH-1211 Aeneve 4, Switzerland

[2] *Group of Applied Physics - Biomedical*
University of Geneva,
20 Ecole-de-Medecine, CH-1211 Geneve 4, Switzerland

Claudio.Vinegoni@physics.unige.ch

Abstract : We have developed a new system combining near-field scanning optical microscopy (NSOM) with single photon detection operating at the wavelength of 1.55 μm. The microscope was used in order to image the splice region between a standard telecom and an Erbium doped fiber. The excellent sensitivity also allowed to detect the Rayleigh scattered light of a standard fiber coming out laterally through the fiber cladding.

SUBMITTED : J. of Optics: A

B.8 Determination of polarization coupling length in telecom fibers exploiting nonlinear polarization rotation.

C. Vinegoni, V. Scarani, M. Wegmuller, and N. Gisin

[1] *Group of Applied Physics - Gap Optique*
University of Geneva,
20 Ecole-de-Medecine, CH-1211 Aeneve 4, Switzerland

Claudio.Vinegoni@physics.unige.ch

Abstract : The polarization coupling length, an important parameter of the PMD probability distribution, is obtained from measurements and modeling of the nonlinear polarization rotation in optical fibers. Results for different types of fibers are presented.

SUBMITTED :

Determination of the polarization coupling length in telecom fibers exploiting the nonlinear polarization rotation

C. Vinegoni, V. Scarani, M. Wegmuller, and N. Gisin

Group of Applied Physics, University of Geneva, CH-1211 Geneve 4, Switzerland

ABSTRACT

The polarization coupling length, an important parameter of the PMD probability distribution, is obtained from measurements and modeling of the nonlinear polarization rotation in optical fibers. Results for different types of fibers are presented.

IEEE INDEXING KEYWORDS

Optical Kerr effect, Optical fiber measurements, Nonlinear optics

Correspondence author:

Dr Claudio Vinegoni
Chalmers University
Dept. of Microelectronics
Photonics Laboratory
Kemivagen 9, 4C
SE-412 96 Göteborg, SWEDEN

Tel: +46.31.772.5044, Fax: +46.31.772 1540
Email: VINEGONI@YAHOO.COM

INTRODUCTION

It is well known that single-mode communication fibers are birefringent and that the orientation and the amount of birefringence is randomly distributed along the fibers. The corresponding polarization mode dispersion (PMD) becomes therefore a statistical quantity, and not only its mean value but also its probability distribution is important to assess the inferred system impairments. This distribution depends on two parameters: on the (mean) local birefringence B and on the coupling length h, which is the length over which the E field loses memory of its initial distribution between the local polarization eigenstates [1]. In fibers having a length L long compared to h, the probability distribution is Maxwellian with a mean PMD value of B, whereas for coupling lengths approaching the fiber lengths, the PMD statistics change considerably. In this paper we present a novel way to directly infer the polarization coupling length from measurements of the nonlinear polarization rotation (NPR) of the fiber.

We demonstrate too that NPR is present non only in polarization maintaining fibers [2] but even in standard single mode fibers. The resulting nonlinear change in the light's state of polarization (dependent on both the channel power and the coupling length) can affect, on long transmission links, the performances of polarization demultiplexing schemes and of first order PMD compensation.

PRINCIPLE OF OPERATION

In a dielectric medium, an intense elliptical input pulse induces birefringence – via the optical Kerr effect - due to the different amounts of intensity along the major and minor axis of the polarization ellipse. In an isotropic medium this self-induced birefringence leads to polarization ellipse self-rotation. In an optical fiber however, the situation is more complex due to the presence of the local intrinsic birefringence. The polarization changes are hard to predict in that case as the linear and nonlinear birefringences interact in a complicated manner. In general, the linear birefringence will however be much larger than the nonlinear one, and the evolution of the polarization vector ψ in a polarization maintaining fiber can then be approximated by [2]:

$$\partial_z \psi \approx i\omega B_{eff} \sigma_\theta \psi \qquad (1)$$

where σ_θ accounts for the linear birefringence with axis θ. The linear birefringence B is replaced by an effective birefringence B_{eff} accounting for the nonlinear birefringence. The solution for Eq.1 is straightforward, and corresponds to a rotation of the input polarization vector around the linear birefringence axis σ_θ, with a rotation angle β given by

$$\beta = \omega B_{eff} z = \omega (B - \frac{\alpha}{2} m_\theta(0)) z \qquad (2)$$

where $\alpha = n_2P/(3cA_{eff})$, n_2 is the nonlinear Kerr coefficient, P the power, and A_{eff} the effective area. $m_\theta(z)$ is defined as the projection of the input SOP on the birefringent axis at the position z along the fiber. In principle the NPR can now be measured by varying the input power P and observing the corresponding change in the output SOP.

However, an inherent problem for this kind of measurements is the stability of the output SOP at the exit of the fiber, subjected to fluctuations of the much larger linear birefringence B due to temperature changes and drafts in the fiber environment. We have recently proposed a method for measuring the NPR [2] by removing the overall linear birefringence -and therefore also its fluctuations- in a purely passive way by employing a Faraday mirror (FM) [3] and a double pass of the fiber under test. Doing so, the nonlinear birefringence (leading to NPR) was shown to remain unaffected, i.e. the NPR of the forward and backward paths add up [2]. In this way we can measure NPR both in polarization maintaining (PM) fibers and in standard fibers. However, the random variations of the intrinsic local birefringence existent in a standard fiber reduce the NPR. The situation becomes more complex, and we therefore resort to numerical simulations. The fiber is modeled as a concatenation of linearly birefringent trunks with a physical length L_C kept constant. Concerning the birefringence, its strength is fixed and the orientation is allowed to vary driven by a white noise process $g_\theta(z)$ characterized by a dispersion σ_θ [1]. For each single trunk, Eq.2 is used to calculate the output SOP from the input one, with the input SOP calculated from the output SOP of the previous trunk. The SOP can therefore be calculated piece by piece, with the

projection m_θ being different for each new trunk. The final SOP will depend on the choice of the birefringence axis orientations, with variations being larger for large values of L_C. We therefore made 200 runs for each specific coupling length to get a mean value of the NPR.

EXPERIMENT

The experimental setup for the measurement of the NPR for the different test fibers is shown in Fig.1. The light source consists of a distributed feedback laser (DFB) operated in pulsed mode at a wavelength of 1559 nm. Typically, pulses with a duration of 30 ns, a repetition rate of 1 kHz, and a peak power of up to 6 W (after amplification by an EDFA) are used. The light is then launched into the fiber under test (FUT) via a 90/10 coupler and a polarization controller (PC1). The coupler is inserted for the detection of the backward traveling light after the double pass of the FUT, with its 90% output port connected to the source in order to maintain high launch powers into the FUT. The polarization controller, PC1, allows to adjust the polarization of the light launched into the FUT, i.e. m_θ which is important for the strength of the NPR as demonstrated by Eq.2. Note that for low launch powers (negligible NPR), the action of PC1 is removed by the Faraday mirror, and its setting is therefore of no importance in that case. The output SOP is examined by an analyzer consisting of a polarization controller

PC2 and a polarizing beam splitter (PBS). To achieve a good sensitivity of the analyzer, it is calibrated for equal power in the two PBS output arms for low power launch signals where no NPR occurs. The two PBS output channels were monitored by a fast photodiode (200 ps response time) and a sampling scope. The measurements were then performed in the following way: for a given launch power, the polarization launched into the FUT was adjusted (PC1) to give the smallest possible output power at the monitored PBS channel. Consequently, the difference between the two PBS output channels is maximized, corresponding to a maximum value of the NPR.

RESULTS AND DISCUSSION

We first measured the NPR in a PM fiber with a length of 200 m. The results shown in [2] indicate that the effect of NPR is negligibly small up to about 0.5 W. For higher lunch powers, NPR manifests itself with a reduction of the power in the monitored PBS channel. In fact, its action becomes so strong that for launch powers above about 2.5 W, the output power starts actually to decrease in spite of the linear increase that would be experienced in the absence of NPR. The measured data agree well with our model, in which $m_\theta(0)$ was varied in order to give a minimum output power from the PBS channel like in the experiment, and only one fiber trunk was used (L_C = fiber length L).

Numerical results for different values of L_C (keeping fixed the total fiber length) show that NPR is reduced for a larger number of couplings resulting in a more and more linear dependence of the output from the input power. This reduction is due to the increased probability that the NPR action in one trunk is compensated for by another. These theoretical predictions were then compared to measurements made on different standard fibers (see Tab.1). The fiber lengths were typically 1 km (simulations were adjusted accordingly to each fiber length and n_2/A_{eff} coefficient). Fig.2 shows the results for 3 standard fibers with large (fiber B) and small PMD (fiber A,C), respectively. The three standard fibers clearly exhibit a different amount of NPR. The fitting of the experimental data is made with two free different parameters; the length of each single trunk of fiber L_C and the dispersion σ_θ. Different combinations of their values can fit the same experimental data but in accordance with the definition of coupling length if the model is consistent the product $\sigma^2_\theta L/L_C$ has to remain constant. This is shown to be the case for our data as shown in the inset of Fig. 2. Here L_C is varying between 5 and 200 m and σ_θ between 10 and 70 degrees.

The coupling length h defined as the length at which the fiber autocorrelation function $<\cos[\theta(z) - \theta(0)]>$ is equal to 1/e, can be shown to be equal to $2/\sigma^2_\theta$. For the case in which each piece of fiber has a fixed length L_C, it's easy to show that $h = 2L_C/\sigma^2_\theta$. The simulations show that for the three different fibers the coupling length can be estimated to be about 160 m for the fiber A and 350 m for the large PMD fiber (fiber B). The coupling length of h~1000 m for the third 'standard' fiber

(fiber C) is quite large, indicating that there might be well defined birefringent axes in that fiber.

The large values we found for the coupling lengts appear to be remarkably high, so we have successively made a different estimation for the coupling length of the same fibers, from PMD and beat length measurements using an Optical Frequency Domain Reflectometer (OFDR) [4]. The values we found in this way are of the order of tens of meters (see Tab.1) except for fiber C that even with this method presents a coupling length of the order of the entire fiber length.

This difference in the estimated coupling length between the two methods is quite surprising so we tested the validity of our model in two ways. One, as mentioned before, consisted in fitting the experimental data using different combinations of the single trunk of fiber L_C and the dispersion σ_θ (keeping the product σ^2_θ L/L_C constant). The inset of Fig.2 shows the consistency of the model.

The other test consisted in demonstrating that the NPR will add even in the presence of a discontinuity in the linear birefringence (i.e. the fiber is a concatenation of two PM fibers spliced together, with a coupling angle different from zero) as is the case of our model. To prove this we considered two PM fibers connected together with a varying coupling angle θ. Depending on the value of θ, the amount of rotation will change (maximum when $\theta = 0$, i.e. fiber aligned). The experimental data are in good agreement with the theoretical ones [5].

From these tests it is not clear at this moment why the values of h we obtained with the nonlinear method are much higher compared with the ones calculated using the OFDR. We clearly showed that the h does play a major role in determining the strength of the NLR, although maybe it is not the only one.

CONCLUSION

Measurements and a model of NPR in optical fibers were presented, allowing for direct determination of the polarization mode coupling length. Coupling length values of several 100 m were obtained for large PMD fibers, whereas it was as low as 160 m in state-of-the-art low PMD fibers. Despite the demonstrated consistency of the model, a high discrepancy is present between the h values measured with the OFDR method and the nonlinear one.

One SMF fiber (fiber C) presented an unusually extremely high coupling length in accordance with both the measurements methods.

The presence of significant NPR in SMF fibers, even in the ones with short coupling lengths as measured from the OFDR method, can constitute a serious problem in particular for first order PMD compensation or polarization demultiplexing schemes.

ACKNOWLEDGMENTS

We acknowledge the financial support from the Swiss Federal Office for Education and Sciences (OFES) in the framework of the European COST 265 action.

REFERENCES

1 P.K.A. Wai, and C.R. Menyuk, “Polarization decorrelation in optical fibers with randomly varying birefringence”, *Opt. Lett.*, 1994, 19 pp. 1517-19

2 C. Vinegoni, M. Wegmuller, and N. Gisin, “Measurement of nonlinear polarization rotation in a highly birefringent optical fiber using a Faraday mirror”, *J. Opt. A* 2000, 2, pp. 314-318

3 M. Martinelli, “A universal compensator for polarization changes induced by birefringence on a retracing beam”, *Opt. Comm.* 1989, 72, pp. 341-344

4 C. Vinegoni, M. Karlsson, M. Wegmuller, V. Scarani, M. Wegmuller, and N. Gisin, “Nonlinear polarization rotation in high birefringent and standard telecom fibers” to be submitted

5 M. Wegmuller, J.P. Von der Weide, P. Oberson, and N. Gisin, “High resolution fiber distributed measurements with coherent OFDR”, *ECOC 2000*, paper 11.3.4

CAPTIONS

Fig. 1 Experimental setup of the NPR measurements. PG pulse generator, DFB distributed feedback laser, EDFA Erbium doped fiber amplifier, PC polarization controller, FUT fiber under test, FM Faraday mirror, PBS polarizing beam splitter

Fig. 2 Minimum output power of PBS channel 1 as a function of the launched power for fibers A (open circles), B (full circles), and C (full squares). Symbols: measured data. Solid curve: prediction from our model. Dashed bold line: prediction in the absence of any NPR. Bold curve: PM fiber. The inset shows the values of the calculated h for different □□ and LC combinations giving curves that fit the experimental data for fibers A and B.

Tab. 1 Parameters for the different fibers: total length, PMD, and beat length L_b. In the last two columns is reported the coupling length as derived from the measured beat length L_b and PMD, and the one estimated through the nonlinear polarization rotation.

FIGURE 1

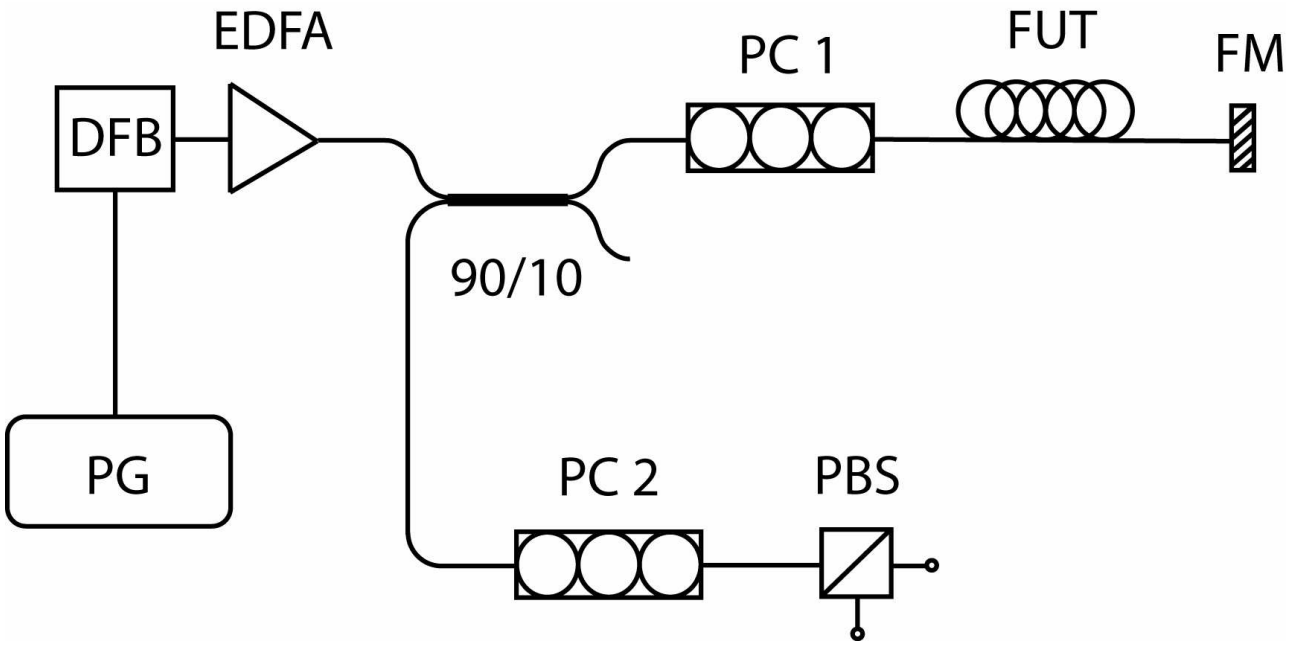

FIGURE 2

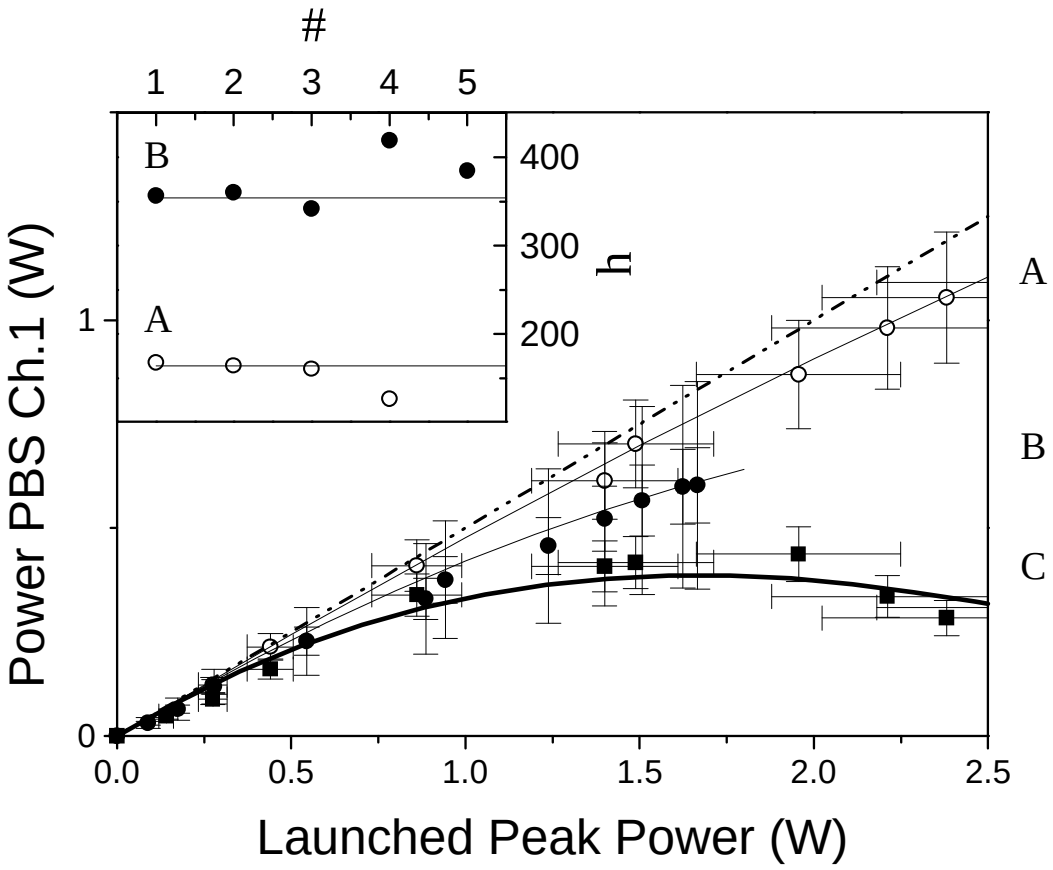

TABLE 1

Fiber	Length (km)	PMD (ps/√km)	L_b (m)	h [OFDR] (m)	h [nonlinear] (m)
A	1.5	0.05	12	15	160
B	1.0	1.9	.5	47	350
B*	1.0	0.05	20	43	350
C	1.0	0.14	30	Fiber length	Fiber length

B.9 Emulator of first and second order polarization mode dispersion.

M. Wegmuller, S. Demma, C. Vinegoni, and N. Gisin

[1] *Group of Applied Physics - Gap Optique*
University of Geneva,
20 Ecole-de-Medecine, CH-1211 Aeneve 4, Switzerland

Claudio.Vinegoni@physics.unige.ch

Abstract : Contrary to approaches which try to mimic a standard fiber as closely as possible, the emulator presented here gives constant (but user-adjustable) values for DGD and ratio of first to second order PMD. Once it is set, the ratio is conserved while the DGD can be easily varied within a range of 0-300 ps. This allows to investigate the low-probability events of large DGD and 2nd order PMD important for system outage.

PUBLISHED : Photonics and Technology Lett. , Vol. 14 (2002) pp. 630-2

Emulator of First- and Second-Order Polarization-Mode Dispersion

M. Wegmuller, S. Demma, C. Vinegoni, and N. Gisin

***Abstract*—Contrary to approaches which try to mimic a standard fiber as closely as possible, the emulator presented here gives constant (but user adjustable) values for differential group delay (DGD) and ratio of first- to second-order polarization-mode dispersion (PMD). Once it is set, the ratio is conserved while the DGD can be easily varied within a range of 0–300 ps. This allows to investigate the low-probability events of large DGD and second-order PMD important for system outage.**

***Index Terms*—Communication system testing, polarization-mode dispersion.**

I. Introduction

UPGRADING the existing telecom systems to high bit rates ($\geq$10 Gb/s) leads to several problems. Already some time ago, the impact of first- and second-order polarization-mode disperison (PMD) in such systems has been analyzed [1], [2]. It was found that second-order PMD, i.e., the frequency dependence of the principle states vector (PSP) $\vec{\Omega}$, can lead to important fluctuations around the mean penalties induced by first-order PMD. For the case of large values of the chromatic dispersion, second-order PMD becomes in fact a major source of performance degradation [1]. Moreover, with the advent of PMD compensators, which typically compensate for first-order effects only (leaving higher orders unaffected or even increasing them), impairments due to accumulated second-order PMD are to be expected [3].

Consequently, second-order PMD is an important issue for a proper assessment of system performance and PMD emulators should therefore not only include the first, but also the second order. The emulators of today have the strategy to mimic as closely as possible long standard fibers with polarization-mode coupling [4]–[6]. They typically consist of pieces of highly birefringent polarization maintaining (PM) fibers joint either by splicing or by rotatable connectors. In the first type, the desired Maxwellian pdf for the DGD is obtained by taking an ensemble over a large wavelength interval. However, the wavelength dependence of the PSP $\vec{\Omega}$ is usually not accounted for in a correct way [4]. Using a fixed wavelength and changing the coupling among the PM fibers (e.g., by changing the temperature or by mechanically varying the birefringence axes directions of the individual trunks) to obtain a Maxwellian distributed DGD, there are indications that second-order PMD could be quite well approximated [5]. However, a large number of trunks ($>$15, [4], [5]) and a large number of different realizations are to be used. This adds to the emulator complexity and measurement time. Moreover, there are indications that the rare events of large DGD values (tail of the Maxwell distribution) in these PMD emulators can be orders of magnitudes smaller than the desired theoretical values [7]—however, it is these large DGD events which are important for the system outage probability!

We, therefore, opt for a different approach, where the user can set a constant value for the DGD and the ratio of DGD to instantaneous second-order PMD[1], independent of the wavelength. Consequently, contrary to the other emulators, no statistics is reproduced (we therefore have a "DGD emulator" rather than a PMD one). The values for DGD and instantaneous second-order PMD are known precisely without having to measure them and can be experimentally linked to the corresponding system penalty. In addition, our emulator also allows to simulate situations—like a first-order compensated system with low DGD and large second-order PMD—not achievable in emulators that mimic long standard fibers.

II. Principle of Operation

The emulator is based on two trunks of PM fiber, with a coupling angle φ between their birefringence axes. The overall PSP $\vec{\Omega}$ then becomes [8]

$$\vec{\Omega}(\omega)=\frac{1}{2}\beta_2\vec{e}_2+\frac{1}{2}\beta_1(\vec{e}_1\cdot\vec{e}_2)\vec{e}_2 +\frac{1}{2}\beta_1\cos(\beta_2\omega)(\vec{e}_1-(\vec{e}_1\cdot\vec{e}_2)\vec{e}_2)+\frac{1}{2}\beta_1\sin(\beta_2\omega)\vec{e}_1\times\vec{e}_2 \quad (1)$$

where $\vec{\Omega}_{1,2}=\beta_{1,2}\vec{e}_{1,2}$ are the PSP of the first and second trunk with DGDs of β_1 and β_2, respectively. Assuming that β_i and $\vec{e}_i$ are independent of wavelength (a very good approximation for PM fibers), one can straightforwardly calculate the overall DGD and instantaneous second-order PMD

$$\left|\vec{\Omega}(\omega)\right|^2=\mathrm{DGD}^2=\beta_1^2+\beta_2^2+2\beta_1\beta_2\cos(\varphi)$$
$$\left|\frac{\partial}{\partial\omega}\vec{\Omega}(\omega)\right|=\left|\vec{\Omega}_\omega\right|=\beta_1\beta_2\sin(\varphi). \quad (2)$$

As one can see, both these quantities are constant with wavelength. The derivative of the modulus of $\vec{\Omega}$, which accounts for about 1/9th of the total amount of second-order PMD in a long

Manuscript received September 14, 2001; revised January 16, 2002. This work was supported in part by the Swiss Federal Office for Education and Science under the European COST265 project and in part by EXFO, Quebec.

The authors are with the Group of Applied Physics, University of Geneva, CH-1211 Geneve 4, Switzerland.

Publisher Item Identifier S 1041-1135(02)03246-9.

[1]In the remainder of the letter, we use the following definitions and terms: first-order PMD: $\sqrt{\left\langle\left|\vec{\Omega}(\omega,t)\right|^2\right\rangle_t}$, DGD: $\left|\vec{\Omega}(\omega,t)\right|$ (varies with time) second-order PMD: $\sqrt{\left\langle\left|(\partial/\partial\omega)\vec{\Omega}(\omega,t)\right|^2\right\rangle_t}$, instantaneous second-order PMD: $\left|(\partial/\partial\omega)\vec{\Omega}(\omega,t)\right|$ (varies with time).

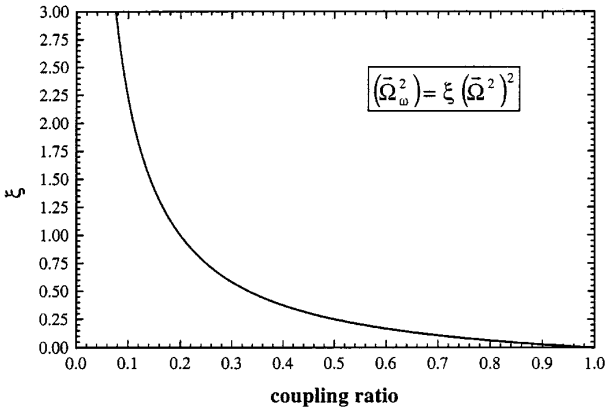

Fig. 1. Ratio of first- to second-order PMD, as a function of the coupling ratio between two PM fibers with arbitrary, but equal DGD [as calculated from (2)].

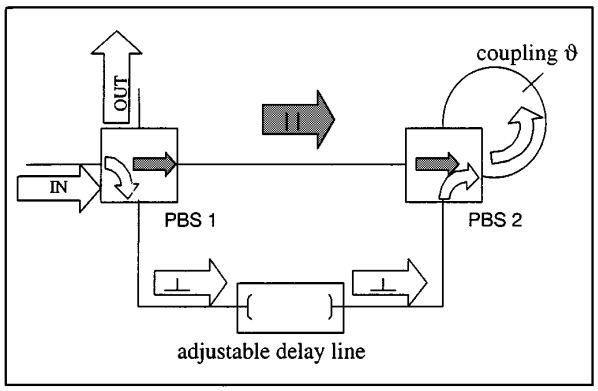

Fig. 2. Experimental setup of the emulator for first- and second-order PMD. The arrows indicate the light path during the forward pass of the emulator, corresponding to the first PM fiber. All fibers in the setup are polarization maintaining. PBS: Polarizing beamsplitter.

standard fiber [2], is therefore zero and the second-order PMD vector $\vec{\Omega}_\omega$ becomes orthogonal to the PSP $\vec{\Omega}$.

Due to the dependence of DGD and instantaneous second-order PMD on the coupling angle φ (2), one can set a desired ratio ξ of the instantaneous second-order PMD to the DGD as is illustrated in Fig. 1 for two PM fibers having the same DGD. Note that rather than the coupling angle φ, the coupling ratio $\cos(\varphi)^2$ has been used as it is this value which can easily be measured for the emulator adjustment. Note that the ratio $\varphi\,\xi = (\tan(\varphi)/2)^2$ is conserved for any values of DGD, as long as they are the same for both fibers. The situation of $\beta_1 = \beta_2 = \beta$ is, therefore, advantageous and consequently employed in our emulator.

III. Experimental Setup and Results

The experimental setup for the emulator is shown in Fig. 2. It is nothing else than the analog to two PM fibers with adjustable DGD and a coupling φ between them.

The parallel and perpendicular orthogonal polarization mode of the input PM fiber are split at the first PBS, allowing to induce a retardation (0–300 ps) on the orthogonal mode using a free space delay line. The two modes are recombined at the second PBS, again with the axes of the following PM fiber aligned. The

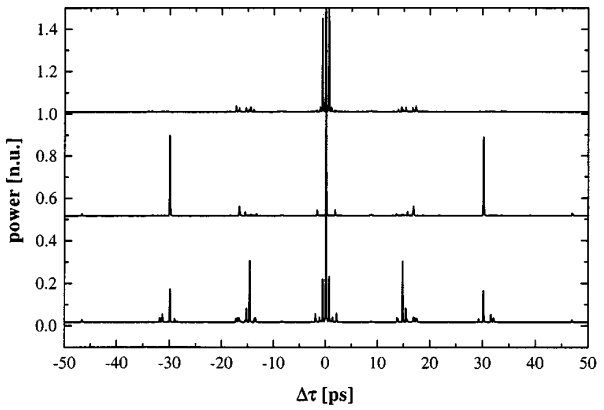

Fig. 3. Interferometric PMD measurements of the emulator for a fixed delay line setting of 15 ps and couplings of $\vartheta = 0°$ (top), 90° (middle) and 41° ($\xi = 1/3$). The power has been normalized so that the central peak is one and the curves were offset vertically for clarity.

light trajectory up to the coupling ϑ, therefore, represents the first PM fiber, with DGD $\Delta\tau_1$. The polarization-mode extinction ratio at the second PBS was measured to be ∼22 dB. The loss up to the coupling point was ∼3 dB for the lower arm and 1 dB for the upper arm. The difference can be explained by the insertion loss of the delay line (∼1 dB) and a bad splice in the lower arm. The loss of the upper arm was thereafter increased to the value of the lower one. The second fiber (after the coupling point) consists of the backward pass through the same polarization interferometer. Note that for the two "quasi-PM" fibers to be aligned ϑ has to be set to 90°. Therefore, in order to have the same situation as for two real PM fibers with a coupling φ, one has to use $\vartheta = 90° - \varphi$. The coupling ratio can be easily determined by adjusting the input light to the $\parallel$ mode (see Fig. 2) and measuring the decrease in power when blocking the delay line. Physically, the coupling was realized by inserting a polarization controller with ultralow PMD (Lefèvre controller), but could be achieved more conveniently using a rotatable connector.

In the first realization of the emulator [9], an important difference in the DGD of the forward ($\Delta\tau_1$) and backward ($\Delta\tau_2$) pass (analog to the first and second PM fiber) was found. As discussed in Section II, the ratio of DGD to instantaneous second-order PMD was, therefore, no longer preserved as a function of the delay line setting. The reason for the discrepancy between $\Delta\tau_1$ and $\Delta\tau_2$ can in fact be easily understood by analyzing the emulator for a setting of $\vartheta = 0°$ (i.e., $\varphi = 90°$). The output for that case should be $|\Delta\tau_1 - \Delta\tau_2| = 0$, but is actually given by the DGD of the empoyed PM fiber (per length) times the total length through the emulator. This is because all the PM fibers in the emulator are aligned: a $\parallel$ input light (see Fig. 2) will remain so throughout its path to the ouput and the same holds for $\perp$ input light. $|\Delta\tau_1 - \Delta\tau_2|$ is independent of the delay line setting (which was also verified experimentally). It was nulled by adding a PM fiber with reversed axes and the correct DGD to the emulator output fiber. Fig. 3 shows interferometric PMD measurements of the emulator for a delay line setting of $\Delta\tau = 15$ ps and different couplings ϑ of 0° (top), 90° (middle) and 41° (corresponding to the statistical case of $\xi = 1/3$ for long fibers, bottom). For $\vartheta = 0°$, the corresponding peak gives $|\Delta\tau_1 - \Delta\tau_2|$.

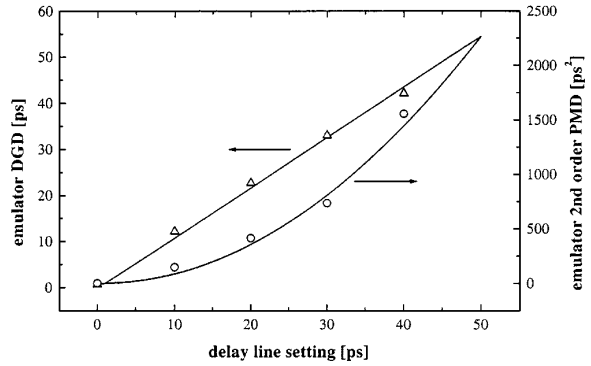

Fig. 4. DGD and instantaneous second-order PMD of the emulator as a function of the delay line setting. The coupling ratio was fixed at $\cos^2\varphi = 0.3$ (roughly corresponding to $\xi = 2 \cdot 1/3$). Solid lines: Theoretical values. Symbols: Measured values.

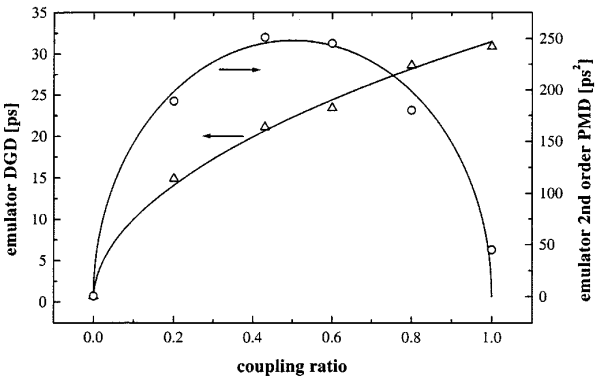

Fig. 5. DGD and instantaneous second-order PMD of the emulator as a function of the coupling ratio. The delay line setting was fixed at 15.75 ps. Solid lines: Theoretical values. Symbols: Measured values.

The measurement shows that a small difference of $\sim$0.6 ps persists because of a slight mismatch in DGD between the original emulator and the PM fiber added to the output. However, this difference is now too small to significantly change the ratio ξ as a function of the delay line setting. Fig. 3 further demonstrates that for a coupling of $\vartheta = 90°$, only a peak at $\Delta\tau_1 + \Delta\tau_2 \approx 2\Delta\tau$ is obtained, whereas for nonaligned fiber axes, peaks at both $\Delta\tau$ and $2\Delta\tau$ appear.

Fig. 4 shows theoretical (2) and measured DGD and instantaneous second-order PMD for a coupling ratio of 0.3 (corresponding to $\xi = 0.59$), as a function of the delay line setting $\Delta\tau$. The original standard Jones Matrix Eigenanalysis (JME) method as presented by Heffner *et al.* [10] was used to extract the PSP as a function of wavelength. For that purpose, the emulator was put into a temperature-controlled box to keep the output polarization stable with time. Using wavelength steps adapted to the DGD and instantaneous second-order PMD [10], a good agreement of the measurements (dots) and the model (lines) was obtained.

Thereafter, we set $\Delta\tau$ to 15.75 ps (giving a DGD of $\sim$20 ps for $\xi = 1/3$, which is about the tolerated limit in a 10-Gb/s link) and varied the coupling ratio, i.e., ξ (Fig. 1 shows their relationship). Fig. 5 shows these results and once more, a remarkable agreement with the theory is found.

IV. Conclusion

A PMD emulator with adjustable DGD and ratio between DGD and instantaneous second-order PMD was presented. Although this emulator does not give any statistical output as real fibers do, it allows even the better to evaluate the impact of low-probability events of large (instantaneous) first- and second-order PMD on the system under test.

The principle of operation is based on two PM fibers, where the coupling between the two fibers sets the ratio of DGD to instantaneous second-order PMD. By changing a variable delay line, the emulator DGD can be easily varied from 0 to 300 ps (while the ratio of DGD to instantaneous second-order PMD is conserved). As the absolute wavelength does not enter the game, the emulator operates in a very broad wavelength region. The emulator performance was tested with JME measurements and the experimental values for DGD and instantaneous second-order PMD were found to agree well with the desired values set by the operator.

Acknowledgment

The authors would like to thank Dr. B. Huttner, Luciol Instruments SA, Nyon, for his initial calculations.

References

[1] F. Buyere, "Impact of first and second order PMD in optical digital transmission systems," *Opt. Fiber Technol.*, vol. 2, pp. 269–280, 1996.

[2] Ph. Ciprut, B. Gisin, N. Gisin, R. Passy, J. P. von der Weid, F. Prieto, and Ch. Zimmer, "Second order polarization mode dispersion: impact on analog and digital transmissions," *J. Lightwave Technol.*, vol. 16, pp. 757–771, May 1998.

[3] J. M. Fini and H. A. Haus, "Accumulation of polarization-mode dispersion in cascades of compensated optical fibers," *IEEE Photon. Technol. Lett.*, vol. 13, pp. 124–126, Feb. 2001.

[4] R. Khosravani, I. T. Lima Jr., P. Ebrahimi, E. Ibragimov, A. E. Willner, and C. R. Menyuk, "Time and frequency domain characteristics of polarization-mode dispersion emulators," *IEEE Photon. Technol. Lett.*, vol. 13, pp. 127–129, Feb. 2001.

[5] A. O. Dal Forno, A. Paradisi, R. Passy, and J. P. von der Weid, "Experimental and theoretical modeling of polarization-mode dispersion in single mode fibers," *IEEE Photon. Technol. Lett.*, vol. 12, pp. 296–298, Mar. 2000.

[6] J. N. Damask, "A programmable polarization-mode dispersion emulator for systematic testing of 10 Gb/s PMD compensators," in *Proc. Optical Fiber Communications Conf. OFC 2000*, Paper ThB3.

[7] G. Biondini, W. L. Kath, and C. R. Menyuk, "Non-Maxwellian DGD distributions of PMD emulators," in *Proc. Optical Fiber Communications Conf. OFC 2001*, Paper ThA5.

[8] N. Gisin and J. P. Pellaux, "Polarization mode dispersion: time versus frequency domains," *Opt. Commun.*, vol. 89, no. 2–4, pp. 316–323, 1992.

[9] M. Wegmuller, S. Demma, C. Vinegoni, and N. Gisin, "First and second order PMD emulator," in *Optical Fiber Measurements Conf. OFMC '01*, Cambridge, U.K., Sept. 2001, pp. 26–28.

[10] B. L. Heffner, "Automated measurement of polarization mode dispersion using Jones Matrix Eigenanalysis," *IEEE Photon. Technol. Lett.*, vol. 4, pp. 1066–1069, Sept. 1992.

B.10 Distributed Measurements of Chromatic Dispersion and Nonlinear Coefficient in Low PMD Dispersion-Shifted Fibers

C. Vinegoni[1,2], H. Chen[2], M. Leblanc[2], G. Schinn[2],M. Wegmuller[1],N. Gisin[1]

[1] *Group of Applied Physics - Gap Optique*
University of Geneva,
20 Ecole-de-Medecine, CH-1211 Aeneve 4, Switzerland

[2] *EXFO Electro-Optical Engineering Inc*
465 Av. Godin, Vanier, Quebec, Canada G1M 3G7

Claudio.Vinegoni@physics.unige.ch

Abstract : We report on the investigation of distributed chromatic dispersion and distributed nonlinear coefficient measurements based on phase mismatched four-wave mixing (FWM) in dispersion-shifted fibers (DSF). Experimental results of the distributed chromatic dispersion maps for low polarization mode dispersion (PMD) DSF fibers are discussed. We also report how non negligible values of PMD can adversely affect the distributed chromatic dispersion measurements. A new method to measure the distributed nonlinear coefficient map in low PMD DSF fibers is also proposed and demonstrated experimentally.

SUBMITTED :

Distributed Measurements of Chromatic Dispersion and Nonlinear Coefficient in Low-PMD Dispersion-Shifted Fibers

C. Vinegoni, Hongxin Chen, M. Leblanc, G. W. Schinn, *Member, IEEE*, M. Wegmuller, and N. Gisin

***Abstract*—We report on the investigation of distributed chromatic dispersion (CD) and distributed nonlinear coefficient (NLC) measurements based on phase mismatched four-wave mixing in dispersion-shifted fibers (DSFs). Experimental results of the distributed CD maps for low polarization-mode dispersion (PMD) DSF fibers are discussed. We also report how nonnegligible values of PMD can adversely affect the distributed CD measurements. A new method to measure the distributed NLC map in low-PMD DSF fibers is also proposed and demonstrated experimentally.**

***Index Terms*—Chromatic dispersion (CD), dispersion-shifted fibers (DSFs), distributed measurements, four-wave mixing (FWM), nonlinear coefficient (NLC), polarization-mode dispersion (PMD).**

I. Introduction

OPTICAL nonlinearities play a significant role in contemporary fiber-optic transmission networks because of the long distances and the high powers present in the optical fibers. In fact, it is well known that nonlinear effects, such as four-wave mixing (FWM) and cross-phase modulation, may seriously affect optical transmission network systems, for example, in dispersion-shifted fibers (DSFs). The efficiency of these processes depends on both the chromatic dispersion (CD) profile and the nonlinear coefficient (NLC) n_2/A_{eff} profile. It is, therefore, highly interesting to have a nondestructive technique that allows us to map these parameters as a function of fiber distance in order to design ultrahigh capacity fiber-optic transmission networks.

In this letter, we report on the investigation of distributed CD measurements based on the method first proposed by Mollenauer *et al.* [1], where we obtained a spatial resolution of 250 m with a high accuracy. The experimental results for the case of fibers with low and nonnegligible values of polarization-mode dispersion (PMD), in particular in the presence of high values of the polarization coupling length (i.e., the distance over which the E field of the travelling wave loses memory of its initial distribution between the local polarization eigenstates) are also discussed. We found that, for nonnegligible values of PMD that can typically be found in the old installed DSF cables, the method is severely limited and data elaboration needs to be refined. At the same time, we propose and also experimentally demonstrate, for the first time to the best of our knowledge, a new method based on the aforementioned one to measure the distributed NLC map in low-PMD DSF fibers.

Manuscript received December 6, 2002; revised January 27, 2003. This work was supported by the Swiss OFES under the European COST 265 Project.

C. Vinegoni is with the Research Division, EXFO Electro-Optical Engineering Inc., Vanier, QC G1M 3G7, Canada, and also with the Group of Applied Physics, University of Geneva, Geneva CH-1211, Switzerland.

H. Chen, M. Leblanc, and G. W. Schinn are with the Research Division, EXFO Electro-Optical Engineering Inc., Vanier, QC G1M 3G7, Canada (e-mail: Hongxin.chen@exfo.com).

M. Wegmuller and N. Gisin are with the Group of Applied Physics, University of Geneva, Geneva CH-1211, Switzerland.

Digital Object Identifier 10.1109/LPT.2003.810249

II. Theory

The optical time-domain reflectometer-like method for measuring a distributed CD map is based on the detection of the fringe periods of the Rayleigh back-scattered FWM signal, either Stokes or anti-Stokes, generated from the fiber under test (FUT), by injecting two powerful lights (pump and probe) with powers P_1 and P_2 and frequencies ω_1 and ω_2 ($\omega_1 < \omega_2$). If we focus on the FWM generated from the Stokes frequency $\omega_S = 2\omega_1 - \omega_2$, the phase-mismatching Δk is given by [1]

$$\Delta k = \Delta k_L + \Delta k_{NL} = -D(\lambda_1)c2\pi\left(\frac{\Delta\lambda}{\lambda_1}\right)^2 + \gamma(2P_1 - P_2) \tag{1}$$

where $\gamma = n_2\omega_0/cA_{\text{eff}}$. The above equation shows that the phase-mismatching Δk depends on both the local CD $D(\lambda)$ (linear term) and NLC γ (nonlinear term). The Stokes signals can also be expressed as a spatial intensity oscillation with period λ_{SP}. Thus, the temporal oscillation frequency ν_T in intensity of the Rayleigh back-scattered light can be expressed as

$$\begin{aligned}\nu_t &= \frac{c}{2n}\frac{1}{\lambda_{Sp}} \\ &= \frac{c}{2n}\frac{\Delta k}{2\pi} \\ &= \nu_L + \nu_{NL} \\ &= -\frac{c}{2n}Dc\left(\frac{\Delta\lambda}{\lambda}\right)^2 + \frac{c\gamma}{4n\pi}(2P_1 - P_2).\end{aligned} \tag{2}$$

If $P_2 = 2P_1$ is satisfied, then the nonlinear term disappears and a measurement of the local frequency provides information of the local CD value versus fiber distance.

It is important to note that (1) does not take into account any polarization-dependent effects. However, it is clear that the relative polarization states of pump and probe will vary according to the PMD of the FUT. This change in their relative state of polarization (SOP) can be characterized by the spatial correlation of the pump and probe SOPs ($\mathbf{S_1}$ and $\mathbf{S_2}$) at the output of the FUT.

When PMD is present, one finds [2] that the correlation between pump and probe SOPs is proportional to $\mathbf{S}_1\mathbf{S}_2 \exp(-\langle\Delta\tau\rangle^2)$ where $\langle\Delta\tau\rangle$ is the overall PMD. This change in the relative SOP has two consequences. First, the FWM efficiency η ($\eta = (1+\mathbf{S_1}\mathbf{S_2})^{1/2}$) is polarization dependent. This implies that the total detected signal oscillations correspond to the sum of the Stokes signal—intensity oscillations related to the phase mismatch (i.e., the local CD)—and an additional modulated signal due to the change in the FWM efficiency by the PMD. However, this effect is usually not important because the length scale of this polarization-dependent fluctuation is normally very short compared with the Stokes signal oscillation scale, so that it is averaged away. The second consequence, however, implies that the phase seen by the pump and the probe can be different because of the local birefringence, thereby introducing an additional term (nonlinear term) to (1). As discussed later, this effect can be important in fibers with little polarization-mode coupling (large values of coupling length) and sufficiently high PMD. In such fibers, polarization-dependent phase shifts of the order of the ones from the CD (which is small in DSF fibers) can be picked up and strongly vary the oscillation frequency of the Stokes signal intensity.

It is interesting to note that in the case of fibers with small values of PMD, once a CD map $D(z, \lambda)$ for a particular fiber is obtained, we can retrieve information of the local NLC $\gamma(z)$ (i.e., n_2/A_{eff}) if we consider a ratio for the pump and probe powers different from two. Unfortunately, local variations due to the coupling length will not allow us to obtain good and reproducible maps of the NLC. An alternative way [3] consists of performing two different measurements keeping the ratio $\alpha = P_1/P_2$ constant (and different from two), but attenuating of the same factor α^* both pump and probe powers. It follows that the difference between the temporal frequencies of two measurements $\Delta\nu_t$ is independent of the CD (the linear term in (2) is equal for both cases, and so it is cancelled out) but contains a dependence in γ

$$\Delta\nu_t = \nu_t(\alpha = 1) - \nu_t(\alpha = \alpha^*) = \frac{c\gamma}{4n\pi}(2P_1 - P_2)\frac{1-\alpha^*}{\alpha^*}. \tag{3}$$

This allows us to obtain a map of the NLC versus fiber distance. Note that typical variations of the refractive index n along FUT will not significantly contribute to the $\Delta\nu_t$ term.

III. Experimental Setup

The experimental setup used for measuring the distributed CD is similar to the one of Mollenauer *et al.* [1] and is shown and described in detail in [3]. Measurements were made on different DSF fibers. The data for the two DSF fibers reported here are as follows. NIST fiber: length = 9700 m, PMD = 0.02 ps/$\sqrt{}$km. AC-2 fiber: length = 7400 m, PMD = 0.19 ps/$\sqrt{}$km. The PMD was measured by using a PMD analyzer (IQ-5500, EXFO).

IV. Distributed CD Map Measurements

Fig. 1 shows the Stokes signal intensity for the NIST fiber, for different input SOPs into the FUT, when pump and probe SOPs are set identical. No significant dependence of the results on the input polarizations was expected for this fiber because the pump and probe lights had no time to acquire significantly different phases due to the frequent coupling among the fast and slow axes and the low value of PMD. Indeed, our results show that we obtained very small changes in both the amplitude and the location of the Stokes signal maxima. The inset of Fig. 1 shows the CD maps obtained from lights launched into the FUT from both ends (one of the profiles was inverted), resulting in good reproducibility and accuracy. A spatial resolution of CD typically of 250 m with a high accuracy was observed.

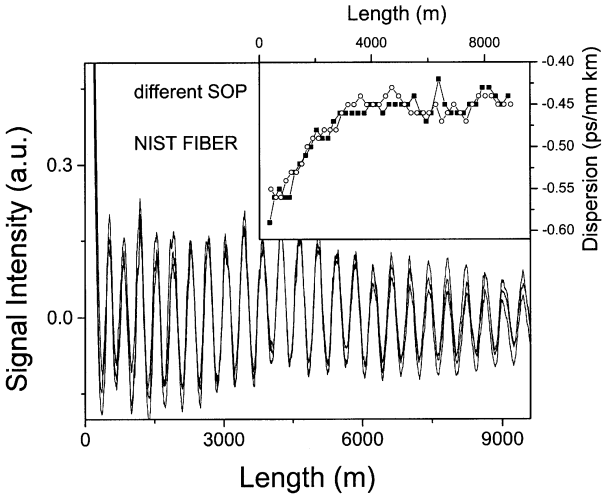

Fig. 1. Measured typical traces of the Rayleigh back-scattered FWM signals from a DSF fiber with low PMD (NIST fiber) for different input SOPs. Inset figure shows the two CD maps when the lights enters from the different fiber ends resulting in a less than ±4% difference of CD magnitudes.

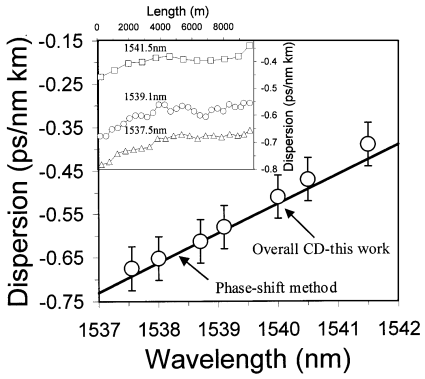

Fig. 2. Overall CD at different wavelengths (open circles) compared with phase-shifted method (solid line), for the NIST fiber. In the inset: CD maps for different wavelengths.

Fig. 2 gives the overall CD at different wavelengths, where open circles are obtained from summing up the FWM dispersion map and the bold line represents results obtained with an EXFO FTB-5800 analyzer using a phase-shift technique [4]. The two methods produce results in excellent agreement. The inset figure in Fig. 2 shows the distributed CD maps at different wavelengths. It clearly appears that CD maps have similar tendencies except for the dispersion values' offset at the different wavelengths.

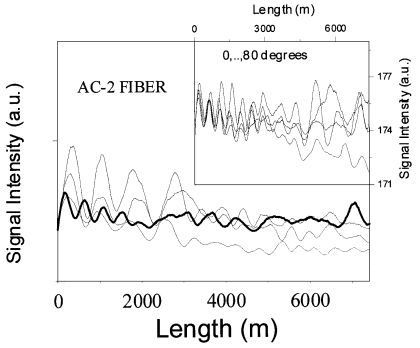

Fig. 3. Measured back-scattered FWM signal intensity profiles for the PMD DSF fiber (AC-2) with different input SOPs. The bold line shows a progressive averaging of the signals during scrambling of pump and probe polarization states. In the inset: the measured FWM signals from the other fiber end.

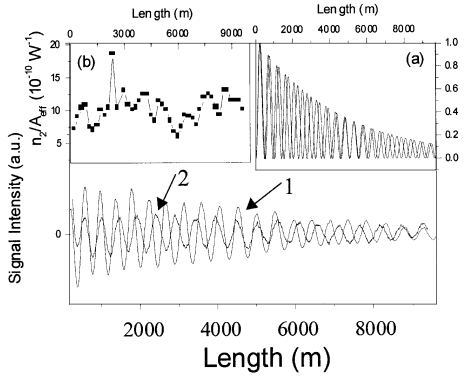

Fig. 4. Measured FWM intensity oscillations versus fiber distance for the low-PMD fiber (NIST fiber) at the wavelength 1541.3 nm for 1) $P_{10} = P_{20} = 1150$ mW and 2) $P_{10} = P_{20} = 115$ mW. In the inset: (a) theoretical simulation and (b) an NLC map.

Fig. 3 shows the data relative to the PMD fiber (AC-2). As it can be seen, the maxima (minima) locations of the Stokes signal vary strongly with the presence of an additional phase due to the PMD. The shift in the maxima (minima) depends on the input SOPs. In fact, the CD map can no longer be estimated from a single trace alone, as the frequency at a given location depends on the (arbitrary) relative polarization states at that location for that input SOP. To remove this arbitrary component, different profiles, each corresponding to a different input SOP, have to be taken. For a given location, the mean value of group-velocity dispersion should then be retained. Note that averaging over all the possible SOPs during an acquisition by means of a polarization scrambler (see bold line in Fig. 3) does not give a useful result as it simply corresponds to the sum of the different individual traces giving a curve that is basically flat due to arbitrary positions of the different maxima.

V. Distributed n_2/A_{eff} Measurement

As discussed in Section II, when the ratio P_2/P_1 is kept different from 2, the fiber nonlinearities produce an additional phase mismatching. Therefore, it is important to maintain $P_2/P_1 = 2$ at any position along the fiber in order to extract an accurate local CD value. However, as discussed before, this effect [i.e., the presence of both linear and nonlinear terms in (1)] can be exploited to obtain a distributed map of the NLC (i.e., n_2/A_{eff}). The method consists of taking at least two measurements while keeping $P_2/P_1 \neq 2$, and inserting a different attenuation for the two different measurements [see (3)]. Fig. 4 shows two FWM signal traces when the launched pump and probe powers had a difference of 10 dB. Two fringes are missed when the attenuation is introduced. This agrees with our theoretical simulation very well [see Fig. 4(a)]. Extracting a distributed NLC map from these curves is possible, as shown in Fig. 4(b) for a distributed NLC (n_2/A_{eff}) map versus fiber length. However, our first results are not accurate enough mainly because of the uncertainty in measuring high peak powers of launched pulses and the noise on the measurements. Note that the NLC map would also be sensitive to power fluctuation along fiber.

VI. Discussion and Conclusion

We have demonstrated highly spatially resolved and accurate distributed CD measurements in low-PMD DSF fibers based on phase mismatched FWM. Because of the sensitivity of the FWM efficiency and the PMD-induced phase mismatching, this method could be severely limited in the determination of accurate and meaningful CD maps for fibers having nonnegligible values of PMD, as reported here for the case of a fiber with PMD > 0.2 ps/$\sqrt{}$km. Further investigations between the interplay of PMD, coupling length, and FWM are in progress. Fortunately, for low-PMD fibers, the input SOP has little effect on the CD map. Thus, it is possible to extract meaningful information about distributed CD values from the detected Stokes signal oscillations. For recently installed fibers with low PMD, precision measurements can be carried out by averaging over all SOPs to avoid ambiguities. We have also demonstrated a useful measurement range of 40 km when using reclity.

Moreover, we have presented a new method in order to measure a distributed map of the NLC n_2/A_{eff}. Preliminary results confirmed the feasibility and the reproducibility of the method and further work is in progress.

Acknowledgment

C. Vinegoni would like to thank EXFO Electro-Optical Engineering, Inc., Vanier, QC, Canada for support during this research.

References

[1] M. L. F. Mollenauer, P. V. Mamyshev, and M. J. Nuebelt, "Method for facile and accurate measurement of optical fiber dispersion maps," *Opt. Lett.*, vol. 21, pp. 1724–1726, 1996.

[2] J. Hansryd, H. Sunnerud, P. A. Andrekson, and M. Karlsson, "Impact of PMD on four-wave-mixing-induced crosstalk in WDM systems," *IEEE Photon. Technol. Lett.*, vol. 12, pp. 1261–1263, Sept. 2000.

[3] C. Vinegoni, H. Chen, M. Leblanc, G. Schinn, M. Wegmuller, and N. Gisin, "Distributed measurements of chromatic dispersion and of nonlinear coefficient in DSF fibers with non negligible values of PMD," presented at the OFC'2002, Anaheim, CA, Paper WA5.

[4] L. G. Cohen, "Comparison of single-mode fiber dispersion measurement techniques," *J. Lightwave Technol.*, vol. LT-3, pp. 958–966, Oct. 1985.

Appendix C

Proceedings of Conferences

1. Faraday mirror stabilization scheme for nonlinear polarization rotation in optical fibers: models and application.
   C. Vinegoni, M. Wegmuller, and N. Gisin
   Cleo 2000 (Nice)

2. Measurements of the polarization coupling length in telecom fiber using nonlinear polarization rotation.
   C. Vinegoni, M. Wegmuller, and N. Gisin
   OFC 2001 (Anaheim, U.S.A.)

3. Estimation of the polarization coupling length in standard telecom fibers from measuremnets of nonlinear polarization rotation.
   C. Vinegoni, M. Wegmuller, and N. Gisin
   NIST 2000 (Boulder, CO)

4. Measurements of the nonlinear coefficient n_2/A_{eff} using a self aligned interferometer and a Faraday mirror.
   C. Vinegoni, M. Wegmuller, and N. Gisin
   NOISE 2000 (Twente, the Netherlands)

5. Measurements of the polarization coupling length in telecom fibers exploiting nonlinear polarization rotation.
   C. Vinegoni, H. Zbinden, V. Scarani, M. Wegmuller, and N. Gisin
   "Applications of nonlinear optical phenomena" 2001 (Budapest, HU)

6. Interlaboratory measurements of the nonlinear coefficient of standard SMF and DSF fibers using an interferometric method and an SPM based cw dual-frequency method.
   C. Vinegoni, M. Wegmuller, N. Gisin, K. Nakajima, and M. Ohashi
   OFMC 2001 (Cambridge, UK)

7. Implementation of a Faraday mirror stabilization scheme for all optical switching in a standard telecom fiber.

C. Vinegoni, M. Wegmuller, and N. Gisin
ICTON 2000 (Warsaw, Poland).

8. Overview of coherent reflectometry techniques: characterization of components and small systems.
M. Wegmuller, P. Oberson, J.P. von der Weid, O. Guinnard, L. Guinnard, C. Vinegoni, M. Legre, and N. Gisin
NIST 2000 (Boulder, CO)

9. Distributed measurements of chromatic dispersion and of the nonlinear coefficient in DSF fibers with non negligible values of PMD
C. Vinegoni, H. Chen, M. Leblanc, G. Schinn,M. Wegmuller, and N. Gisin
OFC 2002 (Anaheim, Ca)

10. First and second order PMD emulator
M. Wegmuller, S. Demma, C. Vinegoni, and N. Gisin
OFMC 2001 (Cambridge, UK)

11. A near infrared SNOM: First results and prospects.
Y. Mugnier, M. Moret, P. Descouts, C. Vinegoni, M. Wegmuller, N. Gisin
WORKSHOP ON NANOSCIENCE 2001 (Twannberg, CH)

12. Measurement of nonlinear polarization rotation in high birefringence optical fibers with a Faraday mirror.
C. Vinegoni, M. Wegmuller, B. Huttner, and N. Gisin
Amalfi Workshop '99 (Amalfi, Italy)

13. Nonlinear polarization rotation in a highly birefringent optical fiber using a Faraday mirror.
C. Vinegoni, M. Wegmuller, B. Huttner, and N. Gisin
Goteborg 2000 (COST 265)

14. Measurement of nonlinear coefficient n_2/A_{eff} in optical fibers using a self-aligned interferometer and a Faraday mirror.
C. Vinegoni, M. Wegmuller, and N. Gisin
Goteborg '00 (COST 265)

15. PMD effect on measurements of distributed chromatic dispersion in DSF fibers
H. Chen, M. Leblanc, and G. Schinn, C. Vinegoni, M. Wegmuller, N. Gisin
Photonics North 2002 (Quebec City, CA)

16. A Comparison of Six techniques for nonlinear coefficient measurements of various single mode optical fibers.
Y. Namihira, K. Miyagi, K. Kaneshima, M. Tadakuma, C. Vinegoni, G. Pietra, K. Kawanami
NIST 2002 Boulder, CO (USA).

C.1 Faraday Mirror Stabilization Scheme for Nonlinear Polarization Rotation in Optical Fibers: Model and Applications.

C. Vinegoni, M. Wegmuller, and N. Gisin

[1] *Group of Applied Physics - Gap Optique*
University of Geneva,
20 Ecole-de-Medecine, CH-1211 Aeneve 4, Switzerland

Claudio.Vinegoni@physics.unige.ch

Abstract : An elegant, passive stabilization method for ultrafast devices employing nonlinear polarization rotation (NPR) is demonstrated both theoretically and experimentally. It allows for a quantitative measurement of NPR in an optical fiber where it is otherwise completely covered by linear fluctuations, and when applied to a wavelength converter excellent stability over hours is obtained.

PRESENTED : Cleo 2000 (Nice)

12.15 CTuI5

Faraday Mirror Stabilization Scheme for Nonlinear Polarization Rotation in Optical Fibers: Model and Applications

C. Vinegoni, M. Wegmuller, N. Gisin

Group of Applied Physics, University of Geneva,
20 Ecole-de-Medecine, CH-1211 Geneve 4, Switzerland
phone: +41 (0)22 702 60 82, fax: +41 (0)22 781 09 80
e-mail: CLAUDIO.VINEGONI@PHYSICS.UNIGE.CH

The potential of nonlinear polarization rotation (NPR) in waveguides is huge as it can be exploited for a large variety of ultrafast devices like optical switches, logic gates, intensity discriminators, nonlinear filters, or pulse shapers. However, an inherent problem to all this applications is the stability of the output polarization state. Fluctuations of the linear birefringence caused by temperature changes, drafts in the fiber environment, and vibrations generally disturb a proper functioning.

We propose an elegant method to remove these detrimental fluctuations in a passive way by employing a Farady mirror (FM) and a double pass of the fiber where NPR takes place. The proposed stabilization scheme has the additional advantage that the double pass allows for a reduction of the fiber length times pump intensity value by almost a factor of two.

A model is developed that allows for an intuitive understanding of the action of the linear and nonlinear birefringence during the go- and return-path. Besides giving good insight in the underlying physical processes, it directly shows that the effect of NPR adds whereas the detrimental effects of the (fluctuating) linear fiber birefringence are removed. This allows to quantitatively measure NPR in an optical fiber, where it is otherwise completely covered by the linear polarization changes (Fig.1).

The successful implementation of our stabilization scheme is then demonstrated both for a self-switch and for a wavelength converter. The converter stability is monitored over several hours and is found to be excellent both for the use of a standard or a PM fiber as the NPR medium (Fig.2). Without our stabilization, the bias of the wavelength converter quickly changes - especially for the PM fiber - in an erratic way.

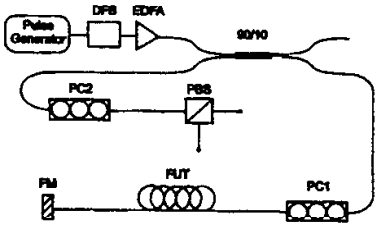

Figure 1: Experimental setup for the measurements of the NPR.

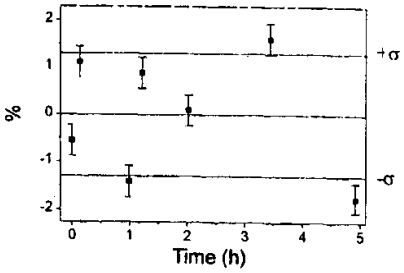

Figure 2: Relative fluctuations of the switch port signal power as a function of time.

C.2 Measurement of the polarization coupling length in telecom fibers exploiting nonlinear polarization rotation.

C. Vinegoni, M. Wegmuller, and N. Gisin

[1] *Group of Applied Physics - Gap Optique*
University of Geneva,
20 Ecole-de-Medecine, CH-1211 Aeneve 4, Switzerland

Claudio.Vinegoni@physics.unige.ch

Abstract : It is well known that single-mode communication fibers are birefringent and that the orientation and the amount of birefringence are randomly distributed along the fibers. The corresponding polarization mode dispersion (PMD) becomes therefore a statistical quantity, and not only its mean value but also its probability distribution is important to assess the inferred system impairments. This distribution depends on two parameters, the (mean) local birefringence B and the coupling length h giving the distance after which a considerable amount of power has coupled into the other polarization mode. In fibers having a length L long compared to the beatlength and to h, the PMD probability distribution is Maxwellian with a mean value of B(hL), whereas for coupling lengths approaching the fiber lengths, the PMD statistics can change considerably. In this work we present a novel way to directly infer the polarization coupling length h from measurements of the amount of nonlinear polarization rotation (NPR) of the fiber. Different values of h were determined for different fibers. Especially noteworthy, a large difference in h was found for two standard fibers having almost the same PMD.

PRESENTED : OFC 2001 (Anaheim, U.S.A.)

Measurement of the Polarization Coupling Length in Telecom Fibers using Nonlinear Polarization Rotation

C. Vinegoni, M. Wegmuller, and N. Gisin
Group of Applied Physics, University of Geneva, 20 Ecole-de-Medecine, CH-1211 Geneve 4, Switzerland
Phone: +41 (0)22 702 69 36, Fax: +41 (0)22 781 09 80 E-mail: CLAUDIO.VINEGONI@PHYSICS.UNIGE.CH

Abstract: The polarization coupling length, an important parameter of the PMD probability distribution, is obtained from measurements and modeling of the nonlinear polarization rotation in optical fibers. Results for different types of fibers are presented.

OCIS codes: (060.2270, 060.4370)

1. Introduction

It is well known that single-mode communication fibers are birefringent and that the orientation and the amount of birefringence is randomly distributed along the fibers. The corresponding polarization mode dispersion (PMD) becomes therefore a statistical quantity, and not only its mean value but also its probability distribution is important to assess the inferred system impairments. This distribution depends on two parameters, on the (mean) local birefringence B and on the coupling length h giving the distance after which a considerable amount of power has coupled into the other polarization mode. In fibers having a length L long compared to h, the probability distribution is Maxwellian with a mean PMD value of $B\sqrt{hL}$, whereas for coupling lengths approaching the fiber lengths, the PMD statistics can change considerably. In this paper we present a novel way to directly infer the polarization coupling length from measurements of the nonlinear polarization rotation (NPR) of the fiber.

2. Theory

In a dielectric medium, an intense elliptical input pulse induces birefringence – via the optical Kerr effect - due to the different amounts of intensity along the major and minor axis of the polarization ellipse. In an isotropic medium this self-induced birefringence leads to polarization ellipse self-rotation. In an optical fiber however, the situation is more complex due to the presence of the local intrinsic birefringence. The polarization changes are hard to predict in that case as the linear and nonlinear birefringences interact in a complicated manner. In general, the linear birefringence will however be much larger than the nonlinear one, and the evolution of the polarization vector ψ in a polarization maintaining fiber can then be approximated by [1]:

$$\partial_z \psi \approx i\omega B_{eff} \sigma_\theta \psi \qquad (1)$$

where σ_θ accounts for the linear birefringence with axis θ. The linear birefringence B is replaced by an effective birefringence B_{eff} accounting for the nonlinear birefringence. The solution for Eq.1 is straightforward, and corresponds to a rotation of the input polarization vector around the linear birefringence axis σ_θ, with a rotation angle β given by

$$b = wB_{eff} z = w(B - \frac{a}{2} m_q(0))z \qquad (2)$$

where $\alpha = n_2 P/(3cA_{eff})$, n_2 is the nonlinear Kerr coefficient, P the power, and A_{eff} the effective area. $m_\theta(0)$ is the projection of the input SOP on the birefringent axis. In principle the NPR can now be measured by varying the input power P and observing the corresponding change in the output SOP.

However, an inherent problem for this kind of measurements is the stability of the output SOP at the exit of the fiber, subjected to fluctuations of the much larger linear birefringence B due to temperature changes and drafts in the fiber environment. We have recently proposed a method for measuring NPR [1] by removing the overall linear birefringence -and therefore also its fluctuations- in a purely passive way by employing a Faraday mirror (FM) and a double pass of the fiber under test. Doing so, the nonlinear birefringence (leading to NPR) was shown to remain unaffected, i.e. the NPR of the forward and backward path add up.

This allows to measure NPR both in polarization maintaining (PM) fibers and in standard fibers. However, the random variations of the intrinsic local birefringence axis in a standard fiber reduce the NPR. The situation becomes more complex, and we therefore resort to numerical simulations. The fiber is modeled as a concatenation of linearly birefringent trunks with a physical length h kept constant and a random birefringence axis orientation. For each of these trunks, Eq.2 is used to calculate the output SOP from the input one, with the input SOP calculated from the output SOP of the previous trunk. The SOP can therefore be calculated piece by piece, with the projection m_θ being different for each new trunk. The final SOP will depend on the choice of the birefringence axis orientations, with variations being larger for large coupling lengths h. We therefore made 100 runs for each specific coupling length to get a mean value of the NPR.

3. Experiment

The experimental setup for the measurement of NPR for different test fibers is shown in Fig.1. The light source consists of a distributed feedback laser (DFB) operated in pulsed mode at a wavelength of 1559 nm. Typically, pulses with a duration of 30 ns, a repetition rate of 1 kHz, and a peak power of up to 6 W (after amplification by an EDFA) are used. The light is then launched into the fiber under test (FUT) via a 90/10 coupler and a polarization controller (PC1). The coupler is inserted for the detection of the backward traveling light after the double pass of the FUT, with its 90% output port connected to the source in order to maintain high launch powers into the FUT. The polarization controller, PC1, allows to adjust the polarization of the light launched into the FUT, i.e. $m_\theta(0)$, which is important for the strength of the NPR as demonstrated by Eq.2. Note that for low launch powers (negligible NPR), the action of PC1 is removed by the Faraday mirror, and its setting is therefore of no importance in that case. The output SOP is examined by an analyzer consisting of a polarization controller PC2 and a polarizing beam splitter (PBS). To achieve a good sensitivity of the analyzer, it is calibrated for equal power in the two PBS output arms for low power launch signals where no NPR occurs. The two PBS output channels were monitored by a fast photodiode (200 ps response time) and a sampling scope. The measurements were then performed in the following way: for a given launch power, the polarization launched into the FUT was adjusted (PC1) to give the smallest possible output power at the monitored PBS channel. Consequently, the difference between the two PBS output channels is maximized, corresponding to a maximum value of the NPR.

4. Results

We first measured the NPR in a PM fiber with a length of 200 m. The results are shown in Fig.2. As can be seen, NPR starts to be important for launch powers above 1 W. In spite of the linear increase that would be experienced in the absence of NPR (straight line), the output power actually starts to decrease for input powers above 2.5 W. The measured data (squares) agree well with our model (solid curve), in which $m_\theta(0)$ was varied in order to give a minimum output power from the PBS channel like in the experiment, and only one fiber trunk was used (coupling length h = fiber length L).

In Fig.3, numerical results for different coupling lengths (indicated on the right) for a fiber length of 1.5 km are given. NPR is reduced for a larger number of couplings resulting in a more and more linear dependence of the output from the input power. This reduction is because of the increased probability that the NPR action in one trunk is compensated for by another. As the figure demonstrates, the results for the different coupling lengths can be clearly distinguished.

These theoretical predictions were then compared to measurements of different standard fibers. The fiber lengths were typically 1 to 1.5 km (of course the simulations were adjusted accordingly). Fig.4 shows the results for 2 standard fibers with large and small PMD, respectively. Note that for a clearer distinction of the curves, the figure gives the strength of NPR, i.e. the reduction of the output power from the value without NPR. As expected, the two standard fibers exhibit a NPR that is much lower than for a PM fiber. But the amount of NPR for the two standard fibers is distinctively different as well. From comparison of the experimental results with the simulations, the coupling lengths can be estimated to about 75 m for the small PMD and 625 m for the large PMD fiber, respectively. A value of $h<100$ m is quite reasonable for a state-of-the-art, low PMD fiber. The coupling length of h~600 m for the high PMD 'standard' fiber is large, but its high PMD value of 1.9 ps/$\sqrt{}$km could indeed indicate that there might be well defined birefringent axes in that fiber. Moreover, a different estimation for the coupling length of these fibers from PMD and beat length measurements using Optical Frequency Domain Reflectometry [2] is in good qualitative agreement with the results presented here.

5. Conclusions

Measurements and a model of NPR in an optical fiber were presented, allowing for direct determination of the polarization mode coupling length. Coupling length values of several 100 m were obtained for large PMD fibers, whereas it was as low as 75 m in state-of-the-art low PMD fibers.

5. References

[1] C. Vinegoni, M. Wegmuller, B. Huttner, and N. Gisin "Measurement of nonlinear polarization rotation in a highly birefringent optical fiber using a Faraday mirror", J. Opt. A **2**, 314-318 (2000).

[2] M. Wegmuller, J.P. von der Weid , P. Oberson, and N. Gisin "High resolution fiber distributed measurements with Coherent OFDR", ECOC 2000, paper 11.3.4

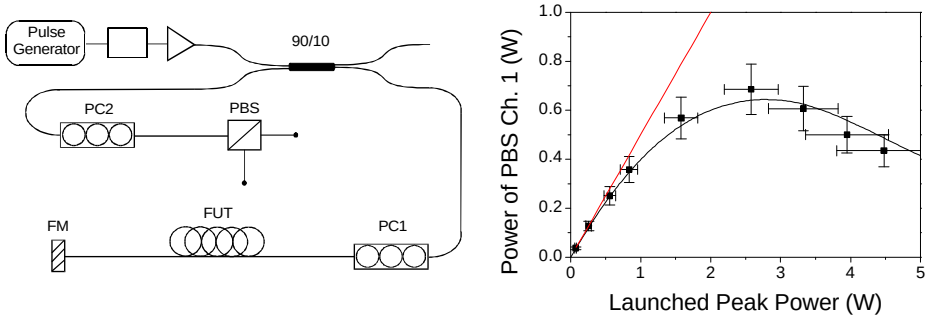

Fig. 1. Experimental setup.
Fig. 2. Minimum output power of PBS channel 1 for a 200 m long PM fiber

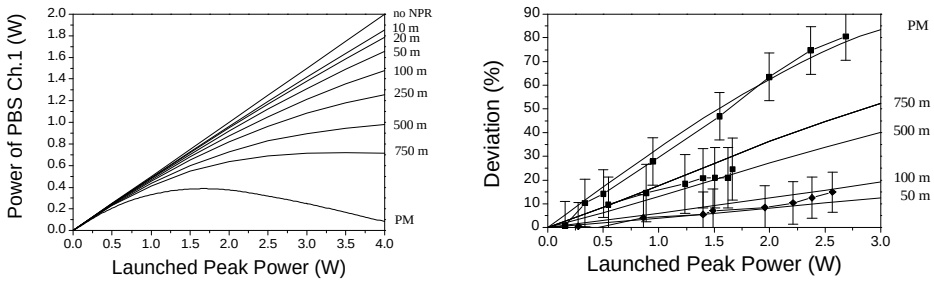

Fig. 3. Numerical results for a fiber length of 1.5 km with different polarization mode coupling lengths h.
Fig. 4. Experimental and numerical results of NPR strength in different fibers.

C.3 Estimation of the Polarization Coupling Length in Standard Telecom Fibers from Measurements of Nonlinear Polarization Rotation.

C. Vinegoni, M. Wegmuller, and N. Gisin

[1] *Group of Applied Physics - Gap Optique*
University of Geneva,
20 Ecole-de-Medecine, CH-1211 Aeneve 4, Switzerland

Claudio.Vinegoni@physics.unige.ch

Abstract : An analytical solution for the influence and strength of nonlinear polarization rotation (NPR) in an optical fiber is presented. It agrees well with our measurements of NPR in a polarization maintaining fiber, made possible by removing the much larger, fluctuating linear birefringence with a Faraday mirror. The same technique is then employed to measure NPR in standard fibers, where its dependence on the polarization mode coupling length can be exploited to get a direct estimate for this important fiber parameter.

PRESENTED : NIST 2000 (Boulder, CO)

Estimation of the Polarization Coupling Length in Standard Telecom Fibers from Measurements of Nonlinear Polarization Rotation

C. Vinegoni, M. Wegmuller, N. Gisin

Group of Applied Physics, University of Geneva,
20 Ecole-de-Medecine, CH-1211 Geneve 4, Switzerland

Abstract:

An analytical solution for the influence and strength of nonlinear polarization rotation (NPR) in an optical fiber is presented. It agrees well with our measurements of NPR in a polarization maintaining fiber, made possible by removing the much larger, fluctuating linear birefringence with a Faraday mirror. The same technique is then employed to measure NPR in standard fibers, where its dependence on the polarization mode coupling length can be exploited to get a direct estimate for this important fiber parameter.

INTRODUCTION

The potential of NPR to build ultrafast devices has been recognized a long time ago and received considerable attention since then. It has been proposed to exploit it for optical switches, logic gates, multiplexers, intensity discriminators, nonlinear filters, or pulse shapers. An inherent problem to all this applications is the stability of the output state of polarization (SOP), generally subjected to fluctuations of the linear birefringence caused by temperature changes and drafts in the fiber environment. We recently proposed a method [1] for removing the overall linear birefringence, and therefore also its fluctuations, in a passive way by employing a Faraday mirror (FM) [2] and a double pass of the fiber under test. It was also demonstrated that the nonlinear birefringence, leading to NPR, remains unaffected, i.e. the NPR of the forward and backward path add up. This allows to measure NPR both in polarization maintaining (PM) fibers and in standard fibers. However, the random variations of the intrinsic local birefringence axes in a standard fiber reduce the NPR. This reduction depends on the polarization mode coupling length h, and can be intuitively understood by examining the extreme case of a fiber with a coupling length close to zero. All orientations of the SOP with respect to the local birefringence axes will be encountered with equal probability, and as the sense of rotation of the NPR depends on exactly this parameter [1], it averages out to zero. Consequently, it should be possible to derive information about the coupling length from the amount of NPR reduction.

The paper is organized as follows: First, the analytical model developed in [1], valid for PM fibers, is reviewed and generalized for standard fibers. We then present results for NPR measurements in a PM and 2 different standard fibers, and compare them with the simulations to obtain information about the coupling length h.

THEORY

In a dielectric medium, an intense elliptical input pulse induces birefringence – via the optical Kerr effect - due to the different amounts of intensity along the major and minor axis of the

polarization ellipse. It is well known that in isotropic media, this self-induced birefringence leads to a rotation of the polarization ellipse while propagating in the medium. In an optical fiber however, the situation becomes more complicated as there is also the local intrinsic birefringence to be considered. Generally, the polarization ellipse changes are hard to predict in that case as the linear and nonlinear birefringence interact in a complicated manner. Starting from the nonlinear Schroedinger equation written in the form as given by Menyuk and assuming that the linear birefringence is much larger than the nonlinear one, it is possible to show that the evolution of the polarization vector ψ is given by [1]:

$$\partial_z \psi \approx i\omega B_{eff} \sigma_\theta \psi \qquad (1)$$

where σ_θ accounts for the linear birefringence with axis θ. The amount of linear birefringence B is replaced by an effective birefringence B_{eff}, which includes the action of the nonlinear birefringence. The solution for Eq.1 is straightforward, $\psi_z = \exp(i\omega B_{eff} \sigma_\theta z)\psi_0$, and corresponds to a rotation of the input polarization vector around the linear birefringence axis σ_θ with a rotation angle β given by

$$\beta = \omega B_{eff} z = \omega(B - \frac{\alpha}{2} m_\theta(0))z \qquad (2)$$

where $\alpha=n_2P/(3cA_{eff})$, n_2 is the nonlinear Kerr coefficient, P the power, and A_{eff} the effective area. $m_\theta(0)$ is the projection of the input SOP on the birefringent axis.

In principle the NPR can now be measured by varying the input power P and observing the corresponding change in the output SOP. However, the contribution of the nonlinear term is negligibly small compared to the linear one, and the slightest change in B will completely cover the NPR. A way out of this problem is to make a double pass of the fiber under test by means of a Faraday mirror. The linear birefringence accumulated during the forward path is thereby automatically removed on the return path. The nonlinear birefringence on the other hand does not cancel out but adds up [1]. This is because after reflection at the FM, which transforms the SOP to its orthogonal counterpart, the sense of rotation of the NPR remains the same as during the forward path.

As mentioned before, the situation is more complex in a standard fiber, and the NPR depends on the polarization mode coupling length h. To calculate the NPR for this case, we therefore resort to numerical simulations. The fiber is modeled as a concatenation of linearly birefringent trunks with length h and random birefringence axis orientation. For each of these trunks, Eq.1 still holds as for typical standard fibers (beatlength of less than 100 m), the linear birefringence is still much larger than the nonlinear one. The SOP can therefore be calculated piece by piece, with the projection m_θ being different for each new trunk. The final SOP will obviously depend on the choice of the (random) birefringence axis orientations, with variations being larger for large coupling lengths h. We therefore made 100 runs for each specific coupling length to get a mean value of the NPR.

EXPERIMENT

The experimental setup is shown in Fig.1. The light source consists of a distributed feedback laser (DFB), operated in pulsed mode at a wavelength of 1559 nm. Typically, pulses with a duration of 30 ns, a repetition rate of 1 kHz, and a peak power of up to 6 W (after amplification by an EDFA) are used. The light is then launched into the fiber under test (FUT) via a 90/10

coupler and a polarization controller (PC1). The coupler is inserted for the detection of the backward traveling light after the double pass of the FUT, with its 90% output port connected to the source in order to maintain high launch powers. The polarization controller, PC1, allows to adjust the polarization of the light launched into the FUT, which is important for the strength of the NPR as demonstrated by Eq.2. Note that for low launch powers (negligible NPR), the action of PC1 is removed by the Faraday mirror, and its setting is therefore of no importance in that case. The output SOP is examined by an analyzer consisting of a polarization controller PC2 and a polarizing beam splitter (PBS). To achieve a good sensitivity of the analyzer, it is calibrated for equal power in the two PBS output arms for low power launch signals where no NPR occurs. The two PBS output channels were monitored by a fast photodiode (200 ps response time) and a sampling scope. The measurements were then performed in the following way: for a given launch power, the polarization launched into the FUT was adjusted (PC1) to give the smallest possible output power at the monitored PBS channel. Consequently, the difference between the two PBS output channels is maximized, corresponding to a maximum value of the NPR.

RESULTS

First, a PM fiber with a length of 200 m was measured. The results are shown in Fig.2. One can see that for this fiber NPR starts to be important for launch powers above 1 W, and that in spite of the linear increase that would be experienced in the absence of NPR (straight line), the output power actually starts to decrease for input powers above 2.5 W. The measured data (squares) are then compared to the calculated values (solid curve) using Eq.1, where $m_\theta(0)$ was varied in order to give a minimum output power from the PBS channel like in the experiment. As Fig.2 shows, the agreement between measurement and model is good.

The same type of measurement was then performed for different standard fibers and compared to the corresponding simulations. The fiber lengths were typically 1 to 1.5 km, so that a large number of couplings is obtained, allowing for comparison with the mean simulation values. An example of the numerical results for a fiber length of 1.5 km is shown in Fig.3. One can see that the mean output power becomes indeed larger for smaller coupling lengths, indicating a reduced NPR.

Fig.4 shows the results for 2 standard fibers with large and small PMD. Note that for ease of comparison, the figure gives the strength of NPR, i.e. the reduction of the output power from the value without NPR. As expected, the two standard fibers exhibit an NPR that is much lower than for a PM fiber (note that the results for the PM fiber had to be rescaled to account for its different length and n_2/A_{eff} parameters). However, the amount of NPR for the two standard fibers is also distinctively different. From comparison of the experimental results with the numerically obtained data (lines), the coupling lengths can be estimated to about 75 m for the small PMD and 625 m for the large PMD fiber. A value of $h<100$ m is quite reasonable for a good (i.e. low PMD) standard fiber. The coupling length of $h\sim600$ m for the high PMD 'standard' fiber is large, but its high PMD value of 1.9 ps/$\sqrt{\text{km}}$ could indeed indicate that there might be well defined birefringent axes in that fiber. Moreover, a different estimation for the coupling length of these fibers from PMD and beat length measurements using Optical Frequency Domain Reflectometry [3] is in good qualitative agreement with the results presented here.

CONCLUSIONS

A model and measurements of NPR in optical fibers were presented. As the amount of NPR depends on the polarization mode coupling length, we were able to retrieve this important fiber parameter by comparing the measured and numerical data.

Acknowledgements: *Financial support from the Swiss OFES in the frame of the COST 265 project is acknowledged*

REFERENCES

[1] C. Vinegoni, M. Wegmuller, B. Huttner, and N. Gisin "Measurement of nonlinear polarization rotation in a highly birefringent optical fiber using a Faraday mirror", *J. Optics A*, accepted for publication in 2000

[2] M. Martinelli, "A universal compensator for polarization changes induced by birefringence on a retracing beam", *Opt. Comm.* 72, 341-344 (1989).

[3] B.Huttner, J.Reecht, N.Gisin, R.Passy, and J.P. von der Weid, "Local birefringence measurements in single-mode fibers with coherent optical frequency-domain reflectometry", *IEEE Photon. Technol. Lett.*, **10** 10, 1458-1460, 1998

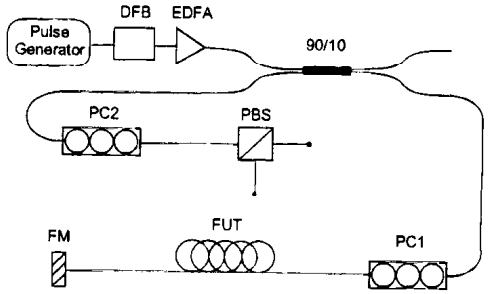

Figure 1: Experimental setup

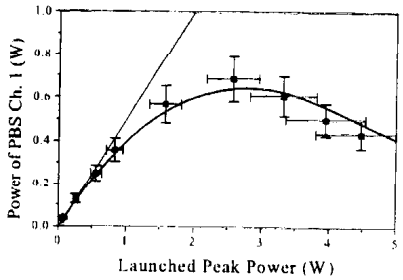

Figure 2: Minimum output power of PBS channel 1 for a 200 m long PM fiber

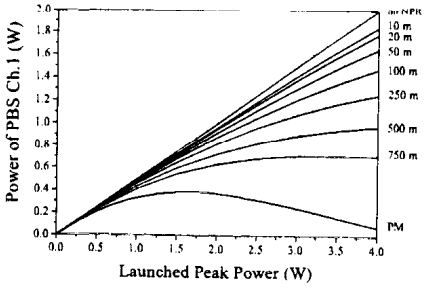

Figure 3: Numerical results for a fiber length of 1.5 km with different polarization mode coupling lengths h

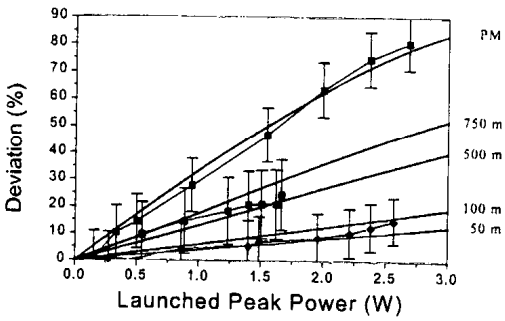

Figure 4: Experimental and numerical results of NPR strength in different fibers

C.4 Measurements of the nonlinear coefficient n_2/A_{eff} using a self-aligned interferometer and a Faraday mirror.

C. Vinegoni, M. Wegmuller, and N. Gisin

[1] *Group of Applied Physics - Gap Optique*
University of Geneva,
20 Ecole-de-Medecine, CH-1211 Aeneve 4, Switzerland

Claudio.Vinegoni@physics.unige.ch

Abstract : A simple, all-fiber implementable method for the measurement of the nonlinear coefficient n_2/A_{eff} in telecom fibers at 1550 nm is demonstrated. The method is based on the interferometric detection of the Kerr phase shift acquired by a laser pulse along the fiber under test. The detection is made by an all-fiber self-aligned interferometer incorporating a Faraday mirror. The self alignment characteristic allows for an easy and quick initial adjustment of the interferometer and leads to a good robustness as the two interferometer arms are always automatically matched.The Faraday mirror, whose property is that it transforms any input polarization state to the orthogonal one upon reflection, completely removes any polarization transformation of the fiber under test. In the same way, any fluctuations of the polarization state due to environmental perturbations (temperature, pressure changes) are removed. The polarization state re-entering the self-aligned interferometer on the backwards path is therefore fixed, so that it can be adjusted once-for-all for maximum visibility at its output. The presence of the Faraday mirror makes the setup robust, leading to a good accuracy in the n_2/A_{eff} value. Moreover, the fiber under test can be easily replaced without necessitating any further readjustment of the interferometer. The proposed scheme is therefore well suited to routinely measure the nonlinear coefficient.

PRESENTED : NOISE 2000 (Twente, the Netherlands)

MEASUREMENTS OF THE NONLINEAR COEFFICIENT N_2/A_{EFF} USING A SELF-ALIGNED INTERFEROMETER AND A FARADAY MIRROR

C. VINEGONI, M. WEGMULLER, N. GISIN
Group of Applied Physics, University of Geneva, 20 Ecole-de-Medecine, CH-1211 Geneve 4, Switzerland

Abstract

A simple, all-fiber implementable method for the measurement of the nonlinear coefficient n_2/A_{eff} in telecom fibers at 1550 nm is demonstrated. The method is based on the interferometric detection of the Kerr phase shift acquired by a laser pulse along the fiber under test. The detection is made by an all-fiber self-aligned interferometer incorporating a Faraday mirror. The self alignment characteristic allows for an easy and quick initial adjustment of the interferometer and leads to a good robustness as the two interferometer arms are always automatically matched. The Faraday mirror, whose property is that it transforms any input polarization state to the orthogonal one upon reflection, completely removes any polarization transformation of the fiber under test. In the same way, any fluctuations of the polarization state due to environmental perturbations (temperature, pressure changes) are removed. The polarization state re-entering the self-aligned interferometer on the backwards path is therefore fixed, so that it can be adjusted once-for-all for maximum visibility at its output. The presence of the Faraday mirror makes the setup robust, leading to a good accuracy in the n_2/A_{eff} value. Moreover, the fiber under test can be easily replaced without necessitating any further readjustment of the interferometer. The proposed scheme is therefore well suited to routinely measure the nonlinear coefficient.

1. Introduction

The implementation of Erbium-doped fiber amplifiers and chromatic dispersion compensation allows for long distance data transmission. Along with the technique of wavelength division multiplexing (WDM), this leads to an important amount of power inside the fiber over long distances, and optical nonlinearities start to play a significant role. Their magnitudes depend on the ratio n_2/A_{eff}, where n_2 is the nonlinear refractive index of the fiber and A_{eff} the effective area of the lightmode. There are different methods to measure n_2/A_{eff}, based on SPM or XPM [1] induced phase shift detection using interferometric and non-interferometric schemes. The interferometric detection scheme [2] has the advantage that it can be implemented more easily - a disadvantage is however its susceptibility to environmental perturbations leading to a poor stability. A

A. Driessen (ed.), Nonlinear Optics for the Information Society, 155–159.

considerable improvement of this technique, is presented in the following, using a self-aligned interferometer [3] with a Faraday mirror. The suggested method has the advantage to be simple and all fiber implementable, and the fluctuations due to environmental perturbations are completely removed.

2. Principle of operation

Due to the power dependence of the refractive index (optical Kerr effect), the phase acquired by a pulse with peak power P and wavelength λ that travels through a fiber of length L is given by

$$\phi(P) = \phi_l + \phi_{nl} = n_0 kL + kL_{eff} \frac{n_2}{A_{eff}} Pm \qquad (1)$$

The decrease in pulse power from the fiber attenuation is accounted for by L_{eff}. The polarization parameter m depends on the polarization characteristics of the test fiber and the input signal polarization state. For the case of a high birefringent fiber and light coupled into one axis only, m = 1. For the case of a long standard telecom fiber with a complete polarization scrambling, it was demonstrated that m = 8/9 [4]. Measuring the acquired phase shift, Eq.1 allows to determine the ratio n_2/A_{eff}.
The setup of the self-aligned interferometer we have used in order to measure this phase shift is shown in Fig.1. High peak power pulses from an EDFA are split at the entry of the first coupler (coupling ratio 50/50) and move along the two arms of the interferometer. These arms are different in length such that the two pulses do not interfere when they recombine at the second coupler (coupling ratio 90/10). Due to the asymmetry of the coupler, the two pulses enter the fiber under test (FUT) with different powers, and according to Eq.1, they will acquire different amounts of phase shift during propagation. The pulses are then reflected at the Faraday mirror (FM) and return back through the FUT and interferometer towards the first coupler. Four different paths are possible during the go- and return trip through the interferometer. A double pass of the long-arm (LL), of the short-arm (SS), and a forward pass of the short (long) arm with a return pass through the opposite arm (SL and LS, respectively). Because of the different arm lengths, three different arrival times at the detector can be discerned. Only the middle pulse, arising from the interference between the SL and the LS pulses, is analyzed. The power of this pulse depends on the phase relationship between the two interfering signals and it can be exploited to calculate the nonlinear phase shift experienced in the FUT. It is important to note that contrary to regular Mach-Zehnder interferometers, the balancing of the interferometer arms is not critical here as the path lengths of the two interfering signals are automatically matched (self-aligned).

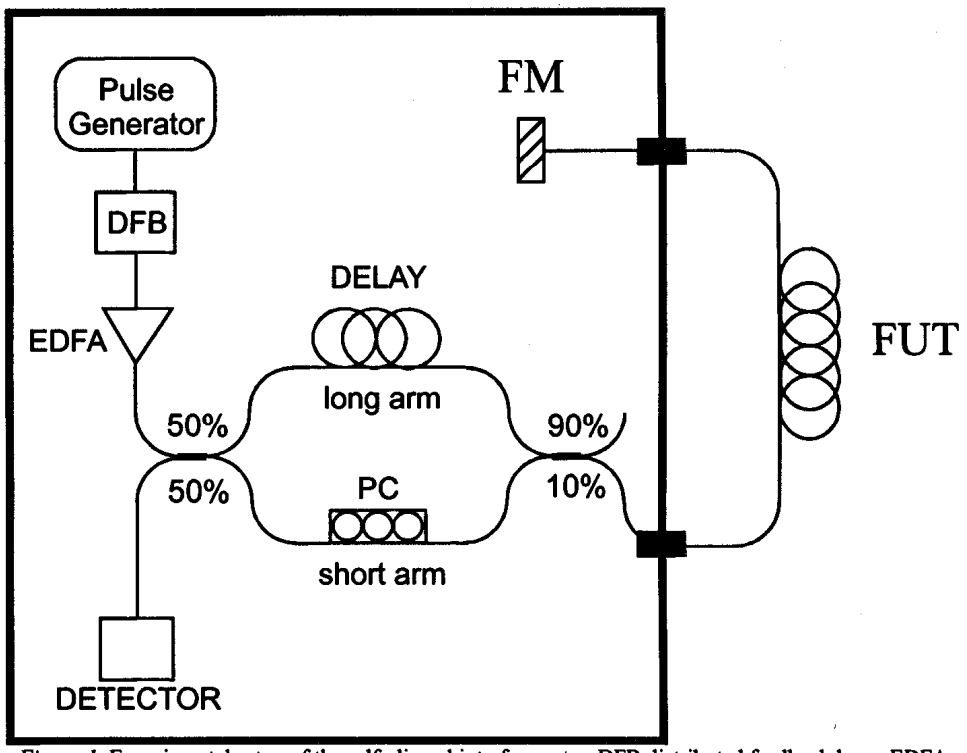

Figure 1. Experimental setup of the self-aligned interferometer. DFB distributed feedback laser, EDFA Erbium doped fiber amplifier, PC polarization controller, FUT fiber under test, FM Faraday mirror, D detector

To calculate the detected power of the middle pulse we have to consider the state of polarization (SOP) of the two interfering pulses. Let R_L, R_S, and R_{FUT} be the polarization transformation operators for the long and short arm of the interferometer and for the FUT, respectively. Knowing that the action of the FM is such that upon reflection, the SOP of the reflected light is always orthogonal to the incoming one, we can describe the double pass of the FUT as

$$m_g = R_{FUT}^{-1} - FR_{FUT}m_0 = R_{FUT}^{-1}(-(R_{FUT}m_0)) = -R_{FUT}^{-1}R_{FUT}m_0 = -m_0$$

So for the pulses that travel through the LS (SL) path, the SOP m_{LS} (m_{SL}) at the exit of the interferometer is given by:

$$m_{LS} = R_S^{-1}\left(R_{FUT}^{-1}FR_{FUT}\right)R_L m_0 = R_S^{-1}(-R_L m_0) = -R_S^{-1}R_L m_0 = Am_0$$

$$m_{SL} = R_L^{-1}\left(R_{FUT}^{-1}FR_{FUT}\right)R_S m_0 = R_L^{-1}(-R_S m_0) = -R_L^{-1}R_{SL}m_0 = Bm_0$$

To have maximum visibility at the exit of the interferometer the two pulses need to have the same SOP, i.e. A=B. This can be done by adjusting the polarization controller (PC) inserted in one of the interferometer arms, e.g. such that R_S=R_L. Note that using a standard mirror in place of the FM, an additional PC would be required [5], making the initial adjustment of the interferometer more difficult. Moreover, both PCs would have to be readjusted for every new FUT. With the FM instead, the interferometer does not require any adjustments after its initial calibration.

Another important point is the possibility to adjust the bias of the interferometer. In the experiment, the PC was adjusted in such a way that the above requirement of A=B was fulfilled. Consequently, all the light was directed towards the detector at the first coupler.
Taking into account this and Eq. (1), the detected power P_{OUT} for a standard fiber becomes

$$P_{OUT}(P) \propto P\cos^2(\Delta\phi) \tag{2}$$

where $\Delta\phi$ is the acquired nonlinear phase shift [5],

$$\Delta\phi(P) = \frac{2\pi}{\lambda} PL_{eff} \frac{16}{45} \frac{n_2}{A_{eff}} \tag{3}$$

3. Results

The pulse source used in the experiment was a directly modulated DFB laser diode. Its wavelength was 1559 nm, the pulse duration 28 ns, and the repetition rate 1 kHz. Note that in some fibers, such long pulses can excite acoustic waves through electrostriction, leading to an erroneous measurement of n_2/A_{eff}.

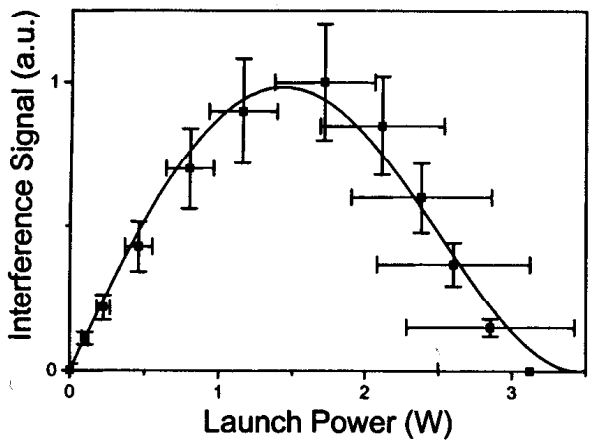

Figure 2. Detected interference signal power as a function of launch power: (squares) measured data, (solid line) theoretical fit

The results for a standard telecom fiber with a length of 1100 m are shown in Fig.2. The interference signal power is plotted as a function of the launch power P. The experimental values (squares) are increasing almost linearly in the beginning, demonstrating that nonlinear effects are of little importance up to about 0.8 W of launched power. Then they set in quite heavily, and the measured power eventually starts to decrease with increasing launch power. The maximum of the interference signal power is reached at a lunch power of 1.4 W, whereas a null value, corresponding to a full $\pi/2$ nonlinear phase shift, is obtained for 3.1 W. From this value, n_2/A_{eff} can be

calculated using Eq.2. The precision is however much better if the whole curve is fitted. This fit is represented by the solid line in Fig.2. As can be seen, the measured data and the fitted values correspond well, with $\chi^2=3x10^{-3}$. From the fit we obtain a value of $(2.76\pm0.04)\ 10^{-10}\ W^{-1}$ for the nonlinear coefficient n_2/A_{eff}.

4. Conclusion

We have presented a simple method for the measurement of the nonlinear coefficient n_2/A_{eff} based on an all fiber, self-aligned interferometer. Self-alignment not only allows for an easy and quick initial adjustment of the interferometer, but along with the use of a Faraday mirror also makes it robust against environmental perturbations. This leads to a good accuracy for the measured n_2/A_{eff} values. The proposed method is well suited to routinely measure the nonlinear coefficient, as the fiber under test can be easily exchanged without necessitating any further readjustments of the interferometer.

Acknowledgements

We acknowledge the financial support from the Swiss Federal Office for Education and Sciences (OFES) in the framework of the European COST 265 action.

References

[1] A. Melloni, L. Amoto, P. Boffi, A. Fellegara, P. Sacchetto, M. Martinelli, Characterization of optical Kerr coefficient in telecommunication fibers, by a polarization insensitive method, *EQEC 1996* p. 102

[2] F. Wittl, J. Vobian, G. Herchenroeder, W. Dultz, Interferometric determination of the nonlinear refractive index n2 of optical fibers, *Technical Digest - Symposium on Optical Fiber Measurements, (NIST SP 905)*, 1996, pp. 71–74

[3] J. Meier, Stabile Interferometrie des nichtlinearen BrechzahlKoeffizienten von Quarzglasfasern der optischen Nachrichtentechnik, *Ph.D. Thesis* (1995)

[4] S.V. Chernikov, J.R. Taylor, Measurement of normalization factor of n_2 for random polarization in optical fibers, *Opt. Lett. 1996, 21*, pp. 1559–1561

[5] C. Vinegoni, M. Wegmuller, N. Gisin, Determination of the nonlinear coefficient n_2/A_{eff} using a self-aligned interferometer and a Faraday mirror, *Elec. Lett.,Accepted for publication.*

C.5 Measurement of the Polarization Coupling Length in Telecom Fibers using Nonlinear Polarization Rotation.

C. Vinegoni, M. Wegmuller, and N. Gisin

[1] *Group of Applied Physics - Gap Optique*
University of Geneva,
20 Ecole-de-Medecine, CH-1211 Aeneve 4, Switzerland

Claudio.Vinegoni@physics.unige.ch

Abstract : The polarization coupling length, an important parameter of the PMD probability distribution, is obtained from measurements and modeling of the nonlinear polarization rotation in optical fibers. Results for different types of fibers are presented.

PRESENTED : "Applications of nonlinear optical phenomena" 2001 (Budapest, HU)

C.6 Interlaboratory measurements of the nonlinear coefficient of standard SMF and DSF fibers using an interferometric method and an SPM based cw dual-frequency method.

C. Vinegoni, M. Wegmuller, and N. Gisin

[1] *Group of Applied Physics - Gap Optique*
University of Geneva,
20 Ecole-de-Medecine, CH-1211 Aeneve 4, Switzerland

Claudio.Vinegoni@physics.unige.ch

Abstract : In this work we present interlaboratory measurements of the nonlinear coefficient n2/Aeff for standard SMF and DSF fibers. Two different measurement methods were used by two different groups. One of the method is based on the detection of the Kerr phase shift by a self-aligned interferometer. The other method is an SPM based cw dual-frequency method. Interlaboratory comparison shows that the values found with the two methods are in good agreement.

PRESENTED : OFMC 2001 (Cambridge, UK)

Interlaboratory measurements of the nonlinear coefficient of standard SMF and DSF fibers using an interferometric method and an SPM based cw dual-frequency method

C. Vinegoni, M. Wegmuller, N. Gisin

Group of Applied Physics, University of Geneva,
20 Ecole-de-Medecine, CH-1211 Geneve 4, Switzerland
phone: +41 (0)22 702 60 82, fax: +41 (0)22 781 09 80
e-mail: CLAUDIO.VINEGONI@PHYSICS.UNIGE.CH

K. Nakajima and M. Ohashi

NTT Access Network Service Systems Laboratories
1-7-1, Hanabatake, Tsukuba, Ibaraki, 305-0805, Japan
phone: +81 298 52 2651, fax: +81 298 52 2500

Abstract:

In this work we present interlaboratory measurements of the nonlinear coefficient n_2/A_{eff} for standard SMF and DSF fibers. Two different measurement methods were used by two different groups. One of the method is based on the detection of the Kerr phase shift by a self-aligned interferometer. The other method is an SPM based cw dual-frequency method. Interlaboratory comparison shows that the values found with the two methods are in good agreement.

INTRODUCTION

The implementation of Erbium-doped fiber amplifiers and chromatic dispersion compensation allows for long distance data transmission. Along with the technique of wavelength division multiplexing (WDM), this leads to an important amount of power inside the fiber over long distances, and optical nonlinearities start to play a significant role. Their magnitudes depend on the ratio n_2/A_{eff}, where n_2 is the nonlinear refractive index of the fiber and A_{eff} the effective area of the mode. There are different methods to measure n_2/A_{eff}, based on SPM or XPM induced phase shift detection using interferometric and non-interferometric schemes [1]. The interferometric detection scheme [2] presents the advantage that it can be implemented more easily. But a disadvantage is constituted by its susceptibility to the environmental perturbations that leads to a poor stability. With one of the setups presented here we reached a considerable improvement of this technique by using a self-aligned interferometer [3] with a Faraday mirror. This method [4] has the advantage to be simple and all fiber implementable and the fluctuations due to the environmental perturbations are completely removed. On the other hand, non-interferometric schemes have the disadvantage that their measurement accuracy strongly depends on the measurement conditions. However, the SPM based cw dual-frequency method [5,6], with its simple measurement setup, gives the accurate value of n_2/A_{eff} according to the measurement conditions given in Refs. [5] and [6].

We give a brief description of the two methods used and present interlaboratory fiber nonlinear coefficient measurements for Dispersion Shifted Fibers (DSF). The values found are in good agreement among the two methods.

INTERFEROMETRIC METHOD (METHOD A) [3,4]

Due to the power dependence of the refractive index, a pulse with peak power P and wave number k, travelling along a fiber of length L, will acquire a power dependent phase change ϕ given by:

$$(1) \qquad \phi(P) = \phi_l + \phi_{nl} = n_0 kL + kL_{eff} \frac{n_2}{A_{eff}} Pm$$

The fiber losses are accounted for by the effective length $L_{eff} = 1/\alpha\,[1-\exp(-\alpha L)]$, with fiber loss coefficient α. The polarization parameter m depends on the polarization characteristics of the test fiber and the signal polarization state. It is equal to 1 for the case of a polarization maintaining fiber if the light is coupled into one of the two axes. For the case of a sufficiently long standard telecom fiber with a complete scrambling of the polarization, it was demonstrated that m=8/9 [7]. Using (1), a measure of the acquired phase shift allows to determine the ratio n_2/A_{eff} or, through an independent measurement of A_{eff}, the value of n_2. The setup of the self-aligned interferometer is shown in Fig. 1 and is described in more detail in Ref. [4]. Due to its robustness against any environmental perturbations the proposed method is well suited to routinely measure the nonlinear coefficient. Moreover the presence of the FM allows to easily exchange the FUT without necessitating any further readjustments of the interferometer. It is possible to show that the detected power P_{OUT} at the exit of the interferometer is equal to

$$(2) \qquad P_{OUT}(P) \propto P\cos^2(\Delta\phi),$$

where $\Delta\phi$ corresponds to the nonlinear phase shift acquired along the FUT [4],

$$(3) \qquad \Delta\phi(P) = \frac{2\pi}{\lambda} PL_{eff} \frac{16}{45} \frac{n_2}{A_{eff}}$$

SPM BASED CW DUAL-FREQUENCY METHOD (METHOD B) [5,6]

When two intense signals with wavelength separation of $\Delta\lambda$ are launched into a fiber, SPM acts on the beat envelope to create sidebands in the frequency domain. Then, the optical power ratio of the input signals (I_0) to the first sideband (I_1) is related to the nonlinear phase shift ϕ_{SPM}. When the chromatic dispersion is negligible, this relationship can be expressed as (4) using n-th order Bessel function J_n.

$$(4) \qquad \frac{I_0}{I_1} = \frac{J_0^2(\phi_{SPM}/2) + J_1^2(\phi_{SPM}/2)}{J_1^2(\phi_{SPM}/2) + J_2^2(\phi_{SPM}/2)}$$

Moreover, the relationship between ϕ_{SPM} and nonlinear coefficient can be expressed as

$$(5) \qquad \phi_{SPM} = \frac{4\pi}{\lambda} L_{eff} P \frac{n_2}{A_{eff}}$$

where P shows the average launched power. Thus, the nonlinear coefficient can be obtained by measuring the optical power ratio I_0/I_1 with various launched power according to the

measurement conditions given in Refs. [5] and [6]. The setup of the SPM based cw dual-frequency method is shown in Fig. 2.

RESULTS

The measurements were done on three different fibers. A DSF fiber with λ_0 = 1556.4 nm, S=0.067 ps/nm^2/km (DSF-1), a DSF fiber with λ_0 = 1548.6 nm, S=0.060 ps/nm^2/km (DSF-2), and a standard single mode fiber with λ_0 = 1300 nm (G-1). Fibers DSF-1 and DSF-2 were also measured at NTT utilizing the self-phase modulation based cw dual-frequency method.

For each fiber different measurements were taken on different days in order to test the reproducibility of our measurements. The corresponding results are summarized in column A of Tab. I for method A. Note that the maximum absolute deviation from the average (MD) is used to characterize the reproducibility. Generally the reproducibility is quite good (<5%) although it varies somewhat from fiber to fiber (see Tab. I). Column B of Tab. 1 reports the values found with method B. Here instead of the MD, the standard deviation (SD) of different measurements is given. As one can see, the values are in good agreement with differences within the experimental errors. Using method A measurements were then performed as a function of the fiber length. We made a fiber cut-back procedure and for each fiber length we measured the nonlinear coefficient on a standard telecom fiber (G-1) with lengths ranging from 12 km to 2 km. For each length at least 3 measurements were taken in order to acquire some statistics and to find the error bars. All values are within a standard deviation of 6% demonstrating that method A is insensitive to the fiber lengths even for large values of chromatic dispersion.

CONCLUSION

In this letter we have presented an interlaboratory comparison of n_2/A_{eff} measurements on the same test fibers as measured by two different institutions using different methods, an interferometric method and a cw dual-frequency method. Good agreement between the measured values was found.

ACKNOWLEDGMENTS

We acknowledge the financial support from the Swiss Federal Office for Education and Sciences (OFES) in the framework of the European COST 265 action.

REFERENCES

[1] G. Agrawal, "Nonlinear fiber optics", Academic Press, Inc., San Diego, CA, 1989.

[2] F. Wittl, J. Vobian, G. Herchenroeder, and W. Dultz, "Interferometric determination of the nonlinear refractive index n_2 of optical fibers", Technical Digest - Symposium on Optical Fiber Measurements, (NIST SP 905), pp. 71–74, 1996.

[3] J. Meier, "Stabile interferometrie des nichtlinearen BrechzahlKoeffizienten von Quarzglasfasern der optischen Nachrichtentechnik", Ph.D. Thesis, 1995.

[4] C. Vinegoni, M. Wegmuller, and N. Gisin, "Determination of the nonlinear coefficient n_2/A_{eff} using a self-aligned interferometer and a Faraday mirror", *Elec. Lett.*, vol. 36, pp. 886-888, 2000.

[5] A. Boskovic, S. V. Chernikov, J. R. Taylor, L. Gruner-Nielsen and O. A. Levring, "Direct continuous-wave measurement of n2 in various types of telecommunication fiber at 1.55 μm", *Opt. Lett.*, vol. 21, pp. 1965–1967, 1996.

[6] T. Omae, K. Nakajima, and M. Ohashi, "Universal conditions for nonlinear refractive index n_2 estimation of dispersion compensating fibers by cw-SPM method", OFC 2001 Anaheim, TuH3, 2001.

[7] S.V. Chernikov, and J.R. Taylor, "Measurement of normalization factor of n_2 for random polarization in optical fibers", *Opt. Lett.*, vol. 21, pp. 1559–1561, 1996.

TABLE I

Values of the nonlinear coefficient n_2/A_{eff} for the different test fiber measured with the two methods proposed in this letter.

Fiber	Length (m)	Zero Wavelength λ_0 (nm)	Nonlinear Coefficient n_2/A_{eff} x 10^{-10} W^{-1}			
			A		B	
			Value	MD	Value	SD
G-1	11840	1302	3.6	5%	-	-
DSF-1	1990	1556.4	6.4	2%	6.3	5%
DSF-2	1990	1548.6	6.3	5%	6.6	5%

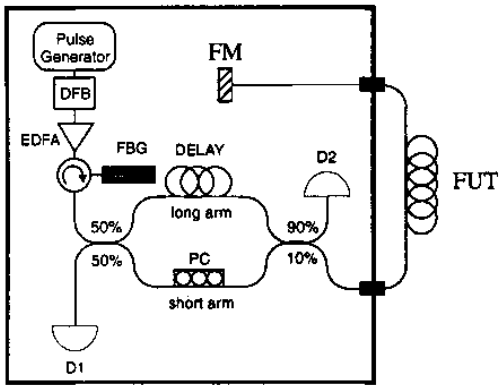

FIGURE 1
Experimental setup of the self-aligned interferometer. DFB distributed feedback laser, EDFA Erbium doped fiber amplifier, PC polarization controller, FUT fiber under test, FM Faraday mirror, D detector, FBG fiber Bragg grating.

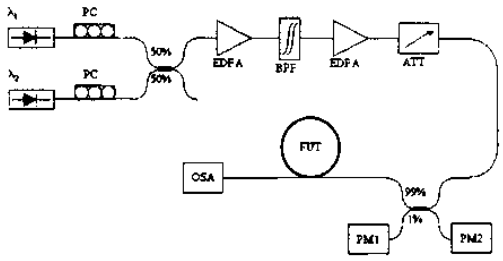

FIGURE 2
Experimental setup of the SPM based cw dual-frequency method. PC polarization controller, EDFA Erbium doped fiber amplifier, BPF Band pass filter, ATT Variable attenuator, PM Power meter, OSA Optical spectrum analyzer, FUT fiber under test. For the values measured with method A, the maximum absolute deviation from the average (MD) is used to characterize the reproducibility. For method B the standard deviation is shown.

C.7 Implementation of a Faraday Mirror Stabilization Scheme for All Optical Switching in a Standard Telecom Fiber.

C. Vinegoni, M. Wegmuller, and N. Gisin

[1] *Group of Applied Physics - Gap Optique*
University of Geneva,
20 Ecole-de-Medecine, CH-1211 Aeneve 4, Switzerland

Claudio.Vinegoni@physics.unige.ch

Abstract : We present an elegant passive stabilization method for ultrafast devices employing nonlinear polarization rotation (NPR) in optical fibers. The fluctuations in the linear birefringence, including temperature and pressure induced ones, that affect the measurement of the NPR are successfully removed in a passive way by using a double pass of the fiber under test with a Faraday mirror at the end of the fiber. This method provides excellent switching stability over long term period when applied to a wavelenght converter.

PRESENTED : ICTON 2000 (Warsaw, Poland).

Implementation of a Faraday Mirror Stabilization Scheme for All Optical Switching in a Standard Telecom Fiber

C. Vinegoni, M. Wegmuller, N. Gisin

Group of Applied Physics, University of Geneva,
20 Ecole-de-Medecine, CH-1211 Geneve 4, Switzerland
phone: +41 (0)22 702 60 82, fax: +41 (0)22 781 09 80
e-mail: CLAUDIO.VINEGONI@PHYSICS.UNIGE.CH

We present an elegant passive stabilization method for ultrafast devices employing nonlinear polarization rotation (NPR) in optical fibers. The fluctuations in the linear birefringence, including temperature and pressure induced ones, that affect the measurement of the NPR are successfully removed in a passive way by using a double pass of the fiber under test with a Faraday mirror at the end of the fiber. This method provides excellent switching stability over long term period when applied to a wavelength converter.

The potential of nonlinear polarization rotation (NPR) to build ultrafast devices has been recognized a long time ago and received considerable attention since then. It has been proposed to exploit it for optical switches, logic gates, multiplexers, intensity discriminators, nonlinear filter, or pulse shapers. However, an inherent problem to all this applications is the stability of the output state of polarization, generally subjected to fluctuations of the linear birefringence caused by temperature changes and drafts in the fiber environment. Of course, the same problem was also encountered in the few experiments dealing with the characterization and measurement of the NPR itself.

As the fluctuations become worse for fibers with a large birefringence, and as the effect of NPR is proportional to the inverse of the wavelength, it is hard to measure NPR directly in a polarization maintaining (PM) fiber at the telecom wavelength of 1.55 μm. Consequently, NPR can not be exploited directly for an optical switch and some stabilization scheme has to be used. We propose a method that removes the overall linear birefringence, and therefore also its fluctuations, in a passive way by employing a Faraday mirror [1] (FM) and a double pass of the fiber under test.

The FM transforms any input polarization state to the orthogonal one upon reflection. Consequently, the signal components that were polarized parallel to one axis of the fiber during the forward propagation will be polarized parallel to the other axis during the return path and vice versa. The overall linear phase acquired is therefore the same for any input polarization, and the intrinsic birefringence is automatically

0-7803-6337-X/00/$10.00 ©2000 IEEE

removed as long as it is stable during a single go-and-return path. In this way, fluctuations with frequencies up to about 0.5 MHz (200 m long fiber) can be removed.

To check how this -nowadays standard- method [2] of removing linear birefringence acts on the NPR, we developed a simple model to calculate the action of linear and nonlinear birefringence. Using this model, one can show that the proposed method removes the overall linear birefringence only, whereas the purposefully induced nonlinear effects of the go and return-path add up. Excellent agreement between the model and some experiments we have made [2] about NPR demonstrates that using the FM, the overall linear birefringence is indeed removed completely, allowing to observe the NPR otherwise hidden within the noisy background of polarization changes due to environmental perturbations. This result validates our method for the implementation of an all optical switch based on NPR.

The principle of the optical Kerr switch presented here is based on NPR induced by a powerful control signal pulse that leads to a different phase-shift (via the optical Kerr effect) for signal components with the same and orthogonal polarization, respectively. The corresponding change in the output signal polarization (maximum angle of rotation) is maximized if the control signal polarization matches the polarization of one of the two signal polarization modes during the entire propagation in the Kerr fiber. By inserting a polarizing beam splitter (PBS), the signal is switched between the two PBS output ports depending on the amount of the induced phase-shift.

For the case of a PM fiber, when the control pulse is linearly polarized along one of the birefringent axis it is easy to show that the phase shift $\Delta\phi$ acquired by a signal linearly polarized at 45 deg is:

$$\Delta\phi = \frac{8}{3}\frac{L_{eff}}{\lambda} n_2 \frac{P}{A_{eff}} \qquad [1]$$

where n_2 is the nonlinear refractive index of the fiber, λ is the signal wavelength, A_{eff} is the effective area of the fiber and P is the peak pump power. Fiber losses are included in the effective length $L_{eff}= 1/\alpha[1-\exp(-\alpha L)]$ where L is the length and α the fiber loss coefficient. For a PBS adjusted so that all the signal is at output port 2 when the control pulse is absent, the signal at output port 1 becomes

$$T = \sin^2\left(\frac{\Delta\phi}{2}\right) \qquad [2]$$

where the induced phase shift $\Delta\phi$ is given by Eq.1. A different wavelength is conveniently used for the control pulses so that they can be combined with the signal using a wavelength division multiplexer (WDM). As a consequence, a walk-off between the control pulses and the signal is introduced, ultimately limiting the switching time. A large walk-off also enlarges the required control peak power because of a reduced interaction length (i.e. smaller L_{eff} in Eq.1). To keep the switch fast and efficient, either a fiber with low group dispersion has to be used, or the wavelength separation should be kept as small as possible.
It is very important to notice that the transmission given in Eq.2 holds only for a fixed intrinsic birefringence of the fiber. Any fluctuation of this birefringence, caused e.g. by temperature drifts or pressure changes, leads to an additional phase-shift randomly

changing the bias of the switch. In order to reduce this effect detrimental for the switch stability, different methods have been proposed.
Here we use the same stability scheme employed for the NPR measurements described above, i.e. a double pass of the fiber by means of a Faraday mirror.

The setup for the Kerr switch is shown in Fig. 1. The control signal and the control pulse are at 1559 and 1556 nm respectively. The experimental data for a 680 m standard telecom fiber are presented in Fig. 2. The output power at the switch is shown for a time period of several hours. After the initial setting the switch was left alone without any readjustment while a normal activity in the lab was maintained with people working around the table. The switch stability was rather good (less than 2% fluctuations) when using a FM. Instead when a normal mirror is employed, thereby removing our stabilization scheme, the output power at the switch port changes randomly from zero to full switch power.
The obtained switching ratio is shown in Fig 3 as a function of the control peak power. The maximum ratio corresponds to 90%. Similar data were obtained for a PM fiber 200 m long. In that case replacing the FM with a standard mirror leads to an output power rapidly changing in the range from zero to full switch power. Indeed it is well known that the polarization of light coupled into both the birefringence axis of a PM fiber is strongly susceptible to any perturbation and the use of a stabilization scheme is therefore absolutely mandatory. With a FM inserted, fluctuations of the switching stability were a little larger than 1%.

In conclusion we demonstrated all-optical switching at 1.5 μm, based on induced nonlinear polarization rotation in both a polarization maintaining and a standard telecom fiber. The presence of the FM at the end of the Kerr fiber removes any fluctuation of the signal providing good stability. In the standard fiber the switching was made possible because the small difference between the control and signal wavelengths allowed for a similar evolution of both signals along the fiber avoiding any scrambling along the fiber with a consequently reduction in the total amount of the NPR.

References

[1] MARTINELLI M., 'A universal compensator for polarization changes induced by birefringence on a retracing beam', *Opt. Comm.* 1989, 72, pp. 341–344

[2] VINEGONI C., WEGMULLER M., HUTTNER B., GISIN N. 'Measurement of nonlinear polarization rotation in a highly birefringent optical fiber using a Faraday mirror', *J. of Optics A*, Accepted.

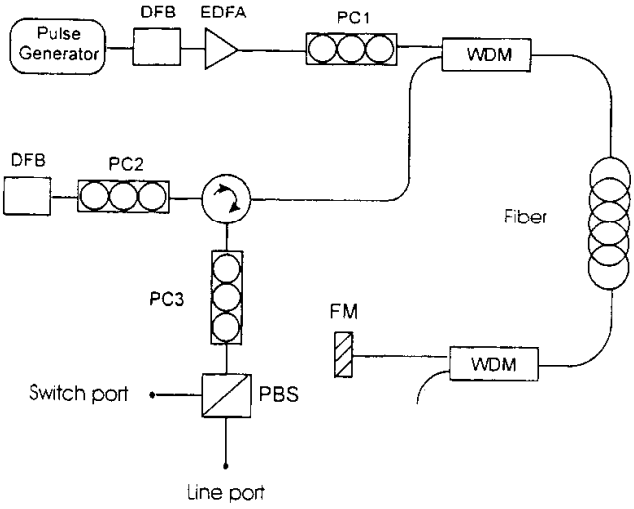

Figure 1: Experimental setup. DFB distributed feedback laser, EDFA Erbium doped fiber amplifier, PC polarization controller, FM Faraday mirror, PBS polarizing beam splitter, WDM wavelength division multiplexer.

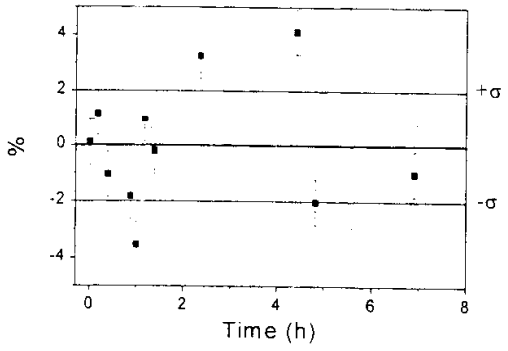

Figure 2: Relative fluctuations of the switch port signal power as a function of time. Measured data (squares), mean value (bold line), and standard deviation (thin lines).

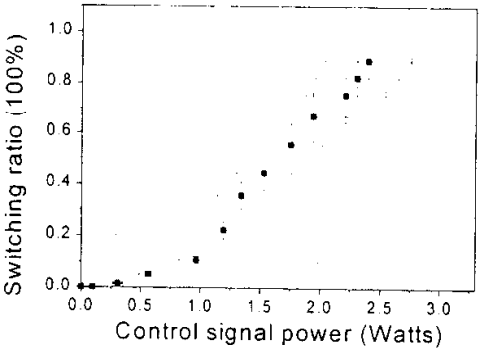

Figure 3: Normalized switching ratio as a function of the control signal power.

C.8 Overview of coherent reflectometry techniques: characterization of components and small systems.

M. Wegmuller, P. Oberson, J.P. von der Weid, O. Guinnard, L. Guinnard, C. Vinegoni, M. Legre, and N. Gisin

[1] *Group of Applied Physics - Gap Optique*
University of Geneva,
20 Ecole-de-Medecine, CH-1211 Aeneve 4, Switzerland

Claudio.Vinegoni@physics.unige.ch

Abstract : Coherent reflectometry techniques have important advantages over direct detection techniques: larger sensitivity, larger dynamic range, better resolution, and spurious light suppression. The measurement range is typically limited to less than 1 meter for optical low coherence reflectometry and to less than 1 km for coherent optical frequency domain reflectometry. Especially the second technique is therefore well suited for measurements of optical modules with extended components and for small systems.

PRESENTED : NIST 2000 (Boulder, CO)

Overview of coherent reflectometry techniques: characterization of components and small systems

M. Wegmüller, P. Oberson, J.P. von der Weid*, O. Guinnard, L. Guinnard, C. Vinegoni, M. Legré, N. Gisin

Group of Applied Physics, University of Geneva, 20 Ecole-de-Médecine, CH-1211 Genève 4, Switzerland, *mark.wegmuller@physics.unige.ch*
* Center for Telecommunications Studies, PUC-Rio, Rio de Janeiro, 22453-900 Brazil

Abstract

Coherent reflectometry techniques have important advantages over direct detection techniques: larger sensitivity, larger dynamic range, better resolution, and spurious light suppression. The measurement range is typically limited to <1 m for Optical Low Coherence Reflectometry, and to <~1 km for Coherent Optical Frequency Domain Reflectometry. Especially the second technique is therefore well suited for measurements of optical modules with extended components and for small systems.

Introduction

The advantages of coherent reflectometry techniques are well known. In fact, they are still the only techniques giving two point resolutions in the mm range. Of the two major coherent reflectometry techniques Optical Low Coherence Reflectometry (OLCR) and Coherent Optical Frequency Domain Reflectometry (OFDR), the first is well established and widely used for component characterization [1]. In typical OLCR implementations, the measurement range is however limited to below 1 m. None of the proposals to extend this value have been retained on a large basis so far, mainly for the sake of having robust and compact OLCR devices.
Although a sub-metric range is well adapted for the characterization of single, compact components, it is too small for larger, more complicated optical modules including several composites as couplers, WDMs, taps, modulators, etc. The path length in such devices can easily reach some tens of meters, and OFDR has to be employed. Although this technique is well known for several years, it has not seen broad commercial implementation so far. The main reason is that the constraints on the source are heavy, and a simple, non-expensive yet reliable source giving the desired performance was lacking. In this paper, a novel OFDR device based on a simple, mechanically tunable fiber laser [2] is presented. After giving the characteristics of this device, several applications relevant for small systems metrology are presented.

Principles of OFDR

To avoid all confusion, let us first stress that only the technique of coherent OFDR is considered here (there exists also a 'normal', non-coherent OFDR technique which is the frequency domain analogous of OTDR and measures the modulation transfer function [1]). The coherent OFDR technique (Fig.1) is based on the detection of a beat signal between the distributed reflections from the fiber under test (Rayleigh backscatter, connectors, etc.) and a fixed Fresnel reflection (local oscillator). Using a linear frequency sweep of the laser, one can straightforwardly map the measured beat frequencies on a distance scale, whereas the normed square power for a given beat frequency gives the reflectivity at the corresponding distance. For a good general overview of the OFDR principles and limits, the reader is referred to [3]. In the OFDR used for the measurements presented here, several important improvements have been implemented described in the following along with the specifications of the present device.

Range: The measurement range of OFDR is limited by the coherence length of the source and by its phase noise. The first one leads to signal fading, the second one reduces the dynamic range [3]. The fiber laser employed presently has a very large coherence length of about 3.3 km (FWHM bandwidth of 10 kHz) [1]. Fig.2 demonstrates the corresponding signal fading of about 5 dB/km, and the reduction in the dynamic range, limiting the useful range to about 2 km. Using more sophisticated (and complicated) sources or signal corrections, an order of magnitude larger ranges have been demonstrated [4]. However, the spatial resolution drops below the one achievable with OTDR, so the interest of such methods is questionable from an applications point of view. Fig.3 demonstrates that the 2 km range of our OFDR device is sufficiently large to assure a smooth transition between OFDR and OTDR applications.

Resolution: The maximum two-point resolution is given by the frequency excursion of the source. However, this value can be seriously deteriorated by nonlinearities in the frequency sweep. In our device, this is corrected for by using the signal from a reference interferometer from which the instantaneous frequency is calculated. For the fiber laser used, a maximum detuning of 0.3 nm is employed (41 GHz), giving a resolution of 5 mm as illustrated by Fig.4. The two point resolution also depends on the measurement range and on the number of points used. This is because the slope of the frequency excursion has to be reduced for a larger range so that no aliasing in the sampling is encountered (i.e. maximum beat frequency<Nyquist-frequency). The two point resolution and the measurement range become

$$\Delta l_{2p} \approx \frac{6.5}{N} L_{max} \quad , \qquad L_{max} \approx \frac{c}{6n} \frac{N}{\delta\nu} \, ,$$

respectively, where N is the number of sampling points (typically 8192), $\delta\nu$ the maximum frequency excursion, c the speed of light, and n the group index. Consequently, for a given range, the resolution is given by 0.08% of the distance range. For the maximum 5 mm resolution, the range is 6.6 m.

The importance of having a good resolution is clear from Fig.5. A line of 6 pigtails connected with FC-APCs was measured using different resolutions. This was achieved by changing the number of points N of the OFDR acquisition. Using 512 points (20 cm resolution, curve at top), the high quality connector at 8 m is covered by the Rayleigh light, and the fiber break after the

last connector can not be discerned from the connector reflection (see inset). With 8192 points (12 mm resolution), the Rayleigh level drops by about 12 dB, and the small reflection from the high quality connector can be easily detected. Further, one clearly sees that the fiber break is after the last connector and not in front of it, an important feature for applications like fault detection in optical modules.
A consequence of having a high spatial resolution is that the Rayleigh backscattering (RBS) becomes very noisy due to the coherent speckle. Note that this is a physical limit (and not a technological one) affecting all high-resolution reflectometry methods. As less scatterers take part in the interference, the RBS becomes more peaked. This can somewhat be reduced by dithering the center frequency and averaging. In our device, the possible change in center frequency is however restricted by mechanical constraints of the fiber laser, and the smoothed RBS still varies somewhat. If one can average over sufficiently large distances, small losses can still be identified, as is demonstrated by Fig.6 which shows a measurement of a bad splice with 0.4 dB loss.

Polarization dependence, sensitivity, and dynamic range: As for all coherent techniques, the signal will depend on the polarization state of the reflected light. This can be advantageous to get information about the beatlength distribution (see below), but is typically an unwanted effect in standard applications. We therefore included a polarization diversity detection scheme in our OFDR device, reducing the polarization dependence of the reflected light to less than 0.5 dB. The sensitivity and dynamic range of the present device is -110 dB and 80 dB, illustrated in Fig.4. As was mentioned before, the dynamic range decreases with distance (see Fig.2) because of the source phase noise. Using time domain averaging, a sensitivity of -152dB with a dynamic range of 106 dB has been demonstrated in earlier work [5]. This technique however requires a very stable phase of the reflected signal, which is only achievable for short measurement distances.

Some measurement examples using OFDR

Due to its high sensitivity, dynamic range, resolution, and accuracy, OFDR is useful for a vast range of different applications in fiber metrology, like e.g. measurements of WDM components [6], distributed gain measurements in EDFAs [7,8], or local birefringence [9.10].

Measurement of distributed gain in EDFAs: The coherent detection scheme of OFDR leads to a strong rejection of background light from ASE or residual pump light. OFDR is therefore ideally suited for non-destructive, distributed gain measurements in EDFA. Fig.7 shows a measurement of the gain distribution in a 12 m long, 500ppm Er-doped fiber pumped by 1480 nm light. The set of curves was obtained by gradually increasing the pump power from no pump at all (lowest curve) to +15 dBm (top curve). Clearly, pump saturation led to gain clamping, with a maximum gain reached at 4.5 m. After that distance, the Er ions were no longer inverted due to a lack of pump power, and the signal is reabsorbed. Cut-back measurements were in very good agreement with the OFDR gain measurements, typically to within the OFDR precision of 0.5dB.
Note that it is difficult to exactly model the gain distribution, as the necessary model parameters are hard to measure with sufficient precision. This is demonstrated in Fig.7 by the solid and dashed lines, where two sets of model parameters obtained in different ways were used [8]. The

dotted line on the other hand was obtained by varying the model parameters for good agreement with the measurement.

Measurement of distributed birefringence: The polarization dependence of the coherent detection used in the OFDR can be exploited to get information about the evolution of the polarization state along the fiber [9,10]. Due to the enhanced range of the OFDR at hand, we can get a much better statistics of the distributed fiber birefringence. Moreover, the polarization independent signal from the polarization diversity detection is used to subtract the (polarization independent) Rayleigh structure, thereby removing the frequencies that are not related with the fiber birefringence. Fig.8 shows the polarization dependent reflections from a 1km long low PMD fiber after removal of the Rayleigh noise and normalization to zero mean power. This curve is then Fourier transformed to get information about the rotation period of the polarization vector, i.e. the beatlength. The figure shows that there is not one specific, well-defined beatlength period, but a distribution of such values. While the structure of the peaks changes somewhat for different launch polarizations, the mean value of the distribution is fairly constant (variations of about 0.5m, i.e. 5%, were observed for the present example). An interesting feature is that the value of birefringence is found to vary along the fiber. From the normalized return signal, it can be seen that the polarization changes slower towards the end of the fiber. Indeed, by Fourier transforming only a section of the curve in Fig.8, mean values for the beatlength of 9.4m and 13.1m were found for fiber sections from 100-300 and 700-900m, respectively. Note that when we inverted the fiber, we found the beatlength to be decreasing, demonstrating that this feature is not an artefact of the measurement technique, but indeed reflects the polarization properties of the fiber. For comparison, we performed a similar measurement on a high PMD fiber (1.9 ps/$\sqrt{}$km). Using the same range of 2km as before, the polarization dependent signal was found to be often flat and 3dB lower than the polarization independent one. This happens if the polarization is rapidly varying on a distance scale smaller than the OFDR resolution, so that only an averaged value is obtained. Looking at these flat sections with an increased resolution indeed revealed fast polarization changes. The measurement was therefore done with a much higher OFDR resolution on a 100m section of the fiber. As Fig.9 shows, two distinctive peaks can be discerned as is expected from the theory in [9] for a fiber with well-defined birefringence. The (mean) beatlength accounts to 55 cm.

Conclusions

For the measurement of optical modules and small systems, the range of typical OLCR devices, very valuable for component characterization, is not sufficient. OTDRs on the other hand lack the advantages of a coherent detection scheme. With the progress of technology, coherent OFDR devices can now be realized that are capable of making the transition between the two techniques.

Such a novel OFDR device, based on a mechanically tuned fiber laser, was presented here. With its range (6 m to 1 km), resolution (0.08% of range), sensitivity (-110 dB), and dynamic range (80 dB), it is well adapted for a vast range of different applications in fiber metrology, like e.g. measurements of all kinds of components and their combinations (connectors, WDMs, couplers, taps, modulators, and to some degree even isolators or circulators), distributed gain measurements in EDFAs, or distributed local birefringence measurements.

Acknowledgements: *Support by the Swiss Department for Education and Research (OFES) in the framework of the European Project COST 265 is acknowledged.*

References

1 W.V. Sorin, "Optical Reflectometry for Component Characterization", in Fiber Optic Test and Measurement, 7Hewlett-Packard, Ed. D.Derickson, Prentice Hall, 1998

2 P.Oberson, B.Huttner, O.Guinnard, L.Guinnard, G.Ribordy, N.Gisin, "OFDR with a narrow linewidth fiber laser", appears in the June issue of *IEEE Photon. Technol. Lett.*, 2000

3 J.P.von der Weid, R.Passy, G.Mussy, N.Gisin, "On the characterization of optical fiber network components with OFDR", *J. Lightwave Technol.*, vol. 15, no. 7, 1997, p. 1131-1141

4 K. Tsuji, K.Shimizu, T.Horiguchi, Y.Koyamada, "Coherent OFDR using phase-decorrelated reflected and reference lightwaves", *J. Lightwave Technol.*, vol. 15, no. 7, 1997, p 1102-1109

5 G.Mussi, N.Gisin, R Passy, J.P. von der Weid, "152.5dB sensitivity high dynamic range OFDR", *Electron. Lett.*, vol. 32, 1996, p. 926-927

6 J.P. von der Weid, R.Passy, A.O.Dal Forno, B.Huttner, N.Gisin, "Return loss measurements of WDM filters with tunable coherent OFDR", *IEEE Photon. Technol. Lett.*, vol. 9, no. 11, 1997, p. 1508-1510

7 M.Wegmuller, P.Oberson, O.Guinnard, B.Huttner, L.Guinnard, N.Gisin, "Non-destructive measurements of the distributed gain in Er doped fibers with improved accuracy using OFDR", *appears in Tech. Digest, CLEO/Europe 2000*

8 M.Wegmuller, P.Oberson, O.Guinnard, B.Huttner, L.Guinnard, C.Vinegoni, N.Gisin, *submitted to J. Lightwave Technol.*

9 B.Huttner, J.Reecht, N.Gisin, R.Passy, J.P. von der Weid, "Local birefringence measurements in single-mode fibers with coherent OFDR", *IEEE Photon. Technol. Lett.*, vol. 10, no. 10, 1998, p.1458-1460

10 M.Wegmuller, J.P. von der Weid, P.Oberson, N.Gisin, "High resolution fiber distributed measurements with coherent OFDR", *appears in Tech. Digest, ECOC 2000*

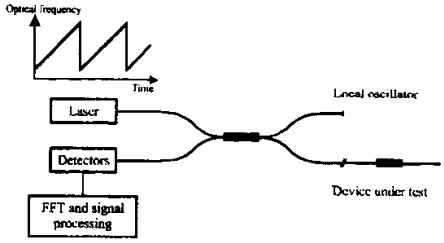

Fig.1: Set-up of the OFDR

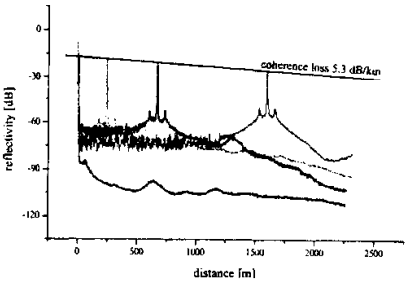

Fig.2: Fresnel reflections at different distances. The two pedestals are from acoustic perturbations

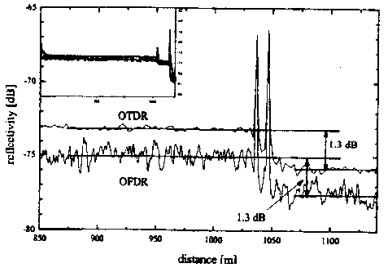

Fig.3: Measurements of a 10m jumper after a 1km SMF using OFDR and OTDR

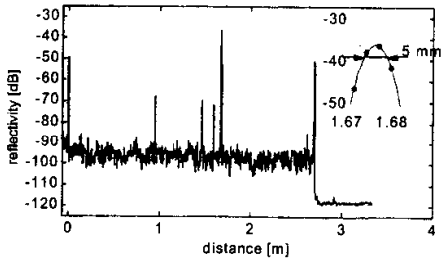

Fig.4: Short range measurement of a series of fibers with FC/PC and FC/APC connectors

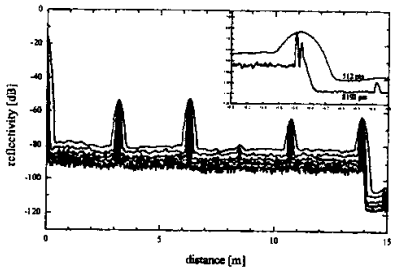

Fig.5: OFDR traces of a line of 6 jumpers using different two point resolution settings

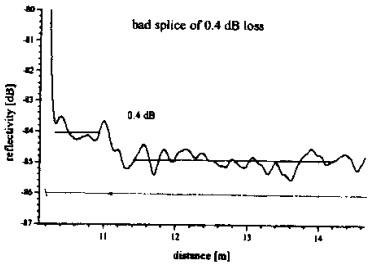

Fig.6: Measurement of a bad splice

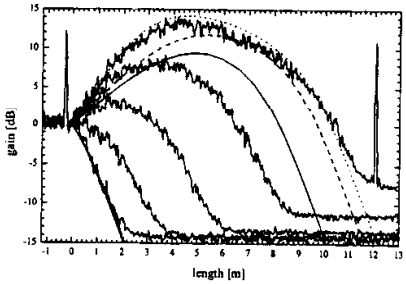

Fig.7: Distributed gain measurements in an 500 ppm Er-doped fiber for different pump powers.

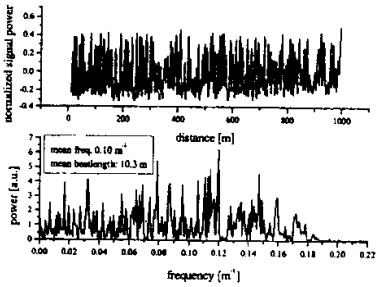

Fig.8: OFDR measurement of distributed birefringence of a low PMD standard fibre

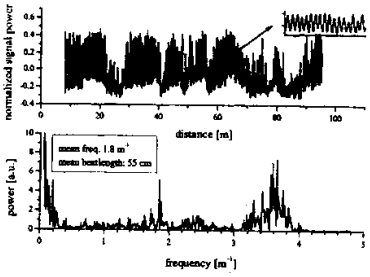

Fig.9: OFDR measurement of distributed birefringence of a large PMD fibre

C.9 Distributed measurements of chromatic dispersion and of the nonlinear coefficient in DSF fibers with non negligible values of PMD.

C. Vinegoni, H. Chen, M. Leblanc, G. Schinn

[1] *EXFO Electro-Optical Engineering Inc*
465 Av. Godin, Vanier, Quebec, Canada G1M 3G7

M. Wegmuller, N. Gisin

[1] *Group of Applied Physics - Gap Optique*
University of Geneva,
20 Ecole-de-Medecine, CH-1211 Aeneve 4, Switzerland

Claudio.Vinegoni@physics.unige.ch

Abstract : We report on the influence of PMD and especially of the polarization coupling length on the measurement of distributed chromatic dispersion in DSF. We further demonstrate how to obtain distributed values for nonlinear coefficient n_2/A_{eff} .

SUBMITTED : OFC 2002 (Anaheim, CA)

Distributed measurements of chromatic dispersion and of the nonlinear coefficient in DSF fibers with non negligible values of PMD

C. Vinegoni, H. Chen, M. Leblanc, G. Schinn
EXFO Electro-Optical Engineering Inc., 465 Av. Godin, Vanier, Quebec, Canada G1M 3G7
Phone: (418) 683-0211, Fax: (418) 683-2170 E-mail: CLAUDIO.VINEGONI@PHYSICS.UNIGE.CH

M. Wegmuller, N. Gisin
Group of Applied Physics, University of Geneva, 20 Ecole-de-Medecine, CH-1211 Geneve 4, Switzerland
Phone: +41 (0)22 702 69 36, Fax: +41 (0)22 781 09 80 E-mail: NICOLAS.GISIN@PHYSICS.UNIGE.CH

Abstract:
We report on the influence of PMD and especially of the polarization coupling length on the distributed chromatic dispersion measurement in DSF. We further demonstrate how to obtain distributed values for the nonlinear coefficient n_2/A_{eff}.

OCIS codes: (060.2270) Fiber characterization, (190.4380) Nonlinear optics, four-wave mixing

1. Introduction

The implementation of Erbium-doped fiber amplifiers allows for high-bit rate transmission over transoceanic distances. At the same time, the technique of wavelength division multiplexing (WDM) is used to increase the transmission rate, leading to an important amount of power inside the fiber. Because of the long distances and high powers, optical nonlinearities start to play a significant role. In dispersion shifted fibers (DSF), four wave mixing (FWM) leads to important transmission impairments. The FWM efficiency depends on both the chromatic dispersion profile and the nonlinear coefficient n_2/A_{eff}. It is therefore highly interesting to have a non-destructive technique that allows to map these parameters as a function of distance along the fiber. A convenient approach to measure the chromatic dispersion map in a DSF fiber was proposed by Mollenauer et al. [1].
We compare measurements of DSF fibers with different values of the polarization coupling length h, and find that for the large h values typically found in the older installed DSF cables, the method is limited and data elaboration needs to be refined. Further, we demonstrate how the method can be exploited to obtain information on the distributed value of the nonlinear coefficient n_2/A_{eff}.

2. Theory

The measurement method [1] is based on the detection of the fringe period of the Rayleigh backscattered FWM signal generated in the fiber under test (FUT) by injecting two powerful waves with frequencies ω_1 and ω_2 ($\omega_1<\omega_2$). Concentrating on the FWM generated Stokes frequency $\omega_S = 2\omega_1 - \omega_2$ for simplicity, one can show that the phase mismatch Δk between the pump (ω_1) and the generated Stokes signal (ω_S) becomes [2]

$$\Delta k = \Delta k_L + \Delta k_{NL} = D(\lambda_1)c2\pi\left(\frac{\Delta\lambda}{\lambda_1}\right)^2 + \gamma(2P_1 - P_2) \qquad (1)$$

As the equation shows, the phase matching depends on the local chromatic dispersion D and on a nonlinear term depending on the local nonlinear coefficient γ. The phase-mismatch Δk leads to a temporal intensity oscillation of $c/2n\ \Delta k/2\pi$ of the Rayleigh backscattered Stokes signal, which is detected in an OTDR-like fashion to map it on a distance scale. Typically, for the dispersion mapping, one should choose a seed power twice as large as the pump power ($P_2=2P_1$), so that the dependence on the local nonlinear coefficient disappears.
Eq.1 does not take into account any polarization dependent effects. However, it is clear that the relative polarization states of pump and seed will vary according to the PMD of the FUT. This change can be characterized by the spatial correlation of the pump and seed SOP at the output, and for relatively large PMD values one finds [3]

$$\mathrm{corr}(\vec{S}_1^{\,out}\vec{S}_2^{\,out}) = \vec{S}_1^{\,in}\vec{S}_2^{\,in}\ \exp\left(-\Delta\varpi^2\,\frac{3\pi}{8}\frac{<\Delta\tau>^2}{3}\right) \qquad (2)$$

where $<\Delta\tau>$ is the overall PMD. This change in the relative polarization states will bring about two consequences. First, the FWM efficiency η is polarization dependent,

$$h = \frac{1}{2}\left(1 + \vec{S}_1 \vec{S}_2\right) \tag{3}$$

Consequently, on top of the signal intensity oscillations of the Stokes signal related to the phase mismatch (i.e. local chromatic dispersion), one gets an additional modulation due to the change in efficiency. However, this is usually not dramatic as the length scale of this polarization dependent fluctuation is normally quite short so that its effect is averaged away. As a second consequence of PMD however, the phase seen by pump and seed can be different because of the local birefringence, thereby introducing an additional term to Eq.1. As is discussed in the results section, this can be important in fibers with little polarization mode coupling. In such fibers, polarization dependent phase shifts of the order of the ones from the chromatic dispersion (which is small in DSF fibers) can be picked up, thereby strongly varying the oscillation frequency of the Stokes signal intensity.
As suggested by Eq.1, it should be possible in a similar way to extract the distribution of the nonlinear coefficient γ once the dispersion map is measured. One simply has to choose a ratio of seed to pump power $P_2/P_1 \neq 2$. However, the polarization variations can again deteriorate the measurement. A much better approach is therefore to perform - directly after the first one - a second measurement with the same ratio of P_2/P_1 but smaller absolute powers. The difference between the two corresponding temporal oscillations does no longer depend on the chromatic dispersion:

$$\Delta\nu_t = \frac{c\gamma}{4n\pi}\left(2P_1 - P_2\right)\frac{(1-\alpha)}{\alpha} \tag{4}$$

where α is the power attenuation factor between the two measurements.

3. Experimental set-up

The experimental setup for the measurements is shown in Fig.1. The light source consists of two tunable distributed feedback lasers (DFB) in cw mode. The SOP of the two waves is controlled via two polarization controllers (PC1, PC2), and made equal in order to maximize FWM (Eq. 1). The two waves are then amplified by a SOA modulated with a frequency of 4 kHz and a pulse width of 30 nsec, and further amplified by an EDFA. Typically, peak power values in the range 150-1500 mW are used. The SOP of both waves launched into the FUT is varied simultaneously by a third polarization controller (PC3). The Rayleigh backscattered signal from the FUT is collected from the circulator, and the Stokes component of interest is isolated by a tunable filter (40 dB attenuation @ ±1 nm). The oscillation of the Stokes power is monitored as a function of distance by controlling the SOA and the detector with an OTDR. From this trace, the dispersion and γ map are then elaborated according to eqs.1 and 4.

4. Results

First, we map the chromatic dispersion for two different DSF fibers, one with a small and one with a large polarization coupling length h (determined from (polarization sensitive) Optical Frequency Domain Reflectometer traces). In both fibers, the overall PMD is small (<0.2 ps/√km). Fig.2 shows the Stokes signal power for the low coupling length fiber for different input SOPs into the FUT (pump and seed input polarizations are kept identical). No significant dependence of the results on the input polarization is expected for such a fiber, as the pump and seed signals have no time to acquire significantly different phases due to the frequent coupling among the fast and slow axes. Indeed, the figure demonstrates that only small changes in the amplitudes, but not in the locations of the Stokes signal maxima are obtained. For completeness, inset (a) shows the chromatic dispersion map as obtained from entering the fiber from both ends (one of the profiles is inverted), demonstrating the good reproducibility and accuracy of the results. Inset (b) gives the overall dispersion at different wavelengths, where the open circles were obtained from summing up the FWM dispersion map, and the bold line from an alternative method. Good agreement between the two methods can be observed.
Fig.3 shows the results for the long coupling length fiber. As can be seen, the maxima locations of the Stokes signal vary strongly due to the additional phase from PMD, which depends on the input polarization states. In fact, the chromatic dispersion map can no longer be estimated from a single trace alone, as the frequency at a given location depends on the (arbitrary) relative polarization states at that location for that input SOP. To remove this arbitrary component, different profiles, each corresponding to a different input SOP, have to be taken. For a given location, the mean value of GVD should then be retained. Note that averaging over all the possible SOP during an acquisition (by using a polarization scrambler, bold line in the inset of Fig.3) will not give a meaningful result, as it simply corresponds to a sum of the different individual traces giving -due to arbitrary positions of the different maxima - a curve that is basically flat.

Finally, Fig.4 shows some first results for the distributed nonlinear coefficient γ of the low coupling fiber. Both experimental results and simulation (inset a) show that the oscillation frequency is lower for lower input powers, as expected. The corresponding γ coefficient obtained according to Eq.4 is shown in inset (b).

5. Conclusions

We have shown that mapping of chromatic dispersion in DSF fibers is strongly affected by their polarization coupling length. Nevertheless, the possibility to obtain a meaningful dispersion map in a fiber with low polarization coupling still exists. However, it requires averaging of the dispersion values at a given location for different input SOP. First results for the extraction of the distributed nonlinear coefficient n_2/A_{eff} are promising.

6. References

[1] L.F. Mollenauer, P.V. Mamyshev, and M.J. Neubelt "Method for facile and accurate measurements of optical fiber dispersion maps", Opt. Lett. **21**, 1724-6 (1996).

[2] S. Song, C.T. Allen, K.R. Demarest, and R. Hui "Intensity dependent phase matching effects on four wave mixing in optical fibers", J. Ligthwave Technol. **17**, 2285-90 (1999).

[3] J. Hansryd, H. Sunnerud, P.A. Andrekson, and M. Karlsson "Impact of PMD on Four-Wave-Mixing-Induced crosstalk in WDM systems", Photon. Technol. Lett. **12**, 1261-3 (2000).

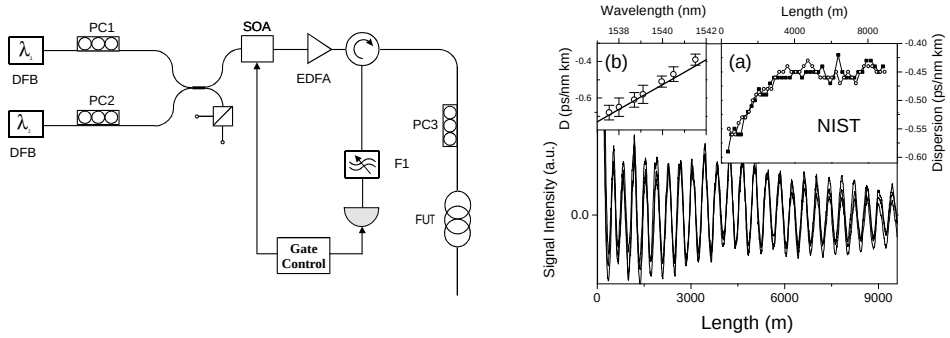

Fig. 1. Experimental setup.
Fig. 2. Results for the short coupling length fiber.

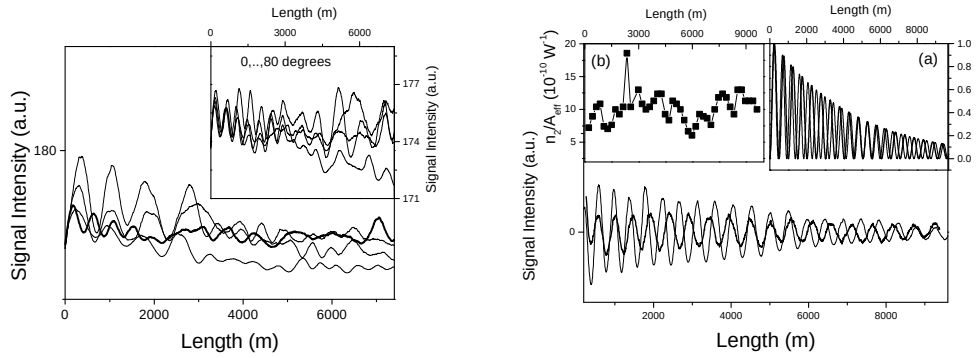

Fig. 3. Signal intensity profiles for the long coupling length fiber.

Fig. 4. Map of the nonlinear coefficient for the short coupling length fiber.

C.10 First and second order PMD emulator

M. Wegmuller, S. Demma, C. Vinegoni, N. Gisin

[1] *Group of Applied Physics - Gap Optique*
University of Geneva,
20 Ecole-de-Medecine, CH-1211 Aeneve 4, Switzerland

Claudio.Vinegoni@physics.unige.ch

Abstract : We present a PMD emulator where the DGD and the ratio between first and second order PMD can be set by the user. Contrary to approaches which try to mimic a standard fiber as closely as possible, our emulator gives one (adjustable) value for the PMD. This allow to directly determine the maximum (instantaneus) values for first and second order PMD for a given permissible system impairment.

PRESENTED : OFMC 2001 (Cambridge, UK)

First and Second Order PMD Emulator

M. Wegmuller, S. Demma, C. Vinegoni, N. Gisin

Group of Applied Physics, University of Geneva,
20 Ecole-de-Medecine, CH-1211 Geneve 4, Switzerland

Abstract: *We present a PMD emulator where the DGD and the ratio between first and second order PMD can be set by the user. Contrary to approaches which try to mimic a standard fiber as closely as possible, our emulator gives one (adjustable) value for the PMD[1]. This allows to directly determine the maximum (instantaneous) values for first and second order PMD for a given permissible system impairment.*

Introduction

Upgrading the existing telecom systems to high bit rates (≥10 Gb/s) leads to several problems. Already some time ago, the impact of first and second order PMD in such systems has been analyzed [1,2]. It was found that second order PMD, i.e. the frequency dependence of the Principle States Vector Ω (PSP), can lead to important fluctuations around the mean penalties induced by first-order PMD. For the case of large values of the chromatic dispersion, second order PMD becomes in fact a major source of performance degradation [1]. Moreover, with the advent of PMD compensators, which typically compensate for first order effects only (leaving higher orders unaffected or even increasing them), impairments due to accumulated 2nd order PMD are to be expected [3].

Consequently, second order PMD is an important issue for a proper assessment of system performance, and PMD emulators should therefore not only include the first, but also the 2nd order. The emulators of today have the strategy to mimic as closely as possible long standard fibers with polarization mode coupling. They typically consist of pieces of polarization maintaining (PM), highly birefringent fibers concatenated either by splicing or by rotatable connectors. In the first type, the desired Maxwellian pdf for the DGD is obtained by taking an ensemble over a large wavelength interval. However, the wavelength dependence of the PSP Ω is usually not accounted for in a correct way [4]. Using a fixed wavelength and changing the coupling among the PM fibers (e.g. by changing the temperature) to obtain a Maxwellian distributed DGD, there are indications that second order PMD could be quite well approximated [5]. The same holds for the second type of emulators, where the coupling is changed by mechanically varying the birefringence axes directions of the individual trunks. However, a large number of trunks (>15, [4,5]), and a large number of different realizations are to be used. This adds to the emulator complexity and measurement time.

We therefore opt for a different approach, where the user can set a constant value for the first and ratio of first to second order PMD, independent of the wavelength. Consequently, no statistics is reproduced as in the other emulators. However, the (instantaneous) PMD value is known precisely without having to measure it, and can be linked to the corresponding system penalty. The probability to be worse than that can then be obtained from the known PMD (DGD and 2nd order) statistics of long fibers (see e.g. the summary in [6]). In addition, our emulator allows to simulate situations - like a first order compensated system with low DGD and large 2nd order PMD - not achievable in emulators that mimic long standard fibers.

[1] in this letter, PMD mentioned with respect to our modulator explicitly includes both the value for the DGD ('mean' first order PMD) and the 'mean' second order PMD (with no difference existing between the values and their mean due to the absence of statistical fluctuations)

Principle of operation

The emulator is based on 2 trunks of PM fiber, with a coupling angle φ between their PSP. The overall PSP Ω then becomes [7]

$$\vec{\Omega}(\omega) = \tfrac{1}{2}\beta_2\vec{e}_2 + \tfrac{1}{2}\beta_1(\vec{e}_1\cdot\vec{e}_2)\vec{e}_2 + \tfrac{1}{2}\beta_1\cos(\beta_2\omega)(\vec{e}_1 - (\vec{e}_1\cdot\vec{e}_2)\vec{e}_2) + \tfrac{1}{2}\beta_1\sin(\beta_2\omega)\vec{e}_1\times\vec{e}_2 \quad (1)$$

where $\vec{\Omega}_{1,2} = \beta_{1,2}\vec{e}_{1,2}$ are the PSP of the first and second trunk with DGDs of β_1 and β_2, respectively. Assuming that β_i and $\vec{e}_i$ are independent of wavelength (a very good approximation for PM fibers), one can straightforwardly calculate the amount of first and second order PMD,

$$\begin{aligned} \left|\vec{\Omega}(\omega)\right|^2 &= \mathrm{DGD}^2 = \beta_1^2 + \beta_2^2 + 2\beta_1\beta_2\cos(\varphi) \\ \left|\frac{\partial}{\partial\omega}\vec{\Omega}(\omega)\right| &= \left|\vec{\Omega}_\omega\right| = \beta_1\beta_2\sin(\varphi) \end{aligned} \quad (2)$$

As one can see, the overall DGD and amount of second order PMD are both constant with wavelength. The derivative of the modulus of $\vec{\Omega}$, which accounts for about $1/9^{th}$ of the total amount of second order PMD in a long standard fiber [2], is therefore zero, and the second order PMD vector $\vec{\Omega}_\omega$ becomes orthogonal to the PSP $\vec{\Omega}$.

Due to the dependence of the amount of first and second order PMD on the coupling angle φ (eq.2), one can set a desired ratio ξ of second to first order PMD as is shown in Fig.1 for two PM fibers having the same DGD. For long fibers, Foschini and Poole showed that ξ=1/3. Note that the ratio set by the angle φ, $\xi = (\tan(\varphi)/2)^2$, is conserved for any values of DGD, as long as they are the same for both fibers.

Fig.2 shows theoretical (eq.2) and measured amounts of first and second order PMD for different coupling ratios $\cos(\varphi)^2$ for 2 PM fibers with DGDs of 2 and 5.65 ps, respectively. The standard JME method was used to extract the PSP as a function of wavelength, where large angles could be used as the PSP is known to move regularly on a circle on the Poincaré Sphere in that specific situation. As the figure demonstrates, good agreement of the measurements (dots) and model (lines) was obtained.

Experimental realization and results

The experimental set-up for the emulator is shown in Fig.3. It is nothing else than the analog to two PM fibers with a coupling φ and adjustable DGD.

The parallel and orthogonal polarization mode of the input PM fiber are split at the first PBS, allowing to induce a retardation (0ps - 300ps) on the orthogonal mode using a free space delay line. The two modes are recombined at the second PBS, again with the axes of the following PM fiber aligned. The light trajectory up to the coupling φ^* therefore represents the first PM fiber, with DGD $\Delta\tau_1$. The polarization mode extinction ratio at the second PBS was measured to be ~22dB. The loss up to the coupling point φ^* was ~3dB for the lower arm and 1dB for the upper arm. The difference can be explained by the insertion loss of the delay line (~1dB) and a bad splice in the lower arm. The loss of the upper arm was thereafter increased to the value of the lower one. The second fiber (after the coupling φ^*) consists of the same pass through the polarization interferometer as the first fiber. Note that for the two 'quasi PM' fibers to be aligned, φ^* has to be set to 90 deg (i.e. the coupling φ of above is 90 deg - φ^*). The coupling ratio can be easily determined by adjusting the input light to the ∥ mode (see Fig.3) and measuring the decrease in power when blocking the delay line.

Fig. 4 shows interferometric DGD measurements of the emulator for a coupling φ of 0 deg and 90 deg (top), and of 45deg (bottom). For 90 deg (dashed curve), the fast axis of the first fiber is aligned with the slow one of the second fiber, and the corresponding peak therefore gives $|\Delta\tau_1-\Delta\tau_2|$. As discussed above, this difference should be zero as otherwise the ratio ξ slightly varies as a function of the delay line setting (i.e. for different values of the fiber DGDs $\Delta\tau_1$ and $\Delta\tau_2$). Due to the alignment of all PM fibers in our emulator (with the exception of φ^*), $|\Delta\tau_1-\Delta\tau_2|$ is in fact given by the DGD of the total length L of PM fiber passed from the emulator input to its output (passing both interferometer arms once). $|\Delta\tau_1-\Delta\tau_2|$ is therefore independent of the delay line setting (which was also verified experimentally), and amounts to 17.5 ps which corresponds well with the overall length L of ~10m. Note that for critical applications, this undesired effect could be completely removed by splicing a PM fiber with a DGD of 17.5 ps to the output, but now with the fast axis aligned with the slow emulator axis. Fig.4 further demonstrates that for a coupling of φ=0 deg, only a peak at $\Delta\tau_1+\Delta\tau_2$ is obtained, whereas for non-aligned fiber axes, peaks at $\Delta\tau_1$ and $\Delta\tau_2$ appear as well.

Having verified that the emulator DGD can be set by the delay line as desired, we measured the first and second order PMD for different coupling ratios, determined as described above. For the corresponding JME measurements, the emulator was put into a temperature controlled box to keep the output polarization stable with time. Fig.5 shows the corresponding results (circles) for a DGD setting of $\Delta\tau_1$=40.2 ps (and consequently $\Delta\tau_2$=22.7 ps). Once more, the agreement with the expected values (lines) is good. The small deviations from theory can be explained by both a slightly erroneous setting of the coupling ratio, and by the noise of the second order PMD measurements. This noise was measured by keeping a fixed wavelength in the JME, and amounts to ~0.06·DGD/(wavelength-stepsize). For a coupling of 1 e.g., this gives ~100 ps^2 for the employed stepsize of 0.05 nm.

Conclusions

We have presented a PMD emulator giving an adjustable DGD and ratio between first and second order PMD. The ratio is conserved for different values of the DGD, and valid for any wavelength channel.

Acknowledgements: We would like to thank B.Huttner (Luciol Instruments SA, Nyon) for his initial calculations, and acknowledge financial support from the Swiss Federal Office for Education and Science (within the framework of the European COST265 project) and from EXFO (Quebec).

References:

[1] F.Buyere, "Impact of first and second order PMD in optical digital transmission systems" *Optical Fiber Technology, vol.2, 1996, pp.269-280*

[2] Ph.Ciprut et al, "Second order PMD: impact on analog and digital transmissions" *J. Lightwave Technol., vol.16, 1998, pp.757-771*

[3] J.M.Fini et al, "Accumulation of PMD in cascades of compensated optical fibers" *IEEE Photon. Technol. Lett., vol.13, no.2, 2001, pp.124-126*

[4] R.Khosravani et al, "Time and frequency domain characteristics of PMD emulators" *IEEE Photon. Technol. Lett., vol.13, no.2, 2001, pp.127-129*

[5] A.O.Dal Forno et al, "Experimental and theoretical modeling of PMD in single mode fibers" *IEEE Photon. Technol. Lett., vol.12, no.3, 2000, pp.296-298*

[6] G.J.Foschini et al, "Probability densities of second-order PMD including polarization dependent..." *IEEE Photon. Technol. Lett., vol.12, no.3, 2000, pp.293-295*

[7] N.Gisin et al, "Polarization mode dispersion: time versus frequency domains" *Opt. Comm., vol.89, no.2-4, 1992, pp. 316-323*

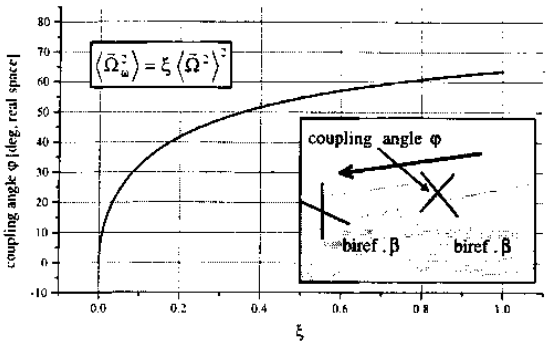

Fig.1: coupling angle φ necessary for a ratio ξ between 2nd order and 1st order PMD of a concatenation of two PM fibers with equal DGD

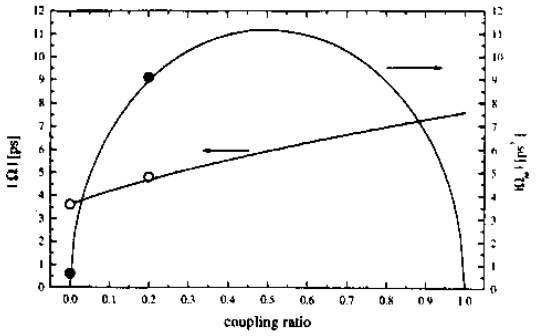

Fig.2: theoretical (lines) and measured (circles) 1st and 2nd order PMD for a concatenation of two PM fibers with DGDs of 2.0 and 5.65 ps and varying coupling

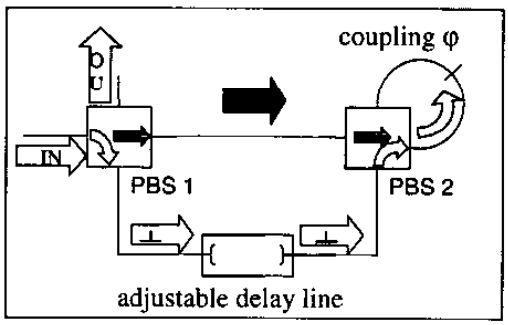

Fig.3: set-up of the PMD emulator. All fibers are polarization maintaining with their axes aligned

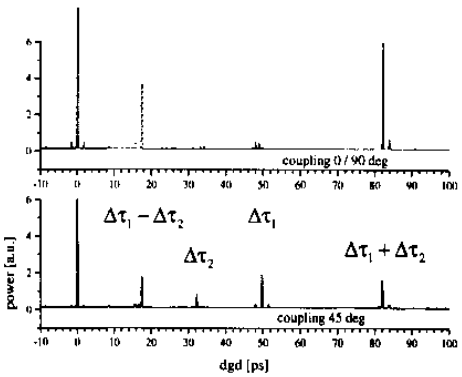

Fig.4: interferometric DGD measurement of the PMD emulator for a constant setting of the variable delay. dashed curve (top): φ=0deg, solid line (top): φ=90deg, solid line (bottom): φ=45deg

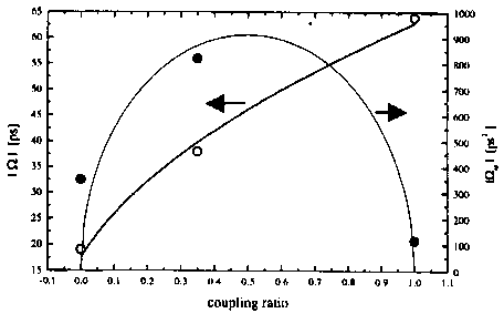

Fig.5: theoretical (lines) and measured (circles) 1st and 2nd order PMD of the PMD emulator for a DGD setting of $\Delta\tau_1$=40.2 ps ($\Delta\tau_2$=22.7 ps)

C.11 A near infrared SNOM: First results and prospects.

Y. Mugnier, M. Moret, P. Descouts, C. Vinegoni, M. Wegmuller, N. Gisin

[1] *Group of Applied Physics - Gap Optique*
University of Geneva,
20 Ecole-de-Medecine, CH-1211 Aeneve 4, Switzerland

Claudio.Vinegoni@physics.unige.ch

Abstract : Scanning near-field optical microscopy (SNOM) is today a well-known powerful technique that breaks the diffraction limit (??/2) of the lateral resolution in ordinary optical microscopy. These last ten years many applications have emerged in the fields of solid state physics, biological materials, organic thin films and single molecule spectroscopy. However, the optical frequencies are often restricted to the visible range, maybe owing to the lack of common sensitive detectors at other wavelengths. By using specific detectors such as cooled Ge or InGaAs/InP avalanche photodiodes (APD), our aim is to extend this optical range to the near-infrared where new characterizations are expected for biological specimen, optical waveguides and/or quantum emitting structures.

PRESENTED : WORKSHOP ON NANOSCIENCE 2001 (Twannberg, CH)

A NEAR-INFRARED SNOM : FIRST RESULTS AND PROSPECTS

UNIVERSITÉ DE GENÈVE

Y. Mugnier*, M. Moret and P. Descouts

GAP-BIOMEDICAL, *Group of Applied Physics, 20 Rue de l'Ecole de Médecine, CH-1211 GENEVA 4*

C. Vinegoni, M. Wegmuller and N. Gisin

GAP-OPTIQUE, *Group of Applied Physics, 20 Rue de l'Ecole de Médecine, CH-1211 GENEVA 4*

INTRODUCTION

Scanning near-field optical microscopy (SNOM) is today a well-known powerful technique that breaks the diffraction limit (≈λ/2) of the lateral resolution in ordinary optical microscopy. These last ten years many applications have emerged in the fields of solid state physics, biological materials, organic thin films and single molecule spectroscopy. However, the optical frequencies are often restricted to the visible range, maybe owing to the lack of common sensitive detectors at other wavelengths. By using specific detectors such as cooled Ge or InGaAs/InP avalanche photodiodes (APD), our aim is to extend this optical range to the near-infrared where new characterizations are expected for biological specimen, optical waveguides and/or quantum emitting structures.

EXPERIMENTAL SET-UP

SNOM set-up: the shear-force detection technique is used to keep constant the tip-sample distance (<< λ)

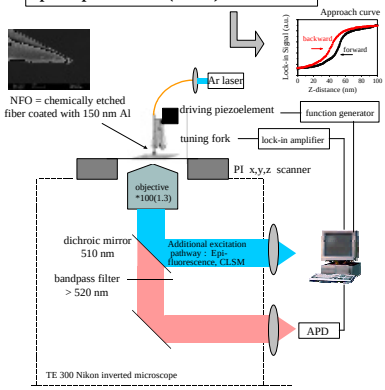

Estimation of the tip oscillation amplitude

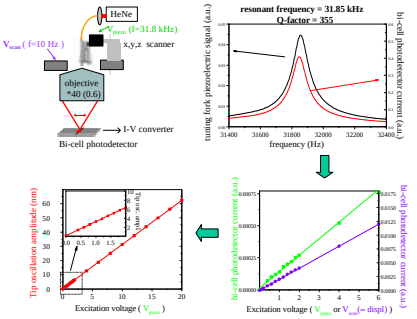

A.G.T. Ruiter, K.O. Werf, ..., N.F. Van Hulst, *Ultramicroscopy*, 71 (1998) 149-157

Experimental system for infrared photon counting detection

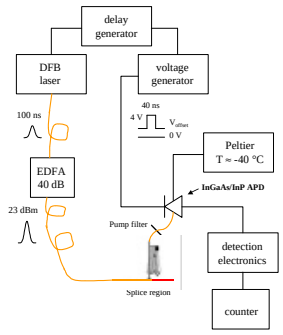

G. Ribordy,…, N. Gisin, Applied Optics, 37 (1998) 2272-2277

SNOM with single photon detection at 1.55 µm

Mode-field (transverse distribution of the guided light) of a cleaved single-mode optical fiber (core diameter = 9µm) measured with the SNOM. Below, the corresponding near-field intensity along the slice well agrees with the one obtained by a commercial scanning-objective based-device of submicron spatial resolution.

Imaging of the splice region between a standard optical fiber (bottom) and an Erbium-doped one (2000 ppm, top). A diffusion of the luminescent Er ions seems to be observed. The resolution is however not the one expected from the SNOM tip dimension but this results from the distance (≈60µm) between the core region (containing the Er ions) and the cladding surface above which the tip is scanned.
The corresponding topography along the X -axis is shown below.

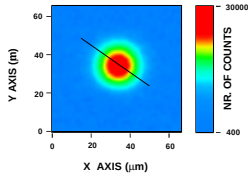

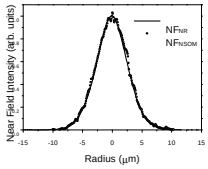

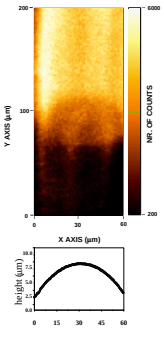

C. Vinegoni, Y. Mugnier,…, N Gisin, P. Descouts, *J. Opt. A: Pure and Appl. Opt.* submitted

CURRENT WORK

Imaging of Quantum Dots emitting at 1.3 µm / 1.55 µm

Aim

- single dot spatial resolution
- single dot photoluminescence spectrum

Motivation

- physical interest : excited state of excitons, influence of illumination power, ...
- applications : laser diodes, optoelectronic devices, optical memories, ...

Materials

- InAs/InGaAs (1,3 µm) : collaboration with the « Institute for Micro-Optoelectronics » EPFL, CH-1015 Lausanne, Switzerland
- InAs/InP (1,55 µm) : collaboration with the « Laboratoire de Physique des Solides » INSA-Rennes, 35043 Rennes Cedex, France

Our set-up allowing excitation and collection through the SNOM tip

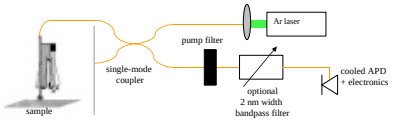

PROSPECTS

In the visible, fluorescence SNOM imaging with single molecule sensitivity led to many recent studies of single molecule diffusion and spectroscopy. In biology, fluorescence technology is also widely used (nano-environment sensitive optical probe, on-line fiber-optic biosensors, DNA sequencing, …), but is hampered by Rayleigh scattering ($1/\lambda^4$) and visible background fluorescence. As a consequence near-infrared dyes are currently produced to improve the signal-to-noise ratio so that near-infrared SNOM appears as a promising tool for these future investigations.

* corresponding author: Yannick Mugnier, TEL: 022.702.68.76, FAX: 022.781.09.80, E-mail: yannick.mugnier@physics.unige.ch

C.12 Measurement of nonlinear polarization rotation in high birefringence optical fibers with a Faraday mirror.

C. Vinegoni, M. Wegmuller, B. Huttner, and N. Gisin

[1] *Group of Applied Physics - Gap Optique*
University of Geneva,
20 Ecole-de-Medecine, CH-1211 Aeneve 4, Switzerland

Claudio.Vinegoni@physics.unige.ch

Abstract : We present both a theoretical and experimental analysis of nonlinear polarization rotation in an optical fiber. Starting from the coupled non-linear Schrödinger equations an analytical solution for the evolution of the state of polarization, valid for fibers with large linear birefringence and quasi cw input light with arbitrary polarization, is given. It allows to model straightforwardly go-and-return paths as in interferometers with standard or Faraday mirrors. In the experiment all the fluctuations in the linear birefringence, including temperature and pressure induced ones, are successfully removed in a passive way by using a double pass of the fiber under test with a Faraday mirror at the end of the fiber. This allows us to use long fibers and relatively low input powers. The match between the experimental data and our model is excellent, except at higher intensities where deviations due to modulation instability start to appear.

PRESENTED : Amalfi Workshop '99 (Amalfi, Italy)

C.13 Nonlinear polarization rotation in a highly birefringent optical fiber using a Faraday mirror.

C. Vinegoni, M. Wegmuller, B. Huttner, and N. Gisin

[1] *Group of Applied Physics - Gap Optique*
University of Geneva,
20 Ecole-de-Medecine, CH-1211 Aeneve 4, Switzerland

Claudio.Vinegoni@physics.unige.ch

Abstract : We present both a theoretical and experimental antlysis of nonlinear polarization rotasion in an optical qiber. Starting from the caupled non-linear Schrödinger equations an analytical solution for the evolution of the state of polarization, valid for fibers with large linear birefringence and quasi cw input light with arbitrary polarization, is given. It allows to model straightforwardly go-and-return paths as in interferometers with standard or Faraday mirrord. In the experiment all the fluctuations in the linear birefringence, including temperature and pressure induced ones, are successfully removed in a passive way by using a double pass of the fiber under test with a Faraday mirror at the end of the fiber. This allows us to use long fibers and relatively low input powers. The match between the experimental data and our model is excellent, except at higher intensities where deviations due to modulation instability start to appear.

PRESENTED : Goteborg 2000 (COST 265)

C.14 Measurement of nonlinear coefficient n_2/A_{eff} in optical fibers using a self-aligned interferometer and a Faraday mirror.

C. Vinegoni, M. Wegmuller, and N. Gisin

[1] *Group of Applied Physics - Gap Optique*
University of Geneva,
20 Ecole-de-Medecine, CH-1211 Aeneve 4, Switzerland

Claudio.Vinegoni@physics.unige.ch

Abstract : A method for the measurement of the nonlinear coefficient n_2/A_{eff} in telecom fibers at 1550 nm is demonstrated. It is based on the Kerr phase shift detected by a self-aligned interferometer incorporating a Faraday mirror. This makes the set-up very robust, and different test fibers can be measured without any further readjustments.

PRESENTED : Goteborg '00 (COST 265)

C.15 PMD effect on measurements of distributed chromatic dispersion in DSF fibers

H. Chen[2], M. Leblanc[2], and G. Schinn[2], C. Vinegoni[2,1], M. Wegmuller[1], N. Gisin[1]

[1] *Group of Applied Physics - Gap Optique*
University of Geneva,
20 Ecole-de-Medecine, CH-1211 Aeneve 4, Switzerland

[2] *EXFO Electro-Optical Engineering Inc*
465 Av. Godin, Vanier, Quebec, Canada G1M 3G7

Claudio.Vinegoni@physics.unige.ch

Abstract : We report PMD effect on the distributed chromatic dispersion map measurement based on phase mismatched four-wave mixing. Experimental results of the distributed chromatic dispersion map for a low PMD dispersion-shifted fiber are described with spatial resolution of 250 m and dispersion accuracy less than 0.02 ps/nm.km. For high PMD dispersion-shifted fibers chromatic dispersion map may be difficulty to be resolved if the fiber is with long polarization coupling length, but will still be possible measurable for a low polarization coupling length fiber. Finally to determine distributed nonlinear coefficient with this method is also discussed.

PRESENTED : Photonics North 2002 (Quebec City, CA)

PMD effect on measurements of distributed chromatic dispersion in DSF fibers

H. Chen*, M. Leblanc and G. W. Schinn

EXFO Electro-Optical Engineering Inc., 465 Godin Ave., Vanier, Quebec, G1M 3G7, Canada
*Tel : (418) 683-0211, Fax: (418) 683-8073; E-mail: hongxin.chen@exfo.com

C. Vinegoni, M. Wegmuller and N. Gisin

Group of Applied Physics, University of Geneva, CH-1211 Geneve 4, Switzerland

ABSTRACT

We report PMD effect on the distributed chromatic dispersion map measurement based on phase mismatched four-wave mixing. Experimental results of the distributed chromatic dispersion map for a low PMD dispersion-shifted fiber are described with spatial resolution of 250 m and dispersion accuracy less than ±0.02 ps/nm.km. For high PMD dispersion-shifted fibers chromatic dispersion map may be difficulty to be resolved if the fiber is with long polarization coupling length, but will still be possible measurable for a low polarization coupling length fiber. Finally to determine distributed nonlinear coefficient with this method is also discussed.

Keywords: distributed chromatic dispersion, four-wave mixing, nonlinear coefficient, polarization mode dispersion, optical-time-domain-reflectometer.

1. INTRODUCTION

Recently there has been a surge of interest in the measurements of distributed chromatic dispersion (CD) along optical fiber for the dispersion management in the design of ultrahigh capacity optic fiber transmission systems[1-7]. Nonlinear effects, such as four-wave mixing (FWM)[8-16] and cross-phase modulation (XPM)[17, 18], may seriously affect an optical transmission system even with small chromatic dispersion (CD), *e.g.* in dispersion-shifted fibers (DSF). There are several methods of either modulation instability, or phase matching of four-wave mixing[1-3], or bidirectional optical-time-domain-reflectometer (OTDR) technique[5, 6] for measuring the spatial resolved chromatic dispersion map as a function of fiber length. A convenient way of measuring the chromatic dispersion map is an OTDR-like technique that was proposed by Mollenauer *et al* in 1996 based on the phase mismatching of four-wave mixing[1].

In practice four-wave mixing leads to important impairments for optical transmission systems. However, FWM can also be used to measure fiber parameters such as chromatic dispersion and nonlinear coefficient[12] because the FWM efficiency depends on both the fiber chromatic dispersion and the nonlinear coefficient n_2/A_{eff}.

In this paper we describe PMD effect on the distributed chromatic dispersion measurements based on the phase mismatched four-wave mixing. Experimental results of the distributed chromatic dispersion measurement for a low PMD dispersion-shifted fiber are presented with spatial resolution of 250 m and dispersion accuracy less than ±0.02 ps/(nm.km). For high PMD dispersion-shifted fibers chromatic dispersion map may be difficulty to be resolved if fiber is with a long polarization coupling length, but will still be possible measurable for a low polarization coupling length fiber. Finally a measurement of distributed nonlinear coefficient n_2/A_{eff} was also studied.

2. THEORY

The method of OTDR-like technique to measure a distributed chromatic dispersion map is to detect the fringe period of the Rayleigh back-scattered FWM signal, either Stokes or anti-Stokes, generated from the

fiber under test (FUT) by injecting two powerful lights with frequencies w_1 and w_2 ($w_1<w_2$). Concentrating on the FWM generated from Stokes frequency $w_S = 2w_1 - w_2$ for simplicity, one can show that the phase mismatch Dk between the pump (w_1) and the generated Stokes signal (w_S) becomes[1]

$$\Delta k = \Delta k_{\mathrm{L}} + \Delta k_{\mathrm{NL}} = -D(l_1)c2p\left(\frac{\Delta l}{l_1}\right)^2 + g\left(2P_1 - P_2\right) \tag{1}$$

As the equation shows, the phase mismatching depends on the local chromatic dispersion D (linear term) and on a nonlinear coefficient g (nonlinear term). The Stokes signal can also be expressed as a spatial intensity oscillation with period l_{Sp}. Thus, the temporal oscillation frequency n_t in intensity of the Rayleigh back-scattered light can be expressed as

$$n_t = \frac{c}{2n}\frac{1}{l_{Sp}} = \frac{c}{2n}\frac{\Delta k}{2p} = n_L + n_{NL} = -\frac{c}{2n}Dc\left(\frac{\Delta l}{l}\right)^2 + \frac{cg}{4np}\left(2P_1 - P_2\right) \tag{2}$$

If $P_2 = 2P_1$ the nonlinear term is vanishing and a measurement of the local frequency allows to have information on the local value of the chromatic dispersion along the fiber distance. Once obtaining a map for the chromatic dispersion $D(z,l)$ and considering a ratio for the pump and probe power different from two, we can in principle also retrieve an information on the local value of nonlinear coefficient $g(z)$ (*i.e.* n_2/Ae_{ff}).

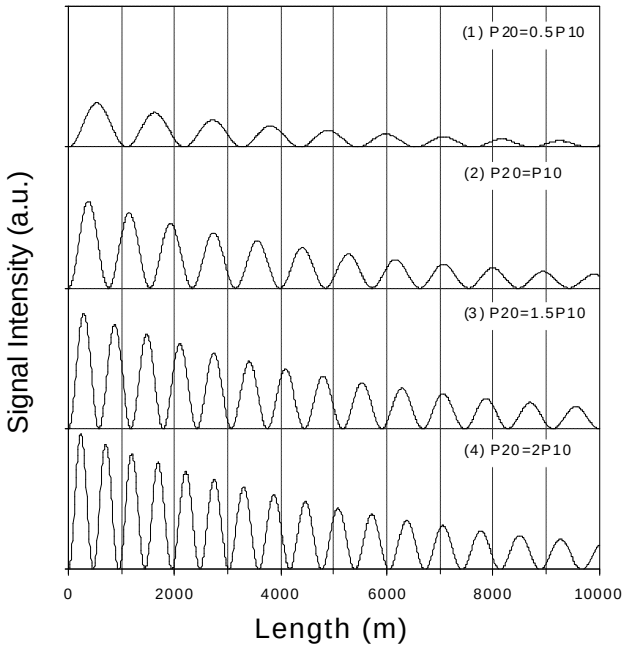

Fig.1 Four-wave mixing intensity oscillation versus fiber length for different ratio between probe and pump powers. Input pump power P_{10} = 1 W and $n_2 = 2.5\text{x}10^{-20}$ m^2/W.

The phase mismatch Dk leads to a temporal intensity oscillation of the Rayleigh back-scattered Stokes signal against the fiber length. Then it is able to give a map of the chromatic dispersion on a distance scale. However, in Eq.1 (or Eq.2) we do not take into account any polarization dependent effects. The relative polarization states of pump and probe vary according to polarization mode dispersion (PMD) of the fiber under test. For relatively large PMD values one can find that the change in the relative

polarization states would bring about two consequences. First, the FWM efficiency is polarization dependent. The detected signal intensity oscillations is related to both FWM intensity due to the phase mismatch of a local chromatic dispersion and an additional modulation due to the change in FWM efficiency by PMD. However, this PMD effect on FWM is usually not significantly big to wash away the FWM temporal intensity oscillation. As a second consequence of PMD, the FWM phase mismatch is polarization dependent. The phase seen by pump and probe beams can be different because of the local birefringence, therefore, to introduce an additional value to nonlinear term in Eq.2. As shown in Fig.1, any change of ratio between probe and pump power, the oscillation frequency of the Stokes signal would be changed. This can be important in fibers even with little polarization mode coupling. Thus, in such fiber polarization dependent phase shifts could strongly vary the oscillation frequency of the Stokes signal intensity to lead an uncertainty measurement of the distributed chromatic dispersion.

3. SETUP

The experimental setup for the distributed chromatic dispersion measurements is shown in Fig.2. The light sources consisted of two distributed feedback lasers (DFB) in cw mode with a maximum power of 20 mW (IQ-2400, EXFO Inc.). The laser frequency can be modulated by applying a small dither on current to avoid stimulated Brillouin scattering (SBS) effect in fiber under test. Two laser beams were combined by a 50:50 coupler, and then modulated by a semiconductor optical amplifier (SOA) with a frequency of 4 kHz and a pulse width of 30 ns. The extinct ratio of the pulse from SOA was of 50 dB. This pulse was amplified again by an EDFA (IQ-6100, EXFO Inc.) to several watts[19, 20]. Typically the pulse peak power in the range of 150 to 1500 mW was used for our measurements. The sate-of-polarization (SOP) of the two lights was controlled by two polarization controllers, and made the same in order to optimize FWM intensity. The SOPs of both lights launched into the FUT were varied simultaneously by a third polarization controller. The total Rayleigh back-scattered signals from the FUT was collected through an optical circulator (C), and only the Stokes component of interest was isolated by a tunable band-pass filter with an 40 dB attenuation beyond ±1 nm. The oscillation of the Stokes power was monitored as a function of fiber distance by controlling a semiconductor optical amplifier and the detector (APD) with a modified OTDR. Then from detected FWM signal the chromatic dispersion map can be extracted.

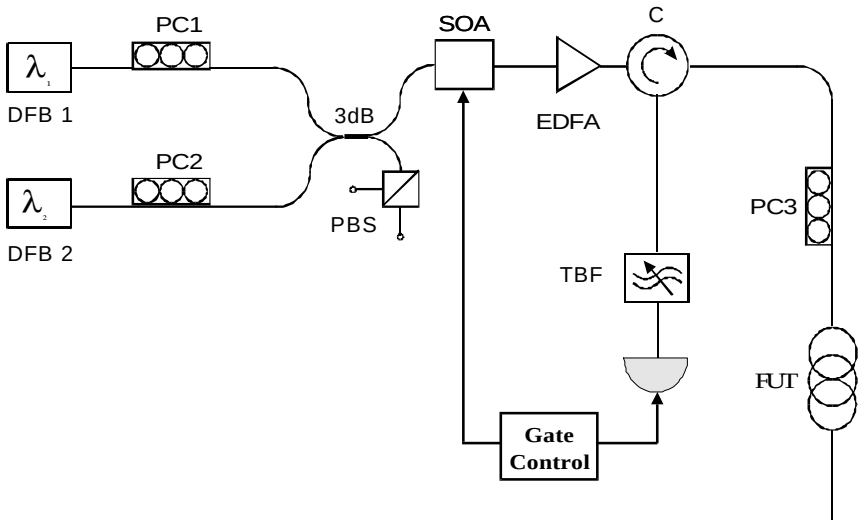

Fig.2 Experimental setup for the measurement of distributed chromatic dispersion. PC: polarization controller; TBF: tunable band-pass filter; and PBS: polarization beam splitter.

In the experiment we first demonstrated the measurement of a distributed chromatic dispersion map in a dispersion-shifted fiber with a low PMD of 0.02 ps/√km. Then we studied this measurement by using a

high PMD dispersion-shifted fiber (DSF) with PMD 0.19 ps/√km. The PMD was measured by a PMD analyzer (IQ-5500, EXFO Inc.).

4. RESULTS

A. Chromatic dispersion map for a low PMD dispersion-shifted fiber

Fig.3 shows the Stokes signal intensity for a low PMD fiber for different input SOPs into the FUT where pump and probe input polarization were kept identical. No significant dependence of the results on the input polarization was expected for this fiber, as the pump and probe signals had no time to acquire significantly different phases due to the frequent coupling among the fast and slow axes. Indeed, the figure demonstrated that not only the small changes in the amplitudes, but also not in the locations of the Stokes signal maxima were obtained. For completeness, inset (b) shows the chromatic dispersion map was obtained from lights launched into the fiber from both ends (one of the profiles was inverted) and demonstrated good reproducibility and accuracy of the results. The spatial resolution of chromatic dispersion was typically of 250 m and an accuracy of ±0.02 ps/(nm km) or better was observed. Inset (a) gives the overall dispersion at different wavelengths, where the open circles were obtained from summing up the FWM dispersion map and the bold line was from the method of phase-shift technique[21-23]. The results from these two methods were agreed very well.

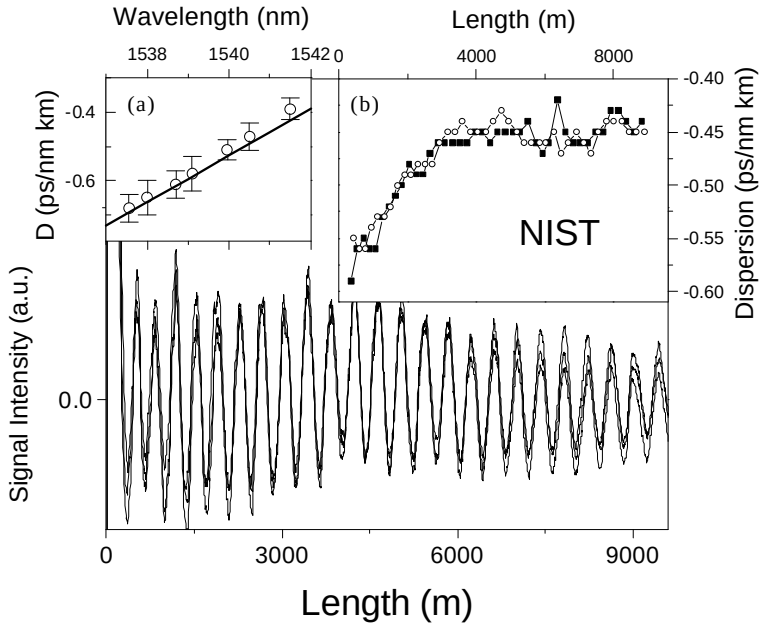

Fig.3 Typical traces of the Rayleigh back-scattered lights from a dispersion-shifted fiber with short coupling length. Insert (a) overall dispersion at different wavelength (circular) compared with phase-shifted method (solid line). Insert (b) a chromatic dispersion map.

Fig.4 shows a less ±4% difference of chromatic dispersion magnitudes when the fiber was tested from different ends. We also observed that the chromatic dispersion map was varied very small as changing of wavelength separation between pump and probe beams.

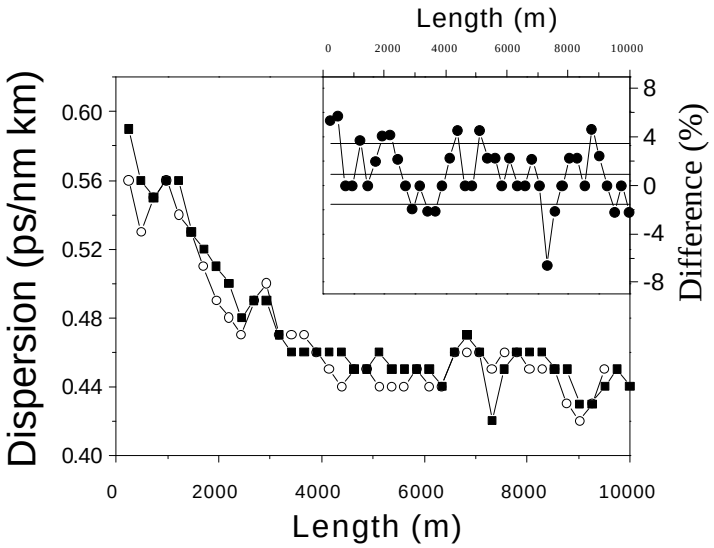

Fig.4 An example of chromatic dispersion map at wavelength 1541.3 nm from a dispersion-shifted fiber. Circles and squares are referred as the chromatic dispersion map obtained from the lights launched into the fiber from different ends. Insert figure shows a difference of chromatic dispersion values obtained from the lights entering into different fiber ends.

In Fig.5 we demonstrated distributed chromatic dispersion maps at different wavelengths. It shows clearly that dispersion maps are with a similar tendency except dispersion values with offsets for different wavelengths. Again we demonstrated a good reproducibility and accuracy of the tested results.

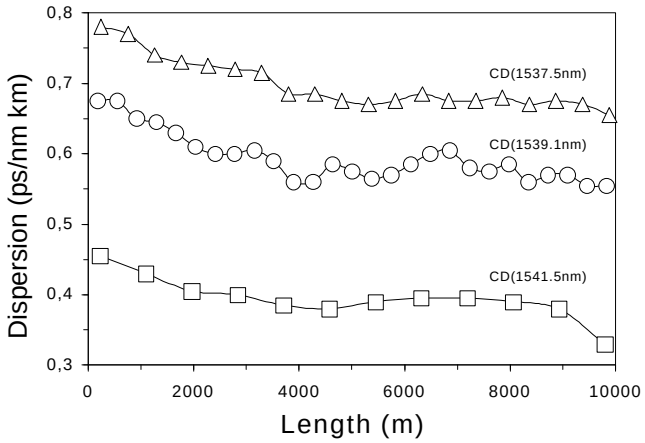

Fig.5 Chromatic dispersion maps for different wavelengths.

B. Effect of PMD

We also measured chromatic dispersion for a high PMD dispersion-shifted fiber with PMD 0.19 ps/√km and found that it was difficulty to extract the dispersion map. Fig.6 shows four-wave mixing intensity along distance for different SOPs. As can be seen, maximum locations of the Stokes signal were varied strongly

due to the additional phase from PMD, which depended on the input light polarization states. In fact, the chromatic dispersion map can no longer be estimated from a single trace alone, as the frequency at a given location depended on the (arbitrary) relative polarization states at that location for that input SOP. To remove this arbitrary component, different profiles, each corresponding to a different input SOP, had to be taken. For a given location, the mean value of group velocity delay (GVD) should then be retained. We point out that an averaging overall possible SOPs during an acquisition (by using a polarization scrambler) did not give a meaningful result, as it simply corresponds to a sum of the different individual traces giving - due to arbitrary positions of the different maxima - a curve that was basically flat. It was nearly impossible to extract a meaningful dispersion map from this measurement.

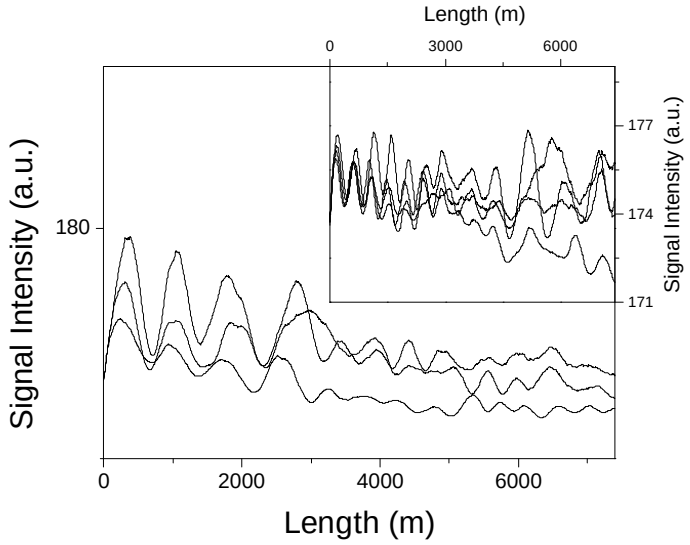

Fig.6 FWM intensity profile for a high PMD DSF fiber. Three traces correspond three input SOPs. The insert figure shows the input lights were launched from another fiber end.

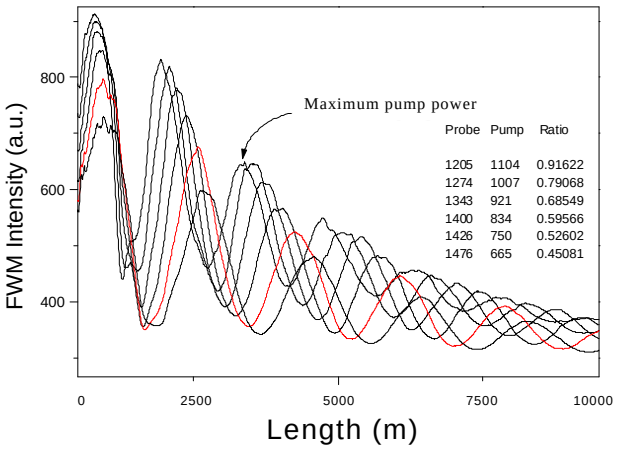

Fig.7 FWM intensity profiles for the different launched probe and pump powers.

C. *Effect of fiber nonlinearity and n_2/Ae_{ff} measurement*

As shown in simulation of Fig.1, the fiber nonlinear effect could introduce some additional phase mismatch if the $P_2/P_1$¹2. Thus it is important to set $P_2/P_1=2$ at any position of fiber in order to extract a precision local CD. Fig.7 shows experimental results of oscillation frequencies in the Stokes signal intensity was varied with ratio of pump and probe powers. This effect not only comes from fiber itself (n_2/Ae_{ff}), but also could come from pump and probe power level and its ratio. This nonlinear phase mismatch makes complicated to extract a precision chromatic dispersion map.

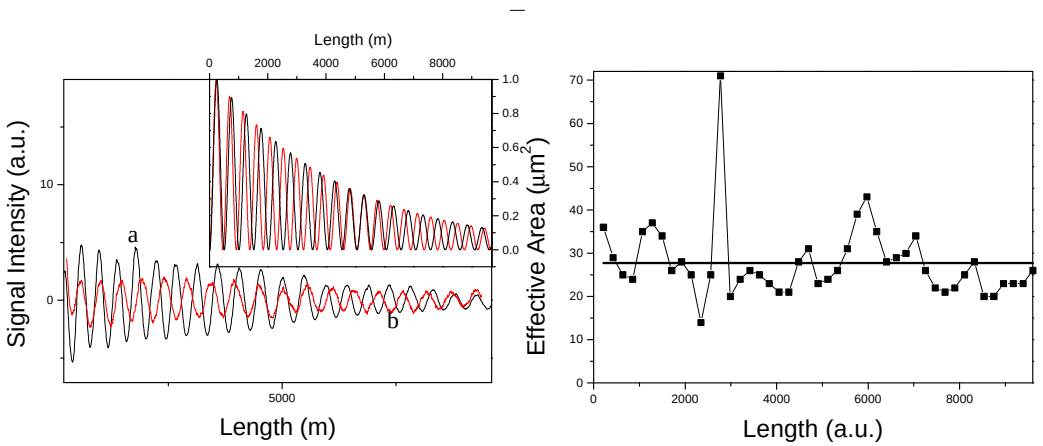

Fig.8 Left: measured FWM intensity for $P_{10} = P_{20}$ = 1150 mW (trace a) and $P_{10} = P_{20}$ = 115 mW (trace b) at wavelength 1541.3 nm and the insert figure is theoretical simulation using experimental parameters. Right: map of the A_{eff} for the short coupling length fiber for $n_2 = 2.6\text{x}10^{-20}$ m^2/W.

However, the method of measurements of distributed chromatic dispersion can also be used to measure distributed nonlinear coefficient g (*i.e.* n_2/Ae_{ff}) by fitting experimental data to the theoretical simulation. One simple method to measure distributed nonlinear coefficient is to take several measurements by using different input pump powers launched into FUT with a viable optical attenuator (VOA). Fig.8 (left) shows two four-wave mixing signal traces where launched pumped light power was attenuated by 10 dB. Clearly there are two fringes being missed from weaker pump power. The inserted figure shows our theoretical simulation using experimental parameters and it agrees with our experimental results very well. To extract a nonlinear coefficient map from above curves was possible[24] as shown in Fig.8 (right) for an A_{eff} map where we set $n_2=2.5\text{x}10^{-20}$ m^2/W but not enough accuracy from these primarily results because of noise on tested curves.

5. DISCUSSION

In the previous sections, we described the spatial resolved chromatic dispersion map measurement in the low PMD or low polarization coupling length dispersion-shifted fibers. In order to increase the dynamic range, we amplified the pulse peak power to about 10 W and predicted that the measurable fiber distance could be of 40 km. In order to avoid the fiber nonlinear effect, one should choose the probe power twice as large as the pump power ($P_2/P_1=2$) so the nonlinear phase mismatch is disappeared.

Even we demonstrated a promising measurement of chromatic dispersion maps with a precision and good spatial resolution. However, due to sensitivity of FWM efficiency and phase mismatch on light polarization by PMD, the meaningful distributed chromatic dispersion map may be impossible to obtain for some fibers where the polarization coupling length is too large. In fibers with low PMD, polarization does not affect the value of chromatic dispersion and a meaningful information about distributed chromatic

dispersion can be possible to be extracted from the resulting Stokes oscillation. For recently installed fibers with a low PMD, it would be possible to achieve a precision measurement by averaging over polarization to avoid ambiguous. We point out here that polarization dependent phase mismatch is strongly depend on probe and pump power level. Thus a relative weak power should be helpful to decrease the polarization effect, but it would limit measurable dynamic range.

The method of the distributed chromatic dispersion measurement using phase mismatched FWM may also be used to measure the distributed nonlinear coefficient of low PMD or low polarization coupling length fibers. Therefore, a meaningful nonlinear coefficient map may be obtained by fitting experimental data to simulation as indicated in second term of Eq.2. In our experiment we could clearly observe the Stokes oscillation moving when the pump and probe power were varied. A clear distributed nonlinear coefficient should be measurable if signal to noise ratio can be improved.

6. CONCLUSION

We demonstrated the distributed chromatic dispersion measurements in low PMD or low polarization coupling length dispersion-shifted fibers with a high spatial resolution and good accuracy based on the phase mismatched four-wave mixing. The impact of PMD and nonlinear effect on the measurements was also studied. In the experiment we observed that the mapping of chromatic dispersion in DSF fibers was strongly affected by their polarization coupling length. Nevertheless, the possibility to obtain a meaningful dispersion map in a fiber with low PMD still exists. However, it requires averaging of the dispersion values at a given location for different input SOPs to avoid ambiguous. The effect of nonlinear phase mismatch on Stokes signal for the measurement of chromatic dispersion map may lead to extract a distributed nonlinear coefficient n_2/A_{eff} as a function of fiber distance.

ACKNOWLEDGMENTS

H. Chen would like to thank Drs G. He and N. Cry of EXFO Electro-Optical Engineering Inc., Quebec, Canada for providing helpful discussion. C. Vinegoni thanks to EXFO Electro-Optical Engineering Inc., Quebec, Canada for financial support during this research.

REFERENCES

1. L.F. Mollenauer, P.V. Mamyshev and M.J. Nuebelt, `Method for facile and accurate measurement of optical fiber dispersion maps`, *Opt. Lett.*, vol.21, no.21, pp.1724, 1996.
2. N.G.R. Broderick, D.J. Richardson and L. Dong, `Distributed dispersion measurements and control within continuously varying dispersion tapered fibers`, *Opt. Lett.*, vol.9, no.11, pp.1511, 1997.
3. J. Gripp, L.F. Mollenauer, `Enhanced range for OTDR-like dispersion map measurements`, *Opt. Lett.*, vol.23, no.20, pp.1603, 1998.
4. M. Ohashi, M. Tateda, `Novel technique for measuring longitudinal chromatic dispersion distribution in singlemode fibres`, *Electron. Lett.*, vol.29, no.5, pp.426, 1993.
5. K.S. Abedin *et al*, `Measurement of the chromatic dispersion of an optical fiber by use of a Sagnac interferometer employing asymmetric modulation`, *Opt. Let*., vol.25, no.5, pp.299, 2000.
6. A. Rossaro, M. Schiano, T. Tambosso and D. D`Alessandro, `Spatially resolved chromatic dispersion measurement by a bidirectional OTDR technique`, *IEEE J. Select. Topic in Quantum Electron*., vol.7, no.3, pp.475-483, 2001.
7. K. Nakajima, M. Ohashi, and M. Tateda, `Chromatic dispersion distribution measurement along a single-mode optical fiber`, *J. of Lightwave Technol*., vol.15, no.7, pp.1095, 1997.
8. K.O. Hill, D.C. Johnson, B.S. Kawasaki and R.I. MacDonald, `CW three-wave mixing in single-mode optics fibers`, *J. App. Phys.*, 49(10), pp.5098, 1978.
9. R.H. Stolen and J.E. Bjorkholm, `Parametric amplification and frequency conversion in optical fibers`, *IEEE J. of Quantum Electron*., vol.QE-18, no.7, pp.1062, 1982.
10. K. Inoue, `Experimental study on channel crosstalk due to fiber four-wave mixing around the zero-dispersion wavelength`, *IEEE J. of Lightwave Technol*., vol.12, no.6, pp.1023, 1994.

11. K. Inoue, `Four-wave mixing in an optical fiber in the zero-dispersion wavelength region`, *J. of Lightwave Technol*., vol.10, no.11, pp.1553, 1992.
12. L. Pringent, J.-P, Hamaide, `Measurement of fiber nonlinear Kerr coefficient by four-wave mixing`, *IEEE Photon. Technol. Lett*., vol.5, no.9, pp.1092, 1993.
13. K. Inoue, `Phase-mismatching characteristic of four-wave mixing in fiber lines with multistage optical amplifiers`, *Opt. Lett*., vol.17, no.11, pp.801, 1992.
14. I. Zacharopoulos, I, Tomkos, G. Guekos, `Influence of phase mismatch on a spectral inverter based on four-wave mixing in dispersion-shifted fiber at 10 Gb/s`, *IEEE Photon. Technol. Lett.*, vol.11, no.4, pp.430, 1999.
15. J. Hansryd, H. Sunnerud, P.A. Andrekson and M. Karlsson, `Impact of PMD on four-wave-mixing-induced crosstalk in WDM system`, *IEEE Photon. Technol. Lett.*, vol.12, pp.1261, 2000.
16. K. Inoue, `Polarization effect on four-wave mixing efficiency in a single-mode fiber`, *IEEE J of Quantum Electron.*, vol.28, no.4, pp.883, 1992.
17. S. Betti, M. Giaconi, `Effect of the cross-phase modulation on WDM optical systems: analysis of fiber propagation`, *IEEE Photon. Technol. Lett*., vol.13, no.4, pp.305-307, 2001.
18. R.I. Killey, H.J. Thiele, P. Bayvel, `Prediction of transmission penalities due to cross-phase modulation in WDM systems using a simplified technique`, *IEEE Photon. Technol. Lett.*, vol.12, no.7, pp.804, 2000.
19. J. Nilsson, B. Jaskorzynska, `Modeling and optimization of low-repetition-rate high-energy pulse amplification in cw-pumped erbium-doped fiber amplifiers`, *Opt. Lett.*, vol.18, no.24, pp.2099, 1993.
20. B. Desthieux, R.I. Laming, R.I., D.N. Payne, `111 kW (0.5 mJ) pulse amplification at 1.5 μm using a gated cascade of three erbium-doped fiber amplifiers`, *Appl. Phys. Lett.*, vol.63, no.5, pp.586, 1993.
21. L.G. Cohen, `Comparison of single-mode fiber dispersion measurement techniques`, *J. of Lightwave Technol*., vol. LT-3, no.5, pp.958-966, 1985.
22. Y. Horiuchi, `Chromatic dispersion measurement in 1.55 μm narrow-band region using a tunable external-cavity laser`, *IEEE Photon. Technol. Lett.*, vol.1, no.12, pp.458, 1989.
23. K. Mori, T. Morioka, and M. Saruwatari, `Ultrawide spectral range group-velocity dispersion measurement utilizing suppercontinuum in an optical fiber pumped by a 1.5μm compact laser source`, *IEEE Trans. on Instrumentation and Measurement*, vol.44, no.3, pp.712, 1995.
24. C. Vinegoni, H. Chen, M. Leblanc, G. Schinn, M. Wegmuller, and N. Gisin, `Distributed measurements of chromatic dispersion and of nonlinear coefficient in DSF fibers with non negligible values of PMD`, Paper WA5, OFC`2002, Anaheim, California, USA, 2002.

C.16 A Comparison of Six techniques for nonlinear coefficient measurements of various single mode optical fibers.

Y. Namihira, K. Miyagi, K. Kaneshima, M. Tadakuma, C. Vinegoni[1], G. Pietra, K. Kawanami

[1] *Group of Applied Physics - Gap Optique*
University of Geneva,
20 Ecole-de-Medecine, CH-1211 Aeneve 4, Switzerland

Claudio.Vinegoni@physics.unige.ch

Abstract : A comparison of six techniques for nonlinear coefficient (n2/Aeff) measurements of various optical fibers using Pulsed-LD SPM, CW-LD SPM, sinusoidally modulated signal-SPM, XPM, self-aligned Interferometric, and FWM methods is first demonstrated. The (n2/Aeff) obtained from the six different methods were in good interlaboratory agreement except for dispersion compensating fiber (DCF).

PRESENTED : NIST 2002 Boulder, CO (USA).

A Comparison of Six Techniques for Nonlinear Coefficient Measurements of various Single Mode Optical Fibers

Y. Namihira [#1], K. Miyagi [#1], K. Kaneshima [#1], M. Tadakuma [#2], C. Vinegoni [#3], G. Pietra [#4] and K. Kawanami [#5]

#2: The Furukawa Electric Co. Ltd., Japan, #3: University of Geneva, Switzerland
#4: Pirelli Labs Innovation, Italy, #5: Muroran Institute of Technology, Japan
#1: University of the Ryukyus, 1 Senbaru, Nishihara, Okinawa 903-0213, Japan
Phone/Fax: +81-98-895-8700, E-mail: namihira@eee.u-ryukyu.ac.jp

Abstract A comparison of six techniques for nonlinear coefficient (n_2/A_{eff}) measurements of various optical fibers using Pulsed-LD SPM, CW-LD SPM, sinusoidally modulated signal-SPM, XPM, self-aligned Interferometric, and FWM methods is first demonstrated. The (n_2/A_{eff}) obtained from the six different methods were in good interlaboratory agreement except for dispersion compensating fiber (DCF).

Introduction: Accurate determination of the nonlinear coefficient (n_2/A_{eff}){n_2 is the nonlinear refractive index, A_{eff} is the effective area} of optical fibers is required for the ultra-long amplified optical transmission systems. To date, the nonlinear coefficient of the optical fibers has been measured by using the self-phase modulation (SPM) method with a pulsed laser diode (LD) (P-SPM)[1], the SPM method with dual CW-LDs (CW-SPM) [2], the cross-phase modulation (XPM) method [3], self-aligned Interferometric (INT) method [4], sinusoidally modulated signal-SPM (S-SPM) method [5], and four wave mixing (FWM) method [6].

Heretofore, ITU-T (n_2/A_{eff}) round robin measurements for various optical fibers were coordinated by Prof. Y. Namihira of University of the Ryukyus (formerly KDD) have been successfully performed [7-9].

This paper first presents the results of the interlaboratory fiber nonlinear coefficient (n_2/A_{eff}) measurements for various optical fibers such as standard single mode fiber (SMF), cut-off shifted fiber (CSF), dispersion shifted fiber (DSF), non-zero DSF (NZDSF) and large effective area DSF (LEDSF), and dispersion compensating fiber (DCF) using six different techniques such as the P-SPM [1] , CW-SPM [2], XPM [3], INT[4], S-SPM [5], and FWM [6] methods at 1550nm.

Experiments: The experimental set-up of the (n_2/A_{eff}) measurements for the various single mode optical fibers are shown in Fig.1. In Fig.1, (a), (b), (c), (d) and (e) are P-SPM method, CW-SPM method, XPM method, INT method, S-SPM, and FWM methods, respectively. Here, n_2 can be estimated by (n_2/A_{eff}) multiplying the A_{eff}. The A_{eff} was measured by the far-field scan (FFS) technique [10]. The parameters of six kinds of single mode optical fibers are shown in Table 1. These fibers were circulated to the five Laboratories such as University of the Ryukyus (formerly KDD), Furukawa, University of Geneva, Pirelli Labs., Muroran Institute of Technology.

P-SPM method: In Fig.1(a), as a pulsed-LD, transform limited (TL) Gaussian pulse-LD were used [1]. The output optical pulse due to SPM was measured by the optical spectrum analyzer (OSA). As the input optical power increases, the maximum phase shift increases in proportion to the input peak power. The (n_2/A_{eff}) can be obtained from the numbers of peaks in the SPM broadened spectra [1].

CW-SPM method: In Fig.1(b), the optical beat signal was derived from dual CW-LDs operating at around 1550nm [2]. The beat signal was then amplified in a preamplifier (EDFA1) and transmitted through a optical band pass filter to suppress the amplified stimulated emission and a polarizer to a following high power erbium amplifier (EDFA2).

XPM method: In Fig.1(c), the probe signal power is set relatively weak so that (n_2/A_{eff}) in FUT is dominantly caused by amplified strong pump CW-LD through XPM and that the effect of SPM is negligible. When pump CW-LD or CW-SLD is modulated in its intensity, probe CW-LD is modulated in this phase through XPM [3].

INT method: In Fig.1(d), the Interferometric method is based on the detection of the Kerr phase shift by a self-aligned interferometer. Here, the distributed feedback laser (DFB), Erbium doped fiber amplifier (EDFA), polarization controller (PC), Farady mirror (FM), and fiber Bragg grating (FBG) were used [4].

S-SPM method: In Fig.1 (e), the S-SPM method is based on SPM effect estimation. This technique consists simply in propagating an optical signal sinusoidally modulated by means of an electro-optical $LiNbO_3$ modulator. The γ -

factor estimation is achieved using a simulation tool capable of reproducing the evolution of signal spectra along the fiber and doing a comparison between acquired experimental data and simulation result [5].

FWM method: In Fig.1(f), pump (DFB-LD1) and probe (DFB-LD2) sources are tunable with a temperature and current controller. The LD1 of pump source was amplified with a EDFA to compensate an insertion loss of polarization optics, and passed through a tunable band-pass filter (BPF) with $\Delta\lambda$=1nm to eliminate the ASE noise of EDFA. The $\lambda/2$ wave plate was used to rotate the input azimuth of linearly polarized light of LD1. In contrast, the output light of LD2 was depolarized with a depolarizer to examine the depolarization effect on FWM efficiency. Otherwise, the depolarizer was deleted in the setup so that the FWM efficiency was measured in linearly polarized states of LD1 and LD2 [6].

Results and discussions: The results of interlaboratory (n_2/A_{eff}) and n_2 measurements at random polarization states (RP) using six different techniques of P-SPM, CW-SPM, XPM, INT, S-SPM, and FWM for a SMF, a CSF, two kinds of DSFs, two kinds of NZDSFs, a LEDSF and a DCF at 1550nm are summarized in Tables 2 and 3, respectively.

In Tables 2 and 3, n2(RP) = η n2(LP), η =1.0 for P-SPM, η =8/9 for CW-SPM, S-SPM, and FWM, and the polarization factor η =2/3 for XPM were used. Here, LP represents the linear polarization state.

Here, concerning the results of the self-aligned Interferometric (INT) method [4], the (n_2/A_{eff}) values were larger than that of the other methods. Then, a correction (scaling) factor of ~0.8 with respect to the mean values of the other methods were used. Such a scaling could easily arise from an erroneous estimation of the absolute peak power used for this measurements (underestimate of the power by a factor of just 0.8). Therefore, the special correction factor of k =0.8 {(*) in Tables 2 , 3, Figs.1,2} were used for the INT method because of the experimental error.

Meanwhile, in FWM method at Muroran Institute of Technology, only one (n_2/A_{eff}) measurement of 20 km long DSF was measured at present, however, they will be measured (n_2/A_{eff}) of another fiber samples in the near future.

Fig. 2 show estimated values of n_2 at random polarization states for various optical fibers as a function of six different measurement methods. Fig. 3 indicates the estimated values of n_2 at random polarization states for six different measurement methods as a function of various optical fibers.

From Tables 2 and 3, it was found that the average values of n_2 at RP of SMF, CSF, DSF, NZDSF, LEDSF, and DCF were ~2.62, 2.43, 4.80, 4.16. 3.19 and 12.1 x 10^{-10} [1/W], respectively. Also, the average values of n_2 at RP for SMF, CSF, DSF, NZDSF, LEDSF and DCF were ~2.21, 2.14, 2.25, 2.31, 2.32, and 2.78 x 10^{-20} [m^2/W], respectively.

The average n_2 values of ~2.25 x 10^{-20} [m^2/W] of DSFs at random polarization states are in good agreement with that of 2.1 - 2.3 x 10^{-20} [m^2/W] range of published results, respectively.

Conclusions: From the interlaboratory nonlinear coefficient (n_2/A_{eff}) measurements for various optical fibers, the (n_2/A_{eff}) obtained from the six different techniques such as pulsed-LD SPM method, CW-SPM method, a XPM method, a self-aligned Interferometric (INT) method, a sinusoidally modulated signal SPM method, and FWM method were found to be a good agreement with each methods except for DCF.

It was confirmed that the average values n_2 at random polarization state obtained from these different methods were 2. □~2.3 x 10^{-20} [m^2/W] for SMF, CSF, DSF, NZDSF and LEDSF except for DCF of ~2.8 x 10^{-20} [m^2/W], respectively.

References□

[1] Y. Namihira:"Higly accurated nonlinear coefficient measurements by SPM method for DSFs and large effective area fibers at 1.55 μm," SOFM 1988, NIST, Boulder, USA, pp.83-86, 1998.

[2] A. Boskovic,et al.,:"Direct continuous-wave measurement of n_2 in various types of telecommunication fiber at 1.55 μm", Optics Letters, vol. 21, no. 24, pp. 1966-1968, 1996.

[3] T. Kato et al.,: "Measurement of nonlinear refractive index in optical fibers by cross phase modulation method using depolarized pump light," Optics Lett.,20, p.988, 1995.

[4] C. Vinegoni et al.,:" Interlaboratory measurements of the nonlinear coefficient of standard SMF and DSF fibers using an interferometric method and an SPM based cw dual-frequency method", OFMC'01, pp.59-62, Canbridge, UK, 2001.

[5] G. Pietra: "Sinusoidally modulated SPM method", Private communications, May, 2002.

[6] K. Kawanami et al.,"Polarization effects on determination of nonlinear refractive index by four-wave mixing in a dispersion shifted fiber", OECC'02, Yokohama, Japan, 2002.

[7] Y. Namihira : "Nonlinear coefficient round robin measurements for various dispersion shifted fibers in Japan and UK", ECOC2000, 8.2.5, pp.97-98, 2000.

[8] Y. Namihira: "KDD nonlinear coefficient round robin measurements for various dispersion shifted fibers in Japan and UK", SOFM 2000, Boulder Co. USA, pp.49-52, 2000.

[9] Y. Namihira et al., "Interim report of ITU-T nonlinear coefficient (n_2/A_{eff}) round robin measurement results in Japan ", OFMC'01, pp.63-66, Canbridge, UK, 2001.

[10] Y. Namihira :"Relationship between nonlinear effective area and mode field diameter for dispersion shifted fibers", Electron. Lett., vol.30, no.3, pp.262-264, 1994.

Table 1 Fiber parameters for various single mode optical fibers.

Fibers	SMF	CSF	DSF	NZDSF	LEDSF	DCF
D@1550nm [ps/(nm-km)]	16.3	19.4	-0.58	-2.19	-2.48	-109.1
Aeff@1550nm [ƒ m²]	84.6	88.2	46.8	55.6	72.8	22.9

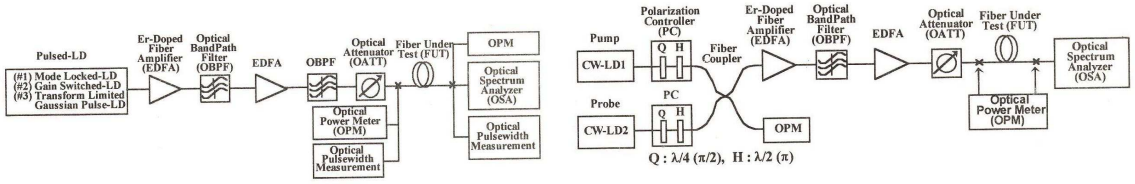

(a) Pulsed-LD SPM (P-SPM)

(b) CW-LD SPM (CW-SPM)

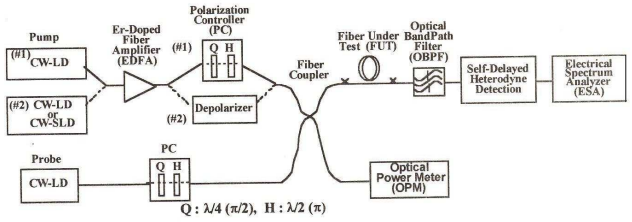

(c) XPM method

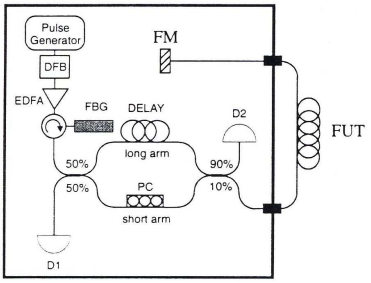

(d) Self-aligned Interferometric

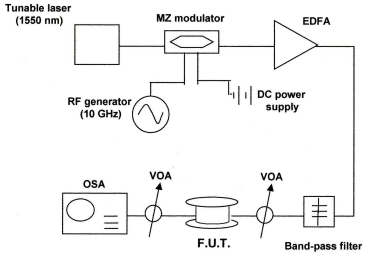

(e) Sinusoidally modulated signal SPM (S-SPM)

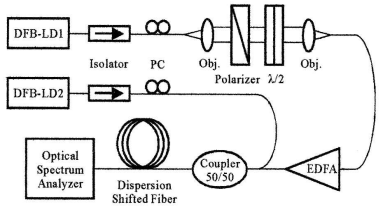

(f) Four wave mixing (FWM)

Fig.1 Experimental set up for six different (n2/Aeff) measurement methods.
(a) Pulsed LD SPM(P-SPM), (b) CW-LD SPM (CW-SPM), (c) XPM
(d) Self-aligned Interferometric (INT), (e) Sinusoidally modulated signal SPM (S-SPM),
(f) Four wave mixing (FWM)

Table 2 Measured values of (n2/Aeff) at random polarization states for various optical fibers using six different methods.

Fibers	(n2/Aeff) ×10⁻¹⁰ [1/W]							
	P-SPM	CW-SPM	XPM	INT (*)	S-SPM	FWM	Ave	ƒ Ð
SMF	2.62	2.60	2.45	2.53	2.90	-	2.62	0.172
CSF	2.45	2.31	2.14	2.58	2.65	-	2.43	0.206
DSF	4.76	5.09	4.69	4.51	5.65	4.70	4.89	0.227
NZDSF	3.94	4.26	3.70	4.18	4.75	-	4.16	0.395
LEDSF	3.01	3.25	3.00	3.18	3.51	-	3.19	0.209
DCF	11.86	11.56	13.00	14.02	10.12	-	12.11	1.481

(*) : Using a correction factor of 0.8. (-) : Not Measured

Table 3 Estimated values of n_2 at random polarization states for various optical fibers using six different methods.

Fibers	n2 ×10⁻²⁰ [m²/W]							
	P-SPM	CW-SPM	XPM	INT (*)	S-SPM	FWM	Ave	ƒ Ð
SMF	2.22	2.20	2.07	2.14	2.45	-	2.21	0.145
CSF	2.16	2.04	1.89	2.27	2.34	-	2.14	0.182
DSF	2.23	2.39	2.19	2.11	2.36	2.22	2.25	0.105
NZDSF	2.20	2.37	2.05	2.33	2.63	-	2.31	0.216
LEDSF	2.19	2.37	2.18	2.31	2.56	-	2.32	0.155
DCF	2.72	2.66	2.97	3.21	2.33	-	2.78	0.331

(*) : Using a correction factor of 0.8. (-) : Not Measured

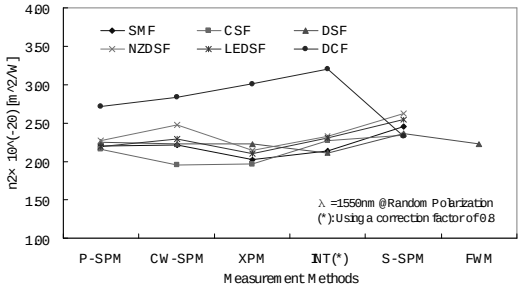

Fig.2 Estimated values of n_2 at random polarization states for various optical fibers as a function of six different measurement methods.

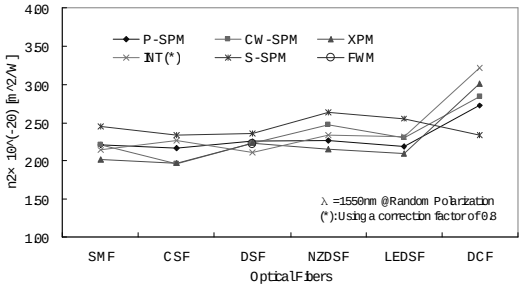

Fig.3 Estimated values of n_2 at random polarization states for six different measurement methods as a function of various single mode optical fibers.

Bibliography

[1] P. Butcher and D. Cotter, *The elements of nonlinear optics*. Cambridge Studies in Modern Optics, 1990.

[2] G. Agrawal, *Nonlinear fiber optics*. Academic Press, 1995.

[3] A. Fellegara, M. Artiglia, S. Andreasen, A. Melloni, F. Espunes, and S. Wabnitz, "Cost 241 intercomparison of nonlinear refractive index measurements in dispersion shifted optical fibers at l=1550 nm," *Electr. Lett.*, vol. 33, pp. 1168–71, 1997.

[4] A. Boskovic, S. V. Chernikov, J. R. Taylor, L. Gruner-Nielsen, and O. A. Levring, "Direct continuous-wave measurement of n_2 in various types of telecommunication fiber at 1.55 μm," *Opt. Lett.*, vol. 21, pp. 1965–7, 1996.

[5] T. Omae, K. Nakajima, and M. Ohashi, "Universal conditions for nonlinear refractive index n_2 estimation of dispersion compensating fibers by cw-spm method," *OFC 2001 Anaheim*, p. TuH3, 2001.

[6] B. Olssono and P. Andrekson, "Polarization independent Kerr-switch using a polarization diversity loop," *Technical Digest ECOC'98 Madrid, Spain*, pp. 185–6, 1998.

[7] K. Kitayama, Y. Kimura, and S. Seikai, "Fiber–optic logic gate," *Appl. Phys. Lett.*, vol. 46, pp. 317–9, 1985.

[8] T. Morioka, M. Saruwatari, and A. Takada, "Ultrafast optical multi/demultiplexer utilizing optical Kerr effect in polarization-maintaining single-mode fibers," *Electr. Lett.*, vol. 23, pp. 453–4, 1987.

[9] R. Stolen, J. Botineau, and A. Ashkin, "Intensity discrimination of optical pulses with birefringent fibers," *Opt. Lett.*, vol. 7, pp. 512–4, 1982.

[10] M. Horowitz and Y. Silberberg, "Nonlinear filtering by use of intensity–dependent polarization rotation in birefringent fibers," *Opt. Lett.*, vol. 22, pp. 1760–2, 1997.

[11] M. Hofer, M. Fermann, F. Haberl, M. Ober, and A. Schmidt, "Mode locking with cross–phase and self–phase modulation," *Opt. Lett.*, vol. 16, pp. 502–4, 1991.

[12] E. Dianov, E. Zakhidov, A. Karasik, M. Kasymdzhanov, and F. Mirtadzhiev, "Optical Kerr effect in glass fiber waveguides with weak and strong birefringence," *Sov. J. Quantum Electron.*, vol. 17, pp. 517–9, 1987.

[13] B. Crosignani, S. Piazzola, P. Spano, and P. D. Porto, "Direct measurement of the nonlinear phase shift between the orthogonally polarized states of a single-mode fiber," *Opt. Lett.*, vol. 10, pp. 89–91, 1985.

[14] M. Martinelli, "A universal compensator for polarization changes induced by birefringence on a retracing beam," *Opt. Comm.*, vol. 72, pp. 341–4, 1989.

[15] G. Ribordy, J. Gautier, N. Gisin, O. Guinnard, and H. Zbinden, "Automated plug and play quantum key distribution," *Electr. Lett.*, vol. 34, pp. 2116–7, 1998.

[16] J. Breguet, J. Pellaux, and N. Gisin, "Photoacoustic detection of trace gases with an optical microphone," *Sens. Actuators A, Phys.*, vol. 1, pp. 29–35, 1995.

[17] S. Yamashita, K. Hotate, and M. Ito, "Polarization properties of a reflective fiber amplifier employing a circulator and a Faraday rotator mirror," *J. Lightwave Technol.*, vol. 14, pp. 385–90, 1996.

[18] E. Alekseev, E. Bazarov, V. Gubin, A. Sazonov, and N. Starostin, "Compensation for spurious polarization modulation in a fiber optic phase modulator with the Faraday mirror," *Radiotekh. Elektron.*, vol. 44, pp. 122–7, 1999.

[19] M. Jinno and T. Matsumoto, "Nonlinear Sagnac interferometer switch and its applications," *IEEE J. Quantum Electr.*, vol. 28, pp. 875–82, 1992.

[20] T. Morioka and M. Saruwatari, "Ultrafast all-optical switching utilizing the optical Kerr effect in polarization-maintaining single-mode fibers," *IEEE J. on Selected Areas in Comm.*, vol. 6, pp. 1186–98, 1988.

[21] K. Byron, "Kerr modulation of signals at 1.3 and 1.5 μm in polrarization maintaining fibers pumped at 1.06 μm," *Electr. Lett.*, vol. 23, pp. 1324–26, 1987.

[22] M. Lagasse, D. Liu-Wong, J. Fujimoto, and H. Haus, "Ultrafast switching with a single-fiber interferometer," *Opt. Lett.*, vol. 14, pp. 311–3, 1989.

[23] C. Vinegoni, M. Wegmuller, B. Huttner, and N. Gisin, "Measurements of nonlinear polarization rotation in a highly birefringent optical fiber using a Faraday mirror," *J. Opt. A: Pure Appl. Opt.*, vol. 2, pp. 314–8, 2000.

[24] Y. Svirko and N. Zheludev, *Polarization of Light in Nonlinear Optics*. John Wiley & Sons, 1998.

[25] J. Dziedzic, R. Stolen, and A. Aschkin, "Optical Kerr effect in long fibers," *Appl. Opt.*, vol. 20, pp. 1403–1406, 1981.

[26] R. Stolen and A. Ashkin, "Optical Kerr effect in glass waveguide," *Appl. Phys. Lett.*, vol. 22, pp. 294–6, 1978.

[27] P. Wai and C. Menyuk, "Polarization decorrelation in optical fibers with randomly varying birefringence," *Opt. Lett.*, vol. 19, pp. 1517–9, 1994.

[28] N. Gisin, J. von der Weid, and J. Pellaux, "Polarization mode dispersion of short and long single-mode fibers," *J. Lightwave Technol.*, vol. 9, pp. 821–7, 1991.

[29] L. Mollenauer, P. Mamyshev, and M. Neubelt, "Method for facile and accurate measurement of optical fiber dispersion maps," *Opt. Lett.*, vol. 21, pp. 1724–6, 1996.

[30] J. Gripp and L. Mollenauer, "Enhanced range for otdr-like dispersion map measurements," *Opt. Lett.*, vol. 23, pp. 1603–7, 1998.

[31] J. Gripp and L. Mollenuaer, "Enhanced range far otdr-like dispersion map measurements.," *Opt. Lett.*, vol. 23, pp. 1603–5, 1998.

[32] F. Wittl, J. Vobian, G. Herchenroeder, and W. Dultz, "Interferometric determination of the nonlinear refractive index n_2 of optical fibers," *Technical Digest - Symposium on Optical Fiber Measurements, (NIST SP 905)*, pp. 71–4, 1996.

[33] S. Chernikov and J. Taylor, "Measurement of normalization factor of n_2 for random polarization in optical fibers," *Opt. Lett.*, vol. 21, pp. 1559–61, 1996.

[34] N. Gisin, R. Passy, and B. Perny, "Optical fiber characterization by simultaneous measurement of the transmitted and refracted near field," *J. Lightwave Technol.*, vol. 11, pp. 1875–83, 1993.

[35] J. Meier, *Stabile interferometrie des nichtlinearen BrechzahlKoeffizienten von Quarzglasfasern der optischen Nachrichtentechnik*. Ph.D. Dissertation, 1995.

[36] C. Vinegoni, M. Wegmuller, N. Gisin, K. Nakajima, and M. Ohashi, "Interlaboratory measurements of the nonlinear coefficient of standard smf and dsf fibers using an interferometric method and an spm based cw dual-frequency method," *OFMC 2001 Cambridge UK*, 2001.

[37] T. Drapela, "Effective area and nonlinear coefficient measurements of single-mode fibers: recent interlaboratory comparison," *in Applications of Photonic Technology 4, Proc. of SPIE*, vol. 4, pp. 293–7, 2000.

[38] P. Maker, R. Terhune, and C. Savage, "Intensity–dependent changes in the refractive index of liquids," *Phys. Rev. Lett.*, vol. 12, pp. 507–9, 1964.

[39] P. Unsbo and C. Flytzanis, "Degenerate four-wave mixing in isotropic nonlinear-optical gyrotropic media," *J. Opt. Soc. Am. B*, vol. 14, pp. 560–69, 1997.

[40] C. Menyuk, "Nonlinear pulse propagation in birefringence optical fibers," *IEEE J. Quantum Electron.*, vol. 23, pp. 174–6, 1987.

[41] K. Inoue, "Four–wave mixing in an optical fiber in the zero–dispersion wavelength region.," *J. Ligthw. Technol.*, vol. 10, pp. 1553–61, 1992.

[42] J. Hansryd, H. Sunnerud, P. Andrekson, and M. Karlsson, "Impact of pmd on four-wave-mixing-induced crosstalk in wdm systems," *Photon. Technol. Lett.*, vol. 12, pp. 1261–3, 2000.

[43] N. Broderick, D. Richardson, and L. Dong, "Distributed dispersion measurements and control within continuously varying dispersion tapered fibers," *Photon. Technol. Lett.*, vol. 9, pp. 1511–3, 1997.

[44] E. Betzig and J. Trautman, "Near-field optics: microscopy, spectroscopy, and surface modification beyond the diffraction limit," *Science*, vol. 257, pp. 189–5, 1992.

[45] E. Betzig, J. Trautman, T. Harris, J. Weiner, and R. Kostelak, "Breaking the diffraction barrier: optical microscopy on a nanometric scale," *Science*, vol. 251, pp. 1468–70, 1991.

[46] J. Trautman, E. Betzig, J. Weiner, D. DiGiovanni, T. Harris, F. Hellman, and E. Gyorgy, "Image contrast in near-field optics," *J. Appl. Phys.*, vol. 71, pp. 4659–63, 1992.

[47] E. Betzig and R. Chichester, "Single molecules observed by near-field scanning optical microscopy," *Science*, vol. 262, pp. 1422–8, 1993.

[48] D. Butler, A. Horsfall, K. Nugent, A. Roberts, I. Basset, and K. Lo, "Measurement of an elliptical fiber mode field using near-field microscopy," *J. Appl. Phys.*, vol. 77, pp. 5514–7, 1995.

[49] K.-B. Song, J.-E. Bae, K. Cho, S.-Y. Yim, and S.-H. Park, "Near-field scanning photoluminescence measurements using an uncoated fiber tip: A potential high resolution diagnostic technique for semiconductor devices," *Appl. Phys. Lett.*, vol. 73, pp. 2260–2, 1998.

[50] J. Mills, C. Hillman, W. Brocklesby, and B. Blott, "Evanescent field imaging of an optical fiber Bragg grating," *Appl. Phys. Lett.*, vol. 75, pp. 4058–60, 1999.

[51] C. Chicanne, S. Emonin, N. Richard, T. David, E. Bourillot, J. Goudonnet, and Y. Lacroute, "Characterization of optogeometric parameters of optical fibers by near-field scanning probe microscopies," *J. Opt. Soc. Am. B*, vol. 17, pp. 1473–82, 2000.

[52] A. Karlsson, M. Bourennane, G. Ribordy, H. Zbinden, J. Brendel, J. Rarity, and P. Tapster, "Long-haul telecom," *Circuits & devices*, vol. 11, pp. 34–40, 1999.

[53] G. Ribordy, J. Gautier, N. Gisin, O. Guinnard, and H. Zbinden, "Fast and user-friendly quantum key distribution," *Journal of Modern Optics*, vol. 47, pp. 517–31, 2000.

[54] K. Karrai and R. Grober, "Piezoelectric tip-sample distance control for near field optical microscope," *Appl. Phys. Lett.*, vol. 66, pp. 1842–44, 1995.

[55] G. Ribordy, J. Gautier, H. Zbinden, and N. Gisin, "Performance of InGaAs/InP avalanche photodiodes as gated-mode photon counters," *Appl. Opt.*, vol. 37, pp. 2272–7, 1998.

[56] S. Cova, M. Ghioni, A. Lacaita, C. Samori, and F. Zappa, "Avalanche photodiodes and quenching circuits for single-photon detection," *Appl. Opt.*, vol. 35, pp. 1956–76, 1996.

[57] D. Stucki, G. Ribordy, A. Stefanov, H. Zbinden, J. Rarity, and T. Wall, "Photon counting for quantum key distribution with Peltier cooled InGaAs/InP APD's," *Submitted for Publication*, 2001.

[58] W. Zheng, O. Hulten, and R. Rylander, "Erbium-doped fiber splicing and splice loss estimation," *J. Lightwave Technol.*, vol. 12, pp. 430–5, 1994.

[59] Y. Zhang, S. Soper, L. Middendorf, J. Wurm, R. Erdmann, and M. Wahl, "Simple near-infrared time-correlated single photon counting instrument with a pulsed diode laser and avalanche photodiode for time-resolved measurements in scanning applications," *Appl. Spectr.*, vol. 53, pp. 497–504, 1999.